USDA Forest Service
U.S. DEPARTMENT OF AGRICULTURE

Southern Research Station | General Technical Report SRS-261 | July 2021

Forest Health Monitoring: National Status, Trends, and Analysis 2020

Editors Kevin M. Potter Barbara L. Conkling

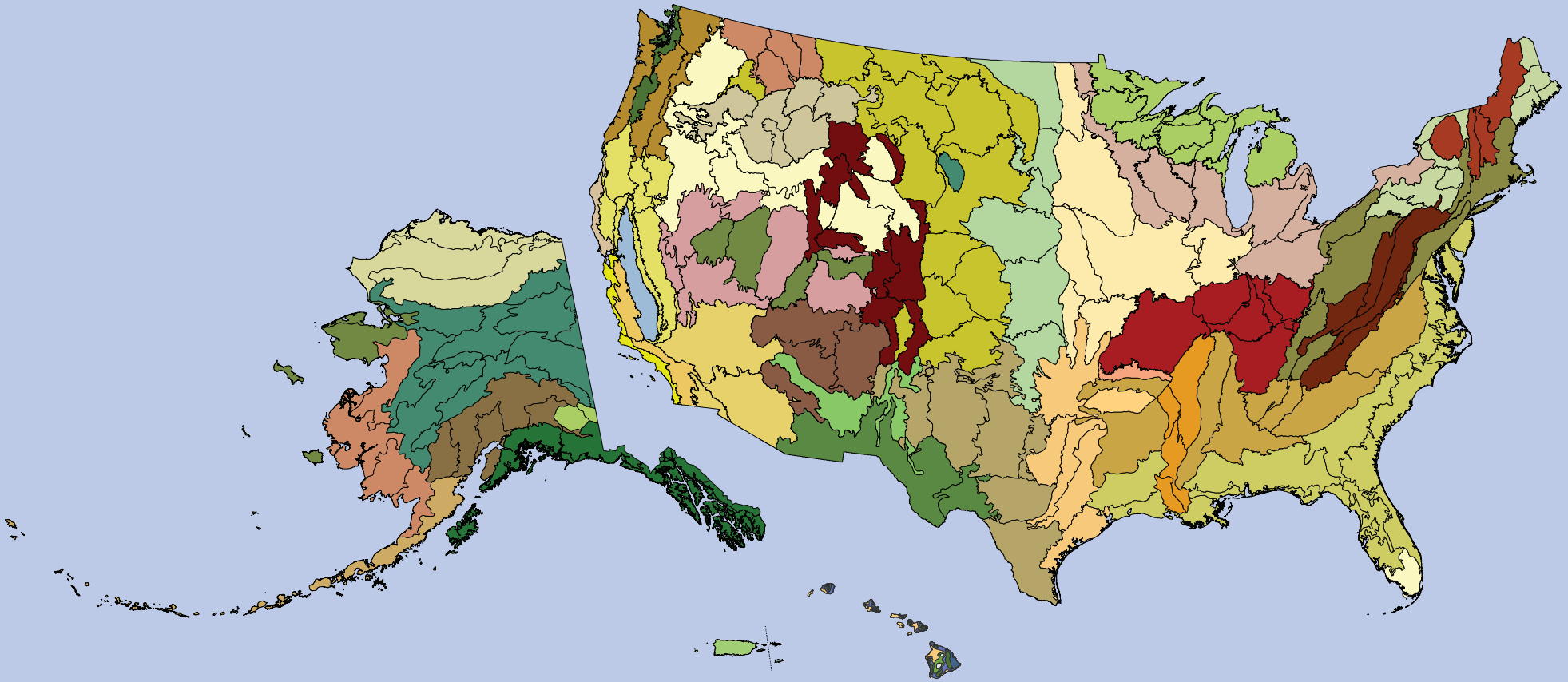

Front cover map:
Ecoregion provinces and ecoregion sections for the conterminous United States (Cleland and others 2007) and for Alaska (Spencer and others 2002), and ecoregions within the islands of Hawaii, along with Puerto Rico and the U.S. Virgin Islands, for which no corresponding ecoregion treatments exist.

Back cover maps:
Tree canopy cover (green) for the conterminous 48 States, Hawaii, Puerto Rico, and the U.S. Virgin Islands based on data from a cooperative project between the Multi-Resolution Land Characteristics Consortium and the U.S. Department of Agriculture Forest Service, Geospatial Technology and Applications Center (GTAC) using the 2011 National Land Cover Database. Forest and shrubland cover for Alaska derived from the 2011 National Land Cover Database.

DISCLAIMER
The use of trade or firm names in this publication is for reader information and does not imply endorsement by the U.S. Department of Agriculture of any product or service.

July 2021

Southern Research Station
200 W.T. Weaver Blvd.
Asheville, NC 28804

www.srs.fs.usda.gov

Forest Health Monitoring:

National Status, Trends, and Analysis 2020

Editors

Kevin M. Potter, Research Professor, North Carolina State University, Department of Forestry and Environmental Resources, Raleigh, NC 27695

Barbara L. Conkling, Research Assistant Professor, North Carolina State University, Department of Forestry and Environmental Resources, Raleigh, NC 27695

ABSTRACT

The annual national report of the Forest Health Monitoring (FHM) program of the Forest Service, U.S. Department of Agriculture, presents forest health status and trends from a national or multi-State regional perspective using a variety of sources, introduces new techniques for analyzing forest health data, and summarizes results of recently completed Evaluation Monitoring projects funded through the FHM national program. In this 20th edition in a series of annual reports, national survey data are used to identify recent geographic patterns of insect and disease activity. Satellite data are employed to detect geographic patterns of forest fire occurrence. Recent drought and moisture surplus conditions are compared across the conterminous United States. Data collected by the Forest Inventory and Analysis (FIA) program are employed to detect regional differences in tree mortality. Nearly 20 years of FIA coarse woody material (CWM) data are examined across spatial scales to assess change over time in CWM biomass, diameter and decay class, and species composition. Case studies demonstrate the potential of rFIA, an open-source R package developed to improve the accessibility of FIA data and offer enhanced flexibility in estimation strategies, to advance forest health evaluation and monitoring. Six recently completed Evaluation Monitoring projects are summarized, addressing forest health concerns at smaller scales.

Keywords—Change detection, coarse woody material, drought, fire, forest health, forest insects and disease, tree canopy, tree mortality.

CONTENTS

LIST OF FIGURES vii

LIST OF TABLES xvi

EXECUTIVE SUMMARY 1

LITERATURE CITED 5

CHAPTER 1.

Introduction 7

Kevin M. Potter

THE FOREST HEALTH MONITORING PROGRAM 14
DATA SOURCES. 16
FHM REPORT PRODUCTION. 16
Box 1.1 17
LITERATURE CITED 18

SECTION 1.

Analyses of Short-Term Forest Health Data . . . 25

CHAPTER 2.

Broad-Scale Patterns of Insect and Disease Activity across the 50 United States from the National Insect and Disease Survey, 2019 27

Kevin M. Potter, Jeanine L. Paschke, Frank H. Koch, and Erin M. Berryman

INTRODUCTION 27
METHODS 28
RESULTS AND DISCUSSION 35
CONCLUSION 54
LITERATURE CITED 54

CHAPTER 3.

Broad-Scale Patterns of Forest Fire Occurrence across the 50 United States and the Caribbean Territories, 2019 59

Kevin M. Potter

INTRODUCTION 59
METHODS 60
RESULTS AND DISCUSSION 64
CONCLUSIONS 81
LITERATURE CITED 81

CHAPTER 4.

Spatial Patterns of Drought and Moisture Surplus in the Conterminous United States: 2019, 2017—2019, and 2015—2019 85

Frank H. Koch and John W. Coulston

INTRODUCTION 85
METHODS 87
RESULTS AND DISCUSSION 90
LITERATURE CITED 100

CHAPTER 5.

Tree Mortality 105

Mark J. Ambrose

INTRODUCTION 105
DATA 105
METHODS 106
RESULTS AND DISCUSSION 108
SUMMARY 118
LITERATURE CITED 119

SECTION 2.

Analyses of Long-Term Forest Health Trends and Presentations of New Techniques 125

CHAPTER 6.

Changes in Coarse Woody Material Attributes, U.S. Forests, 2002—2011 to 2012—2019 127

Christopher W. Woodall, Matthew B. Russell, Shawn Fraver, Brian F. Walters, and Grant M. Domke

INTRODUCTION 127
METHODS 127
RESULTS AND DISCUSSION 129
LITERATURE CITED 141

CHAPTER 7.

Advancing Broad-scale Forest Health Evaluation and Monitoring with rFIA 143

Hunter Stanke, Andrew O. Finley, and Grant M. Domke

INTRODUCTION 143
METHODS 144
RESULTS AND DISCUSSION 147
LITERATURE CITED 154

SECTION 3.

Evaluation Monitoring Project Summaries . . . 155
LITERATURE CITED 155

CHAPTER 8.

Determining What Species Regenerate in Forest Stands Impacted by Heterobasidion Root Disease in Wisconsin and Michigan 157

Michael Hillstrom, Michael Demchik, Monique Sakalidis, Kyoko Scanlon, Trevor Adams, and Katherine Minnix

INTRODUCTION 157
METHODS 157
RESULTS 157
DISCUSSION AND CONCLUSIONS 159
ACKNOWLEDGMENTS 159
LITERATURE CITED 159

CHAPTER 9.

Legacy Effects of Emerald Ash Borer on Vegetation in Riparian Forests and Communities of Woodboring Cerambycid Beetles 161

Patrick Engelken and Deborah G. McCullough

INTRODUCTION 161
LITERATURE CITED 165

CHAPTER 10.

Vulnerability of Rocky Mountain Bristlecone Pine to Mountain Pine Beetle 167

Barbara Bentz, David Soderberg, Justin Runyon, Sharon Hood, Jim Vandygriff, Matt Hansen, and Sky Stephens

INTRODUCTION 167
METHODS 168
RESULTS AND DISCUSSION 170
LITERATURE CITED 174

Chapter 11.

Tree Mortality and Fuel Changes due to Extreme Drought and Concurrent Bark Beetle Outbreaks in California 177

Sharon M. Hood, Charlotte C. Reed, Daniel R. Cluck, Beverly Bulaon, Stacy Hishinuma, Andrea Hefty, and Sheri Smith

INTRODUCTION 177
METHODS 178
RESULTS 179
DISCUSSION AND CONCLUSIONS 182
ACKNOWLEDGMENTS 183
LITERATURE CITED 183

CHAPTER 12.

Accuracy Assessment of Insect and Disease Survey and eDaRT for Monitoring Forest Health . . 187

Michèle R. Slaton, Kayanna Warren, Alexander Koltunov, and Sheri Smith

INTRODUCTION 187
METHODS 187
RESULTS 190
DISCUSSION 192
CONCLUSIONS 193
ACKNOWLEDGMENTS 195
LITERATURE CITED 195

CHAPTER 13.

Emerald Ash Borer Infestation in Arkansas: Extent, Severity, and Progression 197

Mohammad M. Bataineh, Benjamin L. Walters, Stephen R. Clarke, Benjamin Babst, and Robert Ficklin

INTRODUCTION 197
METHODS 197
RESULTS AND DISCUSSION 200
CONCLUSIONS 205
ACKNOWLEDGMENTS 205
LITERATURE CITED 206

ACKNOWLEDGMENTS 207

AUTHOR INFORMATION 208

LIST OF FIGURES

Figure 1.1—Ecoregion provinces and sections for (A) the conterminous United States (Cleland and others 2007) and (B) Alaska (Spencer and others 2002). Ecoregion sections within each ecoregion province are shown in the same color 10

Figure 1.2—Ecoregions, and ecoregion subunits, for Hawaii, developed based on moisture zones and elevation (see box 1.1). Ecoregion subunits are shown in the same color by ecoregion. See table 1.1 for the names of the ecoregion subunits listed on the map 12

Figure 1.3—The design of the Forest Health Monitoring program (FHM 2003) 14

Box 1.1 figure—The Forest Inventory and Analysis mapped plot design. Subplot 1 is the center of the cluster with subplots 2, 3, and 4 located 120 feet away at azimuths of 360°, 120°, and 240°, respectively (Burrill and others 2018) 17

Figure 2.1—The extent of surveys for insect and disease activity conducted in the conterminous United States, Alaska, Hawaii, and the U.S. Caribbean Island territories in 2019. The blue lines delineate Forest Health Monitoring regions. Note: Alaska and Hawaii are not shown to scale with map of the conterminous United States. (Data source: U.S. Department of Agriculture Forest Service, Forest Health Protection) 30

Figure 2.2—The percentage of surveyed tree canopy cover area with insect and disease mortality, by ecoregion section within the conterminous 48 States, for 2019. The gray lines delineate ecoregion sections (Cleland and others 2007). The 240-m tree canopy cover is based on data from a cooperative project between the Multi-Resolution Land Characteristics Consortium (Coulston and others 2012) and the Forest Service Geospatial Technology and Applications Center using the 2011 National Land Cover Database. (Data source: U.S. Department of Agriculture Forest Service, Forest Health Protection) 39

Figure 2.3—Hot spots of percentage of surveyed tree canopy cover area with insect and disease mortality in 2019 for (A) the conterminous 48 States and (B) for separate Forest Health Monitoring (FHM) regions, by hexagons containing >5-percent tree canopy cover. Values are Getis-Ord G_i^* scores, with values >2 representing significant clustering of high mortality occurrence densities and values <-2 representing significant clustering of low mortality occurrence densities. The gray lines delineate ecoregion sections (Cleland and others 2007), and blue lines delineate FHM regions. Tree canopy cover is based on data from a cooperative project between the Multi-Resolution Land Characteristics Consortium (Coulston and others 2012) and the Forest Service Geospatial Technology and Applications Center using the 2011 National Land Cover Database. (Data source: U.S. Department of Agriculture Forest Service, Forest Health Protection) 40

Figures, cont.

Figure 2.4—The percentage of surveyed tree canopy cover area with insect and disease defoliation, by ecoregion section within the conterminous 48 States, for 2019. The gray lines delineate ecoregion sections (Cleland and others 2007). The 240-m tree canopy cover is based on data from a cooperative project between the Multi-Resolution Land Characteristics Consortium (Coulston and others 2012) and the Forest Service Geospatial Technology and Applications Center using the 2011 National Land Cover Database. (Data source: U.S. Department of Agriculture Forest Service, Forest Health Protection) 46

Figure 2.5—Hot spots of percentage of surveyed tree canopy cover area with insect and disease defoliation in 2019 for (A) the conterminous 48 States and (B) for separate Forest Health Monitoring regions, by hexagons containing >5 percent tree canopy cover. Values are Getis-Ord G_i* scores, with values >2 representing significant clustering of high defoliation occurrence densities. (No areas of significant clustering of low densities, <-2, were detected.) The gray lines delineate ecoregion sections (Cleland and others 2007), and blue lines delineate Forest Health Monitoring regions. Tree canopy cover is based on data from a cooperative project between the Multi-Resolution Land Characteristics Consortium (Coulston and others 2012) and the Forest Service Geospatial Technology and Applications Center using the 2011 National Land Cover Database. (Data source: U.S. Department of Agriculture Forest Service, Forest Health Protection) 47

Figure 2.6—Percentage of 2019 surveyed Alaska forest and shrubland area within ecoregions with mortality caused by insects and diseases. The gray lines delineate ecoregion sections (Spencer and others 2002). Forest and shrub cover is derived from the 2011 National Land Cover Database. (Data source: U.S. Department of Agriculture Forest Service, Forest Health Protection) . . . 51

Figure 2.7—Percentage of 2019 surveyed Alaska forest and shrubland area within ecoregions with defoliation caused by insects and diseases. The gray lines delineate ecoregion sections (Spencer and others 2002). Forest and shrub cover is derived from the 2011 National Land Cover Database. (Data source: U.S. Department of Agriculture Forest Service, Forest Health Protection) . . 52

Figure 2.8—Percentage of 2019 surveyed Hawaii tree canopy area within island/ecoregion combinations with mortality caused by insects and diseases. Tree canopy cover is based on data from a cooperative project between the Multi-Resolution Land Characteristics Consortium (Coulston and others 2012) and the Forest Service Geospatial Technology and Applications Center using the 2011 National Land Cover Database. See table 1.1 for ecoregion identification. (Data source: U.S. Department of Agriculture Forest Service, Forest Health Protection) 53

Figure 3.1—Forest fire occurrences detected by Moderate Resolution Imaging Spectroradiometer (MODIS) from 2001 through 2019 for the conterminous United States, Alaska, and Hawaii, and for the entire Nation combined. (Data source: U.S. Department of Agriculture Forest Service, Geospatial Technology and Applications Center, in conjunction with the NASA MODIS Rapid Response group) 65

Figure 3.2—The number of forest fire occurrences, per 100 km^2 (10 000 ha) of tree canopy coverage area, by ecoregion section within the conterminous 48 States, for 2019. The gray lines delineate ecoregion sections (Cleland and others 2007). Tree canopy cover is based on data from a cooperative project between the Multi-Resolution Land Characteristics Consortium (Coulston and others 2012) and the Forest Service Geospatial Technology and Applications Center using the 2011 National Land Cover Database. See figure 1.1A for ecoregion identification. (Source of fire data: U.S. Department of Agriculture Forest Service, Geospatial Technology and Applications Center, in conjunction with the NASA MODIS Rapid Response group) 67

Figure 3.3—The number of forest fire occurrences, per 100 km^2 (10 000 ha) of forest and shrub cover, by ecoregion section within Alaska, for 2019. The gray lines delineate ecoregion sections (Spencer and others 2002). Forest and shrub cover are derived from the 2011 National Land Cover Database. See figure 1.1B for ecoregion identification. (Source of fire data: U.S. Department of Agriculture Forest Service, Geospatial Technology and Applications Center, in conjunction with the NASA MODIS Rapid Response group) 69

Figure 3.4—The number of forest fire occurrences, per 100 km^2 (10 000 ha) of tree canopy coverage area, by island/ecoregion combination in Hawaii, for 2019. Tree canopy cover is based on data from a cooperative project between the Multi-Resolution Land Characteristics Consortium (Coulston and others 2012) and the Forest Service Geospatial Technology and Applications Center using the 2011 National Land Cover Database. See table 1.1 for ecoregion identification. (Source of fire data: U.S. Department of Agriculture Forest Service, Geospatial Technology and Applications Center, in conjunction with the NASA MODIS Rapid Response group) 70

Figure 3.5—The number of forest fire occurrences, per 100 km^2 (10 000 ha) of tree canopy coverage area, by island in Puerto Rico and the U.S. Virgin Islands, for 2019. Tree canopy cover is based on data from a cooperative project between the Multi-Resolution Land Characteristics Consortium (Coulston and others 2012) and the Forest Service Geospatial Technology and Applications Center using the 2011 National Land Cover Database. (Source of fire data: U.S. Department of Agriculture Forest Service, Geospatial Technology and Applications Center, in conjunction with the NASA MODIS Rapid Response group) 72

Figure 3.6—(A) Mean number and (B) standard deviation of forest fire occurrences per 100 km^2 (10 000 ha) of tree canopy coverage area from 2001 through 2018, by ecoregion section within the conterminous 48 States. (C) Degree of 2019 fire occurrence density excess or deficiency by ecoregion relative to 2001–2018 and accounting for variation over that time period. The gray lines delineate ecoregion sections (Cleland and others 2007). Tree canopy cover is based on data from a cooperative project between the Multi-Resolution Land Characteristics Consortium (Coulston and others 2012) and the Forest Service Geospatial Technology and Applications Center using the 2011 National Land Cover Database. (Source of fire data: U.S. Department of Agriculture Forest Service, Geospatial Technology and Applications Center, in conjunction with the NASA MODIS Rapid Response group) 73

Figure 3.7—(A) Mean number and (B) standard deviation of forest fire occurrences per 100 km^2 (10 000 ha) of forest and shrub cover from 2001 through 2018, by ecoregion section in Alaska. (C) Degree of 2019 fire occurrence density excess or deficiency by ecoregion relative to 2001–2018 and accounting for variation over that time period. The gray lines delineate ecoregion sections (Spencer and others 2002). Forest and shrub cover are derived from the 2011 National Land Cover Database. (Source of fire data: U.S. Department of Agriculture Forest Service, Geospatial Technology and Applications Center, in conjunction with the NASA MODIS Rapid Response group) 75

Figure 3.8—(A) Mean number and (B) standard deviation of forest fire occurrences per 100 km^2 (10 000 ha) of tree canopy coverage area from 2001 through 2018, by island/ecoregion combination in Hawaii. (C) Degree of 2019 fire occurrence density excess or deficiency by ecoregion relative to 2001–2018 and accounting for variation over that time period. Tree canopy cover is based on data from a cooperative project between the Multi-Resolution Land Characteristics Consortium (Coulston and others 2012) and the Forest Service Geospatial Technology and Applications Center using the 2011 National Land Cover Database. (Source of fire data: U.S. Department of Agriculture Forest Service, Geospatial Technology and Applications Center, in conjunction with the NASA MODIS Rapid Response group) 77

Figure 3.9—(A) Mean number and (B) standard deviation of forest fire occurrences per 100 km^2 (10 000 ha) of forested area from 2001 through 2018, by island in Puerto Rico and the U.S. Virgin Islands. (C) Degree of 2019 fire occurrence density excess or deficiency by ecoregion relative to 2001–2018 and accounting for variation over that time period. Tree canopy cover is based on data from a cooperative project between the Multi-Resolution Land Characteristics Consortium (Coulston and others 2012) and the U.S. Department of Agriculture Forest Service, Geospatial Technology and Applications Center using the 2011 National Land Cover Database . . . 78

Figure 3.10—Hot spots of fire occurrence across the conterminous United States for 2019. Values are Getis-Ord G_i* scores, with values >2 representing significant clustering of high fire occurrence densities. (No areas of significant clustering of lower fire occurrence densities, <-2, were detected). The gray lines delineate ecoregion sections (Cleland and others 2007). Background tree canopy cover is based on data from a cooperative project between the Multi-Resolution Land Characteristics Consortium (Coulston and others 2012) and the Forest Service Geospatial Technology and Applications Center using the 2011 National Land Cover Database. (Source of fire data: U.S. Department of Agriculture Forest Service, Geospatial Technology and Applications Center, in conjunction with the NASA MODIS Rapid Response group) 79

Figure 4.1—The 100-year (1920–2019) mean annual moisture index, or MI_{1norm}', for the conterminous United States. Ecoregion section (Cleland and others 2007) boundaries and labels are included for reference. Forest cover data (overlaid green hatching) derived from Moderate Resolution Imaging Spectroradiometer (MODIS) imagery by the U.S. Department of Agriculture Forest Service, Remote Sensing Applications Center. (Data source: PRISM Climate Group, Oregon State University) 91

Figure 4.2—The 2019 annual (i.e., 1-year) moisture difference *z*-score, or *MDZ*, for the conterminous United States. Ecoregion section (Cleland and others 2007) boundaries and labels are included for reference. Forest cover data (overlaid green hatching) derived from Moderate Resolution Imaging Spectroradiometer (MODIS) imagery by the U.S. Department of Agriculture Forest Service, Remote Sensing Applications Center. (Data source: PRISM Climate Group, Oregon State University) 93

Figure 4.3—The 2018 annual (i.e., 1-year) moisture difference *z*-score, or *MDZ*, for the conterminous United States. Ecoregion section (Cleland and others 2007) boundaries and labels are included for reference. Forest cover data (overlaid green hatching) derived from Moderate Resolution Imaging Spectroradiometer (MODIS) imagery by the U.S. Department of Agriculture Forest Service, Remote Sensing Applications Center. (Data source: PRISM Climate Group, Oregon State University) 95

Figure 4.4—The 2017–2019 (i.e., 3-year) moisture difference *z*-score (*MDZ*) for the conterminous United States. Ecoregion section (Cleland and others 2007) boundaries are included for reference. Forest cover data (overlaid green hatching) derived from Moderate Resolution Imaging Spectroradiometer (MODIS) imagery by the U.S. Department of Agriculture Forest Service, Remote Sensing Applications Center. (Data source: PRISM Climate Group, Oregon State University) 97

Figures, cont.

Figure 4.5—The 2015–2019 (i.e., 5-year) moisture difference *z*-score (*MDZ*) for the conterminous United States. Ecoregion section (Cleland and others 2007) boundaries are included for reference. Forest cover data (overlaid green hatching) derived from Moderate Resolution Imaging Spectroradiometer (MODIS) imagery by the U.S. Department of Agriculture Forest Service, Remote Sensing Applications Center. (Data source: PRISM Climate Group, Oregon State University) 98

Figure 5.1—Forest cover in the States where mortality was analyzed by ecoregion section (Cleland and others 2007). Mortality in Eastern and Central States was analyzed using a complete remeasurement cycle; in most Western States, mortality was analyzed using a partial cycle of remeasurements, and results there should be considered preliminary. Forest cover was derived from Moderate Resolution Imaging Spectroradiometer (MODIS) satellite imagery (USDA Forest Service 2008) 107

Figure 5.2—Tree mortality expressed as the ratio of annual mortality volume to gross annual volume growth (MRATIO) by ecoregion section (Cleland and others 2007). Data unavailable or insufficient for gray areas. (Data source: U.S. Department of Agriculture Forest Service, Forest Inventory and Analysis program) 109

Figure 5.3—Annual tree mortality expressed as a percentage of live tree volume by ecoregion section (Cleland and others 2007). Data unavailable or insufficient for gray areas. (Data source: U.S. Department of Agriculture Forest Service, Forest Inventory and Analysis program) 117

Figure 6.1—(A) Total coarse woody material (CWM) biomass (2012–2019) for only remeasured, forested down woody material (DWM) plots (2002–2011 to 2012–2019). (B) Total CWM biomass for all plots with at least one forested condition measured between 2012 and 2019.. 130

Figure 6.2—Change in coarse woody material (CWM) biomass (tons per acre) in U.S. forests by survey unit, 2002–2011 to 2012–2019. Gray States/survey units indicate no remeasured plots 131

Figure 6.3—U.S. coarse woody material (CWM) decay class distribution, 2002–2011 to 2012–2019 132

Figure 6.4—Change in coarse woody material (CWM) decay classes, 2002–2011 to 2012–2019 133

Figure 6.5—Change in percentage of moderately to advanced decayed coarse woody material (CWM) biomass, 2002–2011 to 2012–2019. (Note: a positive value indicates that the State's population of CWM biomass is becoming more advanced in decay over nearly 20 years.) 134

Figure 6.6—U.S. coarse woody material (CWM) transect diameter class distribution, 2002–2011 to 2012–2019 134

Figure 6.7—Changes in coarse woody material (CWM) transect diameter class distribution, 2002–2011 to 2012–2019 135

Figure 6.8—Change in percentage of large-sized coarse woody material (CWM) biomass (transect diameter >16.0 inches), 2002–2011 to 2012–2019. (Note: a negative value indicates that the State's population of CWM biomass is becoming increasingly represented by large-sized CWM pieces.) . . 136

Figure 6.9—Coarse woody material (CWM) biomass per forested acre and top three species by State, 2012–2019 138

Figure 6.10—Change in percentage of biomass of top five coarse woody material (CWM) species accounting for total CWM by State, 2002–2011 to 2012–2019. (Note: a positive value indicates that the State's population of CWM biomass is becoming more dominated by fewer species over nearly 20 years.) . . . 140

Figure 7.1—(A) Estimated current 100-hour fuel biomass (tons per acre) and (B) associated uncertainty (percent sampling error [SE]) within HUC6 watershed boundaries across the conterminous United States. All estimates produced using the *dwm* function in the rFIA package, using the temporally indifferent estimator . . 148

Figure 7.2—(A) Estimated trends in lodgepole pine (*Pinus contorta*) mortality rates (trees per acre [TPA] per year) and (B) associated uncertainty (percent sampling error) in the State of Colorado over the period 2002–2018. Estimates were produced using five design-based estimators: annual (ANNUAL), exponential moving average (EMA), linear moving average (LMA), simple moving average (SMA), and temporally indifferent (TI). All estimates were produced using the *growMort* function in the rFIA package 149

Figure 7.3—(A) Variation in short-range and long-range temporal trends of lodgepole pine (*Pinus contorta*) mortality rates (trees per acre [TPA] per year) and (B) associated uncertainty (percent sampling error) in the State of Colorado over the period 2002–2018. Estimates produced by varying the value of λ specified in the exponential moving average (EMA) estimator, where high values of λ characterize long-range temporal trends and low values characterize short-range temporal trends. All estimates produced using the *growMort* function in the rFIA package. . . . 150

Figure 7.4—Estimated annual rate of change (percent per year) in (A) live number of trees per acre (TPA) and (B) live basal area per acre (BAA), and (C, D) associated indices of significance (probability of direction) within ecoregion subsections (Cleland and others 2007) across the conterminous United States from 1999–2019. All estimates produced using a Bayesian hierarchical model fit to plot-level indices of live TPA and BAA on remeasured Forest Inventory and Analysis (FIA) plots. Plot-level indices of live tree abundance produced using the *tpa* function in the rFIA package 152

Figures, cont.

Figure 8.1—Regeneration in *Heterobasidion irregulare*-caused expanding mortality pockets or gaps (number of seedlings per hectare by height class) in Wisconsin and Michigan 158

Figure 8.2—Percentage of sites in Wisconsin and Michigan that included each species or species group. 158

Figure 10.1—Location of Rocky Mountain (RM) bristlecone pine mortality survey (RM 1–13) and defense sample (RM 5, 9, 13, 14, 15) sites. Mortality surveys were conducted in 2017 and defense sampling in 2018 and 2019. Rocky Mountain bristlecone pine distribution based on Little (1971) and Ellenwood and others (2015) 169

Figure 10.2—The proportion of a mountain pine beetle (MPB)-killed pine species at a site over a 10-year period (2006 to 2016) was best predicted by the proportion of basal area (BA) (m^2/ha) of that species in the stand pre-outbreak. Shown is the linear mixed model (SAS version 9.4, GLIMMIX) regression prediction (solid line) and the 95-percent confidence intervals (shaded area) for all species combined (Bentz and others, in press) 172

Figure 10.3—Total secondary metabolites (mg compound/g dry weight) in three pine species at five sites across the range of Rocky Mountain (RM) bristlecone pine (see fig. 10.1). Samples were collected at (A) day 0 (constitutive) and post-inoculation with a mountain pine beetle fungal associate (i.e., simulated attack) on (B) day 1, (C) day 4, and (D) day 30 (Soderberg and others, in preparation). Note the different y-axis scales among the days and that lodgepole pine was sampled at a single site 173

Figure 11.1—Needle retention (percent) of recently killed trees over time by species. ABCO = *Abies concolor* (white fir); PILA = *Pinus lambertiana* (sugar pine); PIMO = *Pinus monophyla* (singleleaf pinyon pine); PIPO = *Pinus ponderosa* (ponderosa pine) 180

Figure 11.2—Change in 1,000-hr fuel loads from 2016 to 2019 by overstory (≥12.7-cm d.b.h.) tree mortality level on the Los Padres National Forest (LPNF) and Sierra National Forest (SNF).. 182

Figure 12.1—Map of study area on the Sierra National Forest, CA, including field plots and Aerial Detection Survey (ADS) polygons (years 2016 and 2018 only used in analysis). 188

Figure 12.2—Error matrices representing disagreement between Aerial Detection Survey (ADS) and plot-based dead trees per acre (TPA) in polygons. Cell values are numbers of ADS polygons. Plot-based trees were >11 inches d.b.h. and included decay classes 1 and 2 for year 2018 (A) and decay classes 2, 3, and 4 for year 2016 (B). Raw values only are displayed; an area-based matrix with corrections following Pontius and Millones (2011) produced almost identical values. 190

Figure 12.3—Dead trees per acre (TPA) estimates from ADS polygons, eDaRT-F3, and plot-measured means with standard error (SE) bars, with plot sample size per polygon for 2 years. 191

Figure 13.1—(A) Green ash basal area distribution along major streams and rivers within the two Arkansas ecoregions that encompass the 17 counties of the study area; (B) the 6- x 6-mile grid used for trapping of emerald ash borer (EAB) and reconstruction of EAB-induced ash tree mortality patterns; (C) EAB detections (positive adult catches), over a 5-year period from 2014 through 2018; (D) EAB county-level yearly confirmation with yearly and 5-year spatial summary statistics (mean, median, and standard distance circle of one standard deviation) of positive detections. Ecoregion level III boundaries (Woods and others 2004) are included for reference. Green ash distribution data derived from Individual Species Parameter Maps by the U.S. Department of Agriculture Forest Service, Forest Health Protection (FHP), Forest Health Assessment and Applied Sciences Team (FHAAST). (Data sources: FHP, FHAAST, and Arkansas GIS Office) . . 198

Figure 13.2—Annual progression in (A) 2013, (B) 2014, (C) 2015, (D) 2016, (E) 2017, and (F) 2018 of emerald ash borer-induced mortality in relation to annual positive trap detections, host abundance and distribution, and other cultural features such as roads, camps, and public lands within an area encompassing the majority of four Arkansas counties. Green ash distribution data derived from Individual Species Parameter Maps by the U.S. Department of Agriculture Forest Service, Forest Health Protection (FHP), Forest Health Assessment and Applied Sciences Team (FHAAST). (Data sources: FHP, FHAAST, and Arkansas GIS Office) . . 202

Figure 13.3—(A) Density of emerald ash borer (EAB) detections and (B) EAB-killed ash snags, counts per square mile, over a 5-year period from 2014 through 2018. Green ash distribution data derived from Individual Species Parameter Maps by the Forest Service, Forest Health Protection, Forest Health Assessment and Applied Sciences Team. (Data sources: Forest Health Protection, FHAAST, and Arkansas GIS Office) 204

LIST OF TABLES

Table 1.1—The six ecoregions and 34 ecoregion subunits for the State of Hawaii . . 13

Table 2.1—Mortality agents and complexes affecting >5000 ha in the conterminous United States during 2019 36

Table 2.2—Beetle taxa included in the "western bark beetle" group. 36

Table 2.3—The top five mortality agents or complexes for each Forest Health Monitoring region, and for Alaska and Hawaii, in 2019 . 37

Table 2.4—Defoliation agents and complexes affecting >5000 ha in the conterminous United States in 2019 43

Table 2.5—The top five defoliation agents or complexes for each Forest Health Monitoring region and for Alaska and Hawaii, in 2019 . . 44

Table 3.1—The 15 ecoregion sections in the conterminous United States with the highest fire occurrence densities in 2019 68

Table 3.2—The 15 ecoregion sections in the conterminous United States with the highest mean annual fire occurrence densities from 2001 to 2018 74

Table 4.1—Moisture difference *z*-score (*MDZ*) value ranges for nine wetness and drought categories, along with each category's approximate theoretical frequency of occurrence 92

Table 5.1—Western States from which repeated Forest Inventory and Analysis Phase 2 measurements were available, the time period spanned by the data, and the effective sample intensity (based on the proportion of plots that had been remeasured) in the available datasets 106

Table 5.2—Ecoregion sections in Eastern and Central States having the highest mortality relative to growth (MRATIO), annual mortality and growth rates, and associated causes of mortality. 111

Table 5.3—Ecoregion sections in West Coast States having the highest mortality relative to growth (MRATIO), annual mortality and growth rates, and associated causes of mortality 114

Table 5.4—Ecoregion sections in Interior West States having the highest mortality relative to standing tree volume and associated causes of mortality 118

Table 10.1—Stand conditions and metrics of mountain pine beetle (MPB)-killed pines at mortality survey sites (non-pines were a minor component) 170

Table 11.1—Number and percentage of new snags created during the drought and bark beetle outbreaks by species that were broken by end of the sampling in 2019 181

Table 11.2—Mortality and fuel loads on the Los Padres and Sierra National Forests by low- (<5 percent) and high- (>40 percent) mortality plots 181

Table 12.1—A decision-making matrix to assist users in data selection for determining tree mortality levels for land management applications and analyses 194

EXECUTIVE SUMMARY

Healthy ecosystems are those that are stable and sustainable, able to maintain their organization and autonomy over time while remaining resilient to stress (Costanza 1992). Healthy forests are vital to our future (Edmonds and others 2011), and consistent, large-scale, and long-term monitoring of key indicators of forest health status, change, and trends is necessary to identify forest resources deteriorating across large regions (Riitters and Tkacz 2004). The Forest Health Monitoring (FHM) program of the Forest Service, U.S. Department of Agriculture, with cooperating researchers within and outside the Forest Service and with State partners, quantifies status and trends in the health of U.S. forests (ch. 1). The analyses and results outlined in sections 1 and 2 of this FHM annual national report offer a snapshot of the current condition of U.S. forests from a national or multi-State regional perspective, incorporating baseline investigations of forest ecosystem health, examinations of change over time in forest health metrics, and assessments of developing threats to forest stability and sustainability. For datasets collected on an annual basis, analyses are presented from 2019 data. For datasets collected over several years, analyses are presented at a longer temporal scale. Finally, section 3 of this report presents six summaries of results from recently completed Evaluation Monitoring (EM) projects that have been funded through the FHM national program to determine the extent, severity, and/or causes of specific forest health problems (FHM 2018).

Monitoring the occurrence of forest pest and pathogen outbreaks is important at regional scales because of the significant impact insects and disease can have on forest health across landscapes (ch. 2). National Insect and Disease Survey data collected in 2019 by the Forest Health Protection program of the Forest Service and partners in State agencies identified 58 different mortality-causing agents and complexes on 2.69 million ha and 64 defoliating agents and complexes on approximately 1.42 million ha in the conterminous United States. In the Western States, fir engraver (*Scolytus ventralis*) caused extensive mortality in California and southwestern Oregon, resulting in several geographic hot spots of mortality. Defoliation was a widespread issue in the northern Rockies, caused by western spruce budworm (*Choristoneura freemani*), hemlock looper (*Lambdina fiscellaria*), and Douglas-fir tussock moth (*Orgyia pseudotsugata*). Meanwhile, emerald ash borer (*Agrilus planipennis*) was a major source of tree mortality across broad areas of the Eastern States, generating a geographic hot spot of extremely high mortality in the Midwest. Several defoliators also caused extensive damage in the East, including baldcypress leafroller (*Archips goyerana)* in Louisiana and forest tent caterpillar (*Malacosoma disstria*), gypsy moth (*Lymantria dispar dispar*), spruce budworm (*C. fumiferana*), and larch casebearer (*Coleophora laricella*) in the Great Lakes States. In Alaska, more defoliation than mortality was detected in 2019, with hemlock sawfly (*Neodiprion tsugae*), birch leafminer (*Fenusa pusilla*), and aspen

leafminer (*Phyllocnistis populiella*) the leading defoliators and spruce beetle (*Dendroctonus rufipennis*) by far the most widely detected mortality agent. In Hawaii, surveyors identified approximately 27 000 ha of mortality, some which may have been caused by rapid ʻōhiʻa death.

Forest fire occurrence outside the historic range of frequency and intensity can result in extensive economic and ecological impacts. The detection of regional patterns of fire occurrence density can allow for the identification of areas at greatest risk of significant impact and for the selection of locations for more intensive analysis (ch. 3). In 2019, the number of satellite-detected forest fire occurrences recorded for the conterminous States was the fewest since 2005 and 43 percent lower than the mean for the previous 18 years. Only in a few ecoregions, mostly in the Northeast, was fire occurrence density higher than normal compared to the previous 18-year mean and accounting for variability over time. Meanwhile, Alaska experienced a dramatic 3,740-percent increase in fire occurrences from 2018 during a year that had the third most fire occurrences in 19 years of data collection and the most since 2005. Forest fire occurrence density was particularly high in east-central Alaska, while several ecoregions in the State had much higher fire occurrence density than normal. In Hawaii, three ecoregions on the islands of Maui, Oʻahu, and Kauaʻi had many more fire occurrences than expected. Finally, in the U.S. Caribbean islands, only Puerto Rico was outside the range of near-normal fire occurrence density in 2019, having moderately more fire occurrences than expected.

Most U.S. forests experience droughts, with varying degrees of intensity and duration between and within forest ecosystems. Arguably, the duration of a drought event is more critical than its intensity. A standardized drought and moisture surplus indexing approach was applied to monthly climate data from 2019 and prior years to map drought conditions and surplus moisture availability across the conterminous United States at a fine scale (ch. 4). Strikingly, much of the conterminous United States experienced moisture surplus conditions in 2019, the second-wettest year on record nationally since 1895 and the wettest for three Great Lakes States. There were areas of mild to moderate drought scattered across the Southeastern and Mid-Atlantic States and very small clusters of severe to extreme drought in southern Texas, southern Colorado, and northwestern Washington. Analyses of longer term (3-year and 5-year) conditions depict disparity between the northern and southern halves of the conterminous United States as well as between the East and West. Only a handful of areas of severe to extreme moisture surplus existed in the Rocky Mountains and to the west, while areas of moisture surplus were more common than areas of drought to the east, with contiguous areas of severe to extreme surplus scattered across much of the Southeast.

Mortality is a natural process in all forested ecosystems, but high levels of mortality at large scales may indicate that the health of forests is declining. Phase 2 data collected by the Forest Inventory and Analysis (FIA) program of the Forest Service offer tree mortality information on a relatively spatially intense basis of approximately one plot per 6,000 acres (ch. 5). An analysis of FIA plots from all the Central and Eastern States found that, in most areas, tree mortality is low relative to tree growth, with areas of highest mortality occurring in the mostly riparian forests of the Great Plains States. The exception was high mortality detected in parts of Michigan, Indiana, and Ohio as a result of emerald ash borer infestation. Preliminary analyses of FIA data from the Western States indicated very high mortality as a percentage of live volume in several West Coast ecoregions, corresponding to locations of insect outbreaks, wildfire, and severe drought. These three mortality-causing agents are related in that drought stresses trees, making them more susceptible to insect attack, while both drought and insect-killed trees create conditions favorable for wildfires.

For decades, coarse woody material (CWM) has been recognized as an important component of forest ecosystems. In recognition of CWM's critical functions, the FIA program has been conducting a nationwide inventory of CWM since ca. 2000 as a component of its strategic-scale forest inventory (ch. 6). As a means to objectively evaluate CWM change across U.S. forests within the context of expected global change impacts, fundamental parameters of CWM resources were examined across spatial scales of inference ranging from inventory survey units to the conterminous United States using FIA's multidecadal inventory (2002–2011 to 2012–2019). Overall, CWM biomass increased across forests of the United States. However, CWM biomass was increasingly represented by larger-sized pieces of more advanced decay with a species composition that is less dominated by a few species. Overall, examinations of CWM resource dynamics provide an insight into past trajectories of forest development across large scales with implications for carbon and nutrient cycles, as well as better understanding of an amenity of ecosystem services.

The extraordinary size of the spatial domain and breadth of forest variables sampled by the FIA program make it a unique and powerful resource for determining the extent and severity of undesirable changes in forest health across large spatial domains in the United States. An open-source R package named rFIA aims to reduce data accessibility hurdles and unlock the potential of FIA for broad-scale forest health evaluation and monitoring (ch. 7). Three case studies demonstrate aspects of rFIA's potential to advance forest health evaluation and monitoring in the United States. One highlights rFIA's spatiotemporal estimation capacity by estimating current down woody material (DWM) biomass within watershed boundaries across the conterminous United States. A second case study illustrates how rFIA enhances the value of FIA for temporal change detection by examining

trends in lodgepole pine (*Pinus contorta*) mortality in Colorado using multiple design-based estimators. Finally, rFIA estimates plot-level live tree density and develops a Bayesian hierarchical model to estimate changes in live tree abundance within ecoregion subsections across the conterminous United States.

Finally, six recently completed Evaluation Monitoring (EM) projects address a wide variety of forest health concerns at a scale smaller than the national or multi-State regional analyses included in the first sections of the report. These EM projects (funded by the FHM program):

- Evaluated the composition of natural regeneration in red pine (*P. resinosa*) stands impacted by Heterobasidion root disease in Wisconsin and Michigan, to better understand what species naturally regenerate in pine plantations infested with the disease (ch. 8)

- Assessed ash mortality and the effects of emerald ash borer in riparian forests in Michigan by quantifying overstory structure, regeneration, and coarse woody debris in riparian forests bordering first-order streams; sampling communities of woodboring cerambycid beetles (Coleoptera: Cerambycidae); and surveying overstory vegetation, regeneration, and coarse woody debris in riparian forests (ch. 9)

- Quantified mortality caused by mountain pine beetle (*D. ponderosae*) in stands where Rocky Mountain bristlecone pine (*P. longaeva*) and limber pine (*P. flexilis*) co-occur, evaluated in the field if mountain pine beetle is capable of successful brood production in Rocky Mountain bristlecone pine, and quantified the timing and concentration of tree defenses in the two pine species growing in the same stands (ch. 10)

- Identified factors relating to conifer tree mortality and monitored changes in vegetation after mortality associated with drought and concurrent bark beetle outbreaks in California from 2012 to 2016, and determined temporal changes in fuel loading and hazard due to bark beetle- and drought-associated tree mortality (ch. 11)

- Provided a rigorous assessment of Aerial Detection Survey (ADS) and Ecosystem Disturbance and Recovery Tracker (eDaRT) products by developing and executing a ground-based sampling strategy to compare ADS and eDaRT to reference validation data, and outlined recommendations for complementary use by land managers (ch. 12)

- Documented the extent, severity, and progression of emerald ash borer infestation in Arkansas and reconstructed emerald ash borer-induced ash tree mortality patterns as a surrogate for realized spread and infestation progression (ch. 13)

The FHM program, in cooperation with forest health specialists and researchers inside and outside the Forest Service, continues to

investigate a broad range of issues relating to forest health using a wide variety of data and techniques. This report presents some of the latest results from ongoing national-scale detection monitoring and smaller scale environmental monitoring efforts by FHM and its cooperators. For more information about efforts to determine the status, changes, and trends in indicators of the condition of U.S. forests, please visit the FHM website at https://www.fs.fed.us/foresthealth/protecting-forest/forest-health-monitoring.

LITERATURE CITED

Costanza, R. 1992. Toward an operational definition of ecosystem health. In: Costanza, R.; Norton, B.G.; Haskell, B.D., eds. Ecosystem health: new goals for environmental management. Washington, DC: Island Press: 239–256.

Edmonds, R.L.; Agee, J.K.; Gara, R.I. 2011. Forest health and protection. Long Grove, IL: Waveland Press, Inc. 667 p.

Forest Health Monitoring (FHM). 2018. Program description. Forest Health Monitoring fact sheet series. https://www.fhm.fs.fed.us/fact/. [Date accessed: September 20, 2018].

Riitters, K.H.; Tkacz, B. 2004. The U.S. Forest Health Monitoring program. In: Wiersma, G.B., ed. Environmental monitoring. Boca Raton, FL: CRC Press: 669–683. https://doi.org/10.1201/9780203495476.ch30.

CHAPTER 1.
Introduction

Kevin M. Potter

Forests and woodlands cover an extremely large area of the United States, 333 million ha or approximately 36 percent of the Nation's land area (Oswalt and others 2019). These forests possess the capacity to provide a broad range of goods and services for current and future generations, to safeguard biological diversity, and to contribute to the resilience of ecosystems, societies, and economies (USDA Forest Service 2011). Their ecological roles include supplying large and consistent quantities of clean water, preventing soil erosion, and providing habitat for a broad diversity of plant and animal species. Their socioeconomic benefits include wood products, nontimber goods, recreational opportunities, and pleasing natural beauty. Both the ecological integrity and the continued capacity of these forests to provide ecological and economic goods and services are of concern, however, in the face of a long list of threats, including insect and disease infestation, drought, fragmentation and forest conversion to other land uses, catastrophic fire, invasive species, and the effects of climate change.

Natural and anthropogenic stresses vary among biophysical regions and local environments; they also change over time and interact with each other. These and other factors make it challenging to establish baselines of forest health and to detect important departures from normal forest ecosystem functioning (Riitters and Tkacz 2004). Monitoring the health of forests is a critically important task, however, reflected within the Criteria and Indicators for the Conservation and Sustainable Management of Temperate and Boreal Forests (Montréal Process Working Group 1995), which the Forest Service, U.S. Department of Agriculture, uses as a forest sustainability assessment framework (USDA Forest Service 2004, 2011). The primary objective of such monitoring is to identify ecological resources whose condition is deteriorating in subtle ways over large regions in response to cumulative stresses, a goal that requires consistent, large-scale, and long-term monitoring of key indicators of forest health status, change, and trends (Riitters and Tkacz 2004). This is best accomplished through the participation of multiple Federal, State, academic, and private partners.

Although the concept of a healthy forest has universal appeal, forest ecologists and managers have struggled with how exactly to define forest health (Teale and Castello 2011), and there is no universally accepted definition. Most definitions of forest health can be categorized as representing either an ecological or a utilitarian perspective (Kolb and others 1994). From an ecological perspective, the current understanding of ecosystem dynamics suggests that healthy ecosystems are those that are able to maintain their organization and autonomy over time while remaining resilient to stress (Costanza 1992), and that evaluations of forest health should emphasize factors that affect the inherent processes and resilience of forests (Edmonds and others 2011, Kolb and others 1994, Raffa and others 2009). On the other hand, the utilitarian

perspective holds that a forest is healthy if management objectives are met, and that a forest is unhealthy if these objectives are not met (Kolb and others 1994). Although this definition may be appropriate when a single, unambiguous management objective exists, such as the production of wood fiber or the maintenance of wilderness attributes, it is too narrow when multiple management objectives are required (Edmonds and others 2011, Teale and Castello 2011). Teale and Castello (2011) incorporate both ecological and utilitarian perspectives into their two-component definition of forest health: first, a healthy forest must be sustainable with respect to its size structure, including a correspondence between baseline and observed mortality; second, a healthy forest must meet the landowner's objectives, provided that these objectives do not conflict with sustainability.

This national report, the 20th in an annual series sponsored by the Forest Health Monitoring (FHM) program of the Forest Service, attempts to quantify the status of, changes to, and trends in a wide variety of broadly defined indicators of forest health. The indicators described in this report encompass forest insect and disease activity, wildland fire occurrence, drought, tree mortality, and coarse woody materials, among others. The previous reports in this series are Ambrose and Conkling (2007, 2009), Conkling (2011), Conkling and others (2005), Coulston and others (2005a, 2005b, 2005c), and Potter and Conkling (2012a, 2012b, 2013a, 2013b, 2014, 2015a, 2015b, 2016, 2017, 2018, 2019, 2020). Visit https://www.fs.fed.us/foresthealth/publications/fhm/fhm-annual-national-reports.shtml for links to each of these reports in their entirety and for searchable lists of links to chapters included in the reports.

This report has three specific objectives. The first is to present information about forest health from a national perspective, or from a multi-State regional perspective when appropriate, using data collected by the Forest Health Protection (FHP) and Forest Inventory and Analysis (FIA) programs of the Forest Service, as well as from other sources available at a wide extent. The chapters that present analyses at a national scale, or multi-State regional scale, are divided between section 1 and section 2 of the report. Section 1 presents results from the analyses of forest health data that are available on an annual basis. Such repeated analyses of regularly collected indicator measurements allow for the detection of trends over time and help establish a baseline for future comparisons (Riitters and Tkacz 2004). Section 2 presents longer-term forest health trends, in addition to describing new techniques for analyzing forest health data at national or regional scales (the second objective of the report). While in-depth interpretation and analysis of specific geographic or ecological regions are beyond the scope of these parts of the report, the chapters in sections 1 and 2 present information that can be used to identify areas that may require investigation at a finer scale.

The second objective of the report is to present new techniques for analyzing forest health data as well as new applications of established techniques, often applied to longer timescales, presented in selected chapters of section 2. Examples in this report are chapters 6 and 7. Chapter 6 presents the results of analyses of nearly 20 years of FIA coarse woody material (CWM) data across spatial scales to assess change over time in CWM biomass, diameter and decay class, and species composition. Chapter 7, meanwhile, uses case studies to demonstrate the potential of rFIA, an open-source R package developed to improve the accessibility of FIA data and offer enhanced flexibility in estimation strategies, to advance forest health evaluation and monitoring.

The third objective of the report is to present results of recently completed Evaluation Monitoring (EM) projects funded through the FHM national program. These project summaries, presented in section 3, determine the extent, severity, and/or cause of forest health problems (FHM 2019), generally at a finer scale than that addressed by the analyses in sections 1 and 2. Each of the six chapters in section 3 contains an overview of an EM project, key results, and contacts for more information.

When appropriate throughout this report, authors use the Forest Service revised ecoregions for the conterminous United States and Alaska (Cleland and others 2007, Spencer and others 2002) as a common ecologically based spatial framework for their forest health assessments (fig. 1.1). Specifically, when the spatial scale of the data and the expectation of an identifiable pattern in the data are appropriate, authors use ecoregion sections, larger-scale provinces, or smaller-scale subsections as assessment units for their analyses. Bailey's hierarchical system bases the two broadest ecoregion scales, domains and divisions, on large ecological climate zones, while each division is broken into provinces based on vegetation macro features (Bailey 1995). Provinces are further divided into sections, which may be thousands of km^2 in area and are expected to encompass regions similar in their geology, climate, soils, potential natural vegetation, and potential natural communities (Cleland and others 1997). Subsections are nested within sections as the smallest level in the hierarchy. This hierarchical system does not address either Hawaii or Puerto Rico beyond including each in a unique, single ecoregion province (Bailey 1995). A set of Hawaii ecoregions based on moisture and elevational characteristics was developed for use in FHM national reports (Potter 2020) because a finer-scale and ecologically oriented spatial assessment framework was needed to estimate the impacts of a destructive forest disease (ch. 2) and of forest fire occurrences (ch. 3) (fig. 1.2, table 1.1).

(A)

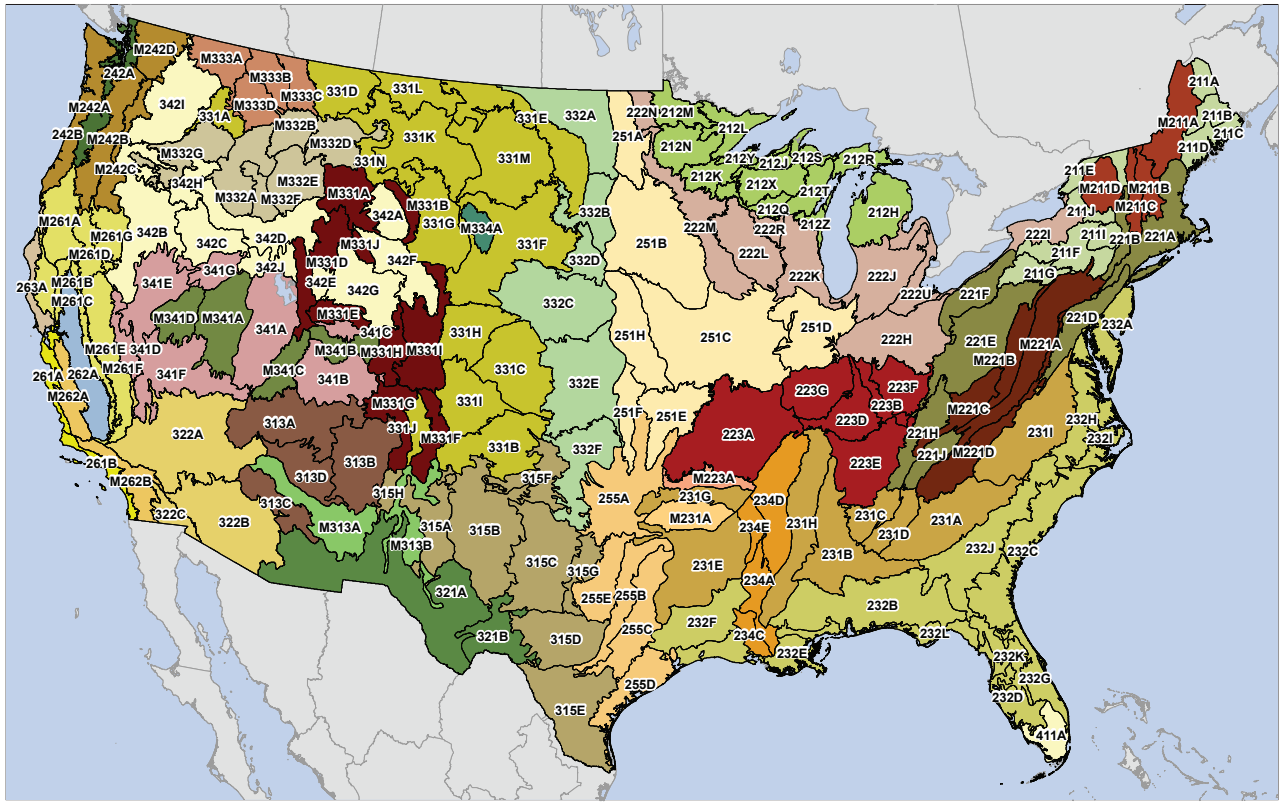

Figure 1.1—Ecoregion provinces and sections for (A) the conterminous United States (Cleland and others 2007) and (B) Alaska (Spencer and others 2002). Ecoregion sections within each ecoregion province are shown in the same color.

Conterminous States ecoregion provinces

- 211: Northeastern Mixed Forest
- M211: Adirondack-New England Mixed Forest—Coniferous Forest—Alpine Meadow
- 212: Laurentian Mixed Forest
- 221: Eastern Broadleaf Forest
- M221: Central Appalachian Broadleaf Forest—Coniferous Forest—Meadow
- 222: Midwest Broadleaf Forest
- 223: Central Interior Broadleaf Forest
- M223: Ozark Broadleaf Forest
- 231: Southeastern Mixed Forest
- M231: Ouachita Mixed Forest—Meadow
- 232: Outer Coastal Plain Mixed Forest
- 234: Lower Mississippi Riverine Forest
- 242: Pacific Lowland Mixed Forest
- 251: Prairie Parkland (Temperate)
- 255: Prairie Parkland (Subtropical)
- M242: Cascade Mixed Forest—Coniferous Forest—Alpine Meadow
- 261: California Coastal Chaparral Forest and Shrub
- M261: Sierran Steppe—Mixed Forest—Coniferous Forest—Alpine Meadow
- 262: California Dry Steppe
- M262: California Coastal Range Open Woodland—Shrub—Coniferous Forest—Meadow
- 263: California Coastal Steppe—Mixed Forest—Redwood Forest
- 313: Colorado Plateau Semi-Desert
- M313: Arizona-New Mexico Mountains Semi-Desert—Open Woodland—Coniferous Forest—Alpine Meadow
- 315: Southwest Plateau and Plains Dry Steppe and Shrub
- 321: Chihuahuan Semi-Desert
- 322: American Semi-Desert and Desert
- 331: Great Plains—Palouse Dry Steppe
- M331: Southern Rocky Mountain Steppe—Open Woodland—Coniferous Forest—Alpine Meadow
- 332: Great Plains Steppe
- M332: Middle Rocky Mountain Steppe—Coniferous Forest—Alpine Meadow
- M333: Northern Rocky Mountain Forest-Steppe—Coniferous Forest—Alpine Meadow
- M334: Black Hills Coniferous Forest
- 341: Intermountain Semi-Desert and Desert
- M341: Nevada-Utah Mountains Semi-Desert—Coniferous Forest—Alpine Meadow
- 342: Intermountain Semi-Desert
- 411: Everglades

Alaska ecoregion provinces

- 121: Arctic Tundra
- M122: Bering Tundra
- M131: Bering Taiga
- M132: Intermontane Boreal
- 133: Alaska Range Transition
- M134: Coastal Mountains Transition
- M241: Coastal Rainforest
- M243: Aleutian Meadows

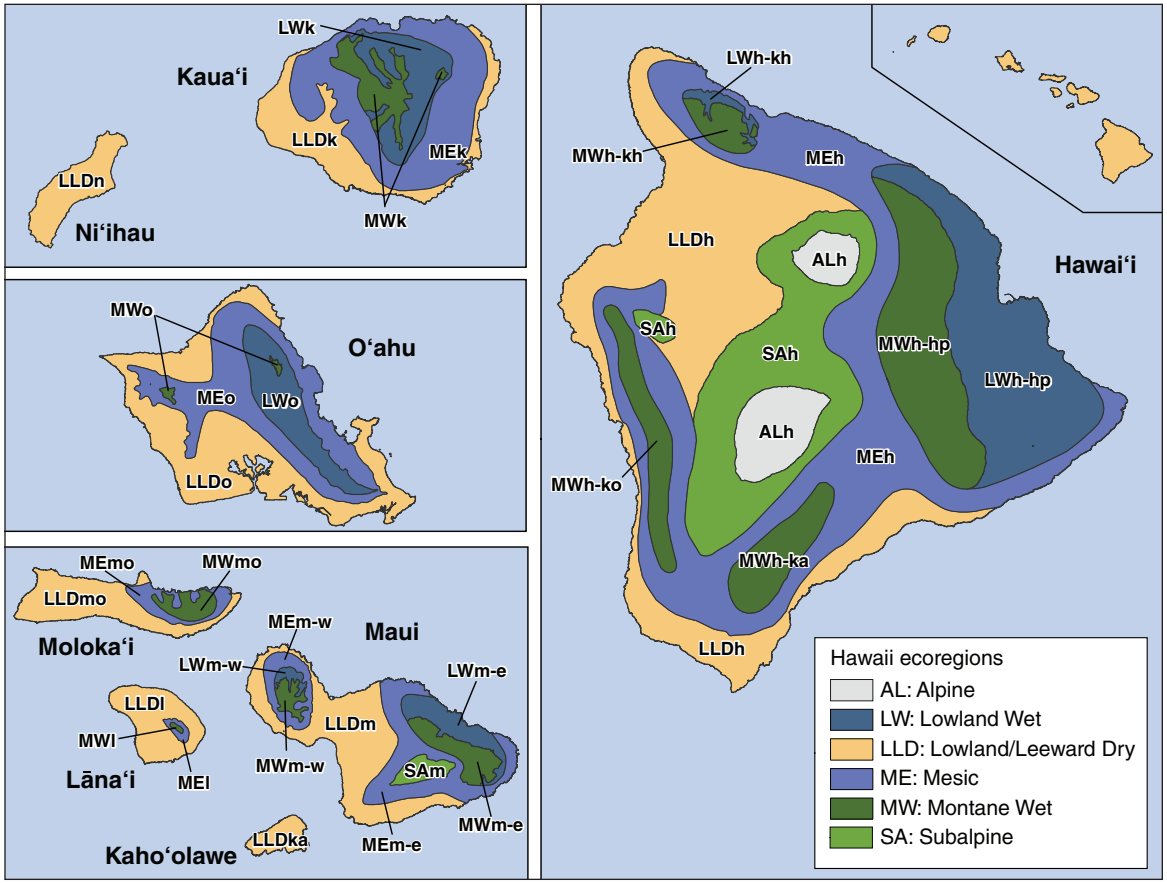

Figure 1.2—Ecoregions, and ecoregion subunits, for Hawaii, developed based on moisture zones and elevation (see box 1.1). Ecoregion subunits are shown in the same color by ecoregion. See table 1.1 for the names of the ecoregion subunits listed on the map.

Table 1.1—The six ecoregions and 34 ecoregion subunits for the State of Hawaii

Ecoregion	Subunit
AL: Alpine	Alh: Alpine-Hawai‘i
LW: Lowland Wet	LWh-hp: Lowland Wet-Hawai‘i-Hilo-Puna
	LWh-kh: Lowland Wet-Hawai‘i-Kohala-Hāmākua
	LWk: Lowland Wet-Kaua‘i
	LWm-e: Lowland Wet-Maui-East
	LWm-w: Lowland Wet-Maui-West
	LWo: Lowland Wet-O‘ahu
LLD: Lowland/ Leeward Dry	LLDh: Lowland/Leeward Dry-Hawai‘i
	LLDka: Lowland/Leeward Dry-Kaho‘olawe
	LLDk: Lowland/Leeward Dry-Kaua‘i
	LLDl: Lowland/Leeward Dry-Lāna‘i
	LLDm: Lowland/Leeward Dry-Maui
	LLDmo: Lowland/Leeward Dry-Moloka‘i
	LLDn: Lowland/Leeward Dry-Ni‘ihau
	LLDo: Lowland/Leeward Dry-O‘ahu
ME: Mesic	MEh: Mesic-Hawai‘i
	MEk: Mesic-Kaua‘i
	MEl: Mesic-Lāna‘i
	MEm-e: Mesic-Maui-East
	MEm-w: Mesic-Maui-West
	MEmo: Mesic-Moloka‘i
	MEo: Mesic-O‘ahu
MW: Montane Wet	MWh-hp: Montane Wet-Hawai‘i-Hilo-Puna
	MWh-ka: Montane Wet-Hawai‘i-Ka‘ū
	MWh-kh: Montane Wet-Hawai‘i-Kohala-Hāmākua
	MWh-ko: Montane Wet-Hawai‘i-Kona
	MWk: Montane Wet-Kaua‘i
	MWl: Montane Wet-Lāna‘i
	MWm-e: Montane Wet-Maui-East
	MWm-w: Montane Wet-Maui-West
	MWmo: Montane Wet-Moloka‘i
	MWo: Montane Wet-O‘ahu
SA: Subalpine	SAh: Subalpine-Hawai‘i
	SAm: Subalpine-Maui

THE FOREST HEALTH MONITORING PROGRAM

The national FHM program is designed to determine the status, changes, and trends in indicators of forest condition on an annual basis and covers all forested lands through a partnership encompassing the Forest Service, State foresters, and other State and Federal agencies and academic groups (FHM 2019). The FHM program utilizes data from a wide variety of data sources, both inside and outside the Forest Service, and develops analytical approaches for addressing forest health issues that affect the sustainability of forest ecosystems. The FHM program has four major components (fig. 1.3):

- Detection Monitoring—nationally standardized aerial and ground surveys to evaluate status and change in condition of forest ecosystems (sections 1 and 2 of this report)

- Evaluation Monitoring—projects to determine the extent, severity, and causes of undesirable changes in forest health identified through Detection Monitoring (section 3 of this report)

- Research on Monitoring Techniques—work to develop or improve indicators, monitoring systems, and analytical techniques, such as urban and riparian forest health monitoring, early detection of invasive species, multivariate analyses of forest health indicators, and spatial scan statistics (section 2 of this report)

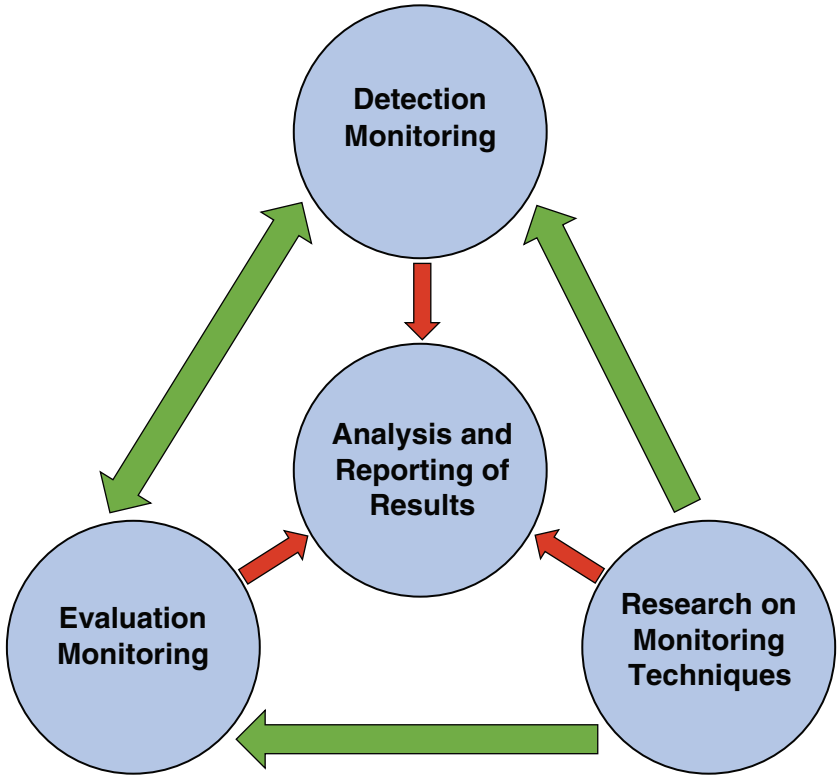

Figure 1.3—The design of the Forest Health Monitoring program (FHM 2003).

- Analysis and Reporting—synthesis of information from various data sources within and external to the Forest Service to produce issue-driven reports on status and change in forest health at national, regional, and State levels (sections 1, 2, and 3 of this report)

The FHM program, in addition to national reporting, generates regional and State reports, often in cooperation with FHM partners, both within the Forest Service and in State forestry and agricultural departments. For example, the FHM regions cooperate with their respective State partners to produce the annual Forest Health Highlights report series, available on the FHM website at https://www.fs.fed.us/foresthealth/protecting-forest/forest-health-monitoring/monitoring-forest-highlights.shtml. Other examples include Steinman (2004) and Harris and others (2011).

The FHM program and its partners also produce reports and journal articles on monitoring techniques and analytical methods (see https://www.fs.fed.us/foresthealth/publications/fhm/fhm-publications.shtml). The emphases of these publications include forest health data (Potter and others 2016, Siry and others 2018, Smith and Conkling 2004); soils as an indicator of forest health (O'Neill and others 2005); urban forest health monitoring (Bigsby and others 2014; Cumming and others 2006, 2007; Lake and others 2006); remote sensing of forest disturbances (Chastain and others 2015, Rebbeck and others 2015); health conditions in national forests (Morin and others 2006); crown conditions (Morin and others 2015; Randolph 2010a, 2010b, 2013; Randolph and Moser 2009; Schomaker and others 2007); indicators of regeneration (McWilliams and others 2015); vegetation diversity and structure (Schulz and Gray 2013, Schulz and others 2009, Simkin and others 2016); forest lichen communities (Jovan and others 2012, Root and others 2014); down woody materials in forests (Woodall and others 2012, 2013); drought (Vose and others 2016); ozone monitoring (Rose and Coulston 2009); patterns of nonnative invasive plant occurrence (Guo and others 2015, 2017; Iannone and others 2015, 2016a, 2016b, 2018; Jo and others 2018; Oswalt and others 2015; Riitters and others 2018a, 2018b); assessments of forest risk or tree species vulnerability to exotic invasive forest insects and diseases (Koch and others 2011, 2014; Krist and others 2014; Potter and others 2019a, 2019b; Vogt and Koch 2016; Yemshanov and others 2014); spatial patterns of landcover and forest fragmentation (Guo and others 2018; Riitters 2011; Riitters and Costanza 2019; Riitters and Wickham 2012; Riitters and others 2012, 2016, 2017); impacts of deer browse on forest structure (Russell and others 2017); broad-scale assessments of forest biodiversity (Guo and others 2019; Potter 2018; Potter and Koch 2014; Potter and Woodall 2012, 2014); predictions and indicators of climate change effects on forests and forest tree species (Fei and others 2017, Heath and others 2015, Potter and Hargrove 2013); and the overall forest health indicator program (Woodall and others 2010).

For more information about the FHM program, visit the FHM website at https://www.fs.fed.us/foresthealth/protecting-forest/forest-health-monitoring/. Among other resources,

this website includes links to all past national forest health reports (https://www.fs.fed.us/foresthealth/publications/fhm/fhm-annual-national-reports.shtml), and annual State Forest Health Highlights reports (https://www.fs.fed.us/foresthealth/protecting-forest/forest-health-monitoring/monitoring-forest-highlights.shtml).

DATA SOURCES

Forest Service data sources in this edition of the FHM national report include FIA annualized Phase 2 survey data (Bechtold and Patterson 2005, Burrill and others 2018, Woodall and others 2010); FHP national Insect and Disease Survey forest mortality and defoliation data for 2019 (FHP 2020); Moderate Resolution Imaging Spectroradiometer (MODIS) Active Fire Detections for the United States data for 2019 (USDA Forest Service 2020); tree canopy cover data generated from the 2011 National Land Cover Database (NLCD) (Homer and others 2015) through a cooperative project between the Multi-Resolution Land Characteristics Consortium and Forest Service Geospatial Technology and Applications Center (GTAC) (Coulston and others 2012); and FIA's publicly available Environmental Monitoring and Assessment Program (EMAP) hexagons (Brand and others 2000). Other sources of data include Parameter-elevation Regression on Independent Slopes Model (PRISM) climate mapping system data (PRISM Climate Group 2020), and Alaskan forest and shrub cover derived from the 2011 NLCD. For more information about the FIA program, which is a major source of data for several FHM analyses, see box 1.1.

FHM REPORT PRODUCTION

This FHM national report, the 20th in a series of such annual documents, is produced by forest health monitoring researchers at the Eastern Forest Environmental Threat Assessment Center (EFETAC) in collaboration with North Carolina State University cooperators in the Forest Health Monitoring Research Group (https://go.ncsu.edu/foresthealth). A unit of the Southern Research Station of the Forest Service, EFETAC was established under the Healthy Forests Restoration Act of 2003 to generate the knowledge and tools needed to anticipate and respond to environmental threats. For more information about the research team and about threats to U.S. forests, please visit https://www.forestthreats.org/about.

Box 1.1

The Forest Inventory and Analysis (FIA) program collects forest inventory information across all forest land ownerships in the United States and maintains a network of more than 130,000 permanent forested ground plots across the conterminous United States, southeastern Alaska, Hawaii, and the Caribbean and Pacific territories with a sampling intensity of approximately one plot/2428 ha (one plot per 6,000 acres). Forest Inventory and Analysis Phase 2 encompasses the annualized inventory measured on plots at regular intervals, with each plot surveyed every 5 to 7 years in most Eastern States, but with plots in the Rocky Mountain and Pacific Northwest regions surveyed once every 10 years (Reams and others 2005). The standard 0.067-ha plot (see figure) consists of four 7.315-m (24-foot) radius subplots (approximately 168.6 m^2 or 1/24th acre), on which field crews measure trees at least 12.7 cm (5 inches) in diameter. Within each of these subplots is nested a 2.073-m (6.8-foot) radius microplot (approximately 13.48 m^2 or 1/300th acre), on which crews measure trees smaller than 12.7 cm (5 inches) in diameter. A core-optional variant of the standard design includes four "macroplots," each with a radius of 17.953 m or 58.9 feet (approximately 0.1012 ha or 1/4 acre) that originates at the center of each subplot (Burrill and others 2018).

Forest Inventory and Analysis Phase 3 plots previously represented a subset of these Phase 2 plots, with one Phase 3 plot for every 16 standard FIA Phase 2 plots. In addition to traditional forest inventory measurements, data for a variety of important ecological indicators were from Phase 3 plots, including tree crown condition, lichen communities, down woody material, soil condition, and vegetation structure and diversity, whereas data on ozone bioindicator plants were collected on a separate grid of plots (Woodall and others 2010, 2011). Most of these additional forest health indicators were measured as part of the Forest Health Monitoring Detection Monitoring ground plot system prior to 2000[1] (Palmer and others 1991). The FIA program recently updated its sampling techniques with flexible spatial and temporal intensities for some of these ecosystem health indicators (including down woody material, vegetation diversity and structure, and crown conditions) to improve field operation efficiency, address emerging user demands, and adjust to evolving forest health science (Castillo and Alvarez 2020). This "Phase 2 Plus Program/ Ecosystem Indicator Program" (P2+) sampling scheme facilitates the collection of a national core set of indicator information on more plots for less cost than the original indicator protocols, with sampling based on a systematic subsample that can change in response to budgetary fluctuations without compromising long-term analytical capabilities. The enhanced indicator protocols collect less-detailed information on each sampled plot than on the previous Phase 3 plots, but substantially more plots are sampled, increasing the statistical power of forest health analyses and improving the reliability of estimates in important national assessments (Castillo and Alvarez 2020).

[1] U.S. Department of Agriculture Forest Service. 1998. Forest Health Monitoring 1998 field methods guide. Research Triangle Park, NC: U.S. Department of Agriculture Forest Service, Forest Health Monitoring program. 473 p. On file with: Forest Health Monitoring program, 3041 Cornwallis Rd., Research Triangle Park, NC 27709.

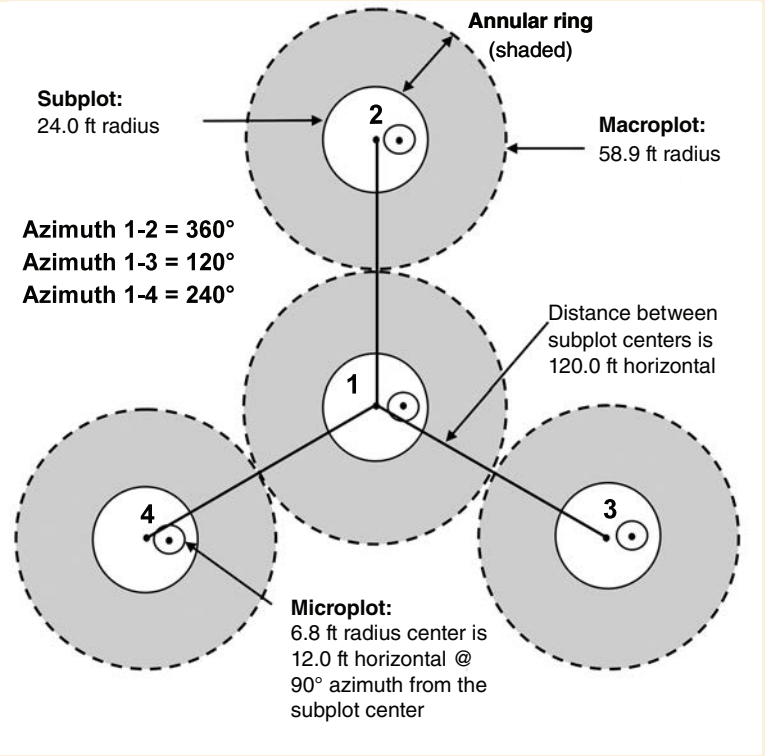

Box 1.1 figure—The Forest Inventory and Analysis mapped plot design. Subplot 1 is the center of the cluster with subplots 2, 3, and 4 located 120 feet away at azimuths of 360°, 120°, and 240°, respectively (Burrill and others 2018).

LITERATURE CITED

Ambrose, M.J.; Conkling, B.L., eds. 2007. Forest Health Monitoring 2005 national technical report. Gen. Tech. Rep. SRS-104. Asheville, NC: U.S. Department of Agriculture Forest Service, Southern Research Station. 76 p.

Ambrose, M.J.; Conkling, B.L., eds. 2009. Forest Health Monitoring 2006 national technical report. Gen. Tech. Rep. SRS-117. Asheville, NC: U.S. Department of Agriculture Forest Service, Southern Research Station. 118 p. https://doi.org/10.2737/SRS-GTR-117.

Bailey, R.G. 1995. Descriptions of the ecoregions of the United States. 2d ed. Misc. Publ. No. 1391. Washington, DC: U.S. Department of Agriculture Forest Service. Map; presentation scale 1:7,500,000. 108 p.

Bechtold, W.A.; Patterson, P.L., eds. 2005. The enhanced Forest Inventory and Analysis program—national sampling design and estimation procedures. Gen. Tech. Rep. SRS-80. Asheville, NC: U.S. Department of Agriculture Forest Service, Southern Research Station. 85 p.

Bigsby, K.M.; Ambrose, M.J.; Tobin, P.C.; Sills, E.O. 2014. The cost of gypsy moth sex in the city. Urban Forestry & Urban Greening. 13(3): 459–468. https://doi.org/10.1016/j.ufug.2014.05.003.

Brand, G.J.; Nelson, M.D.; Wendt, D.G.; Nimerfro, K.K. 2000. The hexagon/panel system for selecting FIA plots under an annual inventory. In: McRoberts, R.E.; Reams, G.A.; Van Deusen, P.C., eds. Proceedings of the first annual Forest Inventory and Analysis symposium. Gen. Tech. Rep. NC-213. St. Paul, MN: U.S. Department of Agriculture Forest Service, North Central Research Station: 8–13.

Burrill, E.A.; Wilson, A.M.; Turner, J.A. [and others]. 2018. The Forest Inventory and Analysis Database: database description and user guide for Phase 2 (version 8.0). Washington, DC: U.S. Department of Agriculture Forest Service. 946 p. http://www.fia.fs.fed.us/library/database-documentation/. [Date accessed: August 23, 2019].

Castillo, P.S.B.; Alvarez, M. 2020. Forest Inventory and Analysis: fiscal year 2018 business report. FS-1153. Washington, DC: U.S. Department of Agriculture Forest Service. 71 p. https://www.fia.fs.fed.us/library/bus-org-documents/docs/17973%20FS%20FIA%20Fiscal%20Year%202018%20Business%20Reportv3%20508.pdf. [Date accessed: September 15, 2020].

Chastain, R.A.; Fisk, H.; Ellenwood, J.R. [and others]. 2015. Near-real time delivery of MODIS-based information on forest disturbances. In: Lippitt, C.D.; Stow, D.A.; Coulter, L.L., eds. Time sensitive remote sensing. New York, NY: Springer: 147–164. https://doi.org/10.1007/978-1-4939-2602-2_10.

Cleland, D.T.; Avers, P.E.; McNab, W.H. [and others]. 1997. National hierarchical framework of ecological units. In: Boyce, M.S.; Haney, A., eds. Ecosystem management applications for sustainable forest and wildlife resources. New Haven, CT: Yale University Press: 181–200.

Cleland, D.T.; Freeouf, J.A.; Keys, J.E. [and others]. 2007. Ecological subregions: sections and subsections for the conterminous United States. Gen. Tech. Rep. WO-76D. Washington, DC: U.S. Department of Agriculture Forest Service. Map; Sloan, A.M., cartographer; presentation scale 1:3,500,000; colored. Also on CD-ROM as a GIS coverage in ArcINFO format or at http://data.fs.usda.gov/geodata/edw/datasets.php. [Date accessed: July 20, 2015].

Conkling, B.L., ed. 2011. Forest Health Monitoring 2007 national technical report. Gen. Tech. Rep. SRS-147. Asheville, NC: U.S. Department of Agriculture Forest Service, Southern Research Station. 159 p.

Conkling, B.L.; Coulston, J.W.; Ambrose, M.J., eds. 2005. Forest Health Monitoring 2001 national technical report. Gen. Tech. Rep. SRS-81. Asheville, NC: U.S. Department of Agriculture Forest Service, Southern Research Station. 204 p.

Costanza, R. 1992. Toward an operational definition of ecosystem health. In: Costanza, R.; Norton, B.G.; Haskell, B.D., eds. Ecosystem health: new goals for environmental management. Washington, DC: Island Press: 239–256.

Coulston, J.W.; Riitters, K.H.; Conkling, B.L., eds. 2005a. Forest Health Monitoring 2002 national technical report. Gen. Tech. Rep. SRS-84. Asheville, NC: U.S. Department of Agriculture Forest Service, Southern Research Station. 97 p.

Coulston, J.W.; Ambrose, M.J.; Riitters, K.H. [and others], eds. 2005b. Forest Health Monitoring 2003 national technical report. Gen. Tech. Rep. SRS-85. Asheville, NC: U.S. Department of Agriculture Forest Service, Southern Research Station. 97 p.

Coulston, J.W.; Ambrose, M.J.; Riitters, K.H.; Conkling, B.L., eds. 2005c. Forest Health Monitoring 2004 national technical report. Gen. Tech. Rep. SRS-90. Asheville, NC: U.S. Department of Agriculture Forest Service, Southern Research Station. 81 p.

Coulston, J.W.; Moisen, G.G.; Wilson, B.T. [and others]. 2012. Modeling percent tree canopy cover: a pilot study. Photogrammetric Engineering and Remote Sensing. 78(7): 715–727. https://doi.org/10.14358/PERS.78.7.715.

Cumming, A.B.; Nowak, D.J.; Twardus, D.B. [and others]. 2007. Urban forests of Wisconsin: pilot monitoring project 2002. NA-FR-05-07. Newtown Square, PA: U.S. Department of Agriculture Forest Service, Northeastern Area State and Private Forestry. 33 p. Low resolution: http://www.na.fs.fed.us/pubs/fhm/pilot/pilot_study_wisconsin_02_lr.pdf. High resolution: http://www.na.fs.fed.us/pubs/fhm/pilot/pilot_study_wisconsin2_02_hr.pdf. [Date accessed: October 19, 2007].

Cumming, A.B.; Twardus, D.B.; Smith, W.D. 2006. National Forest Health Monitoring program, Maryland and Massachusetts street tree monitoring pilot projects. NA-FR-01-06. Newtown Square, PA: U.S. Department of Agriculture Forest Service, Northeastern Area State and Private Forestry. 23 p.

Edmonds, R.L.; Agee, J.K.; Gara, R.I. 2011. Forest health and protection. Long Grove, IL: Waveland Press, Inc. 667 p.

Fei, S.; Desprez, J.M.; Potter, K.M. [and others]. 2017. Divergence of species responses to climate change. Science Advances. 3(5): e1603055. https://doi.org/10.1126/sciadv.1603055.

Forest Health Monitoring (FHM). 2003. Forest Health Monitoring: a national strategic plan. 7 p. https://www.fs.fed.us/foresthealth/fhm/annc/strategic_plan03.pdf. [Date accessed: September 15, 2020].

Forest Health Monitoring (FHM). 2019. Program description. Forest Health Monitoring fact sheet series. https://www.fs.fed.us/foresthealth/protecting-forest/forest-health-monitoring/. [Date accessed: August 23, 2019].

Forest Health Protection (FHP). 2020. Insect and Disease Detection Survey (IDS) data downloads. Fort Collins, CO: U.S. Department of Agriculture Forest Service, Forest Health Technology Enterprise Team. https://www.fs.fed.us/foresthealth/applied-sciences/mapping-reporting/detection-surveys.shtml. [Date accessed: July 6, 2020].

Guo, Q.; Fei, S.; Dukes, J.S. [and others]. 2015. A unified approach to quantify invasibility and degree of invasion. Ecology. 95(10): 2613–2621. https://doi.org/10.1890/14-2172.1.

Guo, Q.; Fei, S.; Potter, K.M. [and others]. 2019. Tree diversity regulates forest pest invasion. Proceedings of the National Academy of Sciences. 116(15): 7382–7386. https://doi.org/10.1073/pnas.1821039116.

Guo, Q.; Iannone, B.V.; Nunez-Mir, G.C. [and others]. 2017. Species pool, human population, and global vs. regional invasion patterns. Landscape Ecology. 32(2): 229–238. https://doi.org/10.1007/s10980-016-0475-6.

Guo, Q.; Riitters, K.H.; Potter, K.M. [and others]. 2018. A subcontinental analysis of forest fragmentation and pest invasion. Forests. 9(12): 744. https://doi.org/10.3390/f9120744.

Harris, J.L., comp.; Region 2 Forest Health Protection staff. 2011. Forest health conditions, 2009–2010: Rocky Mountain Region (R2). R2-11-RO-31. Golden, CO: U.S. Department of Agriculture Forest Service, Renewable Resources, Forest Health Protection, Rocky Mountain Region. 108 p.

Heath, L.S.; Anderson, S.; Emery, M.R. [and others]. 2015. Indicators for climate change impacts for forests: National Climate Assessment indicators. Gen. Tech. Rep. NRS-155. Newtown Square, PA: U.S. Department of Agriculture Forest Service, Northern Research Station. 143 p.

Homer, C.G.; Dewitz, J.A.; Yang, L. [and others]. 2015. Completion of the 2011 National Land Cover Database for the conterminous United States: representing a decade of land cover change information. Photogrammetric Engineering and Remote Sensing. 81(5): 345–354.

Iannone, B.V.; Oswalt, C.M.; Liebhold, A.M. [and others]. 2015. Region-specific patterns and drivers of macroscale forest plant invasions. Diversity and Distributions. 21: 1181–1192. https://doi.org/10.1111/ddi.12354.

Iannone, B.V.; Potter, K.M.; Guo, Q. [and others]. 2016a. Biological invasion hotspots: a trait-based perspective reveals new sub-continental patterns. Ecography. 39: 961–969. https://doi.org/10.1111/ecog.01973.

Iannone, B.V.; Potter, K.M.; Guo, Q. [and others]. 2018. Environmental harshness drives spatial heterogeneity in biotic resistance. NeoBiota. 40: 87–105. https://doi.org/10.3897/neobiota.40.28558.

Iannone, B.V.; Potter, K.M.; Hamil, K.-A.D. [and others]. 2016b. Evidence of biotic resistance to invasions in forests of the Eastern USA. Landscape Ecology. 31: 85–99. https://doi.org/10.1007/s10980-015-0280-7.

Jo, I.; Potter, K.M.; Domke, G.; Fei, S. 2018. Dominant forest tree mycorrhizal type mediates understory plant invasions. Ecology Letters. 21: 217–224. https://doi.org/10.1111/ele.12884.

Jovan, S.; Riddell, J.; Padgett, P.E.; Nash, T.H., III. 2012. Eutrophic lichens respond to multiple forms of N: implications for critical levels and critical loads research. Ecological Applications. 22(7): 1910–1922. https://doi.org/10.1890/11-2075.1.

Koch, F.H.; Yemshanov, D.; Colunga-Garcia, M. [and others]. 2011. Potential establishment of alien-invasive forest insect species in the United States: where and how many? Biological Invasions. 13: 969–985.

Koch, F.H.; Yemshanov, D.; Haack, R.A.; Magarey, R.D. 2014. Using a network model to assess risk of forest pest spread via recreational travel. PLOS ONE. 9(7): e102105. https://doi.org/10.1371/journal.pone.0102105.

Kolb, T.E.; Wagner, M.R.; Covington, W.W. 1994. Concepts of forest health: utilitarian and ecosystem perspectives. Journal of Forestry. 92: 10–15.

Krist, F.J., Jr.; Ellenwood, J.R.; Woods, M.E. [and others]. 2014. 2012–2027 national insect and disease forest risk assessment. FHTET-14-01. U.S. Department of Agriculture Forest Service, Forest Health Technology Enterprise Team. 199 p. http://www.fs.fed.us/foresthealth/technology/pdfs/2012_RiskMap_Report_web.pdf. [Date accessed: July 24, 2014].

Lake, M.; Marshall, P.; Mielke, M. [and others]. 2006. National Forest Health Monitoring program monitoring urban forests in Indiana: pilot study 2002, part 1. Analysis of field methods and data collection. NA-FR-06-06. Newtown Square, PA: U.S. Department of Agriculture Forest Service, Northeastern Area State and Private Forestry. http://www.fhm.fs.fed.us/pubs/ufhm/indianaforests02/indianaforests02.html. [Date accessed: November 6, 2007].

McWilliams, W.H.; Westfall, J.A.; Brose, P.H. [and others]. 2015. A regeneration indicator for Forest Inventory and Analysis: history, sampling, estimation, analytics, and potential use in the Midwest and Northeast United States. Gen. Tech. Rep. NRS-148. Newtown Square, PA: U.S. Department of Agriculture Forest Service, Northern Research Station. 74 p. https://doi.org/10.2737/NRS-GTR-148.

Montréal Process Working Group. 1995. Criteria and indicators for the conservation and sustainable management of temperate and boreal forests. http://www.montrealprocess.org/. [Date accessed: March 4, 2015].

Morin, R.S.; Liebhold, A.M.; Gottschalk, K.W. [and others]. 2006. Analysis of Forest Health Monitoring surveys on the Allegheny National Forest (1998–2001). Gen. Tech. Rep. NE-339. Newtown Square, PA: U.S. Department of Agriculture Forest Service, Northeastern Research Station. 102 p. https://doi.org/10.2737/NE-GTR-339.

Morin, R.S.; Randolph, K.C.; Steinman, J. 2015. Mortality rates associated with crown health for eastern forest tree species. Environmental Monitoring and Assessment. 187(3): 87. https://doi.org/10.1007/s10661-015-4332-x.

O'Neill, K.P.; Amacher, M.C.; Perry, C.H. 2005. Soils as an indicator of forest health: a guide to the collection, analysis, and interpretation of soil indicator data in the Forest Inventory and Analysis program. Gen. Tech. Rep. NC-258. St. Paul, MN: U.S. Department of Agriculture Forest Service, North Central Research Station. 53 p. https://doi.org/10.2737/NC-GTR-258.

Oswalt, C.M.; Fei, S.; Guo, Q. [and others]. 2015. A subcontinental view of forest plant invasions. NeoBiota. 24: 49–54. https://doi.org/10.3897/neobiota.24.4526.

Oswalt, S.N.; Smith, W.B.; Miles, P.D.; Pugh, S.A. 2019. Forest resources of the United States, 2017: a technical document supporting the Forest Service 2020 RPA Assessment. Gen. Tech. Rep. WO-97. Washington, DC: U.S. Department of Agriculture Forest Service, Washington Office. 223 p. https://doi.org/10.2737/WO-GTR-97.

Palmer, C.J.; Riitters, K.H.; Strickland, T. [and others]. 1991. Monitoring and research strategy for forests—Environmental Monitoring and Assessment Program (EMAP). EPA/600/4-91/012. Washington, DC: U.S. Environmental Protection Agency. 189 p.

Potter, K.M. 2018. Do United States protected areas effectively conserve forest tree rarity and evolutionary distinctiveness? Biological Conservation. 224: 34–46. https://doi.org/10.1016/j.biocon.2018.05.007.

Potter, K.M. 2020. Introduction. In: Potter, K.M.; Conkling, B.L., eds. Forest Health Monitoring: national status, trends, and analysis 2019. Gen. Tech. Rep. SRS-250. Asheville, NC: U.S. Department of Agriculture Forest Service, Southern Research Station: 5–24.

Potter, K.M.; Conkling, B.L., eds. 2012a. Forest Health Monitoring 2008 national technical report. Gen. Tech. Rep. SRS-158. Asheville, NC: U.S. Department of Agriculture Forest Service, Southern Research Station. 179 p.

Potter, K.M.; Conkling, B.L., eds. 2012b. Forest Health Monitoring 2009 national technical report. Gen. Tech. Rep. SRS-167. Asheville, NC: U.S. Department of Agriculture Forest Service, Southern Research Station. 252 p.

Potter, K.M.; Conkling, B.L., eds. 2013a. Forest Health Monitoring: national status, trends, and analysis 2010. Gen. Tech. Rep. SRS-176. Asheville, NC: U.S. Department of Agriculture Forest Service, Southern Research Station. 162 p.

Potter, K.M.; Conkling, B.L., eds. 2013b. Forest Health Monitoring: national status, trends, and analysis 2011. Gen. Tech. Rep. SRS-185. Asheville, NC: U.S. Department of Agriculture Forest Service, Southern Research Station. 149 p.

Potter, K.M.; Conkling, B.L., eds. 2014. Forest Health Monitoring: national status, trends, and analysis 2012. Gen. Tech. Rep. SRS-198. Asheville, NC: U.S. Department of Agriculture Forest Service, Southern Research Station. 192 p.

Potter, K.M.; Conkling, B.L., eds. 2015a. Forest Health Monitoring: national status, trends, and analysis 2013. Gen. Tech. Rep. SRS-207. Asheville, NC: U.S. Department of Agriculture Forest Service, Southern Research Station. 199 p.

Potter, K.M.; Conkling, B.L., eds. 2015b. Forest Health Monitoring: national status, trends, and analysis 2014. Gen. Tech. Rep. SRS-209. Asheville, NC: U.S. Department of Agriculture Forest Service, Southern Research Station. 190 p.

Potter, K.M.; Conkling, B.L., eds. 2016. Forest Health Monitoring: national status, trends, and analysis 2015. Gen. Tech. Rep. SRS-213. Asheville, NC: U.S. Department of Agriculture Forest Service, Southern Research Station. 199 p.

Potter, K.M.; Conkling, B.L., eds. 2017. Forest Health Monitoring: national status, trends, and analysis 2016. Gen. Tech. Rep. SRS-222. Asheville, NC: U.S. Department of Agriculture Forest Service, Southern Research Station. 195 p.

Potter, K.M.; Conkling, B.L., eds. 2018. Forest Health Monitoring: national status, trends, and analysis 2017. Gen. Tech. Rep. SRS-233. Asheville, NC: U.S. Department of Agriculture Forest Service, Southern Research Station. 190 p.

Potter, K.M.; Conkling, B.L., eds. 2019. Forest Health Monitoring: national status, trends, and analysis 2018. Gen. Tech. Rep. SRS-239. Asheville, NC: U.S. Department of Agriculture Forest Service, Southern Research Station. 168 p.

Potter, K.M.; Conkling, B.L., eds. 2020. Forest Health Monitoring: national status, trends, and analysis 2019. Gen. Tech. Rep. SRS-250. Asheville, NC: U.S. Department of Agriculture Forest Service, Southern Research Station. 189 p.

Potter, K.M.; Escanferla, M.E.; Jetton, R.M.; Man, G. 2019a. Important insect and disease threats to United States tree species and geographic patterns of their potential impacts. Forests. 10(4): 304. https://doi.org/10.3390/f10040304.

Potter, K.M.; Escanferla, M.E.; Jetton, R.M. [and others]. 2019b. Prioritizing the conservation needs of United States tree species: evaluating vulnerability to forest insect and disease threats. Global Ecology and Conservation. 18: e00622. https://doi.org/10.1016/j.gecco.2019.e00622.

Potter, K.M.; Hargrove, W.W. 2013. Quantitative metrics for assessing predicted climate change pressure on North American tree species. Mathematical and Computational Forestry and Natural Resources Sciences. 5(2): 151–169.

Potter, K.M.; Koch, F.H. 2014. Phylogenetic community structure of forests across the conterminous United States: regional ecological patterns and forest health implications. Forest Science. 60(5): 851–861. https://doi.org/10.5849/forsci.13-115.

Potter, K.M.; Koch, F.H.; Oswalt, C.M.; Iannone, B.V. 2016. Data, data everywhere: detecting spatial patterns in fine-scale ecological information collected across a continent. Landscape Ecology. 31: 67–84. https://doi.org/10.1007/s10980-015-0295-0.

Potter, K.M.; Woodall, C.W. 2012. Trends over time in tree and seedling phylogenetic diversity indicate regional differences in forest biodiversity change. Ecological Applications. 22(2): 517–531. https://doi.org/10.1890/10-2137.1.

Potter, K.M.; Woodall, C.W. 2014. Does biodiversity make a difference? Relationships between species richness, evolutionary diversity, and aboveground live tree biomass across U.S. forests. Forest Ecology and Management. 321: 117–129. https://doi.org/10.1016/j.foreco.2013.06.026.

PRISM Climate Group. 2020. 2.5-arcmin (4 km) gridded monthly climate data. http://www.prism.oregonstate.edu. [Date accessed: July 13, 2020].

Raffa, K.F.; Aukema, B.; Bentz, B.J. [and others]. 2009. A literal use of "forest health" safeguards against misuse and misapplication. Journal of Forestry. 107: 276–277.

Randolph, K.C. 2010a. Equations relating compacted and uncompacted live crown ratio for common tree species in the South. Southern Journal of Applied Forestry. 34(3): 118–123. https://doi.org/10.1093/sjaf/34.3.118.

Randolph, K.C. 2010b. Comparison of the arithmetic and geometric means in estimating crown diameter and crown cross-sectional area. Southern Journal of Applied Forestry. 34(4): 186–189. https://doi.org/10.1093/sjaf/34.4.186.

Randolph, K.C. 2013. Development history and bibliography of the U.S. Forest Service crown-condition indicator for forest health monitoring. Environmental Monitoring and Assessment. 185(6): 4977–4993. https://doi.org/10.1007/s10661-012-2919-z.

Randolph, K.C.; Moser, W.K. 2009. Tree crown condition in Missouri, 2000–2003. Gen. Tech. Rep. SRS-113. Asheville, NC: U.S. Department of Agriculture Forest Service, Southern Research Station. 11 p.

Reams, G.A.; Smith, W.D.; Hansen, M.H. [and others]. 2005. The Forest Inventory and Analysis sampling frame. In: Bechtold, W.A.; Patterson, P.L., eds. The enhanced Forest Inventory and Analysis program—national sampling design and estimation procedures. Gen. Tech. Rep. SRS-80. Asheville, NC: U.S. Department of Agriculture Forest Service, Southern Research Station: 11–26.

Rebbeck, J.; Kloss, A.; Bowden, M. [and others]. 2015. Aerial detection of seed-bearing female *Ailanthus altissima*: a cost-effective method to map an invasive tree in forested landscapes. Forest Science. 61: 1068–1078. https://doi.org/10.5849/forsci.14-223.

Riitters, K.H. 2011. Spatial patterns of land cover in the United States: a technical document supporting the Forest Service 2010 RPA assessment. Gen. Tech. Rep. SRS-136. Asheville, NC: U.S. Department of Agriculture Forest Service, Southern Research Station. 64 p.

Riitters, K.; Costanza, J. 2019. The landscape context of family forests in the United States: anthropogenic interfaces and forest fragmentation from 2001 to 2011. Landscape and Urban Planning. 188: 64–71. https://doi.org/10.1016/j.landurbplan.2018.04.001.

Riitters, K.H.; Costanza, J.K.; Buma, B. 2017. Interpreting multiscale domains of tree cover disturbance patterns in North America. Ecological Indicators. 80: 147–152. https://doi.org/10.1016/j.ecolind.2017.05.022.

Riitters, K.H.; Coulston, J.W.; Wickham, J.D. 2012. Fragmentation of forest communities in the Eastern United States. Forest Ecology and Management. 263: 85–93. https://doi.org/10.1016/j.foreco.2011.09.022.

Riitters, K.; Potter, K.M.; Iannone, B.V. [and others]. 2018a. Exposure of protected forest to plant invasions in the Eastern United States. Forests. 9(11): 723. https://doi.org/10.3390/f9110723.

Riitters, K.; Potter, K.M.; Iannone, B.V. [and others]. 2018b. Landscape correlates of forest plant invasions: a high-resolution analysis across the Eastern United States. Diversity and Distributions. 24: 274–284. https://doi.org/10.1111/ddi.12680.

Riitters, K.H.; Tkacz, B. 2004. The U.S. Forest Health Monitoring program. In: Wiersma, G.B., ed. Environmental monitoring. Boca Raton, FL: CRC Press: 669–683. https://doi.org/10.1201/9780203495476.ch30.

Riitters, K.H.; Wickham, J.D. 2012. Decline of forest interior conditions in the conterminous United States. Scientific Reports. 2: 653. https://doi.org/10.1038/srep00653.

Riitters, K.H.; Wickham, J.D.; Costanza, J.K.; Vogt, P. 2016. A global evaluation of forest interior area dynamics using tree cover data from 2000 to 2012. Landscape Ecology. 31: 137–148. https://doi.org/10.1007/s10980-015-0270-9.

Root, H.T.; McCune, B.; Jovan, S. 2014. Lichen communities and species indicate climate thresholds in southeast and south-central Alaska, USA. The Bryologist. 117(3): 241–252. https://doi.org/10.1639/0007-2745-117.3.241.

Rose, A.K.; Coulston, J.W. 2009. Ozone injury across the Southern United States, 2002–06. Gen. Tech. Rep. SRS-118. Asheville, NC: U.S. Department of Agriculture Forest Service, Southern Research Station. 25 p.

Russell, M.B.; Woodall, C.W.; Potter, K.M. [and others]. 2017. Interactions between white-tailed deer density and the composition of forest understories in the Northern United States. Forest Ecology and Management. 384: 26–33. https://doi.org/10.1016/j.foreco.2016.10.038.

Schomaker, M.E.; Zarnoch, S.J.; Bechtold, W.A. [and others]. 2007. Crown-condition classification: a guide to data collection and analysis. Gen. Tech. Rep. SRS-102. Asheville, NC: U.S. Department of Agriculture Forest Service, Southern Research Station. 78 p. https://doi.org/10.2737/SRS-GTR-102.

Schulz, B.K.; Bechtold, W.A.; Zarnoch, S.J. 2009. Sampling and estimation procedures for the vegetation diversity and structure indicator. Gen. Tech. Rep. PNW-781. Portland, OR: U.S. Department of Agriculture Forest Service, Pacific Northwest Research Station. 53 p. https://doi.org/10.2737/PNW-GTR-781.

Schulz, B.K.; Gray, A.N. 2013. The new flora of Northeastern USA: quantifying introduced plant species occupancy in forest ecosystems. Environmental Monitoring and Assessment. 185: 3931–3957. https://doi.org/10.1007/s10661-012-2841-4.

Simkin, S.M.; Allen, E.B.; Bowman, W.D. [and others]. 2016. Conditional vulnerability of plant diversity to atmospheric nitrogen deposition across the United States. Proceedings of the National Academy of Sciences. 113: 4086–4091. https://doi.org/10.1073/pnas.1515241113.

Siry, J.; Cubbage, F.W.; Potter, K.M.; McGinley, K. 2018. Current perspectives on sustainable forest management: North America. Current Forestry Reports. 4(3): 138–149. https://doi.org/10.1007/s40725-018-0079-2.

Smith, W.D.; Conkling, B.L. 2004. Analyzing forest health data. Gen. Tech. Rep. SRS-077. Asheville, NC: U.S. Department of Agriculture Forest Service, Southern Research Station. 33 p. http://www.srs.fs.usda.gov/pubs/gtr/gtr_srs077.pdf. [Date accessed: November 6, 2007].

Spencer, P.; Nowacki, G.; Fleming, M. [and others]. 2002. Home is where the habitat is: an ecosystem foundation for wildlife distribution and behavior. Arctic Research of the United States. 16: 6–17.

Steinman, J. 2004. Forest Health Monitoring in the Northeastern United States: disturbances and conditions during 1993–2002. NA-TP-01-04. Newtown Square, PA: U.S. Department of Agriculture Forest Service, Northeastern Area State and Private Forestry. 46 p. http://fhm.fs.fed.us/pubs/tp/dist_cond/dc.shtml. [Date accessed: December 8, 2009].

Teale, S.A.; Castello, J.D. 2011. The past as key to the future: a new perspective on forest health. In: Castello, J.D.; Teale, S.A., eds. Forest health: an integrated perspective. New York: Cambridge University Press: 3–16. https://doi.org/10.1017/CBO9780511974977.002.

U.S. Department of Agriculture (USDA) Forest Service. 2004. National report on sustainable forests—2003. FS-766. Washington, DC: U.S. Department of Agriculture Forest Service. 139 p.

U.S. Department of Agriculture (USDA) Forest Service. 2011. National report on sustainable forests—2010. FS-979. Washington, DC: U.S. Department of Agriculture Forest Service. 134 p.

U.S. Department of Agriculture (USDA) Forest Service. 2020. Fire detection GIS data. https://fsapps.nwcg.gov/afm/gisdata.php. [Date accessed: June 24, 2020].

Vogt, J.T.; Koch, F.H. 2016. The evolving role of Forest Inventory and Analysis data in invasive insect research. American Entomologist. 62(1): 46–58. https://doi.org/10.1093/ae/tmv072.

Vose, J.M.; Clark, J.S.; Luce, C.H.; Patel-Weynand, T., eds. 2016. Effects of drought on forests and rangelands in the United States: a comprehensive science synthesis. Gen. Tech. Rep. WO-93b. Washington, DC: U.S. Department of Agriculture Forest Service, Washington Office. 289 p. https://doi.org/10.2737/WO-GTR-93b.

Woodall, C.W.; Amacher, M.C.; Bechtold, W.A. [and others]. 2011. Status and future of the forest health indicators program of the USA. Environmental Monitoring and Assessment. 177: 419–436. https://doi.org/10.1007/s10661-010-1644-8.

Woodall, C.W.; Conkling, B.L.; Amacher, M.C. [and others]. 2010. The Forest Inventory and Analysis database version 4.0: database description and users manual for Phase 3. Gen. Tech. Rep. NRS-61. Newtown Square, PA: U.S. Department of Agriculture Forest Service, Northern Research Station. 180 p. https://doi.org/10.2737/NRS-GTR-61.

Woodall, C.W.; Walters, B.F.; Oswalt, S.N. [and others]. 2013. Biomass and carbon attributes of downed woody materials in forests of the United States. Forest Ecology and Management. 305: 48–59. https://doi.org/10.1016/j.foreco.2013.05.030.

Woodall, C.W.; Walters, B.F.; Westfall, J.A. 2012. Tracking downed dead wood in forests over time: development of a piece matching algorithm for line intercept sampling. Forest Ecology and Management. 277: 196–204. https://doi.org/10.1016/j.foreco.2012.04.031.

Yemshanov, D.; Koch, F.H.; Lu, B. [and others]. 2014. There is no silver bullet: the value of diversification in planning invasive species surveillance. Ecological Economics. 104: 61–72. https://doi.org/10.1016/j.ecolecon.2014.04.024.

SECTION 1.

Analyses of Short-Term Forest Health Data

CHAPTER 2.

Broad-Scale Patterns of Insect and Disease Activity across the 50 United States from the National Insect and Disease Survey, 2019

Kevin M. Potter
Jeanine L. Paschke
Frank H. Koch
Erin M. Berryman

INTRODUCTION

Forest insects and diseases have widespread ecological and economic impacts on the forests of the United States and may represent the most serious threats to the Nation's forests (Logan and others 2003, Lovett and others 2016, Tobin 2015). U.S. law therefore authorizes the U.S. Department of Agriculture Forest Service to "conduct surveys to detect and appraise insect infestations and disease conditions and man-made stresses affecting trees and establish a monitoring system throughout the forests of the United States to determine detrimental changes or improvements that occur over time, and report annually concerning such surveys and monitoring" (FHP 2020). Insects and diseases cause changes in forest structure and function, species succession, and biodiversity, which may be considered negative or positive depending on management objectives (Edmonds and others 2011). Nearly all native tree species of the United States are affected by at least one injury-causing insect or disease agent, with exotic agents on average considerably more severe than native ones (Potter and others 2019a). Additionally, the genetic integrity of several native tree species is highly vulnerable to exotic diseases and insects (Potter and others 2019b).

An important task for forest managers, pathologists, and entomologists is recognizing and distinguishing between natural and excessive mortality, a task that relates to ecologically based or commodity-based management objectives (Teale and Castello 2011). The impacts of insects and diseases on forests vary from natural thinning to extraordinary levels of tree mortality, but insects and diseases are not necessarily enemies of the forest because they kill trees (Teale and Castello 2011). If disturbances, including insects and diseases, are viewed in their full ecological context, then some amount can be considered "healthy" to sustain the structure of the forest (Manion 2003, Zhang and others 2011) by causing tree mortality that culls weak competitors and releases resources that are needed to support the growth of surviving trees (Teale and Castello 2011).

Analyzing patterns of forest insect infestations, disease occurrences, forest declines, and related biotic stress factors is necessary to monitor the health of forested ecosystems and their potential impacts on forest structure, composition, biodiversity, and species distributions (Castello and others 1995). In particular, introduced insects and diseases can extensively damage the biodiversity, ecology, and economy of affected areas (Brockerhoff and others 2006, Mack and others 2000). Few forests remain unaffected by invasive species, and their devastating impacts in forests are undeniable, including, in some cases, wholesale changes to the structure and function of an ecosystem (Parry and Teale 2011).

Examining insect pest occurrences and related stress factors from a landscape-scale perspective is useful, given the regional extent of many infestations and the large-scale complexity of interactions between host

distribution, stress factors, and the development of insect pest outbreaks (Holdenrieder and others 2004, Liebhold and others 2013). One such landscape-scale approach is detecting geographic patterns of disturbance, which allows for the identification of areas at greater risk of significant ecological and economic impacts and for the selection of locations for more intensive monitoring and analysis. National Insect and Disease Survey (IDS) data (FHP 2020), coordinated by the Forest Health Protection (FHP) program of the Forest Service, provide an important source of information about forest disturbances and their causal agents across broad regions. Recent long-term analyses of these data underscored that insects have been much more widespread agents of mortality than diseases, with bark beetles consistently the most important mortality agents across regions and over time (Potter and others 2020a). Additionally, the tree canopy area affected by nonnative invasive agents of mortality and defoliation has remained relatively consistent over time (with a larger relative impact on forests in the North), and tree canopy area affected by defoliation agents has usually exceeded or equaled the area affected by mortality agents (Potter and others 2020a).

METHODS

Data

National Insect and Disease Survey data (FHP 2020) consist of information from low-altitude aerial survey and ground survey efforts by FHP and partners in State agencies. These data can be used to identify forest landscape-scale patterns associated with geographic hot spots of forest insect and disease activity in the conterminous 48 States (CONUS) and to summarize insect and disease activity by regions in the CONUS, Alaska, and Hawaii (Potter 2012, 2013; Potter and Koch 2012; Potter and Paschke 2013, 2014, 2015a, 2015b, 2016, 2017; Potter and others 2018, 2019c, 2020b).

The IDS data identify areas with mortality and defoliation caused by insect and disease activity, although some important forest insects (such as emerald ash borer [*Agrilus planipennis*] and hemlock woolly adelgid [*Adelges tsugae*]), diseases (such as laurel wilt [*Raffaelea lauricola*], Dutch elm disease [*Ophiostoma novo-ulmi*], white pine blister rust [*Cronartium ribicola*], and thousand cankers disease [*Geosmithia morbida*]), and mortality complexes (such as oak decline) are not easily detected or thoroughly quantified through aerial detection surveys. Such pests may attack hosts that are widely dispersed throughout forests with high tree species diversity or may cause mortality or defoliation that is otherwise difficult to detect. A pathogen or insect might be considered a mortality-causing agent in one location and a defoliation-causing agent in another, depending on the level of damage to the forest in an area and the convergence of other stress factors such as drought. In some cases, the identified agents of mortality or defoliation are actually complexes of multiple agents summarized under an impact label related to a specific host tree species (e.g., “beech bark disease complex” or “yellow-cedar decline”). Additionally, differences in data collection, attribute recognition, and

coding procedures among States and regions can complicate data analysis and interpretation of the results. A recent comparison of aerial survey data with ground observations found that the accuracy of the aerial survey data exceeded 70 percent, that damage type observations for tree mortality and defoliation had high levels of accuracy, and that accuracy declined as the specificity for observations went from genera to species level for tree species and damage agents, although many prominent tree species and agents had low to zero commission errors (Coleman and others 2018).

In 2019, IDS surveys of the CONUS covered about 219.00 million ha of both forested and unforested area (fig. 2.1), of which approximately 155.34 million ha encompassed tree canopy cover, or about 49.2 percent of the 315.99-million-ha tree canopy area of the CONUS. The entirety of this area was surveyed using the Digital Mobile Sketch Mapping (DMSM) approach, which recently replaced the legacy Digital Aerial Sketch Mapping (DASM) approach (Berryman and McMahan 2019). Meanwhile, roughly 10.8 percent (8.39 million ha) of Alaska's 77.78 million ha of forest or shrubland were surveyed in 2019, out of a total of 9.88 million ha surveyed across landcover types. In Hawaii, surveyors covered about 798 000 ha during 2019, of which approximately 551 000 ha had tree canopy cover, or about 63.9 percent of the 861 000 ha of total tree cover area in the State. Finally, 2019 surveys in the U.S. Caribbean territories of Puerto Rico and the U.S. Virgin Islands covered 99 percent of the 496 506 ha of tree canopy cover area (491 523 ha). These Caribbean surveys did not record insect and disease damage, however, so these jurisdictions are not included in the analyses for this chapter.

Digital Mobile Sketch Mapping includes tablet hardware, software, and data support processes that allow trained aerial surveyors in light aircraft, as well as ground observers, to record forest disturbances and their causal agents. Digital Mobile Sketch Mapping enhances the quality and quantity of forest health data while having the potential to improve safety by integrating with programs such as operational remote sensing (ORS), which uses satellite imagery to monitor disturbances in areas of higher aviation risk (FHP 2019). Geospatial data collected with DMSM are stored in the national IDS database. In an important change from DASM, the new DMSM approach allows surveyors to both define the extent of an area experiencing damage and to estimate percent range of the area within the polygon that is affected. While additional validation will be required for this new metric, it is expected to increase the accuracy of derived damage metrics because it potentially corrects for previous overestimation caused by "lassoing" areas of undamaged trees into large areas of damage (ch. 12, Coleman and others 2018). For this reason, FHM reports before 2019 did not incorporate any derived damage estimates beyond the areal footprint damage with mortality or defoliation polygon boundaries, but these are now possible because of the inclusion of damage percentage estimates within polygons (see "Analyses" below).

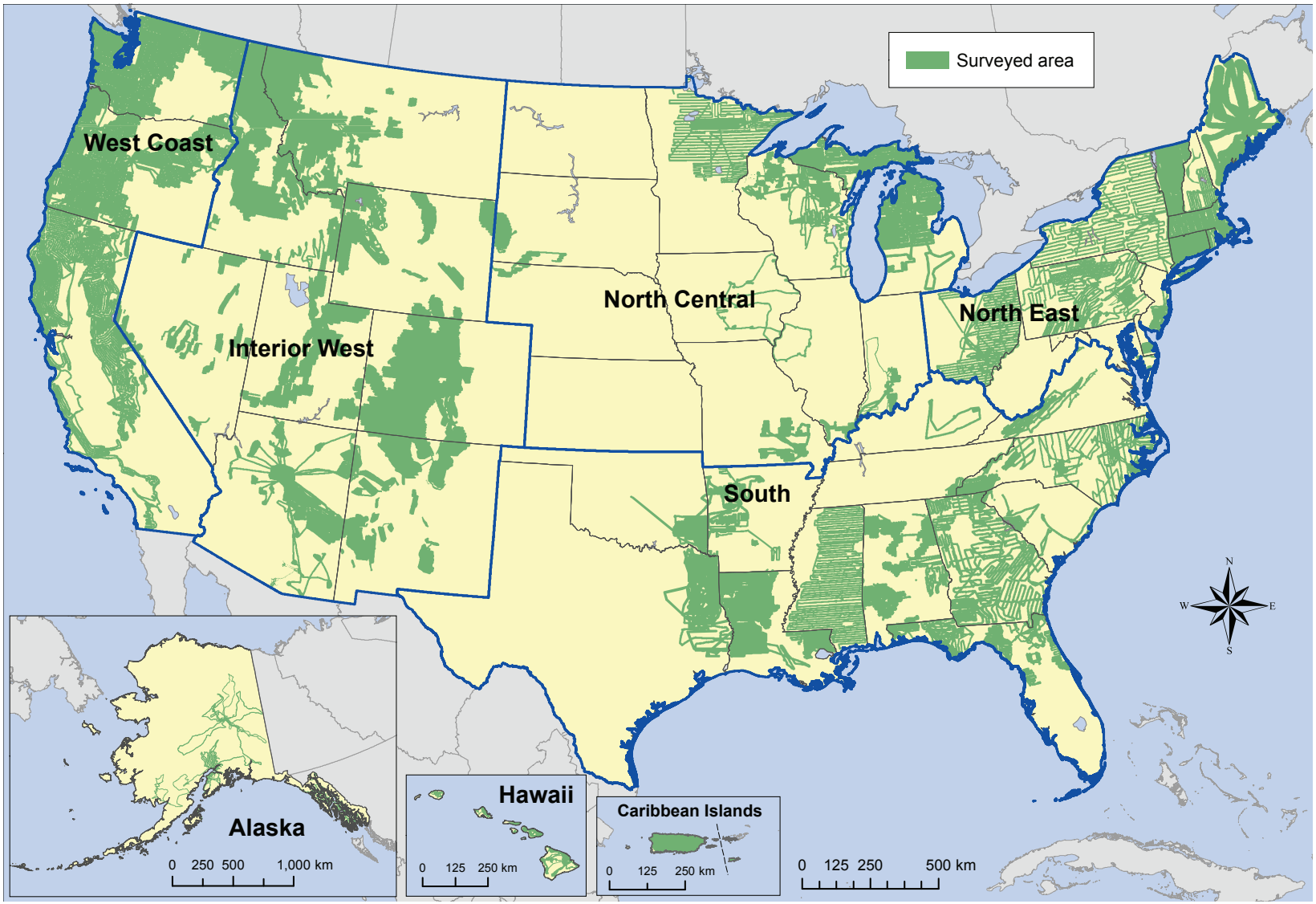

Figure 2.1—The extent of surveys for insect and disease activity conducted in the conterminous United States, Alaska, Hawaii, and the U.S. Caribbean Island territories in 2019. The blue lines delineate Forest Health Monitoring regions. Note: Alaska and Hawaii are not shown to scale with map of the conterminous United States. (Data source: U.S. Department of Agriculture Forest Service, Forest Health Protection)

Digital Mobile Sketch Mapping includes both polygon geometry, used for damage areas where boundaries are discrete and obvious from the air, and point geometry, used for small clusters of damage where the size and shape of the damage are less important than recording the location of damage, such as for sudden oak death (caused by the pathogen *Phytophthora ramorum*), southern pine beetle (*Dendroctonus frontalis*), and some types of bark beetle damage in the West. For the 2019 data, these points were assigned an area of 0.8 ha (about 2 acres). Additionally, DMSM allows for the use of grid cells (240-, 480-, 960-, or 1920-m resolution) to estimate the percentage of trees affected by damages that may be widespread and diffuse, such as those associated with European gypsy moth (*Lymantria dispar dispar*) and emerald ash borer. When calculating the total areas affected by each damage agent, we used the entire areas of these grid cells (e.g., 240-m cell = 5.76 ha).

Analyses

To estimate the extent of damaging insect and disease agents in 2019, we conducted two types of analyses. In the first, we reported the most widely detected mortality and defoliation agents in a series of tables. Specifically, the 2019 mortality and defoliation polygons were used to identify the select mortality and defoliation agents and complexes causing damage on >5000 ha of forest in the CONUS in that year. Similarly, we listed the five most widely reported mortality and defoliation agents and complexes within each of five FHM regions within the CONUS (West Coast, Interior West, North Central, North East, and South), as well as for Alaska and Hawaii where data were available.

Because of the insect and disease aerial sketch-mapping process (i.e., digitization of polygons by a human interpreter aboard the aircraft), all quantities are approximate "footprint" areas for each agent or complex, delineating areas of visible damage within which the agent or complex is present. Unaffected trees may exist within the footprint, and the amount of damage within the footprint is not reflected in the estimates of forest area affected. The sum of areas affected by all agents and complexes is not equal to the total affected area as a result of overlapping polygons and the reporting of multiple agents per polygon in some situations.

In our second set of analyses, we used the IDS data for 2019 to more directly estimate the impacts of insect- and disease-related mortality and defoliation on U.S. forests. These results are reported in a set of figures describing (1) the percentage of surveyed tree canopy cover area with insect- and disease-related mortality or defoliation within ecoregions across the United States and (2) geographic hot spots of insect- and disease-related mortality or defoliation across the CONUS and within the five FHM regions.

As an indicator of the extent of damaging insect and disease agents, we summarized the percentage of surveyed tree canopy cover area experiencing mortality or defoliation for ecoregions within the CONUS and Hawaii, and

for surveyed forest and shrubland in Alaska ecoregions. This is a change from FHM reports before 2019, in which we reported on the percentage of regions *exposed to* mortality and defoliating agents based only on the footprint with mortality or defoliation polygon boundaries (masked by forest cover) because information on the percentage of damage within polygons was not yet completely available. As noted above, DMSM now allows surveyors both to define the extent of an area experiencing damage and to estimate percent range of the area within the polygon that is affected (specifically 1–3 percent, 4–10 percent, 11–29 percent, 30–50 percent, and >50 percent). By multiplying the area of damage within each polygon (after masking by tree canopy cover) by the midpoint of the estimated percent-affected range, it is possible to generate an adjusted estimate of the area affected by each mortality or defoliation agent detection (Berryman and McMahan 2019). These individual estimates can be summed for all the polygons within an ecoregion and divided by the total surveyed tree canopy cover area within the ecoregion to generate an estimate of the percentage of its canopy cover area affected by defoliating or mortality-causing agents. (Digital Mobile Sketch Mapping point data are also included in this estimate. Surveyors have the option to estimate the number of trees affected at a point and are required to assign an area value associated with each point, which is assumed to be 100 percent affected by its mortality or defoliation agent. For simplicity, we transformed each point into a 2-acre [0.809-ha] polygon. These areas for all the points in an ecoregion were then added to the polygon-adjusted affected area estimates for the ecoregion.)

For the CONUS, percentage of surveyed tree canopy area with mortality or defoliation was calculated within each of 190 ecoregion sections (Cleland and others 2007). Similarly, the mortality and defoliation data were summarized for each of the 32 ecoregion sections in Alaska (Spencer and others 2002). In Hawaii, the percentage of surveyed tree canopy area affected by mortality and defoliation agents was calculated by ecoregions on each of the major islands of the archipelago (Potter 2020). Statistics were not calculated for analysis regions in the CONUS or Hawaii with <5 percent of the tree canopy cover area surveyed, nor in Alaska with <2.5 percent of the forest and shrubland area surveyed.

The tree canopy data used for the CONUS and Hawaii were resampled to 240 m from a 30-m raster dataset that estimates percentage of tree canopy cover (from 0 to 100 percent) for each grid cell; this dataset was generated from the 2011 National Land Cover Database (NLCD) (Homer and others 2015) through a cooperative project between the Multi-Resolution Land Characteristics Consortium and the Forest Service Geospatial Technology and Applications Center (GTAC) (Coulston and others 2012). For our purposes, we treated any cell with >0-percent tree canopy cover as forest. Comparable tree canopy cover data were not available for Alaska, so we instead created a 240-m-resolution layer of forest and shrub

cover from the 2011 NLCD. (This is different than Forest Health Monitoring national reports previous to 2019, for which the mortality and defoliation polygons were masked using a forest cover map [1-km resolution] derived from Moderate Resolution Imaging Spectroradiometer [MODIS] imagery by the Forest Service GTAC [USDA Forest Service 2008].)

Additionally, we used the Spatial Association of Scalable Hexagons (SASH) analytical approach to identify statistically significant geographic hot spots of mortality or defoliation in the CONUS. This method identifies locations where ecological phenomena occur at greater or lower frequency than expected by random chance and is based on a sampling frame optimized for spatial neighborhood analysis, adjustable to the appropriate spatial resolution, and applicable to multiple data types (Potter and others 2016). Specifically, it consists of dividing an analysis area into scalable equal-area hexagonal cells within which data are aggregated, followed by identifying statistically significant geographic clusters of hexagonal cells within which mean values are greater or less than those expected by chance. To identify these clusters, we employed a Getis-Ord (G_i*) hot spot analysis (Getis and Ord 1992) in ArcMap® 10.3 (ESRI 2017). We conducted two sets of hot spot analyses for both mortality-causing and defoliation-causing agents: one for the CONUS in its entirety, and one for each of the five FHM regions within the CONUS. The low density of survey data in 2019 from Alaska and the small spatial extent of Hawaii (fig. 2.1) precluded the use of Getis-Ord G_i* hot spot analyses for these States.

The units of analysis were 9,810 hexagonal cells, each approximately 834 km^2 in area, generated in a lattice across the CONUS using intensification of the Environmental Monitoring and Assessment Program (EMAP) North American hexagon coordinates (White and others 1992). These coordinates are the foundation of a sampling frame in which a hexagonal lattice was projected onto the CONUS by centering a large base hexagon over the region (Reams and others 2005, White and others 1992). This base hexagon can be subdivided into many smaller hexagons, depending on sampling needs, and serves as the basis of the plot sampling frame for the Forest Inventory and Analysis (FIA) program (Reams and others 2005). Importantly, the hexagons maintain equal areas across the study region regardless of the degree of intensification of the EMAP hexagon coordinates. In addition, the hexagons are compact and uniform in their distance to the centroids of neighboring hexagons, meaning that a hexagonal lattice has a higher degree of isotropy (uniformity in all directions) than does a square grid (Shima and others 2010). These are convenient and highly useful attributes for spatial neighborhood analyses. These scalable hexagons also are independent of geopolitical and ecological boundaries, avoiding the possibility of different sample units (such as counties, States, or watersheds) encompassing vastly different areas (Potter and others 2016). We selected hexagons

834 km^2 in area because this is a manageable size for making monitoring and management decisions in analyses that are national in extent (Potter and others 2016).

The Getis-Ord G_i^* statistic was then used to identify clusters of hexagonal cells in which the percentage of surveyed tree canopy area with mortality or defoliation was higher than expected by chance. This statistic allows for the decomposition of a global measure of spatial association into its contributing factors, by location, and is therefore particularly suitable for detecting instances of nonstationarity in a dataset, such as when spatial clustering is concentrated in one subregion of the data (Anselin 1992). Hexagons were excluded if they contained <5-percent tree canopy cover or if <1 percent of the tree canopy cover was surveyed in 2019.

The Getis-Ord G_i^* statistic for each hexagon summed the differences between the mean values in a local sample, determined by a moving window consisting of the hexagon and its 18 first- and second-order neighbors (the 6 adjacent hexagons and the 12 additional hexagons contiguous to those 6) and a global mean. Our first analysis encompassed a global mean of all the forested hexagonal cells in the CONUS, while we conducted another set of analyses separately within each of the five FHM regions. The G_i^* statistic was standardized as a *z*-score with a mean of 0 and a standard deviation of 1, with values >1.96 representing significant (p <0.025) local clustering of high values and values <-1.96 representing significant clustering of low values (p <0.025), since 95 percent of the observations under a normal distribution should be within approximately two (exactly 1.96) standard deviations of the mean (Laffan 2006). In other words, a G_i^* value of 1.96 indicates that the local mean of the percentage of forest exposed to mortality-causing or defoliation-causing agents for a hexagon and its 18 neighbors is approximately two standard deviations greater than the mean expected in the absence of spatial clustering, while a G_i^* value of -1.96 indicates that the local mortality or defoliation mean for a hexagon and its 18 neighbors is approximately two standard deviations less than the mean expected in the absence of spatial clustering. Values between -1.96 and 1.96 have no statistically significant concentration of high or low values. In other words, when a hexagon has a G_i^* value between -1.96 and 1.96, mortality or defoliation damage within it and its 18 neighbors is not statistically different from a normal expectation. As described in Laffan (2006), it is calculated as:

$$G_i^*(\boldsymbol{d}) = \frac{\sum_j w_{ij}(d)\, x_j - W_i^* \bar{x}^*}{s^* \sqrt{\frac{(n s_{1i}^*) - W_i^{*2}}{n-1}}}$$

where

G_i^* = the local clustering statistic (in this case, for the target hexagon)

i = the center of local neighborhood (the target hexagon)

d = the width of local sample window (the target hexagon and its first- and second-order neighbors)

x_j = the value of neighbor j

w_{ij} = the weight of neighbor j from location i (all the neighboring hexagons in the moving window were given an equal weight of 1)

n = number of samples in the dataset (the 4,303 hexagons containing >5 percent tree cover and with at least 1 percent of the canopy cover surveyed)

W_i^* = the sum of the weights

s^*_{1i} = the number of samples within d of the central location (19: the focal hexagon and its 18 first- and second-order neighbors)

$\overline{x}$ * = mean of whole dataset (in this case, the 4,303 hexagons)

s* = the standard deviation of whole dataset (for the 4,303 hexagons)

It is worth noting that the -1.96 and 1.96 threshold values are not exact because the correlation of spatial data violates the assumption of independence required for statistical significance (Laffan 2006). The Getis-Ord approach does not require that the input data be normally distributed because the local G_i^* values are computed under a randomization assumption, with G_i^* equating to a standardized z-score that asymptotically tends to a normal distribution (Anselin 1992). The z-scores are reliable, even with skewed data, as long as the distance band used to define the local sample around the target observation is large enough to include several neighbors for each feature (ESRI 2017).

RESULTS AND DISCUSSION

Conterminous United States Mortality

The national IDS data in 2019 identified 58 mortality-causing agents and complexes across the CONUS on an area slightly larger than the combined land area of Vermont and Rhode Island (approximately 2.69 million ha). In comparison, forests cover approximately 252 million ha of the CONUS (Smith and others 2009). Twenty-one of the agents were detected on >5000 ha.

As in 2018 (Potter and others 2020b), fir engraver (*Scolytus ventralis*) was the most widespread mortality agent in 2019, detected on approximately 1.09 million ha (table 2.1), or about 40.5 percent of the total mortality area, followed by emerald ash borer, which was identified on about 517 000 ha. Three additional mortality agents and complexes were detected on >100 000 ha: pinyon ips (*Ips confusus*) on 126 000 ha, mountain pine beetle (*D. ponderosae*) on 122 000 ha, and unknown bark beetles on 116 000 ha (mostly damage on ponderosa pines [*Pinus ponderosa*] in the Interior West by a list of various bark beetle species that are not possible to distinguish from the air). Mortality from the western bark beetle group, including 16 different agents in the IDS data (table 2.2), encompassed about 64 percent of all the 2019 mortality area across the CONUS.

Table 2.1—Mortality agents and complexes affecting >5000 ha in the conterminous United States during 2019

Agents/complexes causing mortality, 2019	Area
	ha
Fir engraver	1 088 757
Emerald ash borer	517 163
Pinyon ips	125 813
Mountain pine beetle	121 932
Unknown bark beetle[a]	116 053
Eastern larch beetle	99 768
Gypsy moth	97 973
Western pine beetle	90 015
Spruce beetle	77 435
Douglas-fir beetle	71 971
Balsam woolly adelgid	69 357
Unknown	42 404
Sudden oak death	37 043
Flatheaded fir borer	34 716
Jeffrey pine beetle	27 155
Subalpine fir decline	24 035
Western balsam bark beetle	23 047
Cedar and cypress bark beetles	18 049
Beech bark disease complex	8959
Roundheaded pine beetle	8790
Ips engraver beetles	7428
Other (37)	28 653
Total, all mortality agents	**2 685 933**

Note: All values are "footprint" areas for each agent or complex. The sum of the individual agents is not equal to the total for all agents due to the reporting of multiple agents per polygon.

[a] In the Interior West, this is primarily damage on ponderosa pines. The group of bark beetles is known and varied but not distinguishable from the air. Regions have characterized it as "Southwest bark beetle complex" consisting mainly of damage caused by roundheaded pine beetle, western pine beetle, and ips beetles.

Table 2.2—Beetle taxa included in the "western bark beetle" group

Western bark beetle mortality agents	
Cedar and cypress bark beetles	*Phloeosinus* spp.
Douglas-fir beetle	*Dendroctonus pseudotsugae*
Douglas-fir engraver	*Scolytus unispinosus*
Fir engraver	*Scolytus ventralis*
Ips engraver beetles	*Ips* spp.
Jeffrey pine beetle	*Dendroctonus jeffreyi*
Mountain pine beetle	*Dendroctonus ponderosae*
Pine engraver	*Ips pini*
Pinyon ips	*Ips confusus*
Root disease and beetle complex	--
Roundheaded pine beetle	*Dendroctonus adjunctus*
Silver fir beetle	*Pseudohylesinus sericeus*
Spruce beetle	*Dendroctonus rufipennis*
Unknown bark beetle	--
Western balsam bark beetle	*Dryocoetes confusus*
Western pine beetle	*Dendroctonus brevicomis*

Also, as in the previous year, the FHM West Coast region in 2019 had the largest area on which mortality agents and complexes were detected, about 1.36 million ha (table 2.3). Three-quarters of this area (1 028 000 ha) was associated with fir engraver mortality. The next most commonly detected mortality agents were western pine beetle (*D. brevicomis*) on 89 000 ha (6.6 percent of the mortality area), mountain pine beetle on 76 000 ha (5.6 percent), sudden oak death on 37 000 ha (2.7 percent), and Douglas-fir beetle (*D. pseudotsugae*) on 36 000 ha

Table 2.3—The top five mortality agents or complexes for each Forest Health Monitoring region, and for Alaska and Hawaii, in 2019

Mortality agents and complexes, 2019	Area
	ha
Interior West	
Pinyon ips	125 798
Unknown bark beetle[a]	114 206
Spruce beetle	76 782
Balsam woolly adelgid	62 517
Fir engraver	60 831
Other mortality agents (16)	151 449
Total, all mortality agents and complexes	**565 807**
North Central	
Emerald ash borer	416 876
Eastern larch beetle	99 768
Beech bark disease complex	8665
Unknown	5338
Unknown bark beetle	1278
Other mortality agents (12)	2683
Total, all mortality agents and complexes	**534 585**
North East	
Gypsy moth	97 973
Emerald ash borer	97 856
Linden looper	4153
Southern pine beetle	3033
Black turpentine beetle	2822
Other mortality agents (21)	8438
Total, all mortality agents and complexes	**214 265**

Mortality agents and complexes, 2019	Area
	ha
South	
Unknown	3795
Emerald ash borer	2430
Ips engraver beetles	1468
Southern pine beetle	286
Black turpentine beetle	<1
Other mortality agents (1)	<1
Total, all mortality agents and complexes	**7979**
West Coast	
Fir engraver	1 027 926
Western pine beetle	89 410
Mountain pine beetle	75 690
Sudden oak death	37 043
Douglas-fir beetle	35 914
Other mortality agents (18)	122 311
Total, all mortality agents and complexes	**1 363 297**
Alaska	
Spruce beetle	53 900
Yellow-cedar decline	8088
Northern spruce engraver	433
Western balsam bark beetle	43
Unknown canker	29
Other mortality agents (1)	4
Total, all mortality agents and complexes	**62 497**

Mortality agents and complexes, 2019	Area
	ha
Hawaii	
Unknown[b]	27 237
Total, all mortality agents and complexes	**27 237**

Note: The total area affected by other agents is listed at the end of each section. All values are "footprint" areas for each agent or complex. The sum of the individual agents is not equal to the total for all agents due to the reporting of multiple agents per polygon.

[a] In the Interior West, this is primarily damage on ponderosa pines. The group of bark beetles is known and varied but not distinguishable from the air. Regions have characterized it as "Southwest bark beetle complex" consisting mainly of damage caused by roundheaded pine beetle, western pine beetle, and ips beetles.

[b] Most of the mortality recorded in Hawaii is coded as "unknown" mortality on ʻōhiʻa lehua. Damage is likely attributed to rapid ʻōhiʻa death but has not been confirmed.

(2.6 percent). Another 18 mortality-causing agents and complexes accounted for 8.9 percent of the mortality area in the West Coast region.

A handful of ecoregion sections in the West Coast region had relatively high percentages of mortality of surveyed tree canopy area, especially the M261E–Sierra Nevada ecoregion section in California (1.47 percent) and the M261A–Klamath Mountains ecoregion section in northwestern California and southwestern Oregon (1.01 percent) (fig. 2.2). The mortality in these regions was primarily caused by infestation of fir engraver in red fir (*Abies magnifica*) and white fir (*A. concolor*) and resulted in a series of geographic hot spots of high mortality in analyses conducted both for the CONUS (fig. 2.3A) and limited to the West Coast FHM region (fig. 2.3B). Fir engraver also impacted neighboring ecoregion sections, including M261D–Southern Cascades (0.68-percent mortality of surveyed canopy area), M261G–Modoc Plateau (0.65 percent), and M261B–Northern California Coast Ranges (0.58 percent). Flatheaded fir borer (*Phaenops drummondi*) in Douglas-fir (*Pseudotsuga menziesii*) was also an issue in the northern (Oregon) portions of M261A–Klamath Mountains.

Fir engraver, along with western pine beetle in ponderosa pine stands, resulted in moderately high mortality (0.70 percent of the surveyed tree canopy cover) in the M332G–Blue Mountains ecoregion section of northeastern Oregon (fig. 2.2), as well as a moderate-mortality hot spot (fig. 2.3). Along with fir engraver, western pine beetle and mountain pine beetle were issues in nearby M242D–Northern Cascades (0.48 percent), M242C–Eastern Cascades (0.35 percent), M333A–Okanogan Highland (0.35 percent), and 342H–Blue Mountain Foothills (0.28 percent).

Elsewhere in the West Coast region, sudden oak death in tanoak (*Notholithocarpus densiflorus*) resulted in 0.48-percent mortality of surveyed canopy area in 263A–Northern California Coast and 0.31 percent in 261A–Central California Coast.

In 2019, the FHM Interior West region had the second most extensive area of insect and disease mortality detection, with 21 agents and complexes identified across 566 000 ha (table 2.3). Unlike in 2018, when spruce beetle (*D. rufipennis*) was the most widely detected agent, pinyon ips damage was recorded on the most area, about 126 000 ha, or 22.2 percent of the total mortality area. Meanwhile, unknown bark beetles affected 20.2 percent of the total mortality area, or 114 000 ha. This was primarily damage on ponderosa pines by a group of known and varied bark beetles that are not distinguishable from the air. This has been characterized as "Southwest bark beetle complex" consisting mainly of damage caused by roundheaded pine beetle (*D. adjunctus*), western pine beetle, and ips beetles. Other widespread mortality agents were spruce beetle detected on 77 000 ha (13.6 percent), balsam woolly adelgid (*Adelges piceae*) on 63 000 ha (11.0 percent), and fir engraver beetle on 61 000 ha (10.8 percent) (table 2.3).

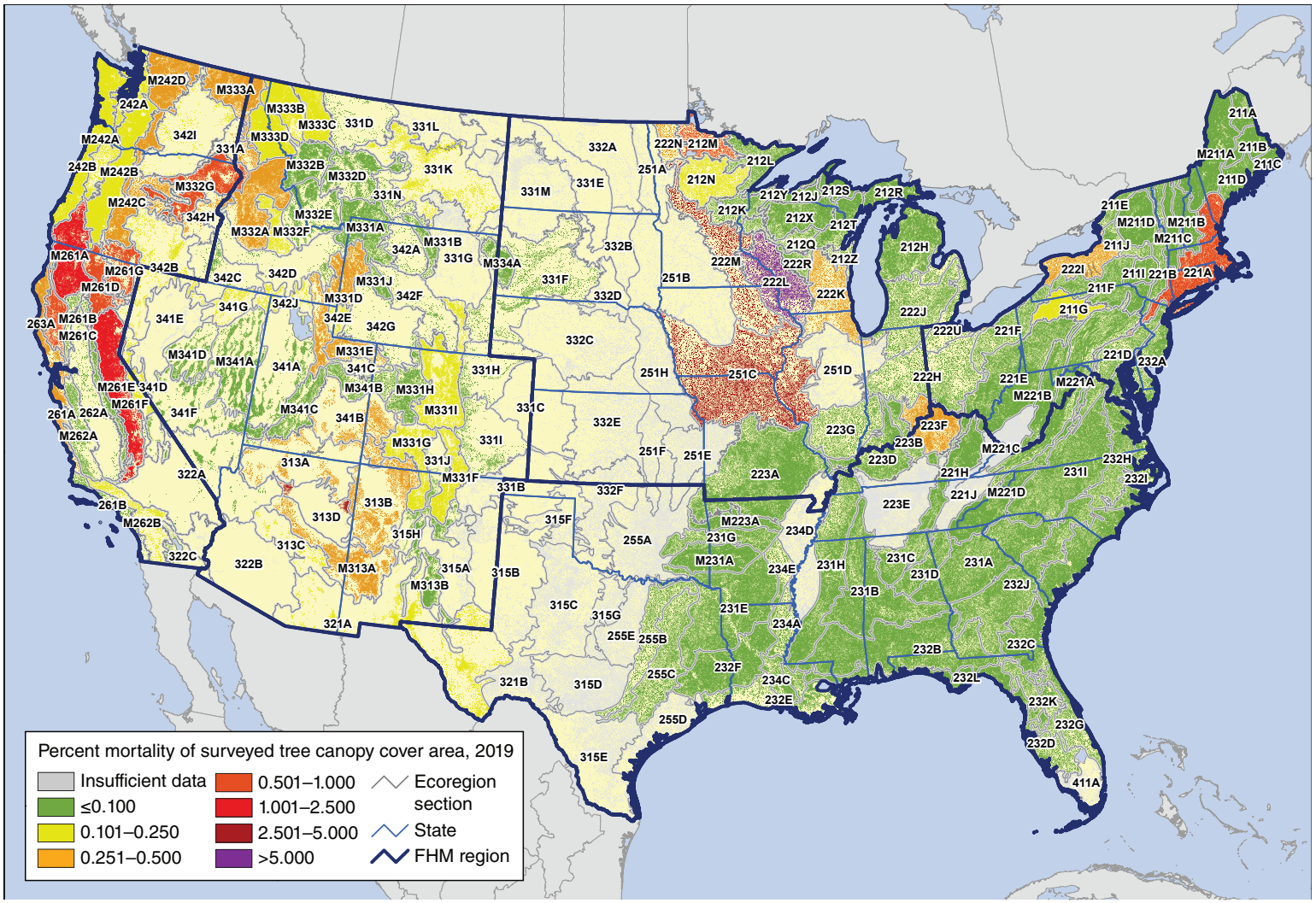

Figure 2.2—The percentage of surveyed tree canopy cover area with insect and disease mortality, by ecoregion section within the conterminous 48 States, for 2019. The gray lines delineate ecoregion sections (Cleland and others 2007). The 240-m tree canopy cover is based on data from a cooperative project between the Multi-Resolution Land Characteristics Consortium (Coulston and others 2012) and the Forest Service Geospatial Technology and Applications Center using the 2011 National Land Cover Database. (Data source: U.S. Department of Agriculture Forest Service, Forest Health Protection)

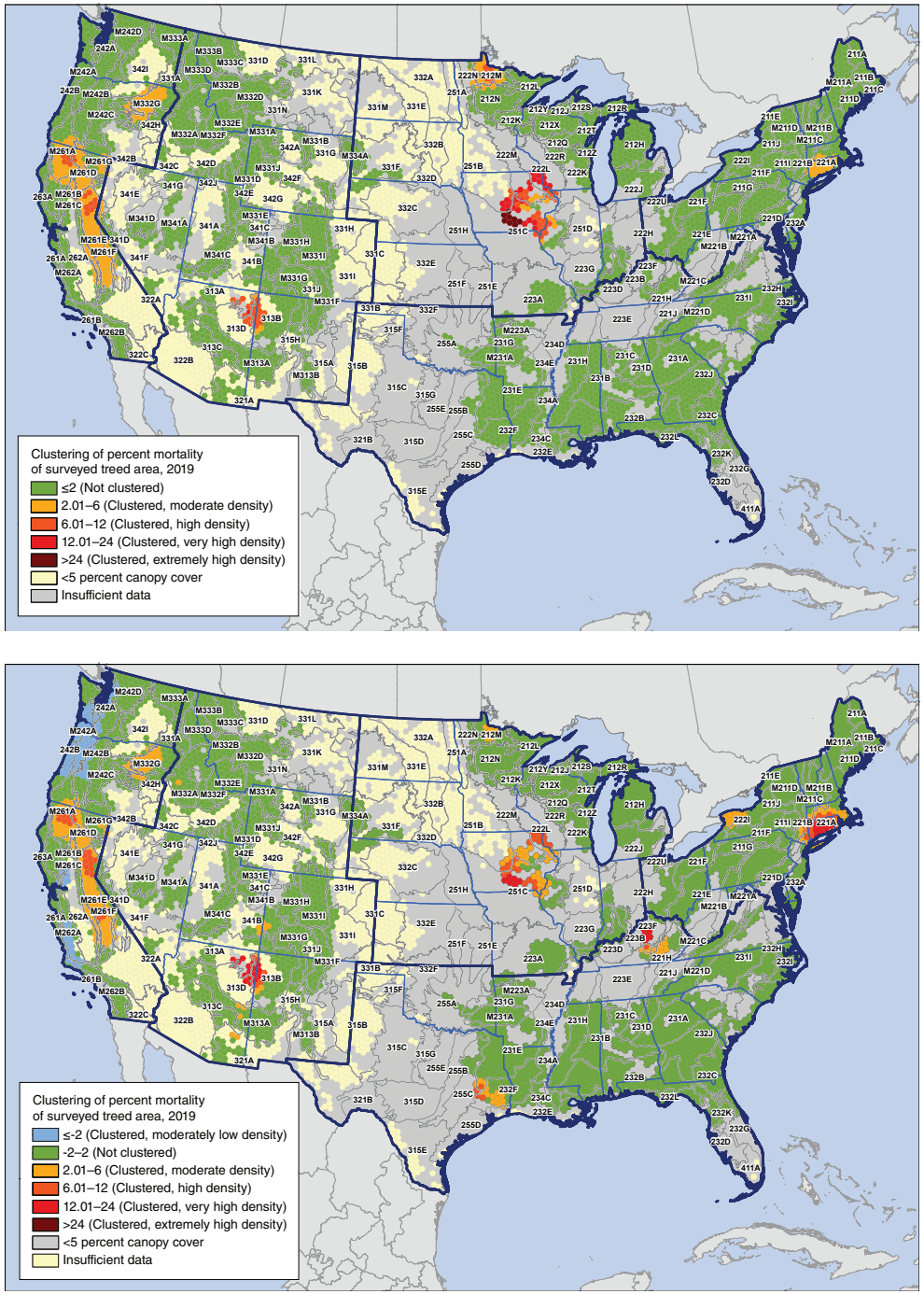

Figure 2.3—Hot spots of percentage of surveyed tree canopy cover area with insect and disease mortality in 2019 for (A) the conterminous 48 States and (B) for separate Forest Health Monitoring (FHM) regions, by hexagons containing >5-percent tree canopy cover. Values are Getis-Ord G_i^* scores, with values >2 representing significant clustering of high mortality occurrence densities and values <-2 representing significant clustering of low mortality occurrence densities. The gray lines delineate ecoregion sections (Cleland and others 2007), and blue lines delineate FHM regions. Tree canopy cover is based on data from a cooperative project between the Multi-Resolution Land Characteristics Consortium (Coulston and others 2012) and the Forest Service Geospatial Technology and Applications Center using the 2011 National Land Cover Database. (Data source: U.S. Department of Agriculture Forest Service, Forest Health Protection)

Interior West mortality was highest in northeastern Arizona and northwestern New Mexico, where two nearly adjacent hot spots were detected of mostly high mortality density in the CONUS hot spot analysis and of very high density in the regional analysis (fig. 2.3). The primary causes of mortality in this area were the "Southwest bark beetle complex" in ponderosa pine stands, described above, and pinyon ips in two-needle pinyon (*P. edulis*) stands. As a result of these agents, the 313D–Painted Desert ecoregion section had the highest percentage of surveyed tree canopy area mortality (4.69) in the Interior West region (fig. 2.2). Adjacent ecoregion sections also had relatively high mortality percentages: 313B–Navajo Canyonlands (0.35), M313A–White Mountains-San Francisco Peaks-Mogollon Rim (0.28), and 313A–Grand Canyon (0.27).

These agents, as well as roundheaded pine beetle (*D. adjunctus*) in ponderosa pine, spruce beetle in Engelmann spruce (*Picea engelmannii*), subalpine fir (*A. lasiocarpa*) decline, and Douglas-fir beetle, resulted in relatively high mortality (0.38 percent of surveyed canopy area) in the 341B–Northern Canyonlands ecoregion section of southwestern Colorado and southeastern Utah (fig. 2.2). The regional hot spot analysis detected an area of moderate mortality density in this area as well (fig. 2.3B). Further north, in northeastern Utah, southeastern Idaho, and western Wyoming, balsam woolly adelgid and subalpine fir decline in subalpine fir stands, as well as spruce beetle in Engelmann spruce stands, caused moderate levels of mortality in M331E–Uinta Mountains (0.34 percent) and M331D–Overthrust Mountains (0.28 percent). Finally, two ecoregion sections in central Idaho (M332A–Idaho Batholith and 331A–Palouse Prairie) both had 0.39-percent mortality in surveyed treed area because of mountain pine beetle in lodgepole pine (*P. contorta*), balsam woolly adelgid and subalpine fir decline in subalpine fir, fir engraver in grand fir (*A. grandis*), and Douglas-fir beetle. A small hot spot of moderate mortality was detected in this area in the regional analysis (fig. 2.3B).

In the FHM North Central region, meanwhile, surveyors recorded approximately 535 000 ha with mortality in 2019.

Of this footprint, about 78 percent was attributed to emerald ash borer (417 000 ha) and 19 percent to eastern larch beetle (*D. simplex*, 100 000 ha) (table 2.3). Of the other 15 mortality agents recorded, beech bark disease complex was the most widespread (1.6 percent of the mortality area).

The ecoregion section with the greatest mortality of surveyed tree canopy cover nationally was 222L–North Central U.S. Driftless and Escarpment of southwestern Wisconsin, northeastern Iowa, and southeastern Minnesota (6.7 percent), where emerald ash borer was detected killing white, green, and black ash (*Fraxinus americana*, *F. pennsylvanica*, and *F. nigra*) (fig. 2.2). Two adjacent ecoregion sections also experienced extensive mortality associated with emerald ash borer: 251C–Central Dissected Till Plains of southeastern Iowa (5.0 percent) and 222M–Minnesota and Northeast Iowa

Morainal-Oak Savannah (2.63 percent). This mortality resulted in a hot spot of extremely high mortality density in the CONUS analysis (fig.2.3A) and of very high mortality density in the regional analysis (fig. 2.3B).

A second hot spot of mortality, of high mortality density in the national analysis and moderate mortality density in the regional analysis, was detected in 212M–Northern Minnesota and Ontario, where an ongoing eastern larch beetle infestation is affecting tamarack (*Larix laricina*). In this ecoregion section, 0.94 percent of surveyed tree canopy cover experienced mortality (fig. 2.2).

In the North East FHM region, 26 mortality agents and complexes were recorded in 2019 on a total of approximately 214 000 ha (table 2.3). The most common were gypsy moth and emerald ash borer, both identified on about 98 000 ha (45.7 percent of the total mortality area in the region). Other less common agents were linden looper (*Erannis tiliaria*, 1.9 percent), southern pine beetle (1.4 percent), and black turpentine beetle (*Dryocoetes confusus*, 1.3 percent).

The 221A–Lower New England ecoregion section experienced 0.77-percent mortality within the surveyed tree canopy cover area, resulting from widespread gypsy moth impacts in deciduous forests in addition to some emerald ash borer-caused mortality in ash stands of Massachusetts, Connecticut, and Rhode Island. This ecoregion also had southern pine southern pine beetle and oak wilt mortality on Long Island (fig. 2.2). The mortality in this area resulted in a hot spot of very high mortality density in the regional analysis, and one of moderate mortality density in the CONUS analysis (fig. 2.3).

Two other ecoregion sections, 222I–Erie and Ontario Lake Plain in western New York (0.33 percent) and 211G–Northern Unglaciated Allegheny Plateau in north-central Pennsylvania (0.12 percent) were also the locations of relatively high mortality associated with emerald ash borer. The former of these caused a moderate mortality hot spot in the regional analysis.

Finally, in the South FHM region, surveyors identified six agents resulting in 8000 ha with mortality (table 2.3). The most common mortality category was “unknown” (3800 ha, 47.6 percent) followed by emerald ash borer (2400 ha, 30.5 percent) and ips engraver beetles (1500 ha, 18.4 percent). Southern pine beetle was found on an additional 286 ha (3.6 percent).

A single ecoregion section in the South had mortality exceeding 0.1 percent of the surveyed tree canopy area. This was 223F–Interior Low Plateau-Bluegrass (0.45 percent) in northern Kentucky where emerald ash borer was relatively widely detected (fig. 2.2). Regional hot spots of mortality were detected here and in three ecoregion sections of eastern Texas (232F–Coastal Plains and Flatwoods-Western Gulf, 255C–Oak Woods and Prairie,

and 231E–Mid Coastal Plains-Western) where there was ips engraver beetle activity in yellow pine forests and hardwood mortality with an unknown cause (fig. 2.3B).

Conterminous United States Defoliation

The national IDS in 2019 identified 64 defoliation agents and complexes affecting approximately 1.42 million ha across the CONUS (table 2.4), which is somewhat smaller than the combined land area of Connecticut and Rhode Island. As in 2018 (Potter and others 2020b), the most widespread defoliation agent was western spruce budworm (*Choristoneura freemani*), detected on approximately 41 percent of the total area with defoliation (589 000 ha). Four additional agents were each detected on >100 000 ha: hemlock looper (*Lambdina fiscellaria*) on 170 000 ha, forest tent caterpillar (*Malacosoma disstria*) on 116 000 ha, spruce budworm (*C. fumiferana*) on 112 000 ha, and Douglas-fir tussock moth (*Orgyia pseudotsugata*) on 100 000 ha (table 2.4).

The FHM region with by far the largest area on which defoliation agents were detected in 2019 was the Interior West, with 957 000 ha of damage associated with 24 defoliators (table 2.5). As in 2018, the majority of this area (61.5 percent) was affected by western spruce budworm (588 000 ha). Hemlock looper affected 168 000 ha (17.6 percent of the total), Douglas-fir tussock moth 92 000 ha (9.6 percent), Marssonina blight (*Drepanopeziza* spp.) 36 000 ha (3.8 percent), and pinyon needle scale (*Matsucoccus acalyptus*) 26 000 ha (2.7 percent).

Table 2.4—Defoliation agents and complexes affecting >5000 ha in the conterminous United States in 2019

Agents/complexes causing defoliation, 2019	Area
	ha
Western spruce budworm	588 591
Hemlock looper	170 011
Forest tent caterpillar	116 395
Spruce budworm	111 754
Douglas-fir tussock moth	100 142
Gypsy moth	93 155
Marssonina blight	37 966
Baldcypress leafroller	35 302
Gelechiid moths/needleminers	30 313
Pinyon needle scale	27 979
Unknown defoliator	25 410
Balsam woolly adelgid	16 212
Jumping oak gall wasp	12 389
Spruce aphid	11 173
White pine needle damage	9419
Maple leafcutter	6543
Aspen blotchminer	6232
Unknown	6087
Yellow poplar weevil	5444
Other (45)	41 456
Total, all defoliation agents	**1 419 839**

Note: All values are "footprint" areas for each agent or complex. The sum of the individual agents is not equal to the total for all agents due to the reporting of multiple agents per polygon.

Table 2.5—The top five defoliation agents or complexes for each Forest Health Monitoring region and for Alaska and Hawaii, in 2019

Defoliation agents and complexes, 2019	Area
	ha
Interior West	
Western spruce budworm	587 931
Hemlock looper	167 884
Douglas-fir tussock moth	92 155
Marssonina blight	36 313
Pinyon needle scale	26 123
Other defoliation agents (19)	56 904
Total, all defoliation agents and complexes	**956 527**
North Central	
Spruce budworm	111 754
Gypsy moth	79 235
Forest tent caterpillar	48 972
Jumping oak gall wasp	12 389
Aspen blotchminer	6232
Other defoliation agents (10)	4665
Total, all defoliation agents and complexes	**263 243**
North East	
Gypsy moth	10 348
White pine needle damage	9419
Maple leafcutter	6543
Browntail moth	4993
Unknown	2493
Other defoliation agents (16)	7087
Total, all defoliation agents and complexes	**40 718**

Defoliation agents and complexes, 2019	Area
	ha
South	
Forest tent caterpillar	65 541
Baldcypress leafroller	35 302
Yellow poplar weevil	5403
Walkingstick	4567
Gypsy moth	3571
Other defoliation agents (4)	3520
Total, all defoliation agents and complexes	**96 742**
West Coast[a]	
Balsam woolly adelgid	16 212
Gelechiid moths/needleminers	8018
Douglas-fir tussock moth	7987
Spruce aphid	7890
Lodgepole needleminer	4764
Other defoliation agents (19)	17 758
Total, all defoliation agents and complexes	**62 610**
Alaska	
Hemlock sawfly	154 050
Birch leafminer	113 382
Aspen leafminer	53 452
Willow leaf blotchminer	12 853
Unknown defoliator	5284
Other defoliation agents (4)	599
Total, all defoliation agents and complexes	**339 601**

Defoliation agents and complexes, 2019	Area
	ha
Hawaii	
ʻŌhiʻa/guava rust	5
Total, all mortality agents and complexes	**5**

Note: The total area affected by other agents is listed at the end of each section. All values are "footprint" areas for each agent or complex. The sum of the individual agents is not equal to the total for all agents due to the reporting of multiple agents per polygon.

[a] There was no Swiss needle cast survey in 2019.

As in 2018, several ecoregion sections of the northern Rockies were severely affected by western spruce budworm in 2019, particularly two in southwestern Montana and east-central Idaho: M332E–Beaverhead Mountains and M332B–Northern Rockies and Bitterroot Valley with 3.94 percent and 2.93 percent of surveyed tree canopy area defoliated, respectively (fig. 2.4). The western spruce budworm defoliation extended into several ecoregion sections to the east, north, and south of these: M332D–Belt Mountains (2.18 percent), M331D–Overthrust Mountains (1.57 percent), M332F–Challis Volcanics (1.95 percent), M331A–Yellowstone Highlands (1.19 percent), M331B–Bighorn Mountains (1.15 percent), and M333C–Northern Rockies: (0.51 percent). To the west, M332A–Idaho Batholith (3.51-percent defoliation) experienced infestations of hemlock looper, Douglas-fir tussock moth, and western spruce budworm, while M333D–Bitterroot Mountains (2.76 percent) had extensive defoliation by hemlock looper. The northern Rockies area was encompassed by several adjacent hot spots of moderate to very high defoliation density in the analyses both for the entire CONUS (fig. 2.5A) and for the Interior West region (fig. 2.5B).

Farther south, an area of relatively high defoliation was centered on two ecoregion sections in south-central Colorado and northern New Mexico, M331F–Southern Parks and Rocky Mountain Range (3.31-percent defoliation) and M331G–South-Central Highlands (2.72 percent). Western spruce budworm was again the leading defoliating agent, along with Marssonina blight in quaking aspen (*Populus tremuloides*) stands and Gelechiid moths/needleminers (*Coleotechnites* spp.) in ponderosa pine stands. The work of these agents resulted in a hot spot of high defoliation density in the CONUS analysis (fig. 2.5A) and a couple of hot spots of moderate defoliation density in the regional analysis (fig. 2.5B).

In south-central Utah, a hot spot of moderate defoliation was the result of a western spruce budworm infestation in M341C–Utah High Plateau (0.99-percent defoliation of surveyed canopy area).

The North Central FHM region, meanwhile, had 263 000 ha with defoliation associated with 15 agents and complexes, with spruce budworm the most widely detected (112 000 ha, 42.5 percent of the total) (table 2.5). Gypsy moth also caused widespread damage (79 000 ha, 30.1 percent), as did forest tent caterpillar (49 000 ha, 18.6 percent). Jumping oak gallwasp (*Neuroterus saltatorius*) and aspen blotchminer (*Phyllonorycter tremuloidiella*) were also somewhat widespread (4.7 percent and 2.4 percent of the regional total defoliation, respectively).

Defoliation in the North Central region was most widespread in the Great Lakes States (fig. 2.4), especially 212R–Eastern Upper Peninsula (2.00 percent of surveyed area with canopy cover), where forest tent caterpillar was the most commonly detected agent along with spruce budworm and jack pine budworm (*C. pinus*). In 212H-Northern Lower Peninsula

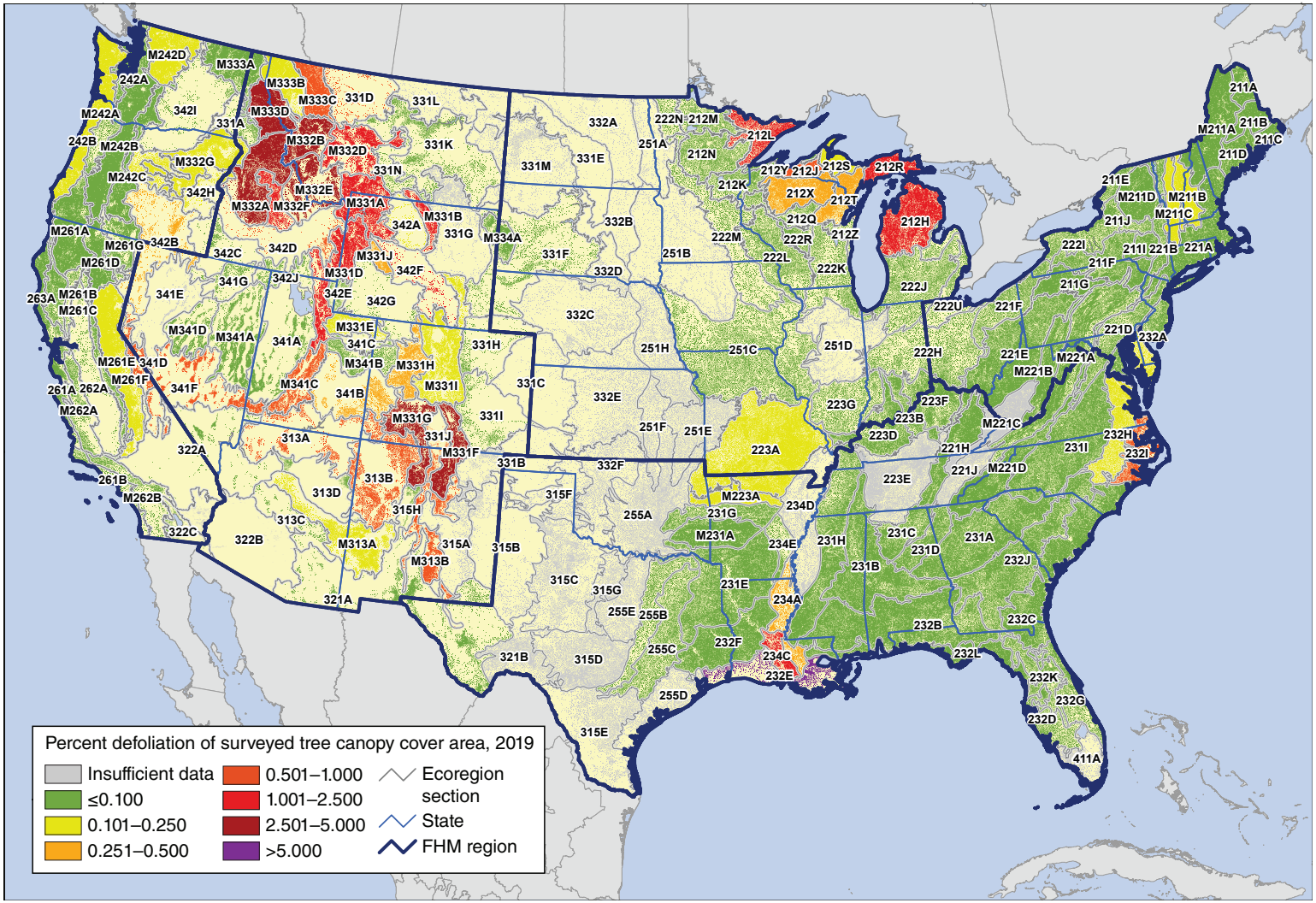

Figure 2.4—The percentage of surveyed tree canopy cover area with insect and disease defoliation, by ecoregion section within the conterminous 48 States, for 2019. The gray lines delineate ecoregion sections (Cleland and others 2007). The 240-m tree canopy cover is based on data from a cooperative project between the Multi-Resolution Land Characteristics Consortium (Coulston and others 2012) and the Forest Service Geospatial Technology and Applications Center using the 2011 National Land Cover Database. (Data source: U.S. Department of Agriculture Forest Service, Forest Health Protection)

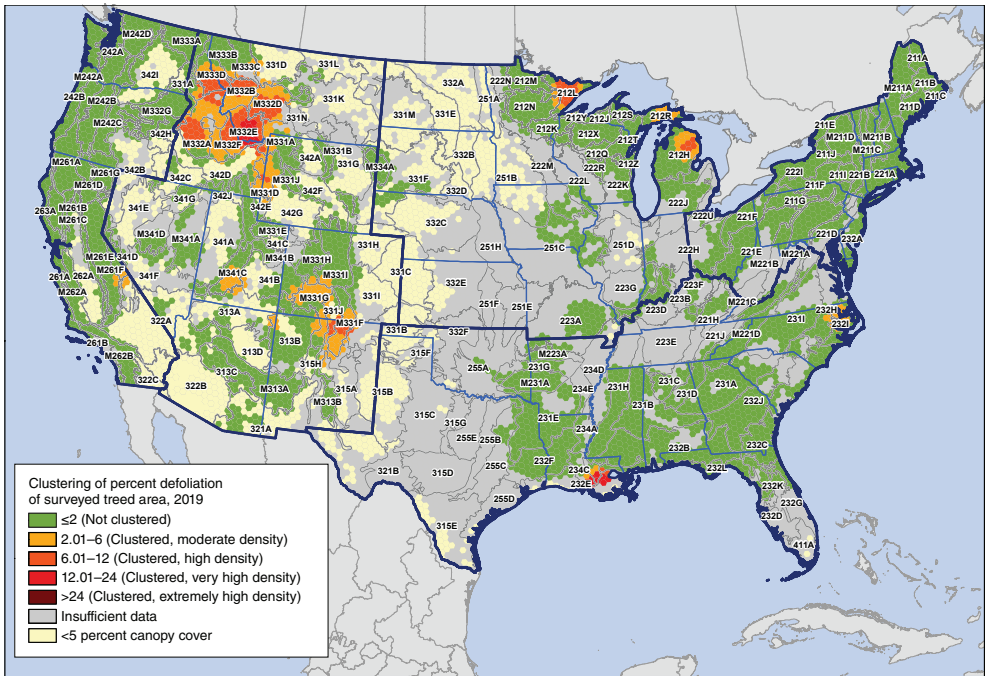

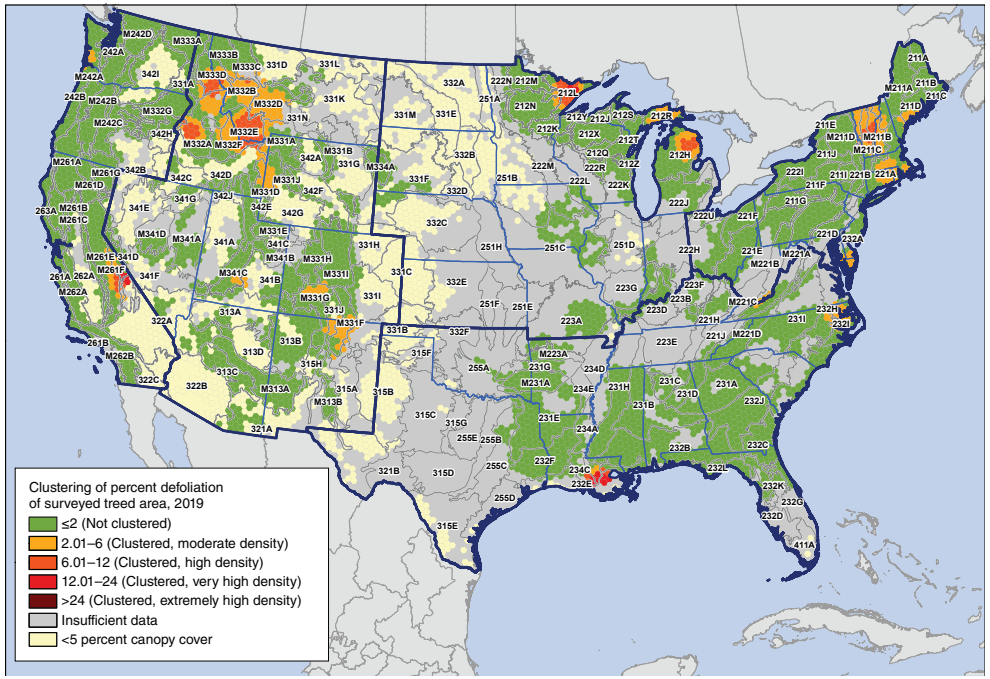

Figure 2.5—Hot spots of percentage of surveyed tree canopy cover area with insect and disease defoliation in 2019 for (A) the conterminous 48 States and (B) for separate Forest Health Monitoring regions, by hexagons containing >5 percent tree canopy cover. Values are Getis-Ord G_i^* scores, with values >2 representing significant clustering of high defoliation occurrence densities. (No areas of significant clustering of low densities, <-2, were detected.) The gray lines delineate ecoregion sections (Cleland and others 2007), and blue lines delineate Forest Health Monitoring regions. Tree canopy cover is based on data from a cooperative project between the Multi-Resolution Land Characteristics Consortium (Coulston and others 2012) and the Forest Service Geospatial Technology and Applications Center using the 2011 National Land Cover Database. (Data source: U.S. Department of Agriculture Forest Service, Forest Health Protection)

(1.75 percent), gypsy moth in oak (*Quercus* spp.) stands was the main agent, in addition to spruce budworm and forest tent caterpillar. Finally, in 212L-Northern Superior Uplands (1.72 percent), spruce budworm was an issue in balsam fir (*A. balsamea*) and white and black spruce (*P. glauca* and *P. mariana*) stands and larch casebearer (*Coleophora laricella*) and forest tent caterpillar were additional but less significant problems. Each of these ecoregion sections was the location of a hot spot of either high or moderate defoliation density in both the CONUS and regional analyses (fig. 2.5). Four other ecoregion sections in the Great Lakes States also had relatively high defoliation as a result of spruce budworm and forest tent caterpillar:

- 212J–Southern Superior Uplands (0.52 percent)
- 212X–Northern Highlands (0.38 percent)
- 212T–Northern Green Bay Lobe (0.30 percent)
- 212S–Northern Upper Peninsula (0.15 percent)

At the southern edge of the North Central region, in 223A–Ozark Highlands in southern Missouri, jumping oak gall wasp was an issue, resulting in 0.16-percent defoliation of surveyed canopy cover.

Surveyors in 2019 documented about 97 000 ha with defoliation in the South (table 2.5), with forest tent caterpillar detected on about 66 000 ha, or 67.7 percent of the area with defoliation, and baldcypress leafroller (*Archips goyerana*) detected on about 35 000 ha, or 36.5 percent of the area with defoliation. Of the seven other defoliating agents detected in 2019, yellow poplar weevil (*Odontopus calceatus*), walkingstick (*Diapheromera femorata*), and gypsy moth were recorded on an additional 5400 ha, 4600 ha, and 3600 ha, respectively.

As in 2018, the southern ecoregion sections with the highest percentage of defoliation were in southern Louisiana, as the result mainly of baldcypress leafroller: 232E–Louisiana Coastal Prairie and Marshes (7.33 percent) and 234C–Atchafalaya and Red River Alluvial Plains (1.42 percent) (fig. 2.4). Forest tent caterpillar was an issue in the neighboring 234A–Southern Mississippi Alluvial Plain (0.45 percent). These defoliators resulted in the area being the location of a hot spot of very high defoliation density (fig. 2.5).

Elsewhere in the South, forest tent caterpillar and, to a lesser degree loblolly pine sawfly (*N. taedae linearis*), caused relatively high levels of defoliation and a hot spot of moderate defoliation in two ecoregion sections of eastern North Carolina: 232I–Northern Atlantic Coastal Flatwoods (0.86-percent defoliation of surveyed canopy cover) and 232H–Middle Atlantic Coastal Plains and Flatwoods (0.20 percent). Additionally, an ongoing infestation of walkingstick in M223A–Boston Mountains of northern Arkansas resulted in 0.12-percent defoliation of surveyed tree canopy area there (fig. 2.4).

In 2019, 24 defoliating agents were recorded in the West Coast FHM region on 63 000 ha (table 2.5). (Unlike 2018, there was no Swiss needle cast survey.) No single agent was responsible for a majority of the defoliation, but balsam woolly adelgid was detected on 16 000 ha (25.9 percent of the regional total), while three agents were found on about 8000 ha: Gelechiid moths/needleminers, Douglas-fir tussock moth, and spruce aphid (*Elatobium abietinum*).

A variety of pests, including Gelechiid moths/needleminers in ponderosa pine forests, Marssonina blight in quaking aspen stands, and pinyon needle scale in singleleaf pinyon (*P. monophylla*) forests, resulted in moderately high levels of defoliation in two ecoregion sections of eastern California, extending into western Nevada and the Interior West FHM region: 341D–Mono and 341F–Southeastern Great Basin (both with 0.73-percent defoliation of surveyed canopy cover area) (fig. 2.4). This defoliation also caused the West Coast region's only national defoliation hot spot (fig. 2.5A) as well as a hot spot of very high defoliation density in the regional analysis (fig. 2.5B). Another regional hot spot, this one of moderate defoliation, was detected on the Pacific Coast border between Washington and Oregon (M242A–Oregon and Washington Coast Ranges), where there was an outbreak of spruce aphid in Sitka spruce (*P. sitchensis*).

In the North East region, two of 21 agents were the most widely identified: gypsy moth on about 10 000 ha (25.4 percent of the regional total) and white pine needle damage on about 9000 ha (23.1 percent). Maple leafcutter (*Paraclemensia acerifoliella*) and browntail moth (*Euproctis chrysorrhoea*) were also relatively widely detected, constituting 16.1 percent and 12.3 percent of the total defoliation, respectively (table 2.5).

White pine needle damage in stands of eastern white pine (*P. strobus*) and maple leafcutter infestation in sugar maple (*Acer saccharum*) forests resulted in moderately high defoliation in the upper New England ecoregion sections of M211C–Green-Taconic-Berkshire Mountains (0.21 percent) and M211B–New England Piedmont (0.22 percent). These caused a regional geographic hot spot of high defoliation in the area (fig. 2.5B). Other North East region hot spots were associated with browntail moth in northern red oak (*Q. rubra*) stands in 211D–Central Maine Coastal and Embayment; with fall cankerworm (*Alsophila pometaria*) in eastern Massachusetts and gypsy moth in Connecticut and central Massachusetts (both in 221A–Lower New England); and with forest tent caterpillar and gypsy moth in the Delmarva Peninsula (232H–Middle Atlantic Coastal Plains and Flatwoods).

Alaska and Hawaii

In Alaska, six mortality agents and complexes were detected on approximately 62 000 ha in 2019 (table 2.3), a decline from the previous year. Spruce beetle was again the most widely detected mortality agent, representing 86.2 percent of the total area with mortality (54 000 ha). Most of the rest of the State's

mortality was associated with yellow-cedar (*Chamaecyparis nootkatensis*) decline (8000 ha, 12.9 percent of the total).

As in 2018, the spruce beetle outbreak was focused in the south-central part of the State (fig. 2.6), where M243B–Alaska Peninsula had the highest mortality of surveyed forest and shrubland (0.45 percent), followed by 133A–Cook Inlet Basin (0.22 percent) and M133B–Alaska Range (0.19 percent).

A much larger area of Alaska was affected by defoliation than by mortality in 2019. Specifically, nine defoliation agents were found together to affect approximately 340 000 ha, with the greatest area (154 000 ha) encompassed by hemlock sawfly (*N. tsugae*), 45.4 percent of the total for the State (table 2.5). Surveyors attributed a further 113 000 ha with defoliation to birch leafminer (*Fenusa pusilla*, 33.4 percent), 53 000 ha to aspen leafminer (*Phyllocnistis populiella*, 15.7 percent), and 13 000 to willow leaf blotchminer (*Micrurapteryx salicifoliella*, 3.8 percent).

Defoliation in 2018 was relatively high across east-central and southeastern parts of Alaska (fig. 2.7). The ecoregion section with the highest defoliation was M241D–Alexander Archipelago in the Alaska panhandle, with 3.52 percent of surveyed area experiencing defoliation from hemlock sawfly in western hemlock (*Tsuga heterophylla*) forests. Meanwhile, birch leafminer resulted in 2.47- and 1.24-percent defoliation in surveyed forest and shrubland areas of 133A–Cook Inlet Basin and M241C–Chugach-St. Elias Mountains, respectively, in south-central Alaska. Aspen leafminer and willow leaf blotchminer were the main defoliation agents in ecoregion sections of east-central Alaska: M132C–Yukon-Tanana Uplands (1.03 percent defoliation), 132C–Tanana-Kuskokwim Lowlands (0.87 percent), 132A–Yukon-Old Crow Basin (0.77 percent), and M132E–Ray Mountains (0.64 percent).

Finally, surveyors delineated about 27 000 ha with mortality in Hawaii during 2019 (table 2.3). While no cause was assigned to any of the mortality, at least some of this was likely caused by rapid ʻōhiʻa death, a wilt disease that affects ʻōhiʻa lehua (*Metrosideros polymorpha*), a highly ecologically and culturally important tree in Hawaiian native forests (University of Hawaiʻi 2020). Rapid *ʻōhiʻa* death is caused by the fungal pathogens *Ceratocystis lukuohia* and *C. huliohia*, but *C. lukuohia* is more aggressive than *C. huliohia*, though both can kill *ʻōhiʻa* (Barnes and others 2018). Both pathogens have been confirmed extensively on the islands of Hawaiʻi (the Big Island) and Kauaʻi, while in 2019 five trees and one tree infected with *C. huliohia* were detected on Oʻahu and Maui, respectively (University of Hawaiʻi 2020).

Montane wet ecoregions across the islands of Maui, Hawaiʻi, and Molokai were those with the highest mortality detected in 2019 (fig. 2.8): Montane Wet-Maui-East (MWm-e) with 4.00 percent of the surveyed tree canopy area, Montane Wet-Maui-West (MWm-w) with 1.36 percent, Montane Wet-Hawaiʻi-Kohala-Hāmākua (MWh-kh) with 1.14 percent,

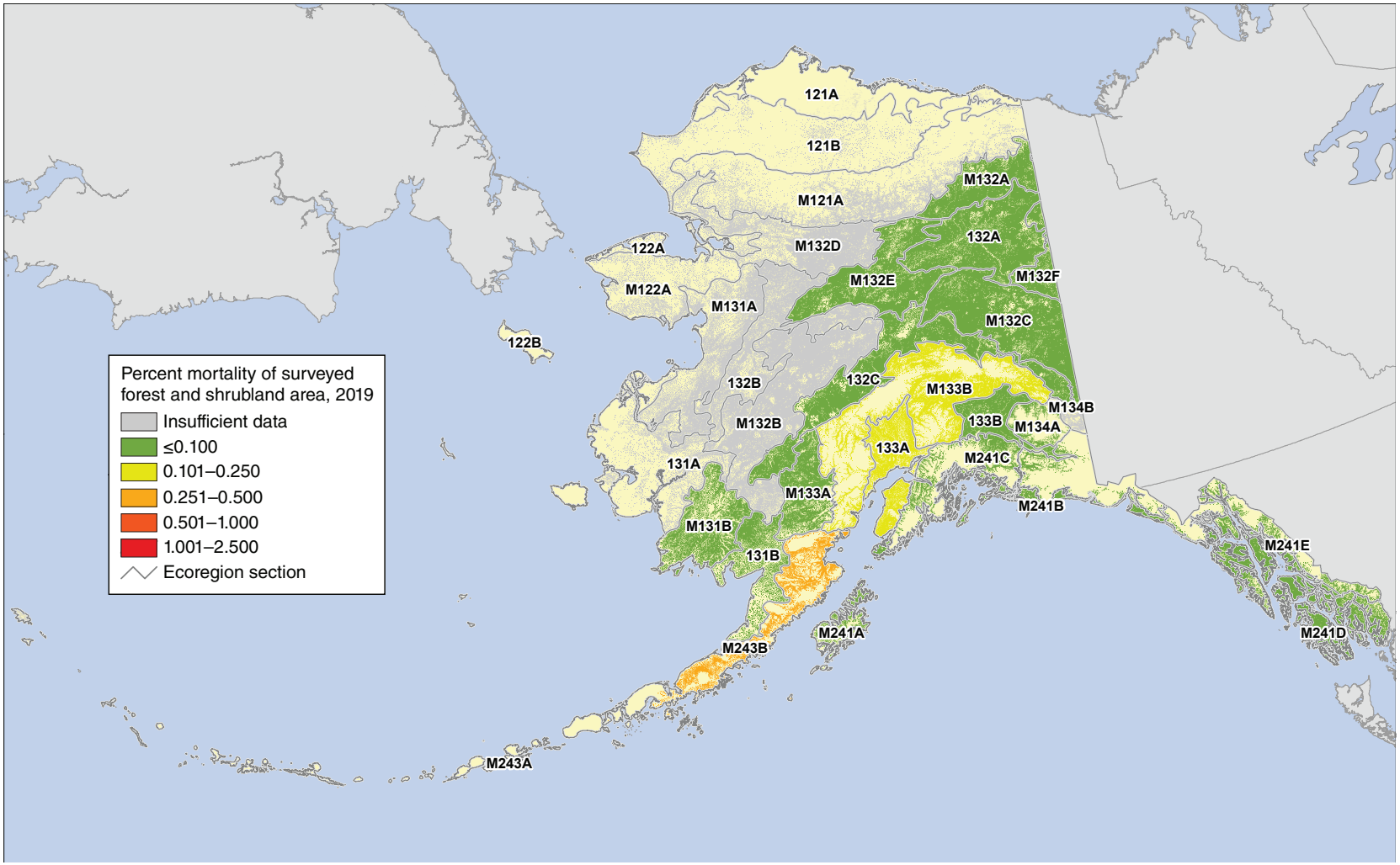

Figure 2.6—Percentage of 2019 surveyed Alaska forest and shrubland area within ecoregions with mortality caused by insects and diseases. The gray lines delineate ecoregion sections (Spencer and others 2002). Forest and shrub cover is derived from the 2011 National Land Cover Database. (Data source: U.S. Department of Agriculture Forest Service, Forest Health Protection)

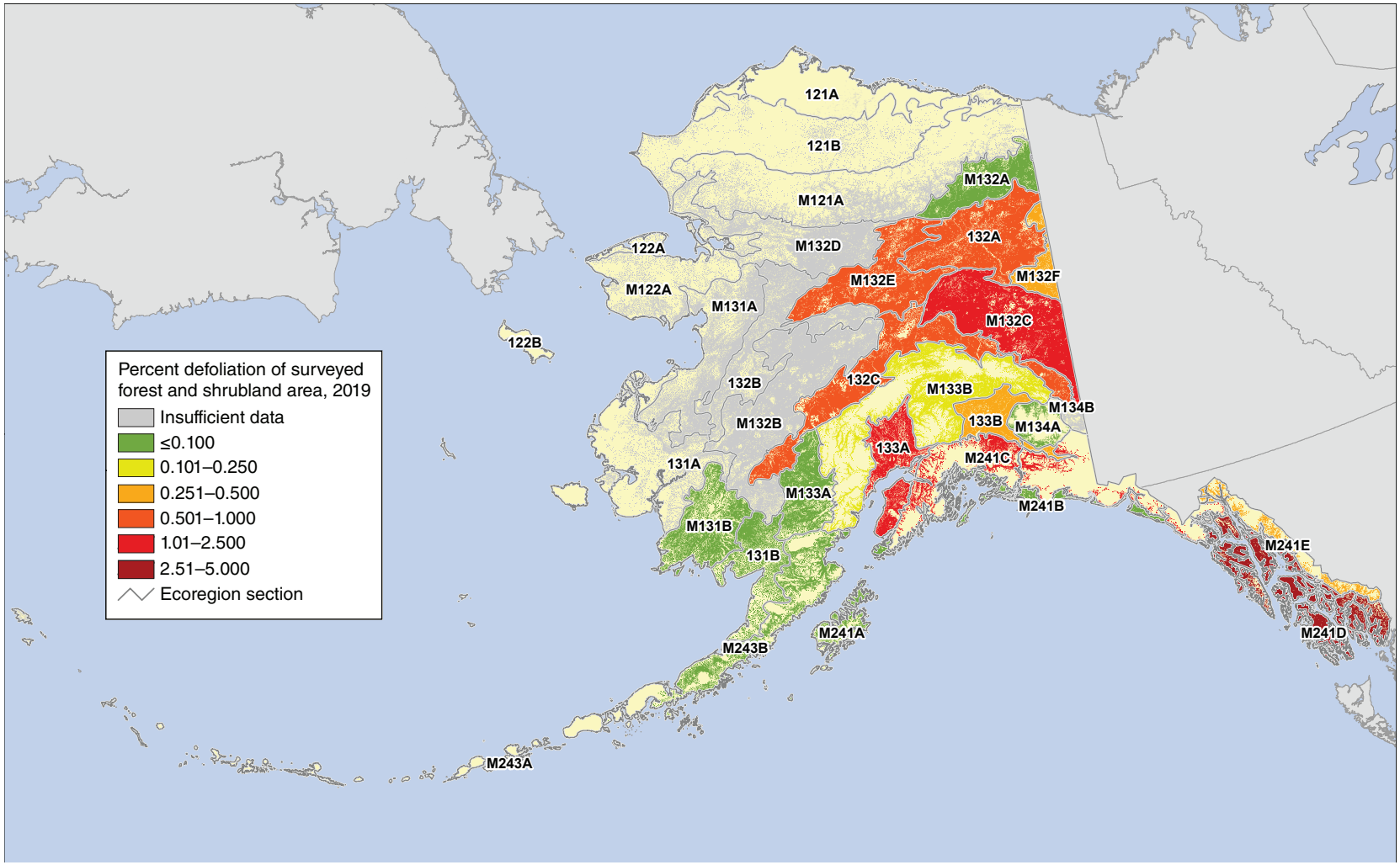

Figure 2.7—Percentage of 2019 surveyed Alaska forest and shrubland area within ecoregions with defoliation caused by insects and diseases. The gray lines delineate ecoregion sections (Spencer and others 2002). Forest and shrub cover is derived from the 2011 National Land Cover Database. (Data source: U.S. Department of Agriculture Forest Service, Forest Health Protection)

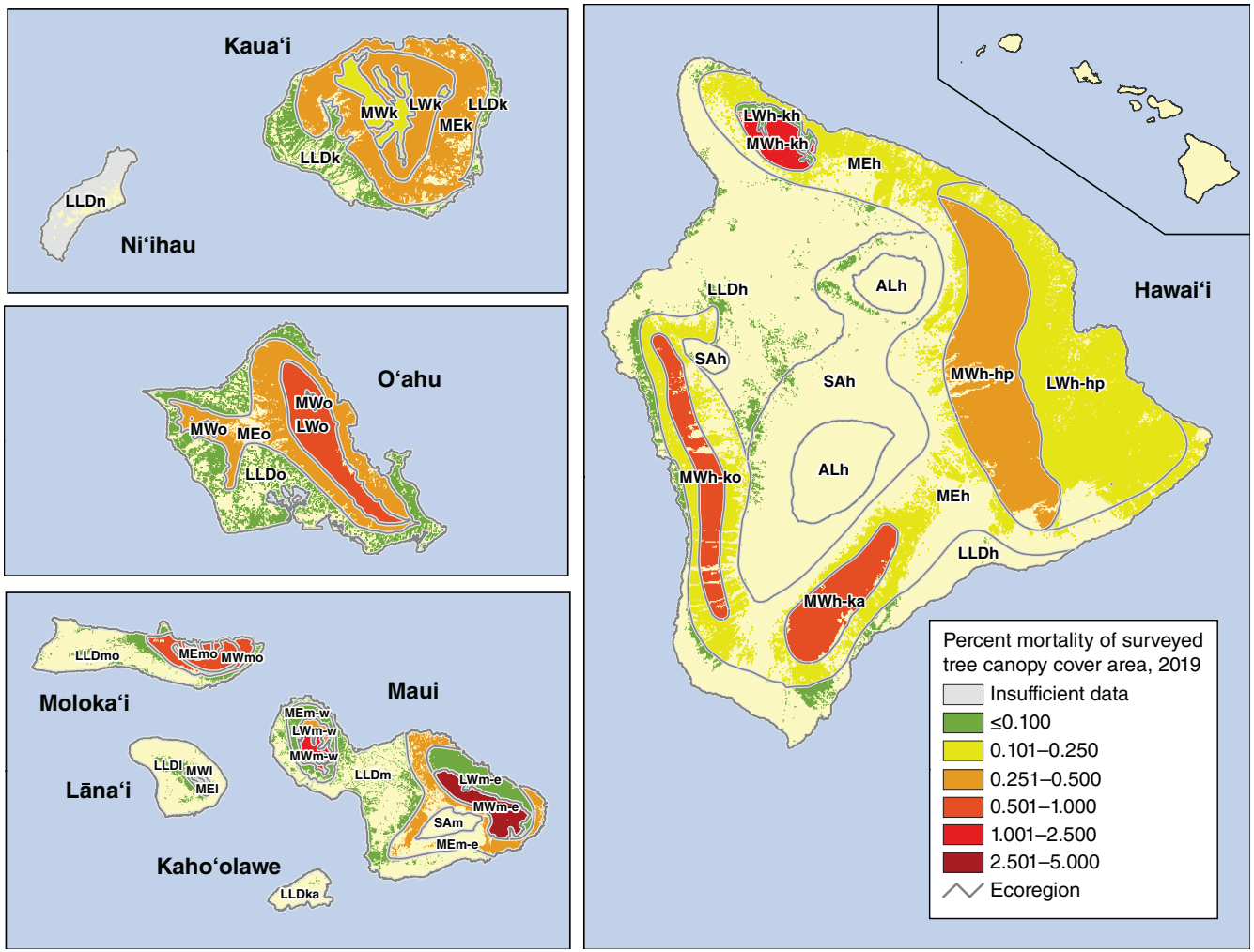

Figure 2.8—Percentage of 2019 surveyed Hawaii tree canopy area within island/ecoregion combinations with mortality caused by insects and diseases. Tree canopy cover is based on data from a cooperative project between the Multi-Resolution Land Characteristics Consortium (Coulston and others 2012) and the Forest Service Geospatial Technology and Applications Center using the 2011 National Land Cover Database. See table 1.1 for ecoregion identification. (Data source: U.S. Department of Agriculture Forest Service, Forest Health Protection)

Montane Wet-Hawai‘i-Kona (MWh-ko) with 0.94 percent, Montane Wet-Moloka‘i (MWmo) with 0.71 percent, and Montane Wet-Hawai‘i-Ka‘ū (MWh-ka) with 0.69 percent. One lowland wet ecoregion (Lowland Wet-O‘ahu [LWo], 0.70 percent) and one mesic ecoregion (Mesic-Moloka‘i [MEmo], 0.53 percent) also had relatively high levels of mortality. These all were areas with mostly very light to moderate ‘ōhi‘a lehua mortality.

A very small area of Hawaii defoliation (5 ha) was detected in 2019 on O‘ahu, attributed to ‘ōhi‘a/guava rust (*Austropuccinia psidii*) (table 2.5).

CONCLUSION

Continued monitoring of insect and disease outbreaks across the United States will be necessary for determining appropriate followup investigation and management activities. Due to the limitations of survey efforts to detect certain important forest insects and diseases, the pests and pathogens discussed in this chapter do not include all the biotic forest health threats that should be considered when making management decisions and budget allocations. However, large-scale assessments of mortality and defoliation severity offer a useful approach for identifying geographic areas where the concentration of monitoring and management activities might be most effective.

LITERATURE CITED

Anselin, L. 1992. Spatial data analysis with GIS: an introduction to application in the social sciences. Tech. Rep. 92-10. Santa Barbara, CA: University of California, National Center for Geographic Information and Analysis. 53 p.

Barnes, I.; Fourie, A.; Wingfield, M.J. [and others]. 2018. New *Ceratocystis* species associated with rapid death of *Metrosideros polymorpha* in Hawaii. Persoonia-Molecular Phylogeny and Evolution of Fungi. 40(1): 154–181. https://doi.org/10.3767/persoonia.2018.40.07.

Berryman, E.; McMahan, A. 2019. Using tree canopy cover data to help estimate acres of damage. In: Potter, K.M.; Conkling, B.L., eds. Forest Health Monitoring: national status, trends, and analysis 2018. Gen. Tech. Rep. SRS-239. Asheville, NC: U.S. Department of Agriculture Forest Service, Southern Research Station: 125–141.

Brockerhoff, E.G.; Liebhold, A.M.; Jactel, H. 2006. The ecology of forest insect invasions and advances in their management. Canadian Journal of Forest Research. 36(2): 263–268. https://doi.org/10.1139/x06-013.

Castello, J.D.; Leopold, D.J.; Smallidge, P.J. 1995. Pathogens, patterns, and processes in forest ecosystems. BioScience. 45(1): 16–24. https://doi.org/10.2307/1312531.

Cleland, D.T.; Freeouf, J.A.; Keys, J.E. [and others]. 2007. Ecological subregions: sections and subsections for the conterminous United States. Gen. Tech. Rep. WO-76D. Washington, DC: U.S. Department of Agriculture Forest Service. Map; Sloan, A.M., cartographer; presentation scale 1:3,500,000; colored. Also on CD-ROM as a GIS coverage in ArcINFO format or at http://data.fs.usda.gov/geodata/edw/datasets.php. [Date accessed: July 20, 2015].

Coleman, T.W.; Graves, A.D.; Heath, Z. [and others]. 2018. Accuracy of aerial detection surveys for mapping insect and disease disturbances in the United States. Forest Ecology and Management. 430: 321–336. https://doi.org/10.1016/j.foreco.2018.08.020.

Coulston, J.W.; Moisen, G.G.; Wilson, B.T. [and others]. 2012. Modeling percent tree canopy cover: a pilot study. Photogrammetric Engineering and Remote Sensing. 78(7): 715–727. https://doi.org/10.14358/PERS.78.7.715.

Edmonds, R.L.; Agee, J.K.; Gara, R.I. 2011. Forest health and protection. Long Grove, IL: Waveland Press, Inc. 667 p.

ESRI. 2017. ArcMap® 10.5.1. Redlands, CA: Environmental Systems Research Institute.

Forest Health Protection (FHP). 2019. Digital Mobile Sketch Mapping user's manual 2.1. Fort Collins, CO: U.S. Department of Agriculture Forest Service, Forest Health Assessment and Applied Sciences Team. https://www.fs.fed.us/foresthealth/technology/docs/DMSM_Tutorial/story_content/external_files/DMSM_User_Guide.pdf. [Date accessed: July 10, 2020].

Forest Health Protection (FHP). 2020. Insect and Disease Detection Survey (IDS) data downloads. Fort Collins, CO: U.S. Department of Agriculture Forest Service, Forest Health Technology Enterprise Team. https://www.fs.fed.us/foresthealth/applied-sciences/mapping-reporting/detection-surveys.shtml. [Date accessed: July 6, 2020].

Getis, A.; Ord, J.K. 1992. The analysis of spatial association by use of distance statistics. Geographical Analysis. 24(3): 189–206. https://doi.org/10.1111/j.1538-4632.1992.tb00261.x.

Holdenrieder, O.; Pautasso, M.; Weisberg, P.J.; Lonsdale, D. 2004. Tree diseases and landscape processes: the challenge of landscape pathology. Trends in Ecology & Evolution. 19(8): 446–452. https://doi.org/10.1016/j.tree.2004.06.003.

Homer, C.G.; Dewitz, J.A.; Yang, L. [and others]. 2015. Completion of the 2011 National Land Cover Database for the conterminous United States: representing a decade of land cover change information. Photogrammetric Engineering and Remote Sensing. 81(5): 345–354.

Laffan, S.W. 2006. Assessing regional scale weed distributions, with an Australian example using *Nassella trichotoma*. Weed Research. 46(3): 194–206. https://doi.org/10.1111/j.1365-3180.2006.00491.x.

Liebhold, A.M.; McCullough, D.G.; Blackburn, L.M. [and others]. 2013. A highly aggregated geographical distribution of forest pest invasions in the USA. Diversity and Distributions. 19: 1208–1216. https://doi.org/10.1111/ddi.12112.

Logan, J.A.; Regniere, J.; Powell, J.A. 2003. Assessing the impacts of global warming on forest pest dynamics. Frontiers in Ecology and the Envionment. 1: 130–137. https://doi.org/10.1890/1540-9295(2003)001[0130:ATIOGW]2.0.CO;2.

Lovett, G.M.; Weiss, M.; Liebhold, A.M. [and others]. 2016. Nonnative forest insects and pathogens in the United States: impacts and policy options. Ecological Applications. 26: 1437–1455. https://doi.org/10.1890/15-1176.

Mack, R.N.; Simberloff, D.; Lonsdale, W.M. [and others]. 2000. Biotic invasions: causes, epidemiology, global consequences, and control. Ecological Applications. 10(3): 689–710. https://doi.org/10.1890/1051-0761(2000)010[0689:BICEGC]2.0.CO;2.

Manion, P.D. 2003. Evolution of concepts in forest pathology. Phytopathology. 93: 1052–1055. https://doi.org/10.1094/PHYTO.2003.93.8.1052.

Parry, D.; Teale, S.A. 2011. Alien invasions: the effects of introduced species on forest structure and function. In: Castello, J.D.; Teale, S.A., eds. Forest health: an integrated perspective. New York: Cambridge University Press: 115–162. https://doi.org/10.1017/CBO9780511974977.006.

Potter, K.M. 2012. Large-scale patterns of insect and disease activity in the conterminous United States and Alaska from the national Insect and Disease Detection Survey database, 2007 and 2008. In: Potter, K.M.; Conkling, B.L., eds. Forest Health Monitoring 2009 national technical report. Gen. Tech. Rep. SRS-167. Asheville, NC: U.S. Department of Agriculture Forest Service, Southern Research Station: 63–78.

Potter, K.M. 2013. Large-scale patterns of insect and disease activity in the conterminous United States and Alaska from the national Insect and Disease Detection Survey, 2009. In: Potter, K.M.; Conkling, B.L., eds. Forest Health Monitoring: national status, trends, and analysis 2010. Gen. Tech. Rep. SRS-176. Asheville, NC: U.S. Department of Agriculture Forest Service, Southern Research Station: 15–29.

Potter, K.M. 2020. Introduction. In: Potter, K.M.; Conkling, B.L., eds. Forest Health Monitoring: national status, trends, and analysis 2019. Gen. Tech. Rep. SRS-250. Asheville, NC: U.S. Department of Agriculture Forest Service, Southern Research Station: 5–24.

Potter, K.M., Canavin, J.C.; Koch, F.H. 2020a. A forest health retrospective: national and regional results from 20 years of Insect and Disease Survey data. In: Potter, K.M.; Conkling, B.L., eds. Forest Health Monitoring: national status, trends, and analysis 2019. Gen. Tech. Rep. SRS-250. Asheville, NC: U.S. Department of Agriculture Forest Service, Southern Research Station: 125–149.

Potter, K.M.; Escanferla, M.E.; Jetton, R.M.; Man, G. 2019a. Important insect and disease threats to United States tree species and geographic patterns of their potential impacts. Forests. 10(4): 304. https://doi.org/10.3390/f10040304.

Potter, K.M.; Escanferla, M.E.; Jetton, RM. [and others]. 2019b. Prioritizing the conservation needs of United States tree species: evaluating vulnerability to forest insect and disease threats. Global Ecology and Conservation. 18: e00622. https://doi.org/10.1016/j.gecco.2019.e00622.

Potter, K.M.; Koch, F.H. 2012. Large-scale patterns of insect and disease activity in the conterminous United States and Alaska, 2006. In: Potter, K.M.; Conkling, B.L., eds. Forest Health Monitoring 2008 national technical report. Gen. Tech. Rep. SRS-158. Asheville, NC: U.S. Department of Agriculture Forest Service, Southern Research Station: 63–72.

Potter, K.M.; Koch, F.H.; Oswalt, C.M.; Iannone, B.V. 2016. Data, data everywhere: detecting spatial patterns in fine-scale ecological information collected across a continent. Landscape Ecology. 31: 67–84. https://doi.org/10.1007/s10980-015-0295-0.

Potter, K.M.; Paschke, J.L. 2013. Large-scale patterns of insect and disease activity in the conterminous United States and Alaska from the national Insect and Disease Detection Survey database, 2010. In: Potter, K.M.; Conkling, B.L., eds. Forest Health Monitoring: national status, trends, and analysis 2011. Gen. Tech. Rep. SRS-185. Asheville, NC: U.S. Department of Agriculture Forest Service, Southern Research Station: 15–28.

Potter, K.M.; Paschke, J.L. 2014. Large-scale patterns of insect and disease activity in the conterminous United States and Alaska from the national Insect and Disease Survey database, 2011. In: Potter, K.M.; Conkling, B.L., eds. Forest Health Monitoring: national status, trends, and analysis 2012. Gen. Tech. Rep. SRS-198. Asheville, NC: U.S. Department of Agriculture Forest Service, Southern Research Station: 19–34.

Potter, K.M.; Paschke, J.L. 2015a. Large-scale patterns of insect and disease activity in the conterminous United States and Alaska from the national Insect and Disease Survey, 2012. In: Potter, K.M.; Conkling, B.L., eds. Forest Health Monitoring: national status, trends, and analysis 2013. Gen. Tech. Rep. SRS-207. Asheville, NC: U.S. Department of Agriculture Forest Service, Southern Research Station: 19–36.

Potter, K.M.; Paschke, J.L. 2015b. Large-scale patterns of insect and disease activity in the conterminous United States, Alaska, and Hawaii from the national Insect and Disease Survey, 2013. In: Potter, K.M.; Conkling, B.L., eds. Forest Health Monitoring: national status, trends, and analysis 2014. Gen. Tech. Rep. SRS-209. Asheville, NC: U.S. Department of Agriculture Forest Service, Southern Research Station: 19–38.

Potter, K.M.; Paschke, J.L. 2016. Large-scale patterns of insect and disease activity in the conterminous United States and Alaska from the national Insect and Disease Survey, 2014. In: Potter, K.M.; Conkling, B.L., eds. Forest Health Monitoring: national status, trends, and analysis 2015. Gen. Tech. Rep. SRS-213. Asheville, NC: U.S. Department of Agriculture Forest Service, Southern Research Station: 21–40.

Potter, K.M.; Paschke, J.L. 2017. Large-scale patterns of insect and disease activity in the conterminous United States and Alaska from the national Insect and Disease Survey, 2015. In: Potter, K.M.; Conkling, B.L., eds. Forest Health Monitoring: national status, trends, and analysis 2016. Gen. Tech. Rep. SRS-222. Asheville, NC: U.S. Department of Agriculture Forest Service, Southern Research Station: 21–42.

Potter, K.M., Paschke, J.L.; Koch, F.H.; Berryman, E.M. 2020b. Large-scale patterns of insect and disease activity in the conterminous United States, Alaska, and Hawaii from the national Insect and Disease Survey, 2018. In: Potter, K.M.; Conkling, B.L., eds. Forest Health Monitoring: national status, trends, and analysis 2019. Gen. Tech. Rep. SRS-250. Asheville, NC: U.S. Department of Agriculture Forest Service, Southern Research Station: 27–55.

Potter, K.M.; Paschke, J.L.; Koch, F.H.; Zweifler, M. 2019c. Large-scale patterns of insect and disease activity in the conterminous United States, Alaska, and Hawaii from the national Insect and Disease Survey, 2017. In: Potter, K.M.; Conkling, B.L., eds. Forest Health Monitoring: national status, trends, and analysis 2018. Gen. Tech. Rep. SRS-239. Asheville, NC: U.S. Department of Agriculture Forest Service, Southern Research Station: 21–49.

Potter, K.M.; Paschke, J.L.; Zweifler, M. 2018. Large-scale patterns of insect and disease activity in the conterminous United States, Alaska, and Hawaii from the national Insect and Disease Survey, 2016. In: Potter, K.M.; Conkling, B.L., eds. Forest Health Monitoring: national status, trends, and analysis 2017. Gen. Tech. Rep. SRS-233. Asheville, NC: U.S. Department of Agriculture Forest Service, Southern Research Station: 23–44.

Reams, G.A.; Smith, W.D.; Hansen, M.H. [and others]. 2005. The Forest Inventory and Analysis sampling frame. In: Bechtold, W.A.; Patterson, P.L., eds. The enhanced Forest Inventory and Analysis program—national sampling design and estimation procedures. Gen. Tech. Rep. SRS-80. Asheville, NC: U.S. Department of Agriculture Forest Service, Southern Research Station: 11–26.

Shima, T.; Sugimoto, S.; Okutomi, M. 2010. Comparison of image alignment on hexagonal and square lattices. In: 2010 IEEE international conference on image processing. [Place of publication unknown]: Institute of Electrical and Electronics Engineers, Inc.: 141–144. https://doi.org/10.1109/ICIP.2010.5654351.

Smith, W.B.; Miles, P.D.; Perry, C.H.; Pugh, S.A. 2009. Forest resources of the United States, 2007. Gen. Tech. Rep. WO-78. Washington, DC: U.S. Department of Agriculture Forest Service. 336 p.

Spencer, P.; Nowacki, G.; Fleming, M. [and others]. 2002. Home is where the habitat is: an ecosystem foundation for wildlife distribution and behavior. Arctic Research of the United States. 16: 6–17.

Teale, S.A.; Castello, J.D. 2011. Regulators and terminators: the importance of biotic factors to a healthy forest. In: Castello, J.D.; Teale, S.A., eds. Forest health: an integrated perspective. New York: Cambridge University Press: 81–114. https://doi.org/10.1017/CBO9780511974977.005.

Tobin, P.C. 2015. Ecological consequences of pathogen and insect invasions. Current Forestry Reports. 1: 25–32. https://doi.org/10.1007/s40725-015-0008-6.

University of Hawai‘i, College of Tropical Agriculture and Human Resources. 2020. Rapid ʻōhiʻa death. http://rapidohiadeath.org. [Date accessed: September 4, 2020].

U.S. Department of Agriculture (USDA) Forest Service. 2008. National forest type data development. http://svinetfc4.fs.fed.us/rastergateway/forest_type/. [Date accessed: May 13, 2008].

White, D.; Kimerling, A.J.; Overton, W.S. 1992. Cartographic and geometric components of a global sampling design for environmental monitoring. Cartography and Geographic Information Systems. 19(1): 5–22. https://doi.org/10.1559/152304092783786636.

Zhang, L.; Rubin, B.D.; Manion, P.D. 2011. Mortality: the essence of a healthy forest. In: Castello, J.D.; Teale, S.A., eds. Forest health: an integrated perspective. New York: Cambridge University Press: 17–49. https://doi.org/10.1017/CBO9780511974977.003.

CHAPTER 3.

Broad-Scale Patterns of Forest Fire Occurrence across the 50 United States and the Caribbean Territories, 2019

Kevin M. Potter

INTRODUCTION

As a pervasive disturbance agent operating at many spatial and temporal scales, wildland fire is a key abiotic factor affecting forest health both positively and negatively. In some ecosystems, for example, wildland fires have been essential for regulating processes that maintain forest health (Lundquist and others 2011). Wildland fire is an important ecological mechanism that shapes the distributions of species, maintains the structure and function of fire-prone communities, and acts as a significant evolutionary force (Bond and Keeley 2005). At the same time, wildland fires have created forest health (i.e., sustainability) problems in some ecosystems (Edmonds and others 2011).

Current fire regimes on more than half of the forested area in the conterminous United States have been moderately or significantly altered from historical regimes (Barbour and others 1999), potentially altering key ecosystem components such as species composition, structural stage, stand age, canopy closure, and fuel loadings (Schmidt and others 2002). Fires in some regions and ecosystems have become larger, more intense, and more damaging because of the accumulation of fuels as a result of prolonged fire suppression (Pyne 2010). In some regions, plant communities have experienced or are undergoing rapid compositional and structural changes as a result of fire suppression (Nowacki and Abrams 2008). Additionally, changes in fire intensity and recurrence could result in decreased forest resilience and persistence (Lundquist and others 2011), and fire regimes altered by global climate change could cause large-scale shifts in vegetation spatial patterns (McKenzie and others 1996).

At the same time, large wildland fires also can have long-lasting social and economic consequences, which include the loss of human life and property, smoke-related human health impacts, and the economic cost and dangers of fighting the fires themselves (Gill and others 2013, Richardson and others 2012).

This chapter presents analyses of daily satellite-based fire occurrence data that map and quantify the locations and intensities of fire occurrences spatially across the conterminous United States, Alaska, Hawaii, and the Caribbean territories in 2019. It also compares 2019 fire occurrences, within a geographic context, to all the recent years for which such data are available. Quantifying and monitoring such large-scale patterns of fire occurrence across the United States can help improve our understanding of the ecological and economic impacts of fire as well as the appropriate management and prescribed use of fire. Specifically, large-scale assessments of fire occurrence can help identify areas where specific management activities may be needed, or where research into the ecological and socioeconomic impacts of fires may be required. Additionally, given the potential for climate change and shifting species distributions to alter historic fire regimes, quantifying the location and frequency

of forest fire occurrences across the United States can help us to better understand emerging spatiotemporal patterns of fire occurrence.

METHODS

Data

Annual monitoring and reporting of active wildland fire events using the Moderate Resolution Imaging Spectroradiometer (MODIS) Active Fire Detections for the United States database (USDA Forest Service 2020) allow analysts to spatially display and summarize fire occurrences across broad geographic regions (Coulston and others 2005; Potter 2012a, 2012b, 2013a, 2013b, 2014, 2015a, 2015b, 2016, 2017, 2018, 2019, 2020a). A fire occurrence is defined as one daily satellite detection of wildland fire in a 1-km pixel, with multiple fire occurrences possible on a pixel across multiple days resulting from a single wildland fire that lasts more than 1 day. The data are derived using the MODIS Rapid Response System (Justice and others 2002, 2011) to extract fire location and intensity information from the thermal infrared bands of imagery collected daily by two satellites at a resolution of 1 km, with the center of a pixel recorded as a fire occurrence (USDA Forest Service 2020). The Terra and Aqua satellites' MODIS sensors identify the presence of a fire at the time of image collection, with Terra observations collected in the morning and Aqua observations collected in the afternoon. The resulting fire occurrence data represent only whether a fire was active because the MODIS data bands may not differentiate between a hot fire in a relatively small area (0.01 km^2, for example) and a cooler fire over a larger area (1 km^2, for example) if the foreground to background temperature contrast is not sufficiently high. The MODIS Active Fire database does well at capturing large fires during cloud-free conditions but may underrepresent rapidly burning, small, and low-intensity fires, as well as fires in areas with frequent cloud cover (Hawbaker and others 2008). For large-scale assessments, the dataset represents a good alternative to the use of information on ignition points, which may be preferable but can be difficult to obtain or may not exist (Tonini and others 2009). More information about the performance of this product is available in Justice and others (2011). The fire occurrence data additionally do not identify fires intentionally set for management purposes (controlled burns), which are common in some parts of the United States, particularly in the South.

It is important to underscore that estimates of burned area and calculations of MODIS-detected fire occurrences are two different metrics for quantifying fire activity within a given year. Most importantly, the MODIS data contain both spatial and temporal components because persistent fire will be detected repeatedly over several days on a given 1-km pixel. In other words, a location can be counted as having a fire occurrence multiple times, once for each day a fire is detected at the location. Analyses of the MODIS-detected fire occurrences, therefore, measure the total number of daily

1-km pixels with fire during a year, as opposed to quantifying only the area on which fire occurred at some point during the course of the year. A fire detected on a single pixel for every day in the month of July, for example, would be equivalent to 31 fire occurrences.

The Terra and Aqua satellites, which carry the MODIS sensors, were launched in 1999 and 2002, respectively, and will eventually be decommissioned. An alternative fire occurrence data source is the Visible Infrared Imaging Radiometer Suite (VIIRS) sensor on board the Suomi National Polar-orbiting Partnership (Suomi NPP) weather satellite. The transition to this new data source will require a comparison of fire occurrence detections between it and MODIS. This is because VIIRS data are available from 2014 onward (USDA Forest Service 2020), but it will be important for assessments of fire occurrence trends to be able to analyze as long a window of time as possible (i.e., from the beginning of MODIS data availability).

Analyses

These MODIS products for 2019, and for the 18 preceding full years of data, were processed in ArcMap® (ESRI 2017) to determine forest fire occurrence density (that is, the number of fire occurrences/100 km^2 [10 000 ha] of tree canopy cover area) for each ecoregion section in the conterminous United States (Cleland and others 2007), for ecoregions on each of the major islands of Hawaii (Potter 2020b), and for the islands of the Caribbean territories of Puerto Rico and the U.S. Virgin Islands. For the current analyses, the forest fire occurrence density metrics for the conterminous 48 States, Hawaii, and the Caribbean territories (the number of fire occurrences/100 km^2 of tree canopy cover area) were calculated after screening out wildland fires that did not intersect with tree canopy data. The tree canopy data had been resampled to 240 m from a 30-m raster dataset that estimates percentage of tree canopy cover (from 0 to 100 percent) for each grid cell; this dataset was generated from the 2011 National Land Cover Database (NLCD) (Homer and others 2015) through a cooperative project between the Multi-Resolution Land Characteristics Consortium and the U.S. Department of Agriculture Forest Service, Geospatial Technology and Applications Center (GTAC) (Coulston and others 2012). For our purposes, we treated any cell with >0-percent tree canopy cover as forest. Comparable tree canopy cover data were not available for Alaska, so we instead created a 240-m-resolution layer of forest and shrub cover from the 2011 NLCD. The MODIS fire occurrence detection data were then intersected with this layer and with ecoregion sections for the State (Spencer and others 2002) to calculate the number of fire occurrences/100 km^2 of forest and shrub cover within each ecoregion section in Alaska. In Forest Health Monitoring national reports before 2019, the number of fire occurrences/100 km^2 of forest was determined for the conterminous States, Alaska, and Hawaii using a forest cover mask derived from MODIS imagery by the Forest Service GTAC (USDA Forest Service 2008).

The total numbers of forest fire occurrences were also determined separately for the conterminous States, Alaska, Hawaii, and the Caribbean territories after clipping the MODIS fire occurrences by the canopy cover or tree and shrub cover data.

The fire occurrence density value for each of the ecoregions of the States and for the Caribbean islands in 2019 was then compared with the mean fire density values for the first 18 full years of MODIS Active Fire data collection (2001–2018). Specifically, the difference of the 2019 value and the previous 18-year mean for an ecoregion was divided by the standard deviation across the previous 18-year period, assuming a normal distribution of fire density over time in the ecoregion. The result for each ecoregion was a standardized *z*-score, which is a dimensionless quantity describing the degree to which the fire occurrence density in the ecoregion in 2019 was higher, lower, or the same relative to all the previous years for which data have been collected, accounting for the variability in the previous years. The *z*-score is the number of standard deviations between the observation and the mean of the historic observations in the previous years. Approximately 68 percent of observations would be expected within one standard deviation of the mean, and 95 percent within two standard deviations. Near-normal conditions are classified as those within a single standard deviation of the mean, although such a threshold is somewhat arbitrary. Conditions between about one and two standard deviations of the mean are moderately different from mean conditions but are not significantly different statistically. Those outside about two standard deviations would be considered statistically greater than or less than the long-term mean (at $p < 0.025$ at each tail of the distribution).

Additionally, we used the Spatial Association of Scalable Hexagons (SASH) analytical approach to identify forested areas in the conterminous United States with higher-than-expected fire occurrence density in 2019. This method identifies locations where ecological phenomena occur at greater or lower occurrences than expected by random chance and is based on a sampling frame optimized for spatial neighborhood analysis, adjustable to the appropriate spatial resolution, and applicable to multiple data types (Potter and others 2016). Specifically, it consists of dividing an analysis area into scalable equal-area hexagonal cells within which data are aggregated, followed by identifying statistically significant geographic clusters of hexagonal cells within which mean values are greater or less than those expected by chance. To identify these clusters, we employed a Getis-Ord G_i^* hot spot analysis (Getis and Ord 1992) in ArcMap® 10.5.1 (ESRI 2017).

The spatial units of analysis were 9,810 hexagonal cells, each approximately 834 km^2 in area, generated in a lattice across the conterminous United States using intensification of the Environmental Monitoring and Assessment Program (EMAP) North American hexagon coordinates (White and others 1992). These coordinates are the foundation of a sampling frame in which a hexagonal lattice

was projected onto the conterminous United States by centering a large base hexagon over the region (Reams and others 2005, White and others 1992). The hexagons are compact and uniform in their distance to the centroids of neighboring hexagons, meaning that a hexagonal lattice has a higher degree of isotropy (uniformity in all directions) than does a square grid (Shima and others 2010). These are convenient and highly useful attributes for spatial neighborhood analyses. These scalable hexagons also are independent of geopolitical and ecological boundaries, avoiding the possibility of different sample units (such as counties, States, or watersheds) encompassing vastly different areas (Potter and others 2016). We selected hexagons 834 km^2 in area because this is a manageable size for making monitoring and management decisions in analyses across the conterminous United States (Potter and others 2016).

Fire occurrence density values for each hexagon were quantified as the number of forest fire occurrences/100 km^2 of tree canopy cover area within the hexagon. The Getis-Ord G_i^* statistic was used to identify clusters of hexagonal cells with fire occurrence density values higher than expected by chance. This statistic allows for the decomposition of a global measure of spatial association into its contributing factors, by location, and is therefore particularly suitable for detecting outlier assemblages of similar conditions in a dataset, such as when spatial clustering is concentrated in one subregion of the data (Anselin 1992).

Briefly, G_i^* sums the differences between the mean values in a local sample, determined in this case by a moving window of each hexagon and its 18 first- and second-order neighbors (the 6 adjacent hexagons and the 12 additional hexagons contiguous to those 6) and the global mean of the 9,644 hexagonal cells with tree canopy cover (of the total 9,810) in the conterminous United States. As described in Laffan (2006), it is calculated as

$$G_i^*(\boldsymbol{d}) = \frac{\sum_j w_{ij}(\boldsymbol{d})\, x_j - W_i^* \bar{x}^*}{s^* \sqrt{\frac{(ns_{1i}^*) - W_i^{*2}}{n-1}}}$$

where

G_i^* = the local clustering statistic (in this case, for the target hexagon)

i = the center of local neighborhood (the target hexagon)

d = the width of local sample window (the target hexagon and its first- and second-order neighbors)

x_j = the value of neighbor j

w_{ij} = the weight of neighbor j from location i (all the neighboring hexagons in the moving window were given an equal weight of 1)

n = number of samples in the dataset (the 9,644 hexagons containing tree cover)

W_i^* = the sum of the weights

$s^*_1 i$ = the number of samples within d of the central location (19: the focal hexagon and its 18 first- and second-order neighbors)

$\bar{x}^*$ = the mean of whole dataset (in this case, for all 9,644 hexagons containing tree cover)

s^* = the standard deviation of whole dataset (for all 9,644 hexagons containing tree cover)

G_i^* is standardized as a z-score with a mean of 0 and a standard deviation of 1, with values >1.96 representing significant local clustering of higher fire occurrence densities (p <0.025) and values <-1.96 representing significant clustering of lower fire occurrence densities (p <0.025), because 95 percent of the observations under a normal distribution should be within approximately two standard deviations of the mean (Laffan 2006). Values between -1.96 and 1.96 have no statistically significant concentration of high or low values; a hexagon and its 18 neighbors, in other words, have a normal range of both high and low numbers of fire occurrences/100 km^2 of tree canopy cover area. It is worth noting that the threshold values are not exact because the correlation of spatial data violates the assumption of independence required for statistical significance (Laffan 2006). In addition, the Getis-Ord approach does not require that the input data be normally distributed, because the local G_i^* values are computed under a randomization assumption, with G_i^* equating to a standardized z-score that asymptotically tends to a normal distribution (Anselin 1992). The z-scores are considered to be reliable, even with skewed data, as long as the local neighborhood encompasses several observations (ESRI 2017), in this case, via the target hexagon and its 18 first- and second-order neighbors.

RESULTS AND DISCUSSION

Trends in Forest Fire Occurrence Detections for 2019

The MODIS Active Fire database recorded 40,657 forest fire occurrences across the conterminous United States in 2019, the fifth lowest in 19 full years of data collection and the least in a year since 2005 (fig. 3.1). This was a decline of approximately 47 percent from 2018 (76,692 total forest fire occurrences), and 43 percent lower than the mean of the previous 18 years of data. At the same time, Alaska experienced a dramatic 3,740-percent increase in fire occurrences from 2018, from 690 to 26,493, as well as a 157-percent increase over the mean of the previous years. This was the third most fire occurrences in Alaska in 19 years of data collection, and the most since 2005. Hawaii had only 36 fire occurrences in 2019, which was a 74-percent drop from 2018 (136) and an 88-percent decrease from the 2001–2018 average. Finally, 18 fire occurrences were detected in Puerto Rico, an increase from the single occurrence in 2018 and about 85 percent above the average of 9.7 per year.

The decrease in fire occurrences in the conterminous United States along with the stark upsurge in fire occurrences in Alaska are in keeping with the official national wildland fire statistics, which are based on numbers of wildfires reported and area burned (National

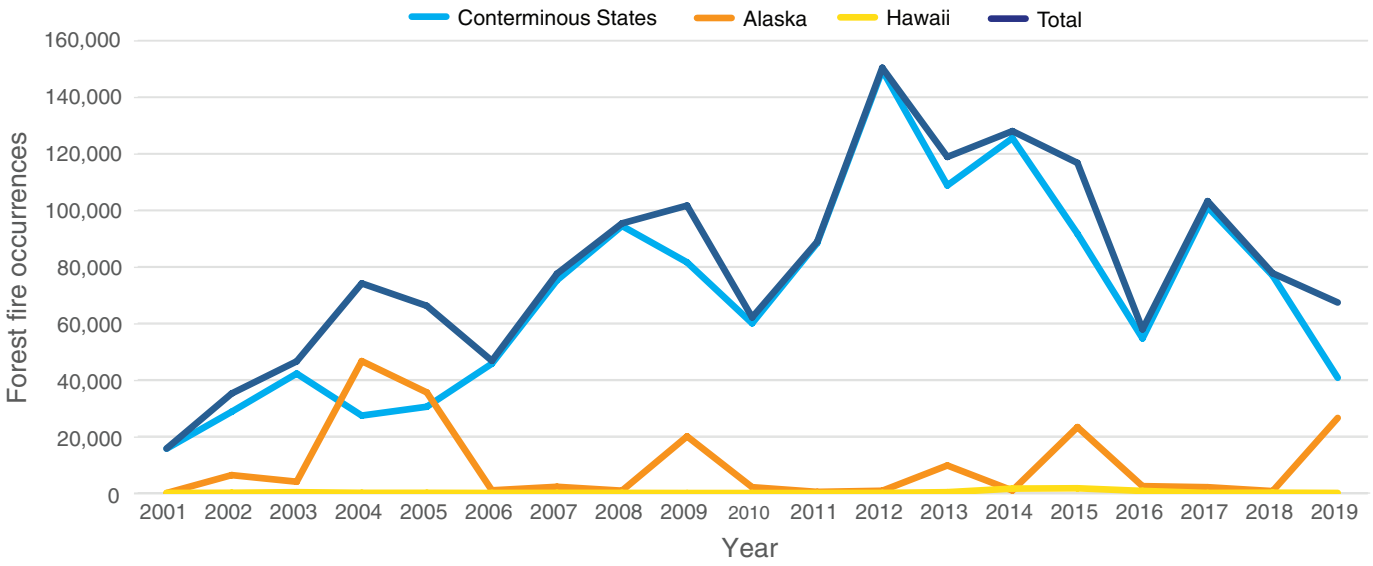

Figure 3.1—Forest fire occurrences detected by Moderate Resolution Imaging Spectroradiometer (MODIS) from 2001 through 2019 for the conterminous United States, Alaska, and Hawaii, and for the entire Nation combined. (Data source: U.S. Department of Agriculture Forest Service, Geospatial Technology and Applications Center, in conjunction with the NASA MODIS Rapid Response group)

Interagency Coordination Center 2020). According to these statistics, there were 50,477 wildfires nationally in 2019 compared to 58,083 in 2018, while the area burned declined 47 percent from 3 548 078 ha in 2018 to 1 887 601 ha in 2019, and was 33 percent less than the 10-year average (National Interagency Coordination Center 2019, 2020). Alaska was the only region in the United States with a larger-than-average area burned as well as the only region with a significant increase in number of fires reported. Across the United States in 2019, the number of wildland fires and fire complexes exceeding 16 187 ha (40,000 acres, a benchmark threshold for the National Interagency Coordination Center) was only 27, compared to 49 in 2018 and 44 in 2017 (National Interagency Coordination Center 2018, 2019, 2020). Of these, all but two of the 15 largest U.S. fires in 2019 occurred in Alaska (National Interagency Coordination Center 2020). As noted in the Methods section above, estimates of burned area and numbers of reported fires are different metrics for quantifying fire activity than calculations of MODIS-detected fire occurrences, though they may be correlated.

This was not the first time that a peak fire year in Alaska corresponded with a decrease in fire occurrences in the conterminous

United States (fig. 3.1). In 2004 and 2005, in fact, the number of fire occurrences in Alaska exceeded those of the conterminous States, the only times during the MODIS period that this happened. Additionally, peaks of Alaska fire occurrences in 2009 and 2015 were followed the next year by a marked decrease in conterminous States fire occurrences. Such broad-scale patterns of wildfire throughout North America are the result of the interaction between climate and vegetation development across a range of spatial and temporal scales, with climate influencing fine fuel moisture, ignition frequency, and rates of wildfire spread at annual to interannual timescales (Gedalof 2011) and with years of high fire activity in the West characterized by widespread and regionally distinct summer droughts (Trouet and others 2010). Interannual to multidecadal variability in sea surface temperatures, associated with the El Niño-Southern Oscillation (ENSO), Pacific Decadal Oscillation (PDO), and Atlantic Multidecadal Oscillation (AMO), drive intermediate-term patterns in wildfire occurrence in North America (Kitzberger and others 2007). Further research could help illuminate the relationships between climate and wildfire occurrences within and between regions of the conterminous 48 States and Alaska.

Areas with the highest fire occurrence densities in 2019 were in southwestern Idaho, central California, and eastern Kansas (fig. 3.2). The Owyhee Uplands (342C) was the ecoregion section with the highest fire occurrence density in 2019, with 8.8 fire occurrences/100 km^2 of tree canopy cover (table 3.1). (In the previous year, the ecoregion section with the highest fire occurrence density was the Northern California Coast Ranges [M261B], which experienced 31.8 fire occurrences/100 km^2 of tree canopy cover [Potter 2020a]). Two other ecoregion sections had relatively high fire occurrence densities: 262A–Great Valley in California (8.4 fire occurrences/100 km^2 of tree canopy cover) and 251F–Flint Hills in Kansas (6.7 fire occurrences/100 km^2 of tree canopy cover). A handful of ecoregion sections in the Southeast, in Arizona and New Mexico, in northern California, and in Oregon and Washington had moderate fire occurrence densities (fig. 3.2). The relatively low fire occurrence densities across the conterminous 48 States were attributable at least in part to the atypical summer of 2019, during which spring-like temperatures held until early July, and long-duration and hot high-pressure ridge events did not develop in the West (National Interagency Coordination Center 2020).

On the other hand, Alaska experienced extraordinarily hot and dry conditions in June and July, with July 2019 being the hottest month on record for the State; conditions were critically dry in the interior as the summer rains arrived later than usual in August and missed the south-central part of Alaska (National Interagency Coordination Center 2020). As a result, fire occurrence densities across large swaths of central and south-central Alaska were moderate, with densities very high in 132A–Yukon-Old Crow Basin (19.4 fire occurrences/100 km^2 of forest and shrub cover) (fig. 3.3). This ecoregion section

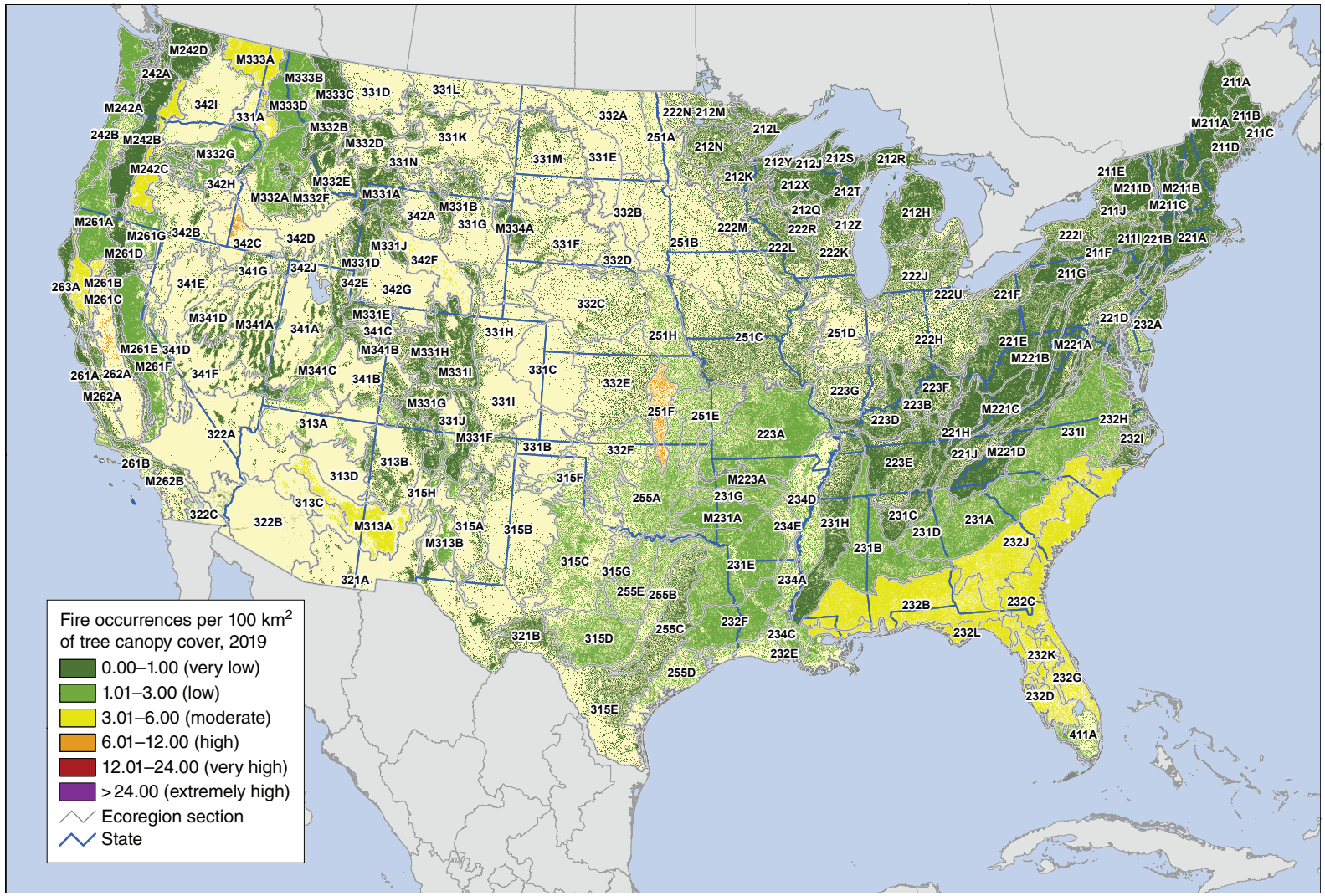

Figure 3.2—The number of forest fire occurrences, per 100 km^2 (10 000 ha) of tree canopy coverage area, by ecoregion section within the conterminous 48 States, for 2019. The gray lines delineate ecoregion sections (Cleland and others 2007). Tree canopy cover is based on data from a cooperative project between the Multi-Resolution Land Characteristics Consortium (Coulston and others 2012) and the Forest Service Geospatial Technology and Applications Center using the 2011 National Land Cover Database. See figure 1.1A for ecoregion identification. (Source of fire data: U.S. Department of Agriculture Forest Service, Geospatial Technology and Applications Center, in conjunction with the NASA MODIS Rapid Response group)

Table 3.1—The 15 ecoregion sections in the conterminous United States with the highest fire occurrence densities in 2019

Section	Name	Tree canopy area	Fire occurrences	Density[a]
		km²	*number*	
342C	Owyhee Uplands	16.7	148	8.8
262A	Great Valley	19.4	164	8.4
251F	Flint Hills	57.8	387	6.7
232B	Gulf Coastal Plains and Flatwoods	888.7	4770	5.4
232J	Southern Atlantic Coastal Plains and Flatwoods	604.0	2,865	4.7
342F	Central Basin and Hills	16.5	77	4.7
232K	Florida Coastal Plains Central Highlands	149.0	632	4.2
M261C	Northern California Interior Coast Ranges	18.2	73	4.0
M261B	Northern California Coast Ranges	114.1	439	3.8
M333A	Okanogan Highland	247.9	919	3.7
232D	Florida Coastal Lowlands-Gulf	134.9	491	3.6
M313A	White Mountains-San Francisco Peaks-Mogollon Rim	202.5	717	3.5
232G	Florida Coastal Lowlands-Atlantic	138.5	471	3.4
331A	Palouse Prairie	33.4	107	3.2
313C	Tonto Transition	17.5	55	3.2

[a] Density = fire occurrences/100 km^2 of tree canopy coverage area.

was the location of the Chalkyitsik Complex of fires, which burned 204 463 ha and cost approximately $7 million to contain (National Interagency Coordination Center 2020).

In Hawaii, only a single area had at least moderate fire occurrence density in 2019, the Lowland/Leeward Dry ecoregion on Maui island (LLDm) with fire occurrence density of 5.5/100 km^2 of tree canopy cover (fig. 3.4).

All other ecoregions in the State had 2019 fire occurrence densities of ≤3/100 km^2 of tree canopy cover. This followed a year during which a dramatic Big Island lava eruption in the lower east rift zone of the Kīlauea volcano burned forests and homes at the very eastern tip of the island (Andrews 2018), resulting in a high fire occurrence density (7.4/100 km^2 of tree canopy cover) in the island's Lowland Wet-Hilo-Puna ecoregion (LWh-hp) (Potter 2020a).

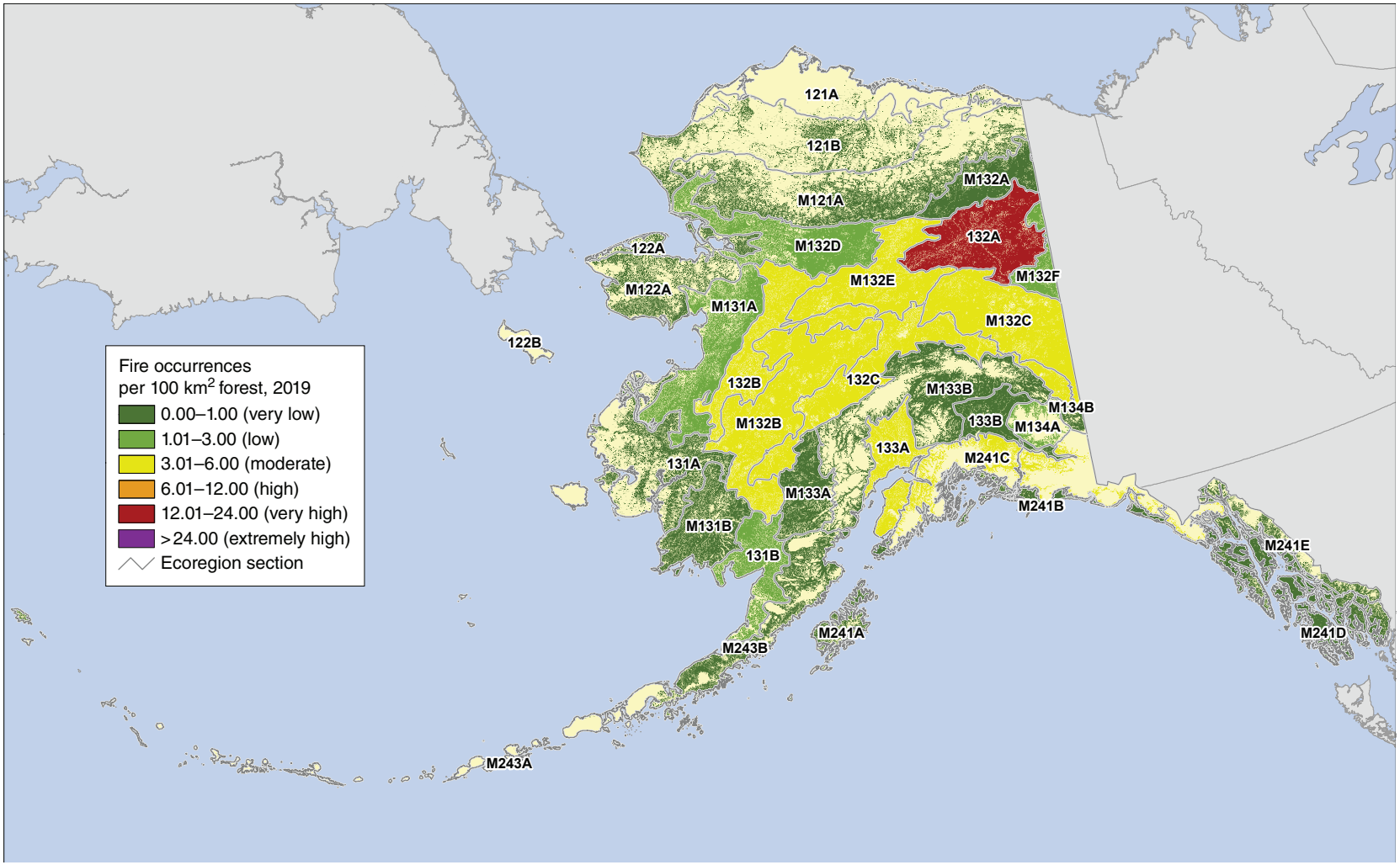

Figure 3.3—The number of forest fire occurrences, per 100 km^2 (10 000 ha) of forest and shrub cover, by ecoregion section within Alaska, for 2019. The gray lines delineate ecoregion sections (Spencer and others 2002). Forest and shrub cover are derived from the 2011 National Land Cover Database. See figure 1.1B for ecoregion identification. (Source of fire data: U.S. Department of Agriculture Forest Service, Geospatial Technology and Applications Center, in conjunction with the NASA MODIS Rapid Response group)

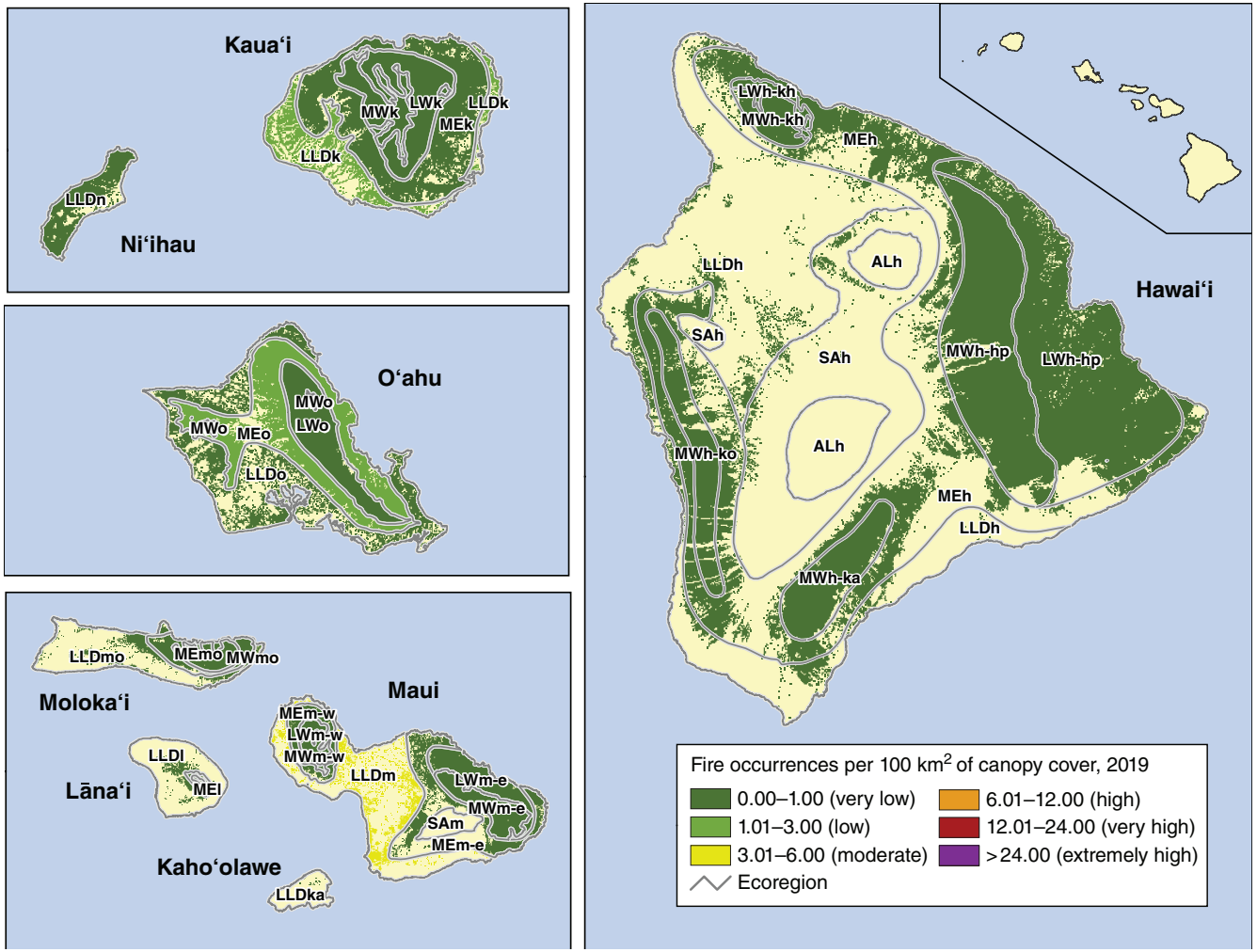

Figure 3.4—The number of forest fire occurrences, per 100 km^2 (10 000 ha) of tree canopy coverage area, by island/ecoregion combination in Hawaii, for 2019. Tree canopy cover is based on data from a cooperative project between the Multi-Resolution Land Characteristics Consortium (Coulston and others 2012) and the Forest Service Geospatial Technology and Applications Center using the 2011 National Land Cover Database. See table 1.1 for ecoregion identification. (Source of fire data: U.S. Department of Agriculture Forest Service, Geospatial Technology and Applications Center, in conjunction with the NASA MODIS Rapid Response group)

Finally, 2019 fire occurrence densities were ≤1/100 km^2 of tree canopy cover for all of the islands of the U.S. Caribbean territories (Puerto Rico and the U.S. Virgin Islands) (fig. 3.5).

Comparison to Longer Term Trends

The nature of the MODIS Active Fire data makes it possible to contrast short-term (2019) forest fire occurrence densities with longer term trends encompassing the first 18 full years of data collection (2001–2018) for ecoregions in the conterminous States, Alaska, and Hawaii, and for Caribbean islands. Across that multiyear period, the highest mean annual fire occurrences in the conterminous States are in ecoregion sections of the northern Rocky Mountains, California, the Southwest, the southern Great Plains, and the Southeastern Coastal Plain (fig. 3.6A). Meanwhile, ecoregions elsewhere generally experienced ≤3 fire occurrences/100 km^2 of tree canopy cover annually, with the Northeast and most of the Midwest having ≤1. The M332A–Idaho Batholith in central Idaho had the highest fire occurrence density on average (mean annual fire occurrence density of 12.8), followed by M261A–Klamath Mountains of northwestern California and southeastern Oregon (10.6) (table 3.2). Other ecoregion sections with high mean fire occurrence densities (6.01–12.00 fire occurrences/100 km^2 of canopy cover) were located along the Gulf Coast in the Southeast; in coastal, northern, and central areas of California; in north-central Washington; in central Arizona and New Mexico; in the northern Rocky Mountains; and in central Kansas and northeastern Oklahoma (table 3.2). The ecoregion section with the greatest annual variation in fire occurrence densities from 2001 to 2018 was again M332A–Idaho Batholith, with more moderate variation in California, northeastern Washington and northwestern Idaho, southern Oregon, western Montana, and central Arizona and west-central New Mexico (fig. 3.6B). The Northeast and most of the Midwest had the lowest variation, while relatively low variation was also present across the Southeast, the central Rocky Mountain States, the Great Basin, and central Oregon and Washington.

Most of the conterminous United States experienced near-normal fire occurrence densities in 2019, compared to the previous 17-year mean and accounting for variability over time (fig. 3.6C). As determined by the calculation of standardized fire occurrence *z*-scores, a few ecoregions in the Northeast and scattered elsewhere had significantly higher fire occurrence densities than normal. The ecoregion section with the highest *z*-score in 2019 was 212J–Southern Superior Uplands, an area with typically very few fire occurrences. Other similar ecoregion sections were 211A–Aroostook Hills and Lowlands of northern Maine, 221A–Lower New England along the Atlantic Coast from New York to Maine, 342C–Southern Superior Uplands in southwest Idaho, 315B–Texas High Plains in western Texas and eastern New Mexico, 331J–Northern Rio Grande Basin in north-central New Mexico and south-central Colorado, and 262A–Great Valley in central California.

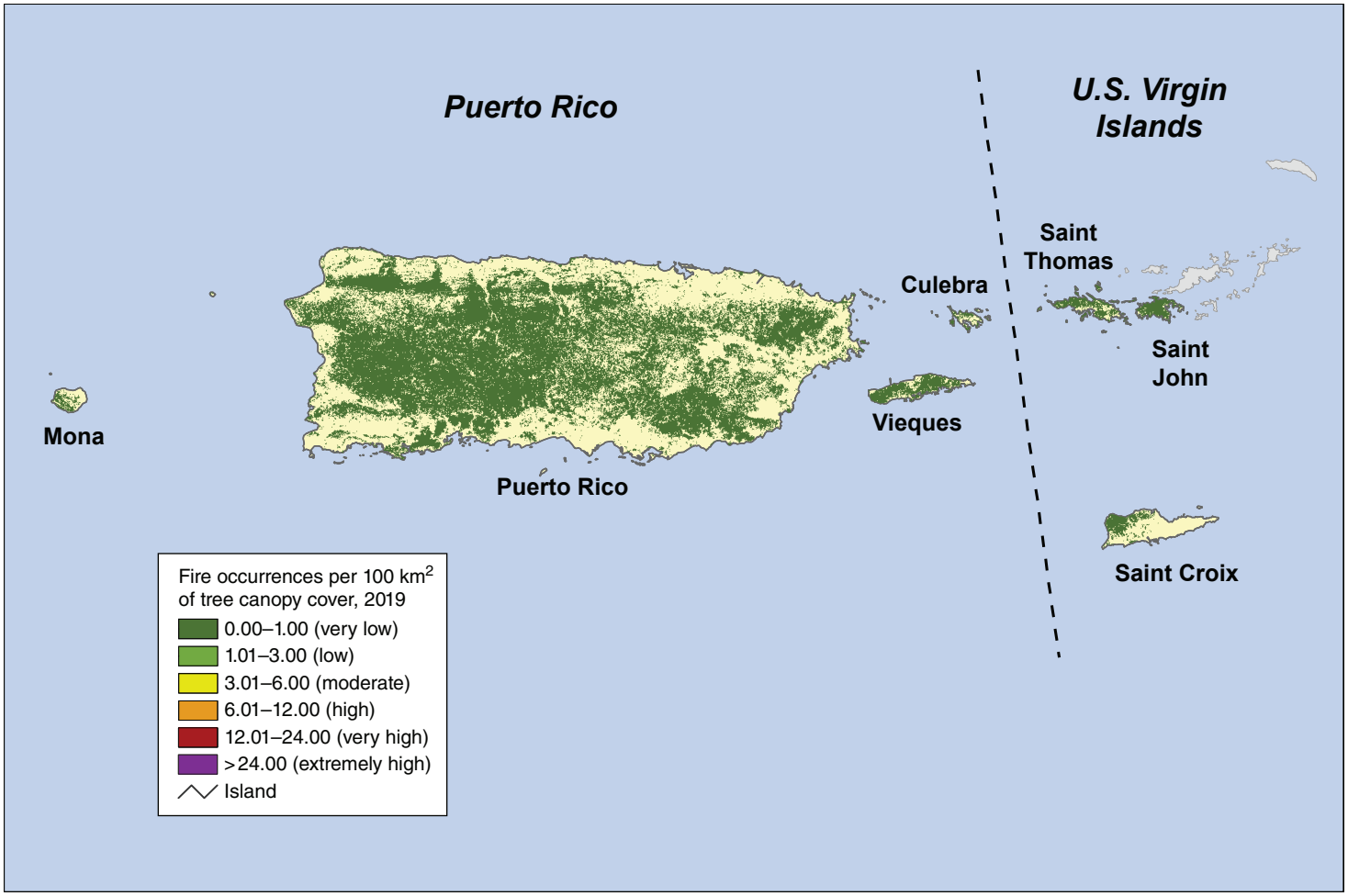

Figure 3.5—The number of forest fire occurrences, per 100 km^2 (10 000 ha) of tree canopy coverage area, by island in Puerto Rico and the U.S. Virgin Islands, for 2019. Tree canopy cover is based on data from a cooperative project between the Multi-Resolution Land Characteristics Consortium (Coulston and others 2012) and the Forest Service Geospatial Technology and Applications Center using the 2011 National Land Cover Database. (Source of fire data: U.S. Department of Agriculture Forest Service, Geospatial Technology and Applications Center, in conjunction with the NASA MODIS Rapid Response group)

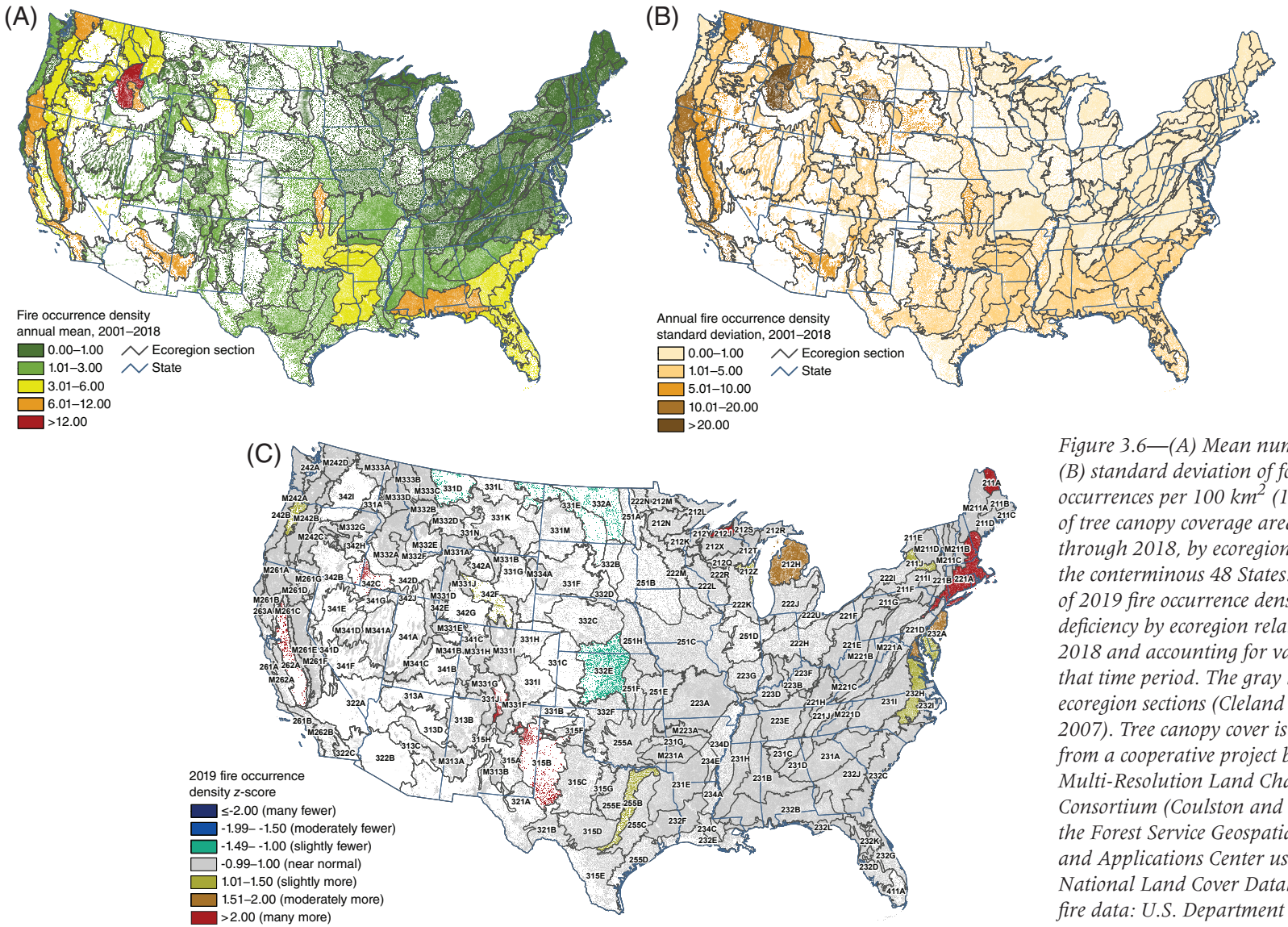

Figure 3.6—(A) Mean number and (B) standard deviation of forest fire occurrences per 100 km^2 (10 000 ha) of tree canopy coverage area from 2001 through 2018, by ecoregion section within the conterminous 48 States. (C) Degree of 2019 fire occurrence density excess or deficiency by ecoregion relative to 2001–2018 and accounting for variation over that time period. The gray lines delineate ecoregion sections (Cleland and others 2007). Tree canopy cover is based on data from a cooperative project between the Multi-Resolution Land Characteristics Consortium (Coulston and others 2012) and the Forest Service Geospatial Technology and Applications Center using the 2011 National Land Cover Database. (Source of fire data: U.S. Department of Agriculture Forest Service, Geospatial Technology and Applications Center, in conjunction with the NASA MODIS Rapid Response group)

Table 3.2—The 15 ecoregion sections in the conterminous United States with the highest mean annual fire occurrence densities from 2001 to 2018

Section	Name	Tree canopy area	Mean annual fire occurrence density[a]
		km^2	
M332A	Idaho Batholith	338.9	12.8
M261A	Klamath Mountains	338.5	10.6
M262B	Southern California Mountain and Valley	58.1	8.8
M261E	Sierra Nevada	427.8	7.9
M313A	White Mountains-San Francisco Peaks-Mogollon Rim	202.5	7.7
313C	Tonto Transition	17.5	7.5
251F	Flint Hills	57.8	6.9
M261B	Northern California Coast Ranges	114.1	6.7
M242D	Northern Cascades	251.1	6.7
261A	Central California Coast	66.8	6.3
232B	Gulf Coastal Plains and Flatwoods	888.7	6.1
M332F	Challis Volcanics	72.2	6.1
M333C	Northern Rockies	176.3	5.9
331A	Palouse Prairie	33.4	5.8
M332B	Northern Rockies and Bitterroot Valley	154.9	5.7

[a] Mean annual fire occurrence density = fire occurrences/100 km^2 of tree canopy coverage area.

A few ecoregion sections in the middle part of the country had 2019 fire occurrence densities that were lower than the longer term as indicated by *z*-scores that were ≤-1: 331E–Northeastern Glaciated Plains in central and northwest North Dakota and northeastern Montana; 332E–South-Central Great Plains in central Kansas and south-central Nebraska; 332A–Northeastern Glaciated Plains in central North Dakota; and 331D–Northwestern Glaciated Plains in north-central Montana (fig. 3.6C). Each of these has a relatively low proportion of tree canopy cover, and each had a very low fire occurrence density score in 2019.

In Alaska, meanwhile, the central and east-central parts of the State had moderate mean annual fire occurrence densities for 2001–2018, specifically in 132A–Yukon-Old Crow Basin and M132E–Ray Mountains (fig. 3.7A). These ecoregion sections, along with M132C–Yukon-Tanana Uplands and M132F–North Ogilvie Mountains, were the most variable over the

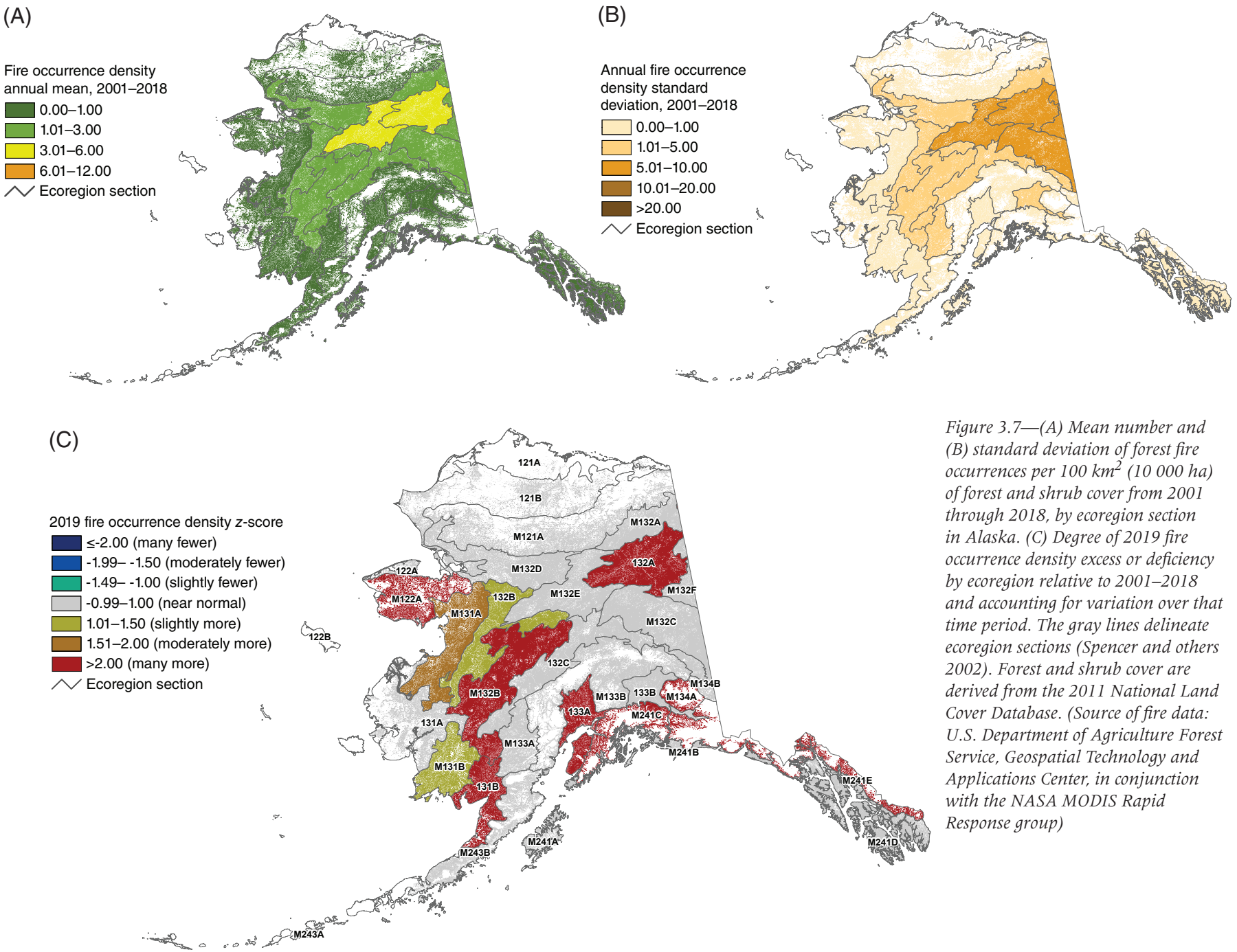

Figure 3.7—(A) Mean number and (B) standard deviation of forest fire occurrences per 100 km^2 (10 000 ha) of forest and shrub cover from 2001 through 2018, by ecoregion section in Alaska. (C) Degree of 2019 fire occurrence density excess or deficiency by ecoregion relative to 2001–2018 and accounting for variation over that time period. The gray lines delineate ecoregion sections (Spencer and others 2002). Forest and shrub cover are derived from the 2011 National Land Cover Database. (Source of fire data: U.S. Department of Agriculture Forest Service, Geospatial Technology and Applications Center, in conjunction with the NASA MODIS Rapid Response group)

18-year period preceding 2019 (fig. 3.7B). In 2019, much of the State had higher fire occurrence densities compared to the previous 18 years and accounting for variability (fig. 3.7C). The ecoregion sections that had many more fire occurrence densities than expected were 132A–Yukon-Old Crow Basin in the east; M122A–Seward Peninsula in the west; M132B–Kuskokwim Mountains and 131B–Bristol Bay Lowlands in the southwest; 133A–Cook Inset Basin, M241C–Chugach-St. Elias Mountains, and M134A–Wrangell Mountains in the south-central and southeastern parts of the State; and M241E–Northern Coast Mountains in the panhandle. Other ecoregions in western Alaska had fire occurrence densities that were moderately or slightly higher than expected.

In Hawaii, the Lowland Wet-Hilo-Puna ecoregion (LWh-hp) of the Big Island had both the highest annual fire occurrence density mean (fig. 3.8A) and variability (fig. 3.8B) during the 2001–2018 period. The annual mean was ≤1 fire occurrence/100 km^2 of tree cover for all other ecoregions with the exception of the Mesic region on the Big Island (MEh), which was 2.7. In 2019, ecoregions on three other islands had fire occurrence densities higher than expected, controlling for variability over the previous 18 years (z-score >1). Three ecoregions had many more fire occurrences than expected: Lowland/Leeward Dry ecoregion on Maui (LLDm), Mesic on O‘ahu (MEo), and Lowland/Leeward Dry on Kaua‘i (LLDk) (fig. 3.7C). An additional ecoregion had moderately more fire occurrences than expected: Lowland Wet on O‘ahu (LWo).

Finally, the 2001–2018 fire occurrence means and standard deviations were ≤1 for all the islands of the Caribbean territories of Puerto Rico and the U.S. Virgin Islands (figs. 3.9A and 3.9B). Only Puerto Rico was outside the range of near-normal fire occurrence density (z-score ≤-1 or >1) in 2019, having moderately more fire occurrences than expected (fig. 3.9C).

Geographical Hot Spots of Fire Occurrence Density

The results presented thus far summarize the 2019 fire occurrence data at the ecoregion scale (or by island in the Caribbean territories). Geographic hot spot analyses, conducted across the conterminous United States using analysis units smaller than ecoregions, can offer additional insights into where, statistically, fire occurrences are more concentrated than expected by chance. As noted above, the 2019 wildfire season was relatively mild in the conterminous States compared to recent years. The hot spot analysis, however, is limited to a single year and therefore identifies areas that have higher-than-expected fire occurrence densities in 2019 compared to the entire study region. For 2019, the SASH method detected two geographic hot spots of very high fire occurrence density (G_i* >12 and ≤24) as well as several hot spots of high density (G_i* >6 and ≤12) (fig. 3.10).

The hot spots of very high fire occurrence density were in southern Arizona (322B–Sonoran Desert and 321A–Basin and Range) and in southeastern Georgia (232B–Gulf Coastal Plains and Flatwoods). Hot spots of

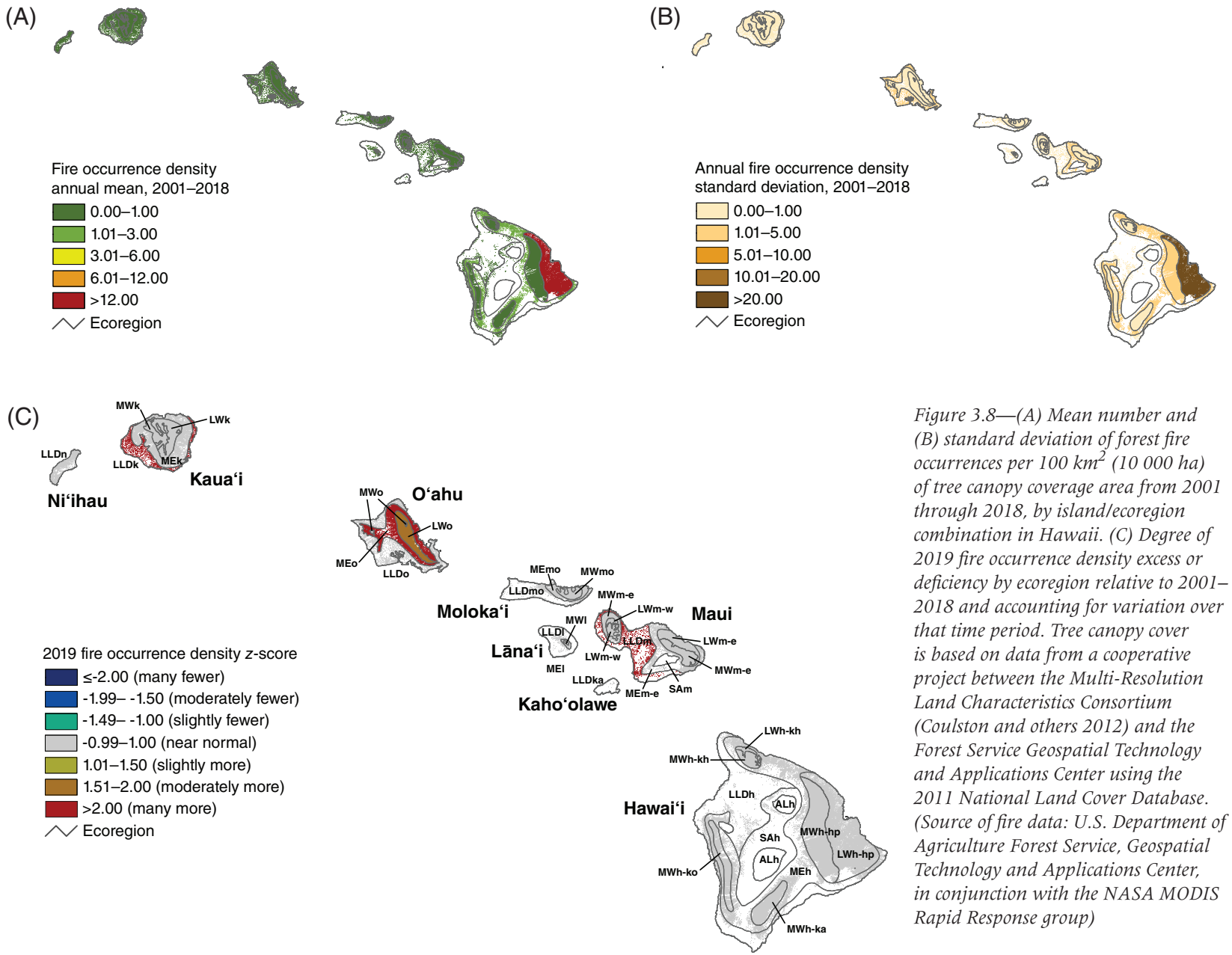

Figure 3.8—(A) Mean number and (B) standard deviation of forest fire occurrences per 100 km^2 (10 000 ha) of tree canopy coverage area from 2001 through 2018, by island/ecoregion combination in Hawaii. (C) Degree of 2019 fire occurrence density excess or deficiency by ecoregion relative to 2001–2018 and accounting for variation over that time period. Tree canopy cover is based on data from a cooperative project between the Multi-Resolution Land Characteristics Consortium (Coulston and others 2012) and the Forest Service Geospatial Technology and Applications Center using the 2011 National Land Cover Database. (Source of fire data: U.S. Department of Agriculture Forest Service, Geospatial Technology and Applications Center, in conjunction with the NASA MODIS Rapid Response group)

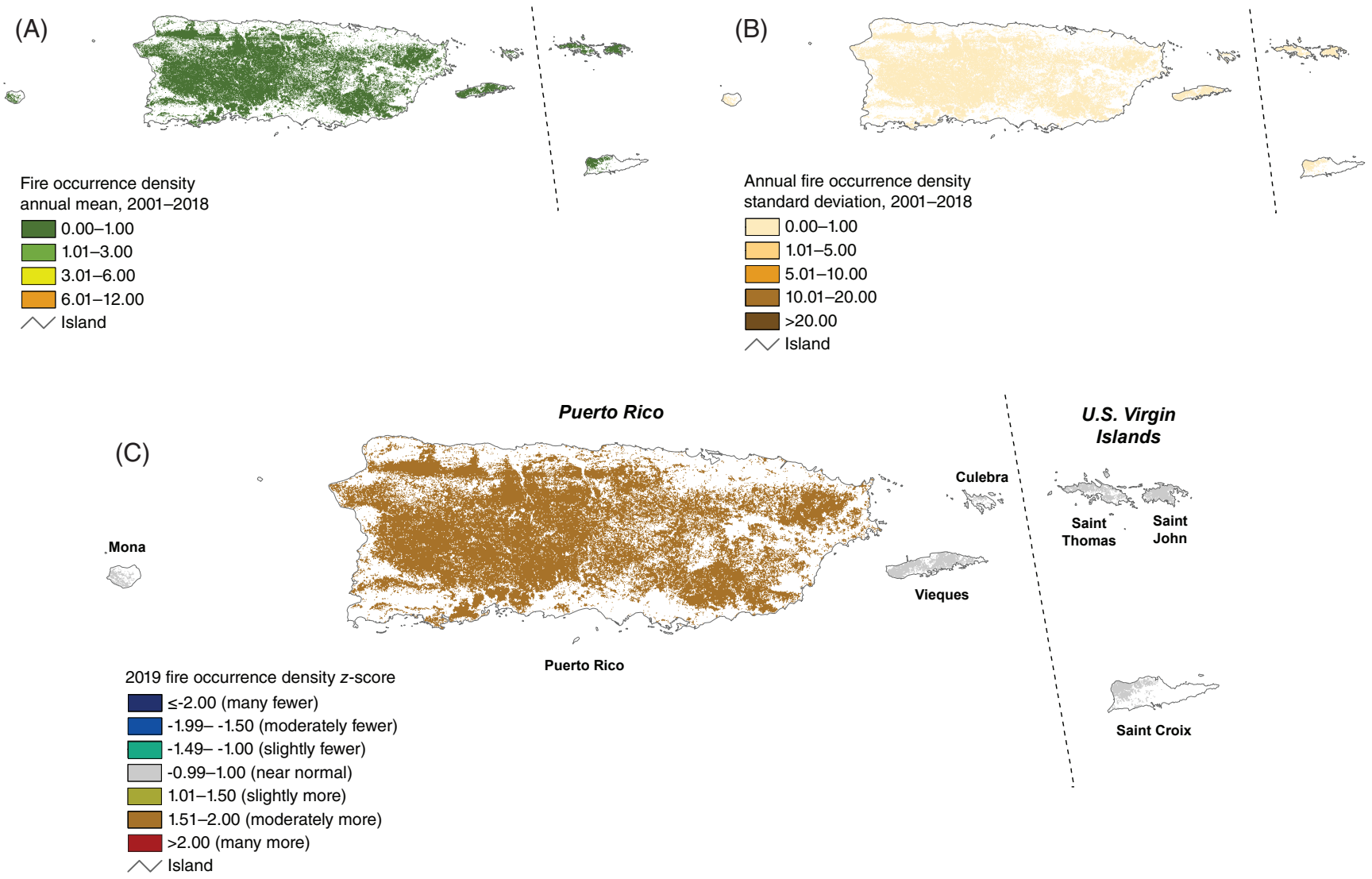

Figure 3.9—(A) Mean number and (B) standard deviation of forest fire occurrences per 100 km^2 (10 000 ha) of forested area from 2001 through 2018, by island in Puerto Rico and the U.S. Virgin Islands. (C) Degree of 2019 fire occurrence density excess or deficiency by ecoregion relative to 2001–2018 and accounting for variation over that time period. Tree canopy cover is based on data from a cooperative project between the Multi-Resolution Land Characteristics Consortium (Coulston and others 2012) and the U.S. Department of Agriculture Forest Service, Geospatial Technology and Applications Center using the 2011 National Land Cover Database.

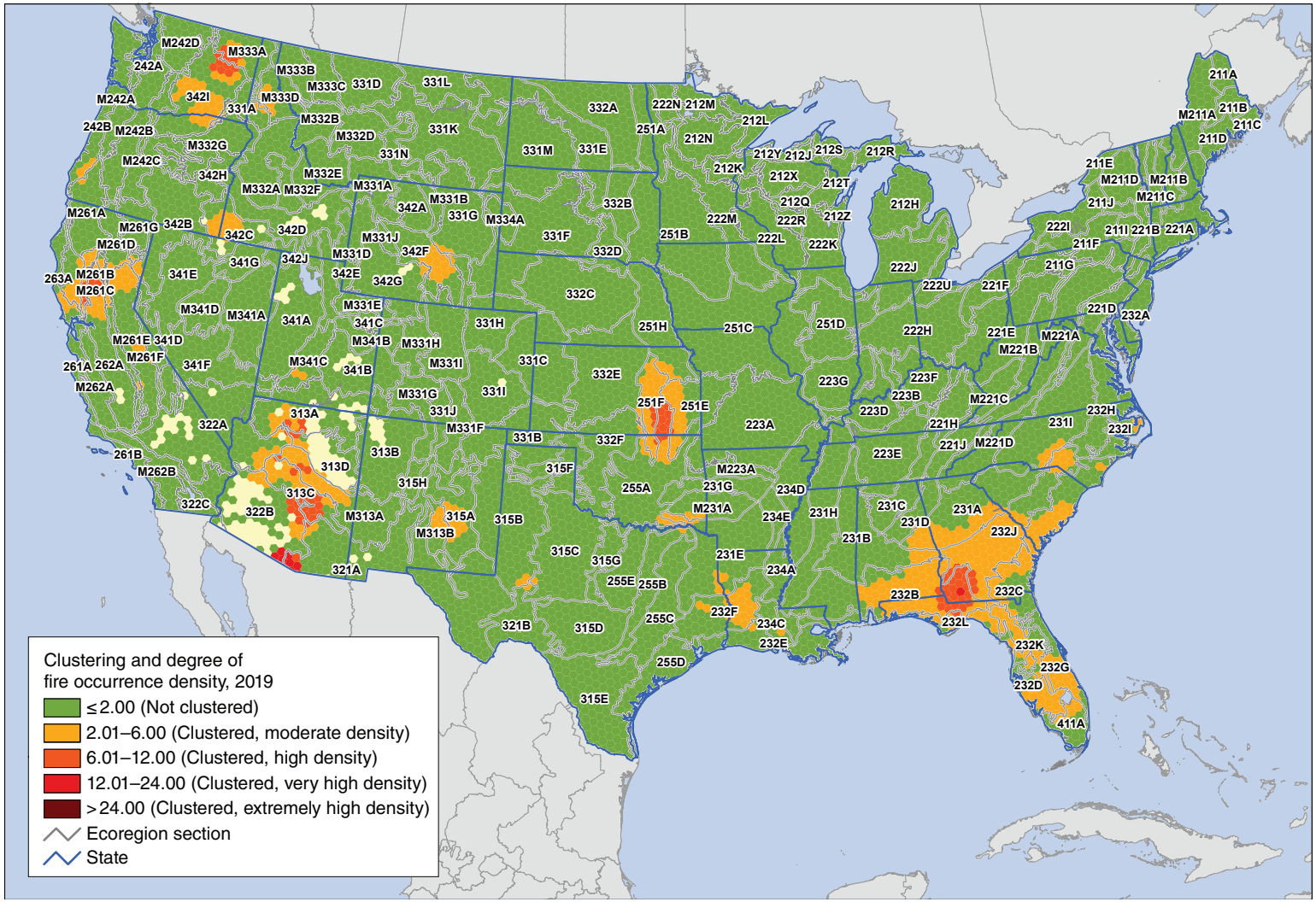

Figure 3.10—Hot spots of fire occurrence across the conterminous United States for 2019. Values are Getis-Ord G_i^* scores, with values >2 representing significant clustering of high fire occurrence densities. (No areas of significant clustering of lower fire occurrence densities, <-2, were detected). The gray lines delineate ecoregion sections (Cleland and others 2007). Background tree canopy cover is based on data from a cooperative project between the Multi-Resolution Land Characteristics Consortium (Coulston and others 2012) and the Forest Service Geospatial Technology and Applications Center using the 2011 National Land Cover Database. (Source of fire data: U.S. Department of Agriculture Forest Service, Geospatial Technology and Applications Center, in conjunction with the NASA MODIS Rapid Response group)

high fire occurrence density were detected in eastern Kansas (255A–Cross Timbers and Prairie and 251F–Flint Hills), northeastern Washington (M333A–Okanogan Highland and 342I–Columbia Basin), north-central California (262A–Great Valley and M261C–Northern California Interior Coast Ranges), northern Arizona (313A–Grand Canyon and 313D–Painted Desert), and central Arizona (M313A–White Mountains-San Francisco Peaks-Mogollon Rim, 313C–Tonto Transition, and 322B–Sonoran Desert) (fig. 3.10).

Hot spots of moderate fire density in 2019 (G_i^* >2 and ≤6) were identified in scattered locations in the Pacific Coast States, the Rocky Mountain States, and the Southeast (fig. 3.10). From west to east, these were detected in:

- Southwestern Oregon (M242A–Oregon and Washington Coast Ranges)
- East-central California (M261E–Sierra Nevada)
- South-central Washington (342I–Columbia Basin)
- Southeastern Oregon and southwestern Idaho (342C–Owyhee Uplands)
- Northern Idaho (M333D–Bitterroot Mountains)
- South-central Utah (M341C–Utah High Plateau)
- South-central Wyoming (342F–Central Basin and Hills)
- Southeastern New Mexico (M313B–Sacramento-Monzano Mountains and 315A–Pecos Valley)
- West-central Texas (315B–Texas High Plains, 315C–Rolling Plains, and 321B–Stockton Plateau)
- Southeastern Kansas and northeastern Oklahoma (251F–Flint Hills, 255A–Cross Timbers and Prairie, and 251E–Osage Plains)
- Southeastern Oklahoma (M231A–Ouachita Mountains, 231E–Mid Coastal Plains-Western, and 255A–Cross Timbers and Prairie)
- Eastern Texas and west-central Louisiana (234C–Atchafalaya and Red River Alluvial Plains)
- South-central Louisiana (232F–Coastal Plains and Flatwoods-Western Gulf and 231E–Mid Coastal Plains-Western)
- Southeastern Alabama, southern and central Georgia, southern South Carolina, and Florida panhandle (232B–Gulf Coastal Plains and Flatwoods, 232J–Southern Atlantic Coastal Plains and Flatwoods, 231A–Southern Appalachian Piedmont, 232C–Atlantic Coastal Flatwoods, and 232L–Gulf Coastal Lowlands)
- Central and southern Florida (232K–Florida Coastal Plains Central Highlands, 232D–Florida Coastal Lowlands-Gulf, 232G–Florida Coastal Lowlands-Atlantic, and 411A–Everglades)
- South-central North Carolina (231I–Central Appalachian Piedmont and 232J–Southern Atlantic Coastal Plains and Flatwoods)
- Southeastern North Carolina (232C–Atlantic Coastal Flatwoods)
- Eastern North Carolina (232I–Northern Atlantic Coastal Flatwoods)

CONCLUSIONS

In 2019, the number of MODIS satellite-detected forest fire occurrences recorded for the conterminous States was uncharacteristically small compared to recent years: the fifth fewest in 19 full years of data collection and the least since 2005. Alaska, however, experienced a particularly severe fire season, with the most fire occurrences since 2005. The relatively low densities of fire occurrences in the conterminous 48 States were attributable at least in part to mild conditions in the early summer, while Alaska experienced extremely hot and dry conditions in June and July.

Ecoregions in southwestern Idaho, central California, and eastern Kansas had the highest forest fire occurrence densities. Geographic hot spots of very high fire occurrence density were detected in southern Arizona and southeast Georgia. Most of the conterminous United States experienced near-normal fire occurrence densities in 2019, compared to the previous 18-year mean and accounting for variability over time, although a few ecoregions in the Northeast and scattered elsewhere had significantly higher fire occurrence densities than normal. Meanwhile, much of Alaska had much higher fire occurrence densities than normal. In Hawaii, ecoregions in Maui, Oʻahu, and Kauaʻi had many more fire occurrences than expected. In the Caribbean, the island of Puerto Rico had moderately more fire occurrences than a normal year.

The results of these geographic analyses are intended to offer insights into where fire occurrences have been concentrated spatially in a given year and compared to previous years but are not intended to quantify the severity of a given fire season. Given the limits of MODIS active fire detection using 1-km-resolution data, these products also may underrepresent the number of fire occurrences in some ecosystems where small and low-intensity fires are common, and where high cloud frequency can interfere with fire detection. These products can also have commission errors. However, these high-temporal-fidelity products currently offer the best means for daily monitoring of forest fire occurrences.

Ecological and forest health impacts relating to fire and other abiotic disturbances are scale-dependent properties, which in turn are affected by management objectives (Lundquist and others 2011). Information about the concentration of fire occurrences may help pinpoint areas of concern for aiding management activities and for investigations into the ecological and socioeconomic impacts of forest fire potentially outside the range of historic frequency.

LITERATURE CITED

Andrews, R.G. 2018. America's most hazardous volcano erupted this year. Then it erupted and erupted. The New York Times. December 12. https://www.nytimes.com/2018/12/12/science/kilauea-hawaii-volcano-eruption.html. [Date accessed: July 15, 2019].

Anselin, L. 1992. Spatial data analysis with GIS: an introduction to application in the social sciences. Tech. Rep. 92-10. Santa Barbara, CA: University of California, National Center for Geographic Information and Analysis. 53 p.

Barbour, M.G.; Burk, J.H.; Pitts, W.D. [and others]. 1999. Terrestrial plant ecology. Menlo Park, CA: Addison Wesley Longman, Inc. 649 p.

Bond, W.J.; Keeley, J.E. 2005. Fire as a global "herbivore": the ecology and evolution of flammable ecosystems. Trends in Ecology & Evolution. 20(7): 387–394. https://doi.org/10.1016/j.tree.2005.04.025.

Cleland, D.T.; Freeouf, J.A.; Keys, J.E. [and others]. 2007. Ecological subregions: sections and subsections for the conterminous United States. Gen. Tech. Rep. WO-76D. Washington, DC: U.S. Department of Agriculture Forest Service. Map; Sloan, A.M., cartographer; presentation scale 1:3,500,000; colored. Also on CD-ROM as a GIS coverage in ArcINFO format or at http://data.fs.usda.gov/geodata/edw/datasets.php. [Date accessed: July 20, 2015].

Coulston, J.W.; Ambrose, M.J.; Riitters, K.H.; Conkling, B.L. 2005. Forest Health Monitoring 2004 national technical report. Gen. Tech. Rep. SRS-90. Asheville, NC: U.S. Department of Agriculture Forest Service, Southern Research Station. 81 p.

Coulston, J.W.; Moisen, G.G.; Wilson, B.T. [and others]. 2012. Modeling percent tree canopy cover: a pilot study. Photogrammetric Engineering and Remote Sensing. 78(7): 715–727. https://doi.org/10.14358/PERS.78.7.715.

Edmonds, R.L.; Agee, J.K.; Gara, R.I. 2011. Forest health and protection. Long Grove, Illinois: Waveland Press, Inc. 667 p.

ESRI. 2017. ArcMap® 10.5.1. Redlands, CA: Environmental Systems Research Institute.

Gedalof, Z. 2011. Climate and spatial patterns of wildfire in North America. In: McKenzie, D.; Miller, C.; Falk, D.A., eds. The landscape ecology of fire. Dordrecht: Springer Netherlands: 89–115. https://doi.org/10.1007/978-94-007-0301-8_4.

Getis, A.; Ord, J.K. 1992. The analysis of spatial association by use of distance statistics. Geographical Analysis. 24(3): 189–206. https://doi.org/10.1111/j.1538-4632.1992.tb00261.x.

Gill, A.M.; Stephens, S.L.; Cary, G.J. 2013. The worldwide "wildfire" problem. Ecological Applications. 23(2): 438–454. https://doi.org/10.1890/10-2213.1.

Hawbaker, T.J.; Radeloff, V.C.; Syphard, A.D. [and others]. 2008. Detection rates of the MODIS active fire product. Remote Sensing of Environment. 112: 2656–2664. https://doi.org/10.1016/j.rse.2007.12.008.

Homer, C.G.; Dewitz, J.A.; Yang, L. [and others]. 2015. Completion of the 2011 National Land Cover Database for the conterminous United States: representing a decade of land cover change information. Photogrammetric Engineering and Remote Sensing. 81(5): 345–354.

Justice, C.O.; Giglio, L.; Korontzi, S. [and others]. 2002. The MODIS fire products. Remote Sensing of Environment. 83(1–2): 244–262. https://doi.org/10.1016/S0034-4257(02)00076-7.

Justice, C.O.; Giglio, L.; Roy, D. [and others]. 2011. MODIS-derived global fire products. In: Ramachandran, B.; Justice, C.O.; Abrams, M.J., eds. Land remote sensing and global environmental change: NASA's earth observing system and the science of ASTER and MODIS. New York: Springer: 661–679. https://doi.org/10.1007/978-1-4419-6749-7_29.

Kitzberger, T.; Brown, P.M.; Heyerdahl, E.K. [and others]. 2007. Contingent Pacific-Atlantic Ocean influence on multicentury wildfire synchrony over western North America. Proceedings of the National Academy of Sciences. 104(2): 543–548. https://doi.org/10.1073/pnas.0606078104.

Laffan, S.W. 2006. Assessing regional scale weed distributions, with an Australian example using *Nassella trichotoma*. Weed Research. 46(3): 194–206. https://doi.org/10.1111/j.1365-3180.2006.00491.x.

Lundquist, J.E.; Camp, A.E.; Tyrrell, M.L. [and others]. 2011. Earth, wind and fire: abiotic factors and the impacts of global environmental change on forest health. In: Castello, J.D.; Teale, S.A., eds. Forest health: an integrated perspective. New York: Cambridge University Press: 195–243. https://doi.org/10.1017/CBO9780511974977.008.

McKenzie, D.; Peterson, D.L.; Alvarado, E. 1996. Predicting the effect of fire on large-scale vegetation patterns in North America. Res. Pap. PNW-489. Portland, OR: U.S. Department of Agriculture Forest Service, Pacific Northwest Research Station. 38 p. https://doi.org/10.5962/bhl.title.87888.

National Interagency Coordination Center. 2018. Wildland fire summary and statistics annual report: 2017. https://www.predictiveservices.nifc.gov/intelligence/2017_statssumm/intro_summary17.pdf. [Date accessed: April 30, 2018].

National Interagency Coordination Center. 2019. Wildland fire summary and statistics annual report: 2018. https://www.predictiveservices.nifc.gov/intelligence/2018_statssumm/intro_summary18.pdf. [Date accessed: June 27, 2019].

National Interagency Coordination Center. 2020. Wildland fire summary and statistics annual report: 2019. https://www.predictiveservices.nifc.gov/intelligence/2019_statssumm/intro_summary19.pdf. [Date accessed: April 3, 2020].

Nowacki, G.J.; Abrams, M.D. 2008. The demise of fire and "mesophication" of forests in the Eastern United States. BioScience. 58(2): 123–138. https://doi.org/10.1641/B580207.

Potter, K.M. 2012a. Large-scale patterns of forest fire occurrence in the conterminous United States and Alaska, 2005–07. In: Potter, K.M.; Conkling, B.L., eds. Forest Health Monitoring 2008 national technical report. Gen. Tech. Rep. SRS-158. Asheville, NC: U.S. Department of Agriculture Forest Service, Southern Research Station: 73–83.

Potter, K.M. 2012b. Large-scale patterns of forest fire occurrence in the conterminous United States and Alaska, 2001–08. In: Potter, K.M.; Conkling, B.L., eds. Forest Health Monitoring 2009 national technical report. Gen. Tech. Rep. SRS-167. Asheville, NC: U.S. Department of Agriculture Forest Service, Southern Research Station: 151–161.

Potter, K.M. 2013a. Large-scale patterns of forest fire occurrence in the conterminous United States and Alaska, 2009. In: Potter, K.M.; Conkling, B.L., eds. Forest Health Monitoring: national status, trends, and analysis 2010. Gen. Tech. Rep. SRS-176. Asheville, NC: U.S. Department of Agriculture Forest Service, Southern Research Station: 31–39.

Potter, K.M. 2013b. Large-scale patterns of forest fire occurrence in the conterminous United States and Alaska, 2010. In: Potter, K.M.; Conkling, B.L., eds. Forest Health Monitoring: national status, trends, and analysis 2011. Gen. Tech. Rep. SRS-185. Asheville, NC: U.S. Department of Agriculture Forest Service, Southern Research Station: 29–40.

Potter, K.M. 2014. Large-scale patterns of forest fire occurrence in the conterminous United States and Alaska, 2011. In: Potter, K.M.; Conkling, B.L., eds. Forest Health Monitoring: national status, trends, and analysis 2012. Gen. Tech. Rep. SRS-198. Asheville, NC: U.S. Department of Agriculture Forest Service, Southern Research Station: 35–48.

Potter, K.M. 2015a. Large-scale patterns of forest fire occurrence in the conterminous United States and Alaska, 2012. In: Potter, K.M.; Conkling, B.L., eds. Forest Health Monitoring: national status, trends, and analysis 2013. Gen. Tech. Rep. SRS-207. Asheville, NC: U.S. Department of Agriculture Forest Service, Southern Research Station: 37–53.

Potter, K.M. 2015b. Large-scale patterns of forest fire occurrence in the conterminous United States and Alaska, 2013. In: Potter, K.M.; Conkling, B.L., eds. Forest Health Monitoring: national status, trends, and analysis 2014. Gen. Tech. Rep. SRS-209. Asheville, NC: U.S. Department of Agriculture Forest Service, Southern Research Station: 39–55.

Potter, K.M. 2016. Large-scale patterns of forest fire occurrence in the conterminous United States, Alaska, and Hawaii, 2014. In: Potter, K.M.; Conkling, B.L., eds. Forest Health Monitoring: national status, trends, and analysis 2015. Gen. Tech. Rep. SRS-213. Asheville, NC: U.S. Department of Agriculture Forest Service, Southern Research Station: 41–60.

Potter, K.M. 2017. Large-scale patterns of forest fire occurrence in the conterminous United States, Alaska, and Hawaii, 2015. In: Potter, K.M.; Conkling, B.L., eds. Forest Health Monitoring: national status, trends, and analysis 2016. Gen. Tech. Rep. SRS-222. Asheville, NC: U.S. Department of Agriculture Forest Service, Southern Research Station: 43–62.

Potter, K.M. 2018. Large-scale patterns of forest fire occurrence in the conterminous United States, Alaska, and Hawaii, 2016. In: Potter, K.M.; Conkling, B.L., eds. Forest Health Monitoring: national status, trends, and analysis 2017. Gen. Tech. Rep. SRS-233. Asheville, NC: U.S. Department of Agriculture Forest Service, Southern Research Station: 45–64.

Potter, K.M. 2019. Large-scale patterns of forest fire occurrence across the 50 United States and the Caribbean territories, 2017. In: Potter, K.M.; Conkling, B.L., eds. Forest Health Monitoring: national status, trends, and analysis 2018. Gen. Tech. Rep. SRS-239. Asheville, NC: U.S. Department of Agriculture Forest Service, Southern Research Station: 51–76.

Potter, K.M. 2020a. Large-scale patterns of forest fire occurrence across the 50 United States and the Caribbean territories, 2018. In: Potter, K.M.; Conkling, B.L., eds. Forest Health Monitoring: national status, trends, and analysis 2019. Gen. Tech. Rep. SRS-250. Asheville, NC: U.S. Department of Agriculture Forest Service, Southern Research Station: 57–82.

Potter, K.M. 2020b. Introduction. In: Potter, K.M.; Conkling, B.L., eds. Forest Health Monitoring: national status, trends, and analysis 2019. Gen. Tech. Rep. SRS-250. Asheville, NC: U.S. Department of Agriculture Forest Service, Southern Research Station: 5–24.

Potter, K.M.; Koch, F.H.; Oswalt, C.M.; Iannone, B.V. 2016. Data, data everywhere: detecting spatial patterns in fine-scale ecological information collected across a continent. Landscape Ecology. 31: 67–84. https://doi.org/10.1007/s10980-015-0295-0.

Pyne, S.J. 2010. America's fires: a historical context for policy and practice. Durham, NC: Forest History Society. 91 p.

Reams, G.A.; Smith, W.D.; Hansen, M.H. [and others]. 2005. The Forest Inventory and Analysis sampling frame. In: Bechtold, W.A.; Patterson, P.L., eds. The enhanced Forest Inventory and Analysis program—national sampling design and estimation procedures. Gen. Tech. Rep. SRS-80. Asheville, NC: U.S. Department of Agriculture Forest Service, Southern Research Station: 11–26.

Richardson, L.A.; Champ, P.A.; Loomis, J.B. 2012. The hidden cost of wildfires: economic valuation of health effects of wildfire smoke exposure in southern California. Journal of Forest Economics. 18(1): 14–35. https://doi.org/10.1016/j.jfe.2011.05.002.

Schmidt, K.M.; Menakis, J.P.; Hardy, C.C. [and others]. 2002. Development of coarse-scale spatial data for wildland fire and fuel management. Gen. Tech. Rep. RMRS-87. Fort Collins, CO: U.S. Department of Agriculture Forest Service, Rocky Mountain Research Station. 41 p. https://doi.org/10.2737/RMRS-GTR-87.

Shima, T.; Sugimoto, S.; Okutomi, M. 2010. Comparison of image alignment on hexagonal and square lattices. In: 2010 IEEE international conference on image processing. [Place of publication unknown]: Institute of Electrical and Electronics Engineers, Inc.: 141–144. https://doi.org/10.1109/ICIP.2010.5654351.

Spencer, P.; Nowacki, G.; Fleming, M. [and others]. 2002. Home is where the habitat is: an ecosystem foundation for wildlife distribution and behavior. Arctic Research of the United States. 16: 6–17.

Tonini, M.; Tuia, D.; Ratle, F. 2009. Detection of clusters using space-time scan statistics. International Journal of Wildland Fire. 18(7): 830–836. https://doi.org/10.1071/WF07167.

Trouet, V.; Taylor, A.H.; Wahl, E.R.; Skinner, C.N. 2010. Fire-climate interactions in the American West since 1400 CE. Geophysical Research Letters. 37(4): L04702. https://doi.org/10.1029/2009GL041695.

U.S. Department of Agriculture (USDA) Forest Service. 2008. National forest type data development. http://svinetfc4.fs.fed.us/rastergateway/forest_type/. [Date accessed: May 13, 2008].

U.S. Department of Agriculture (USDA) Forest Service. 2020. Fire detection GIS data. https://fsapps.nwcg.gov/afm/gisdata.php. [Date accessed: June 24, 2020].

White, D.; Kimerling, A.J.; Overton, W.S. 1992. Cartographic and geometric components of a global sampling design for environmental monitoring. Cartography and Geographic Information Systems. 19(1): 5–22. https://doi.org/10.1559/152304092783786636.

CHAPTER 4.

Spatial Patterns of Drought and Moisture Surplus in the Conterminous United States: 2019, 2017–2019, and 2015–2019

Frank H. Koch
John W. Coulston

INTRODUCTION

In forests, droughts can cause considerable tree stress, particularly when they coincide with periods of abnormally hot weather, i.e., heat waves (L.D.L. Anderegg and others 2013, Peters and others 2015, Williams and others 2013). Trees and other plants respond to this stress by restricting fundamental growth processes. Photosynthesis, which is less sensitive than other fundamental processes, decreases slowly at low levels of drought stress but decreases more rapidly as the stress becomes more severe (Kareiva and others 1993, Mattson and Haack 1987). Ultimately, prolonged drought stress can lead to failure of a tree's hydraulic system, resulting in crown death and subsequent tree mortality (Choat and others 2018). Evidence suggests that large trees are more sensitive to drought stress than small trees, experiencing comparatively higher rates of growth decline and mortality (Bennett and others 2015). In addition, drought stress often makes trees vulnerable to attack by damaging insects and diseases (Clinton and others 1993, Kolb and others 2016, Mattson and Haack 1987, Raffa and others 2008). Droughts also increase wildfire risk by inhibiting organic matter breakdown and diminishing the moisture content of down woody debris and other potential fire fuels (Clark 1989, Collins and others 2006, Keetch and Byram 1968, Schoennagel and others 2004, Trouet and others 2010). Although relationships between fire occurrence and drought are complex at a regional scale, projections of greater drought frequency and severity under a warming climate suggest that wildfires will become increasingly prevalent and extensive in many U.S. forest systems, especially in the Western United States (Abatzoglou and Williams 2016, Dennison and others 2014, Littell and others 2016).

Ecologists are inconsistent in how they define the concept of drought and disagree about how best to measure its severity (Slette and others 2019, 2020; Zang and others 2020). One general and widely accepted definition that applies to forests is that a drought is a period of precipitation deficit that persists long enough to deplete available soil water, leading to impacts on trees and other plants; in some cases, these impacts include injury or death (Anderegg and others 2012, Hanson and Weltzin 2000). By this definition, droughts affect most forests in the United States, although drought frequency, timing, and intensity vary between geographic regions (Hanson and Weltzin 2000). These variations characterize the regions' predominant drought regimes. Because they receive most of their precipitation during a relatively brief period of 2–3 months, most forests in the Western United States experience seasonal droughts each year. By comparison, forests in the Eastern United States usually exhibit one of the following drought patterns: random (i.e., occurring at any time of year) but occasional droughts, as observed in the Appalachian Mountains and the Northeast, or frequent late-summer droughts, as commonly observed in the Southeastern Coastal Plain and the eastern Great Plains (Hanson and Weltzin 2000).

Most forests are resistant to short-term droughts, although individual tree species vary in their degree of drought tolerance (Archaux and Wolters 2006, Berdanier and Clark 2016, Peters and others 2015). Because of this resistance, drought duration may be a more critical factor for forests than drought intensity (Archaux and Wolters 2006). For example, forests that endure multiple consecutive years of drought are much more likely to experience high tree mortality or other negative impacts than forests subject to a single year of extreme drought (Bigler and others 2006, Guarín and Taylor 2005, Jenkins and Pallardy 1995, Millar and others 2007). Indeed, a 1-year drought is likely brief enough that any impacts on tree growth and function are still reversible for most forests (Bigler and others 2006). Stated differently, forests may have to undergo a prolonged period of comparatively intense drought conditions before they encounter effects like those observed with shorter term droughts in other (e.g., rangeland) systems. Thus, a comprehensive evaluation of drought impact in forests should include analysis of moisture conditions over multiyear time windows. Such an approach has been rare among similarly broad-scale assessments (Norman and others 2016).

In the 2010 Forest Health Monitoring (FHM) National Technical Report, we described a method for mapping drought conditions across the conterminous United States (Koch and others 2013b). Our objective was to generate fine-scale, drought-related spatial datasets that improve upon similar products available from sources such as the National Oceanic and Atmospheric Administration's National Centers for Environmental Information (e.g., Vose and others 2014) or the U.S. Drought Monitor program (Svoboda and others 2002). The primary inputs are gridded climate data (i.e., monthly raster maps of precipitation and temperature over a 100-year period) created with the Parameter-elevation Regression on Independent Slopes (PRISM) climate mapping system (Daly and others 2002). The method uses a standardized indexing approach that facilitates comparison of a given location's moisture status during different time windows, regardless of their length. The index is more straightforward to calculate than the commonly used Palmer Drought Severity Index, or PDSI (Palmer 1965), and avoids some criticisms of the PDSI (see Alley 1984) regarding its underlying assumptions and limited comparability across space and time. Here, we applied the method outlined in the 2010 FHM report to the most currently available climate data (i.e., the monthly PRISM data through 2019), thereby providing the 11th installment in an ongoing series of annual drought assessments for the conterminous United States (Koch and Coulston 2015, 2016, 2017, 2018, 2019, 2020; Koch and others 2013a, 2013b, 2014, 2015).

This is the sixth year in which we also mapped levels of moisture surplus across the conterminous United States during multiple time windows. While recent refereed literature (e.g., Adams and others 2009, Allen and others 2010, Martínez-Vilalta and others 2012, Peng and others 2011, Williams and others 2013) has usually focused on reports of regional-scale forest decline and mortality due to persistent drought conditions, surplus moisture availability can also be damaging to forests. Abnormally high moisture can be a short-term stressor (e.g., an extreme rainfall event with subsequent flooding) or a long-term stressor (e.g., persistent wetness caused by a macroscale climatic pattern such as the El Niño-Southern Oscillation), either of which may lead to tree dieback and mortality (Rozas and García-González 2012, Rozas and Sampedro 2013). Such impacts have been observed in tropical, temperate, and boreal forest systems (Hubbart and others 2016, Laurance and others 2009, Rozas and García-González 2012). For example, larch (*Larix*) species that predominate in eastern Siberian forests appear to be drought-resistant yet highly sensitive to excessively wet conditions (Tei and others 2019). While surplus-induced impacts in forests may not be as common as drought-induced impacts, a single index that depicts moisture surplus as well as deficit conditions provides a more complete indicator of potential forest health issues.

METHODS

We acquired grids for monthly precipitation and monthly mean temperature for the conterminous United States from the PRISM Climate Group web site (PRISM Climate Group 2020). At the time of these analyses, gridded datasets were available for all years from 1895 to 2019. The spatial resolution of the grids was approximately 4 km (cell area = 16 km^2). For future applications and to ensure better compatibility with other spatial datasets, all output grids were resampled to a spatial resolution of approximately 2 km (cell area = 4 km^2) using a nearest neighbor approach. The nearest neighbor approach is a computationally simple resampling method that avoids the smoothing of data values observed with methods such as bilinear interpolation or cubic convolution.

Potential Evapotranspiration (PET) Maps

As in our previous drought mapping efforts (in particular, see Koch and others 2013b), we adopted an approach in which a moisture index value is calculated for each location of interest (i.e., each grid cell in a map of the conterminous United States) during a given time period. Moisture indices are intended to reflect the amount of water available in a location (e.g., to support plant growth). In our case, the index is computed using an approach that considers both the amount of precipitation that falls on

a location during the period of interest as well as the level of potential evapotranspiration during this period. Potential evapotranspiration measures the loss of soil moisture through plant uptake and transpiration (Akin 1991). It does not measure actual moisture loss but rather the loss that would occur if there was no possible shortage of moisture for plants to transpire (Akin 1991, Thornthwaite 1948). Potential evapotranspiration serves as a basic measure of moisture demand. By incorporating potential evapotranspiration along with precipitation, our index thus documents the long-term balance between moisture demand and supply for each location of interest.

To complement the available PRISM monthly precipitation grids, we computed monthly potential evapotranspiration (*PET*) grids using Thornthwaite's formula (Akin 1991, Thornthwaite 1948):

$$PET_m = 1.6 L_{lm} \left(10 \frac{T_m}{I}\right)^a \qquad (1)$$

where

PET_m = the potential evapotranspiration for a given month m in cm

L_{lm} = a correction factor for the mean possible duration of sunlight during month m for all locations (i.e., grid cells) at a particular latitude l (see Table V in Thornthwaite [1948] for a list of L correction factors by month and latitude)

T_m = the mean temperature for month m in degrees C

I = an annual heat index ranging from 0 to 160, calculated as

$I = \sum_{m=1}^{12} \left(\frac{T_m}{5}\right)^{1.514}$, where T_m is the mean temperature for each month m of the year

a = an exponent calculated as $a = 6.75 \times 10^{-7} I^3 - 7.71 \times 10^{-5} I^2 + 1.792 \times 10^{-2} I + 0.49239$ (see Appendix I in Thornthwaite [1948] regarding calculation of I and the empirical derivation of a in relation to I)

Although only a simple approximation, a key advantage of Thornthwaite's formula is that it has modest input data requirements (i.e., mean temperature values) compared to more sophisticated methods of estimating potential evapotranspiration such as the Penman-Monteith equation (Monteith 1965), which requires less readily available data on factors such as humidity, radiation, and wind speed. To implement equation (1) spatially, we created a grid of latitude values for determining the L adjustment for any given grid cell (and any given month) in the conterminous United States. We extracted the T_m values for the grid cells from the corresponding PRISM mean monthly temperature grids.

Moisture Index Maps

To estimate baseline conditions, we used the precipitation (*P*) and *PET* grids to generate moisture index grids for the past 100 years

(i.e., 1920–2019) for the conterminous United States. We used a moisture index described by Willmott and Feddema (1992), which has been applied in a variety of contexts, including global vegetation modeling (Potter and Klooster 1999) and climate change analysis (Grundstein 2009). Willmott and Feddema (1992) devised the index as a refinement of one described earlier by Thornthwaite (1948) and Thornthwaite and Mather (1955). Their revised index, *MI′*, has the following form:

$$MI' = \begin{cases} P/PET - 1 & , \quad P < PET \\ 1 - PET/P & , \quad P \geq PET \\ 0 & , \quad P = PET = 0 \end{cases} \qquad (2)$$

where

P = precipitation

PET = potential evapotranspiration, as calculated using equation (1)

(*P* and *PET* must be in equivalent measurement units, e.g., mm)

This set of equations yields a symmetric, dimensionless index scaled between -1 and 1. A primary advantage of this symmetry is that it enables valid comparisons between any set of locations in terms of their balance between moisture demand and supply. *MI′* can be calculated for any time period but is commonly calculated on an annual basis using *P* and *PET* values summed across the entire year (Willmott and Feddema 1992). An alternative to this summation approach is to calculate *MI′* on a monthly basis (i.e., from total measured precipitation and estimated potential evapotranspiration in each month), and then, for a given time window of interest, calculate its moisture index as the mean of the *MI′* values for all months in the time window. This "mean-of-months" approach limits the ability of short-term peaks in either precipitation or potential evapotranspiration to negate corresponding short-term deficits, as would happen under a summation approach.

For each year in our study period (i.e., 1920–2019), we used the mean-of-months approach to calculate moisture index grids for three different time windows: 1 year (MI_1'), 3 years (MI_3'), and 5 years (MI_5'). Briefly, the MI_1' grids are the mean (i.e., the mean value for each grid cell) of the 12 monthly *MI′* grids for each year in the study period, the MI_3' grids are the mean of the 36 monthly grids from January of 2 years prior through December of the target year, and the MI_5' grids are the mean of the 60 consecutive monthly *MI′* grids from January of 4 years prior through December of the target year. Thus, the MI_1' grid for the year 2019 is the mean of the monthly *MI′* grids from January to December 2019, while the MI_3' grid is the mean of the grids from January 2017 to December 2019, and the MI_5' grid is the mean of the grids from January 2015 to December 2019.

Annual and Multiyear Drought Maps

To determine degree of departure from typical moisture conditions, we first created a normal grid, $MI'_{i\,norm}$, for each of our three

time windows, representing the mean (i.e., the mean value for each grid cell) of the 100 corresponding moisture index grids (i.e., the MI_1', MI_3', or MI_5' grids, depending on the window; see fig. 4.1). We also created a standard deviation grid, $MI'_{i\,SD}$, for each time window, calculated from the window's 100 individual moisture index grids as well as its $MI'_{i\,norm}$ grid. We subsequently calculated moisture difference *z*-scores, MDZ_{ij}, for each time window using these derived datasets:

$$MDZ_{ij} = \frac{MI'_{ij} - MI'_{i\,norm}}{MI'_{i\,SD}} \qquad (3)$$

where

i = the analytical time window (i.e., 1, 3, or 5 years)

j = a particular target year in our 100-year study period (i.e., 1920–2019)

MDZ scores may be classified in terms of degree of moisture deficit or surplus (table 4.1). The classification scheme includes categories (e.g., severe drought, extreme drought) like those associated with the PDSI. The scheme has also been adopted for other drought indices such as the Standardized Precipitation Index, or SPI (McKee and others 1993). Moreover, the breakpoints between *MDZ* categories resemble those used for the SPI, such that we expect the *MDZ* categories to have theoretical frequencies of occurrence that are similar to their SPI counterparts (e.g., approximately 2.3 percent of the time for extreme drought; see McKee and others 1993, Steinemann 2003). More importantly, because of the standardization in equation (3), the breakpoints between categories remain the same regardless of the size of the time window of interest. For comparative analysis, we generated and classified *MDZ* maps of the conterminous United States, based on all three time windows, for the target year 2019.

RESULTS AND DISCUSSION

The 100-year (1920–2019) mean annual moisture index, or $MI_1'_{norm}$, grid (fig. 4.1) provides an overview of long-term moisture regimes in the conterminous United States. (The 100-year $MI_3'_{norm}$ and $MI_5'_{norm}$ grids were very similar to the mean $MI_1'_{norm}$ grid, and so are not shown here.) Wet climates ($MI' > 0$) are typical in the Eastern United States, especially the Northeast. An exception worth noting is southern Florida, primarily ecoregion sections (Cleland and others 2007) 232D–Florida Coastal Lowlands-Gulf, 232G–Florida Coastal Lowlands-Atlantic, and 411A–Everglades. This region appears to be dry relative to other parts of the East. This is an effect of its tropical climate, which has distinct wet (primarily summer months) and dry (late fall to early spring) seasons. Although southern Florida usually receives a high level of precipitation during the wet season, it can be insufficient to offset the region's lengthy dry season (Duever and others 1994) or its high level of temperature-driven evapotranspiration, especially during the late spring and summer months, resulting in negative MI' values. This differs from the pattern

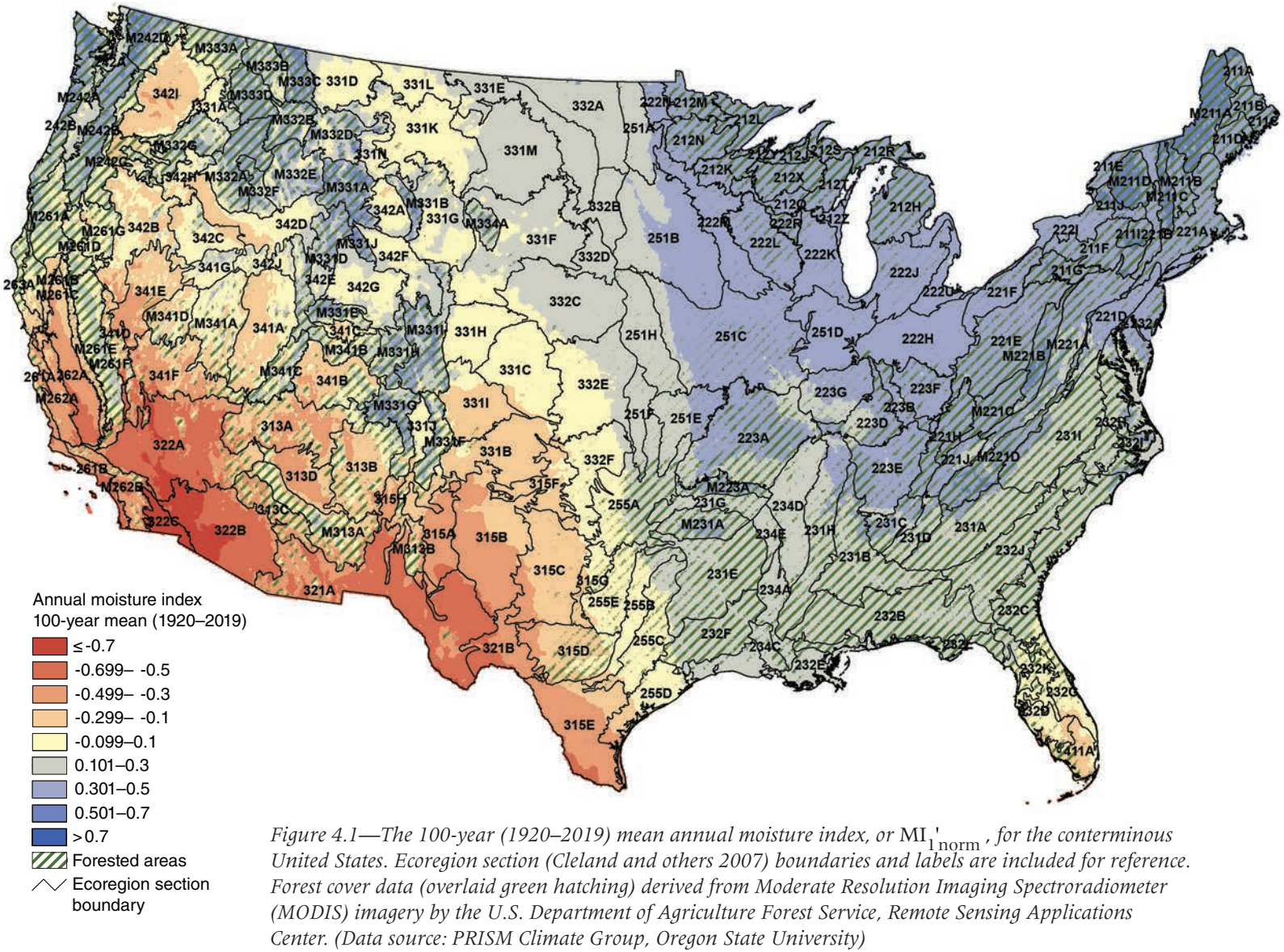

Figure 4.1—The 100-year (1920–2019) mean annual moisture index, or MI_{1norm}' *, for the conterminous United States. Ecoregion section (Cleland and others 2007) boundaries and labels are included for reference. Forest cover data (overlaid green hatching) derived from Moderate Resolution Imaging Spectroradiometer (MODIS) imagery by the U.S. Department of Agriculture Forest Service, Remote Sensing Applications Center. (Data source: PRISM Climate Group, Oregon State University)*

Table 4.1—Moisture difference *z*-score (*MDZ*) value ranges for nine wetness and drought categories, along with each category's approximate theoretical frequency of occurrence

MDZ	Category	Frequency
≤-2	Extreme drought	2.3%
-1.999 to -1.5	Severe drought	4.4%
-1.499 to -1	Moderate drought	9.2%
-0.999 to -0.5	Mild drought	15%
-0.499 to 0.5	Near normal conditions	38.2%
0.501 to 1	Mild moisture surplus	15%
1.001 to 1.5	Moderate moisture surplus	9.2%
1.501 to 2	Severe moisture surplus	4.4%
>2	Extreme moisture surplus	2.3%

observed in the driest parts of the Western United States, especially the Southwest (e.g., sections 322A–Mojave Desert, 322B–Sonoran Desert, and 322C–Colorado Desert), where potential evapotranspiration is very high, as in southern Florida, but precipitation levels are typically very low. In fact, because of generally lower precipitation than the East, dry climates (*MI'* <0) are typical across much of the Western United States. Nevertheless, mountainous areas in the central and northern Rocky Mountains as well as the Pacific Northwest are relatively wet, such as ecoregion sections M242A–Oregon and Washington Coast Ranges, M242B–Western Cascades, M331G–South Central Highlands, and M333C–Northern Rockies. In part, this is driven by large amounts of winter snowfall in these regions (Hanson and Weltzin 2000).

Figure 4.2 shows the annual (i.e., 1-year) *MDZ* map for 2019 for the conterminous United States. A striking feature of the map is the presence of moisture surplus conditions across much of the country. Nationally, 2019 was the second-wettest year since 1895, and several States had their wettest years on record, including Michigan, Wisconsin, and Minnesota (NOAA NCEI 2020a, 2020b). Although contiguous areas of extreme moisture surplus (*MDZ* >2) were extensive, many of them occurred in portions of the conterminous United States with little forest cover, such as the Northern Great Plains and the Desert Southwest. But, a few places that were extremely wet in 2019 do have significant forest cover, including eastern Maine (ecoregion sections 211B–Maine - New Brunswick Foothills and Lowlands and 211C–Fundy Coastal and Interior), the Great Lakes region (e.g., 212H–Northern Lower Peninsula, 212T–Northern Green Bay Lobe, and 222R–Wisconsin Central Sands), the Ozark Mountains (M223A–Boston Mountains), and the Black Hills (M334A). Another contiguous area of moderate to extreme surplus (*MDZ* >1) extended into northeastern and central Texas, most notably into forested portions of ecoregion sections 315G–Eastern Rolling Plains, 255E–Texas Cross Timbers and Prairie, 255B–Blackland Prairie, and 255C–Oak Woods and Prairie. These sections, which fall in a transition zone between wet and dry moisture regimes (see fig 4.1), experienced high levels of forest mortality in the years after a historically exceptional drought affected Texas in 2011 (Moore and others 2016).

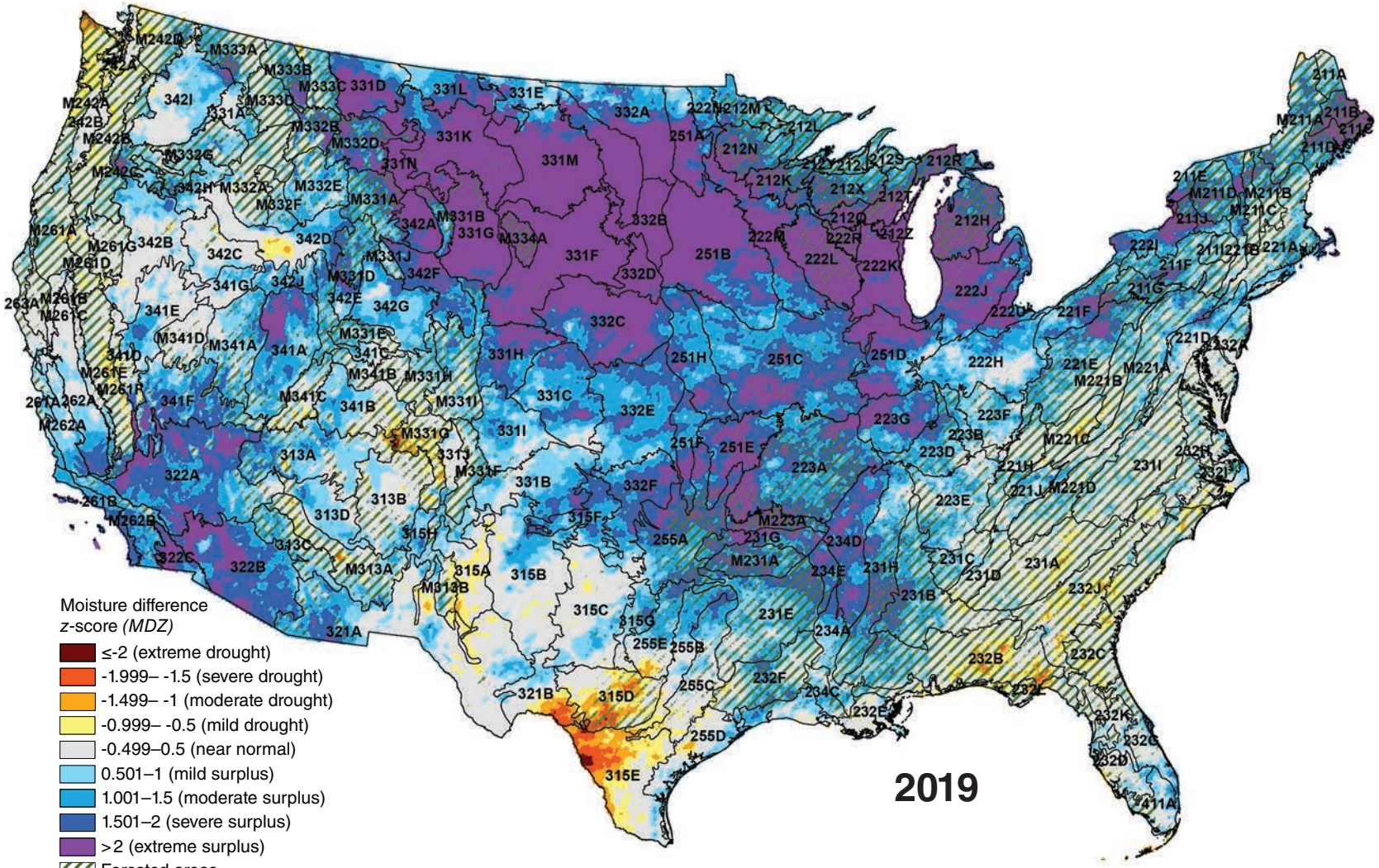

Figure 4.2—The 2019 annual (i.e., 1-year) moisture difference z-score, *or* MDZ, *for the conterminous United States. Ecoregion section (Cleland and others 2007) boundaries and labels are included for reference. Forest cover data (overlaid green hatching) derived from Moderate Resolution Imaging Spectroradiometer (MODIS) imagery by the U.S. Department of Agriculture Forest Service, Remote Sensing Applications Center. (Data source: PRISM Climate Group, Oregon State University)*

Areas of mild to moderate drought were scattered across the Southeastern and Mid-Atlantic United States in 2019 (fig. 4.2). Very small clusters of severe to extreme drought (*MDZ* ≤-1.5) occurred in the western portion of section M331G–South Central Highlands and at the northwestern tip of M242A–Oregon and Washington Coast Ranges. Both of these hot spots co-occurred with more widespread, but mild, drought conditions in nearby areas. The largest hot spot of severe to extreme drought during 2019 was in southern Texas, although this hot spot affected only one ecoregion section (315D–Edwards Plateau) with a significant amount of forest.

The 2019 *MDZ* map is consistent with summary metrics reported for the year (NOAA NCEI 2020b). According to the U.S. Drought Monitor, the percentage of conterminous U.S. area experiencing drought conditions reached an annual low of 2.3 percent in April, following a wet start to the year. The percentage of drought area peaked at 21.2 percent in October, after an unusually hot summer (and increased evapotranspiration) worsened conditions across the southern half of the conterminous United States. However, the percentage of drought area fell to 11.2 percent by the end of 2019, facilitated by wet conditions in the Southwest during November and December. The only parts of the country where precipitation levels for the year were much below average were southern Texas and coastal portions of Washington and Oregon (NOAA NCEI 2020a). These account for two of the three drought hot spots observed in the 2019 *MDZ* map (fig. 4.2).

By contrast, the 2018 *MDZ* map (fig. 4.3) shows a more pronounced dichotomy in moisture conditions between the eastern and western halves of the country. Surplus conditions were prevalent in the Eastern United States during 2018, with the exception of northern New England and southern Florida; indeed, the only sizeable cluster of severe to extreme drought was in section 411A–Everglades. In the Western United States, most forested areas were subjected to mild or worse drought conditions (*MDZ* ≤-0.5), although contiguous areas of severe to extreme drought were mostly limited to the central Rocky Mountains (e.g., M331G–South Central Highlands and M331I–Northern Parks and Ranges, both of which are heavily forested) and the Pacific Northwest (primarily M242B–Western Cascades).

The preponderance of near-normal to surplus conditions across the West in 2019 (fig. 4.2) relative to 2018 (fig. 4.3) may suggest an improved outlook for some areas that recently have experienced substantial forest health impacts due to drought, such as the central and southern Sierra Nevada Mountains (Fettig and others 2019). Nonetheless, any improvement is probably short-lived. The relatively wet conditions in 2019 obscure the fact that temperatures were above average for much of the conterminous United States; for the Southeast, it was the warmest year since 1895 (NOAA NCEI 2020a, 2020b). This accords with a steady warming trend since the 1970s that has been observed worldwide (Rahmstorf and others 2017). Under a warming climate,

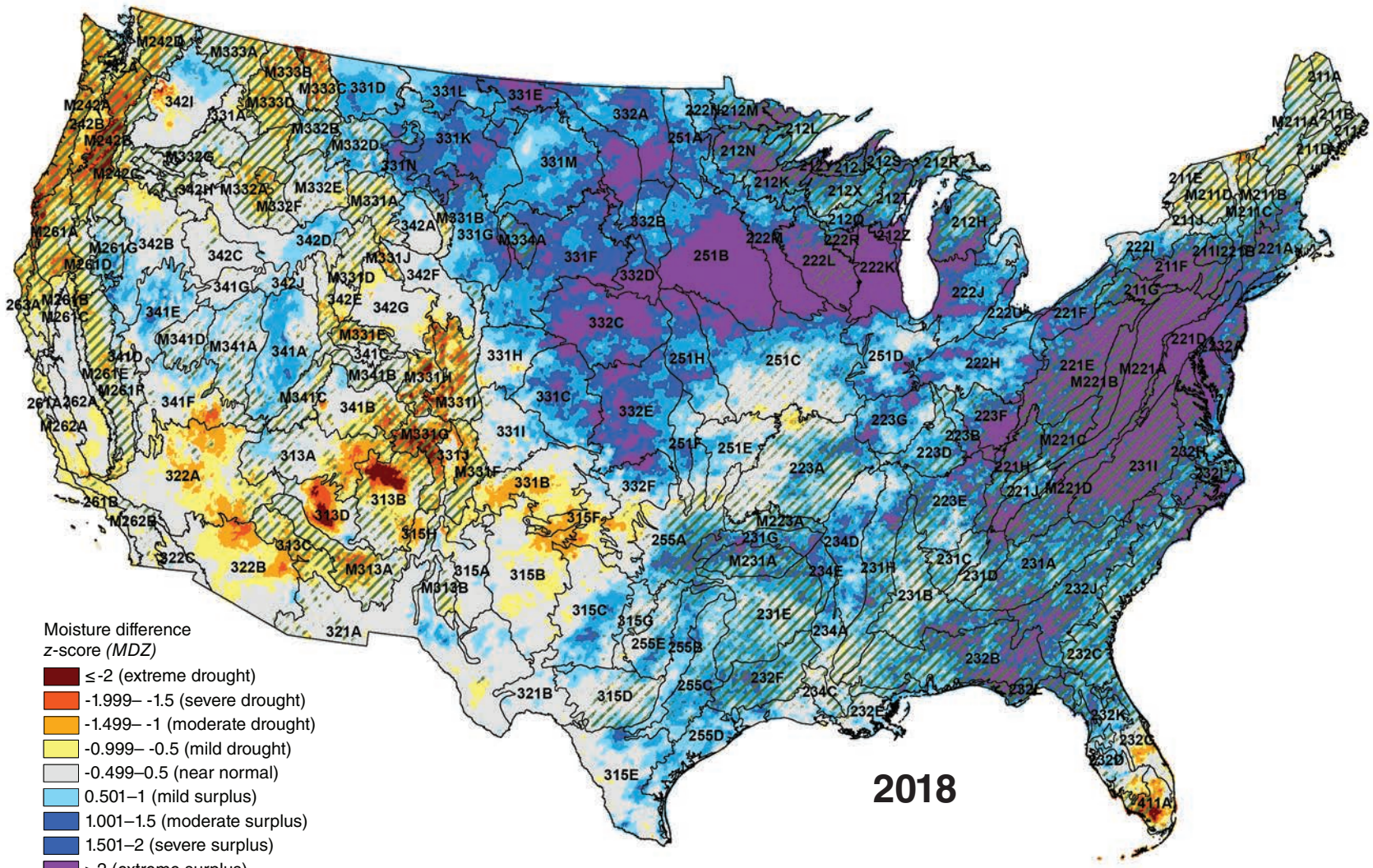

Figure 4.3—The 2018 annual (i.e., 1-year) moisture difference z*-score, or* MDZ*, for the conterminous United States. Ecoregion section (Cleland and others 2007) boundaries and labels are included for reference. Forest cover data (overlaid green hatching) derived from Moderate Resolution Imaging Spectroradiometer (MODIS) imagery by the U.S. Department of Agriculture Forest Service, Remote Sensing Applications Center. (Data source: PRISM Climate Group, Oregon State University)*

drought frequency, severity, and duration are expected to increase, particularly in the Western United States (Peltier and Ogle 2019, Williams and others 2013). Indeed, warmer temperatures have already shown the capacity to magnify moderate drought conditions into "megadroughts" that can have devastating impacts on forest systems (Brodribb and others 2020, Williams and others 2020). They have also triggered severe droughts in parts of the West where they have been relatively infrequent, including the Pacific Northwest (Marlier and others 2017).

Despite the amplifying effect of a warming climate, the Eastern United States has recorded few instances of persistent and intense drought in recent years. Generally, when such conditions have developed, they have been limited in geographic extent. Examples of this are captured in the 3-year (2017–2019; fig. 4.4) and 5-year (2015–2019; fig. 4.5) *MDZ* maps. With respect to the Eastern United States, the only sizeable hot spots of moderate or worse drought conditions (*MDZ* ≤-1) that appeared in both the 3- and 5-year *MDZ* maps were in sections 411A–Everglades and 232G–Florida Coastal Lowlands-Atlantic, although the latter hot spot was in an area with limited forest cover. Another small area of moderate or worse drought conditions occurred along the northern border of Maine (section M211A–White Mountains). Elsewhere in the East, scattered areas that exhibited moderate or worse drought conditions in one map had mild drought or near-normal conditions in the other, supporting the notion that prolonged drought has rarely been a concern in recent years for Eastern U.S. forests.

In the Western United States, most forested areas outside of the Four Corners region showed lower *MDZ* values in the 5-year map (fig. 4.5) than in the 3-year map (fig. 4.4). This indicates recent, albeit modest, improvement in moisture conditions for areas such as the northern Rocky Mountains (e.g., sections M333B–Flathead Valley and M333D–Bitterroot Mountains) and the Cascade Range (e.g., M242B–Western Cascades and M261B–Southern Cascades). Nevertheless, the practical significance of such changes is downplayed considerably by a historical record of chronic drought in many parts of the West extending back 3 or more decades (Clark and others 2016), as well as the aforementioned future projections of increased drought impacts in Western U.S. forests (Williams and others 2013).

With respect to moisture surplus conditions, the 3-year (fig. 4.4) and 5-year (fig. 4.5) *MDZ* maps depict disparity between the northern and southern halves of the conterminous United States as well as between the East and West. From the Rocky Mountains westward, the maps show only a handful of areas of severe to extreme moisture surplus (*MDZ* >1.5); furthermore, the locations where those surpluses persisted for 5 years (i.e., the northern portion of 341A–Bonneville Basin and the southwestern corner of 342B–Northwestern Basin and Range) contain little forest. In the Eastern United States,

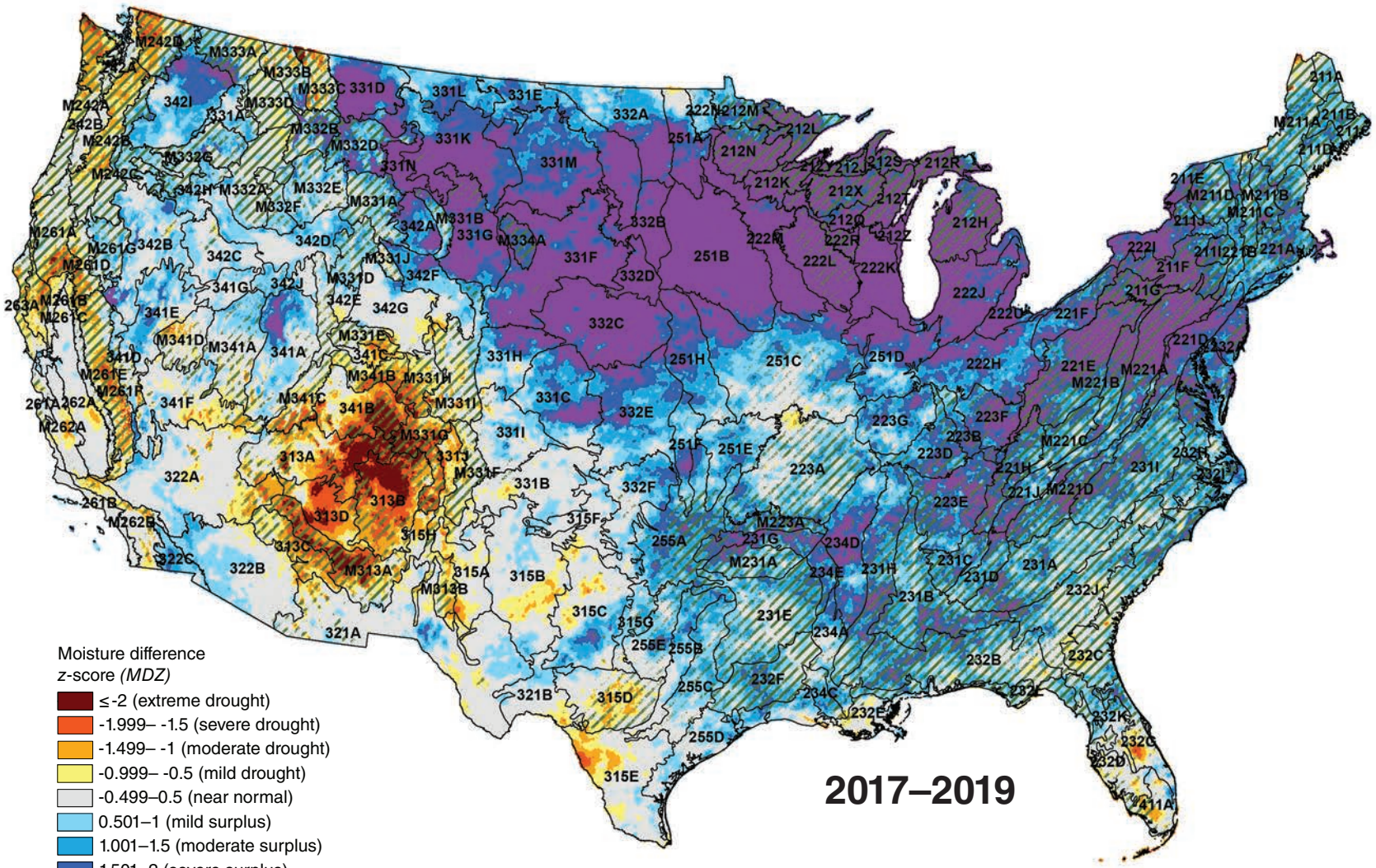

Figure 4.4—The 2017–2019 (i.e., 3-year) moisture difference z*-score (*MDZ*) for the conterminous United States. Ecoregion section (Cleland and others 2007) boundaries are included for reference. Forest cover data (overlaid green hatching) derived from Moderate Resolution Imaging Spectroradiometer (MODIS) imagery by the U.S. Department of Agriculture Forest Service, Remote Sensing Applications Center. (Data source: PRISM Climate Group, Oregon State University)*

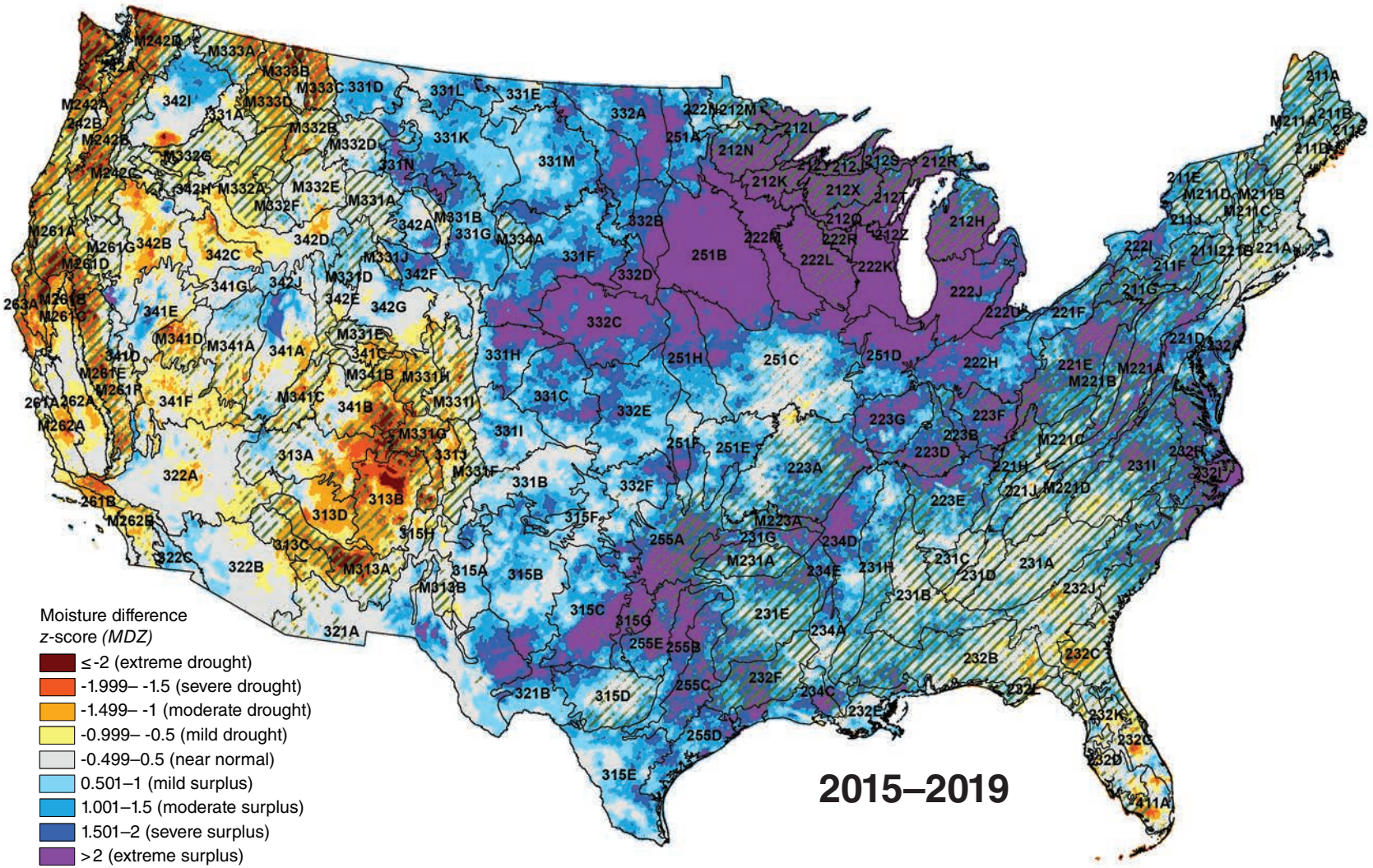

*Figure 4.5—The 2015–2019 (i.e., 5-year) moisture difference z-score (*MDZ*) for the conterminous United States. Ecoregion section (Cleland and others 2007) boundaries are included for reference. Forest cover data (overlaid green hatching) derived from Moderate Resolution Imaging Spectroradiometer (MODIS) imagery by the U.S. Department of Agriculture Forest Service, Remote Sensing Applications Center. (Data source: PRISM Climate Group, Oregon State University)*

areas of moisture surplus were more common than areas of drought. Contiguous areas of severe to extreme surplus were scattered across much of the Southeast, although the clusters were smaller on average in the 3-year *MDZ* map (fig. 4.4) than in the 5-year map (fig. 4.5). More noteworthy is the nearly continuous swath of extreme moisture surplus (*MDZ* >2) shown in the 3-year map, which extended from section 331D–Northwestern Glaciated Plains to 232A–Northern Atlantic Coastal Plain. Although some areas in this swath are sparsely forested, it encompassed a number of forested sections in the Great Lakes region (e.g., 211F–Northern Glaciated Allegheny Plateau, 211G–Northern Unglaciated Allegheny Plateau, 212J–Southern Superior Uplands, 212K–Western Superior Uplands, 212Q–North Central Wisconsin Uplands, 212R–Eastern Upper Peninsula, 212X–Northern Highlands, 212Y–Southwest Lake Superior Clay Plain, 221E–Southern Unglaciated Allegheny Plateau, and 222R–Wisconsin Central Sands). Although the 3-year and 5-year maps are relatively short-term depictions, the observations described above are in line with historical trends and future projections: since the mid-1900s, the Midwest and Northeast have experienced greater numbers of extreme precipitation events than other parts of the country, and that trend is expected to continue under a warming climate (Swanston and others 2018). In combination with milder winters, this could lead to increased frequency and severity of flooding.

Localized damage due to flooding is typical in U.S. forests, but other impacts related to prolonged surpluses are not fully understood. Recent research has suggested that persistent excess moisture can increase vulnerability of forests to pathogens and other disease-causing agents (Hubbart and others 2016). In particular, these agents may be enabled during times of high climatic variability, such as when a period of drought occurs immediately before or after a period of moisture surplus, or when wet and warm conditions co-occur (Hubbart and others 2016). In fact, rapid swings between drought and surplus conditions may induce tree mortality directly (Tei and others 2019). This argues for continued monitoring of forested areas that experience persistent moisture surpluses.

Future Efforts

The 1-year, 3-year, and 5-year *MDZ* maps of the conterminous United States are a recurring component of national forest health reporting. For interpretive purposes, it is critical to understand their limitations. Most notably, the *MDZ* approach omits certain factors that influence a location's moisture supply at finer spatial scales, such as winter snowpack, surface runoff, or groundwater storage. Furthermore, while the maps use a standardized index scale that can be used with time windows of any size, it is still important to choose a window size that is analytically appropriate. For example, an extreme drought that lasts for 5 years will have different forest health ramifications than

an extreme drought that ends after only 1 year. While the 1-year, 3-year, and 5-year *MDZ* maps provide a reasonably complete short-term picture, a region's longer term moisture trajectory may also be meaningful with respect to forest health. For instance, in regions where droughts have been frequent historically, some tree species are better drought-adapted than others (McDowell and others 2008). In any case, long periods of persistent moisture extremes could lead to eventual changes in regional forest composition (McEwan and others 2011, Mueller and others 2005). Such changes are likely to affect responses to future drought or surplus conditions, fire regimes, and the status of ecosystem services such as nutrient cycling and wildlife habitat (W.R.L. Anderegg and others 2013, DeSantis and others 2011). In the future, we hope to deliver quantitative evidence to forest managers and other decision makers regarding relationships between moisture extremes and significant forest health impacts such as regional-scale tree mortality (e.g., Edgar and others 2019, Mitchell and others 2014); ascertaining such relationships can be challenging, especially at broader spatial scales. Nevertheless, we also intend to investigate the capacity of moisture extremes to serve as inciting factors for other forest threats such as wildfire or pest outbreaks.

LITERATURE CITED

Abatzoglou, J.T.; Williams, A.P. 2016. Impact of anthropogenic climate change on wildfire across Western US forests. Proceedings of the National Academy of Sciences. 113(42): 11770–11775. https://doi.org/10.1073/pnas.1607171113.

Adams, H.D.; Guardiola-Claramonte, M.; Barron-Gafford, G.A. [and others]. 2009. Temperature sensitivity of drought-induced tree mortality portends increased regional die-off under global-change-type drought. Proceedings of the National Academy of Sciences. 106(17): 7063–7066. https://doi.org/10.1073/pnas.0901438106.

Akin, W.E. 1991. Global patterns: climate, vegetation, and soils. Norman, OK: University of Oklahoma Press. 370 p.

Allen, C.D.; Macalady, A.K.; Chenchouni, H. [and others]. 2010. A global overview of drought and heat-induced tree mortality reveals emerging climate change risks for forests. Forest Ecology and Management. 259(4): 660–684. https://doi.org/10.1016/j.foreco.2009.09.001.

Alley, W.M. 1984. The Palmer Drought Severity Index: limitations and assumptions. Journal of Climate and Applied Meteorology. 23(7): 1100–1109. https://doi.org/10.1175/1520-0450(1984)023<1100:TPDSIL>2.0.CO;2.

Anderegg, L.D.L.; Anderegg, W.R.L.; Berry, J.A. 2013. Not all droughts are created equal: translating meteorological drought into woody plant mortality. Tree Physiology. 33(7): 672–683. https://doi.org/10.1093/treephys/tpt044.

Anderegg, W.R.L.; Berry, J.A.; Field, C.B. 2012. Linking definitions, mechanisms, and modeling of drought-induced tree death. Trends in Plant Science. 17(12): 693–700. https://doi.org/10.1016/j.tplants.2012.09.006.

Anderegg, W.R.L.; Kane, J.M.; Anderegg, L.D.L. 2013. Consequences of widespread tree mortality triggered by drought and temperature stress. Nature Climate Change. 3(1): 30–36. https://doi.org/10.1038/nclimate1635.

Archaux, F.; Wolters, V. 2006. Impact of summer drought on forest biodiversity: what do we know? Annals of Forest Science. 63: 645–652. https://doi.org/10.1051/forest:2006041.

Bennett, A.C.; McDowell, N.G.; Allen, C.D.; Anderson-Teixeira, K.J. 2015. Larger trees suffer most during drought in forests worldwide. Nature Plants. 1(10): 15139. https://doi.org/10.1038/nplants.2015.139.

Berdanier, A.B.; Clark, J.S. 2016. Multiyear drought-induced morbidity preceding tree death in Southeastern U.S. forests. Ecological Applications. 26(1): 17–23. https://doi.org/10.1890/15-0274.

Bigler, C.; Bräker, O.U.; Bugmann, H. [and others]. 2006. Drought as an inciting mortality factor in Scots pine stands of the Valais, Switzerland. Ecosystems. 9(3): 330–343. https://doi.org/10.1007/s10021-005-0126-2.

Brodribb, T.J.; Powers, J.; Cochard, H.; Choat, B. 2020. Hanging by a thread? Forests and drought. Science. 368(6488): 261–266. https://doi.org/10.1126/science.aat7631.

Choat, B.; Brodribb, T.J.; Brodersen, C.R. [and others]. 2018. Triggers of tree mortality under drought. Nature. 558(7711): 531–539. https://doi.org/10.1038/s41586-018-0240-x.

Clark, J.S. 1989. Effects of long-term water balances on fire regime, north-western Minnesota. Journal of Ecology. 77: 989–1004. https://doi.org/10.2307/2260818.

Clark, J.S.; Iverson, L.; Woodall, C.W. [and others]. 2016. The impacts of increasing drought on forest dynamics, structure, and biodiversity in the United States. Global Change Biology. 22(7): 2329–2352. https://doi.org/10.1111/gcb.13160.

Cleland, D.T.; Freeouf, J.A.; Keys, J.E. [and others]. 2007. Ecological subregions: sections and subsections for the conterminous United States. Gen. Tech. Rep. WO-76D. Washington, DC: U.S. Department of Agriculture Forest Service. Map; Sloan, A.M., cartographer; presentation scale 1:3,500,000; colored. Also on CD-ROM as a GIS coverage in ArcINFO format.

Clinton, B.D.; Boring, L.R.; Swank, W.T. 1993. Canopy gap characteristics and drought influences in oak forests of the Coweeta Basin. Ecology. 74(5): 1551–1558. https://doi.org/10.2307/1940082.

Collins, B.M.; Omi, P.N.; Chapman, P.L. 2006. Regional relationships between climate and wildfire-burned area in the Interior West, USA. Canadian Journal of Forest Research. 36(3): 699–709. https://doi.org/10.1139/x05-264.

Daly, C.; Gibson, W.P.; Taylor, G.H. [and others]. 2002. A knowledge-based approach to the statistical mapping of climate. Climate Research. 22: 99–113. https://doi.org/10.3354/cr022099.

Dennison, P.E.; Brewer, S.C.; Arnold, J.D.; Moritz, M.A. 2014. Large wildfire trends in the Western United States, 1984–2011. Geophysical Research Letters. (41): 2928–2933. https://doi.org/10.1002/2014GL059576.

DeSantis, R.D.; Hallgren, S.W.; Stahle, D.W. 2011. Drought and fire suppression lead to rapid forest composition change in a forest-prairie ecotone. Forest Ecology and Management. 261(11): 1833–1840. https://doi.org/10.1016/j.foreco.2011.02.006.

Duever, M.J.; Meeder, J.F.; Meeder, L.C.; McCollum, J.M. 1994. The climate of south Florida and its role in shaping the Everglades ecosystem. In: Davis, S.M.; Ogden, J.C., eds. Everglades: the ecosystem and its restoration. Delray Beach, FL: St. Lucie Press: 225–248.

Edgar, C.B.; Westfall, J.A.; Klockow, P.A. [and others]. 2019. Interpreting effects of multiple, large-scale disturbances using national forest inventory data: a case study of standing dead trees in east Texas, USA. Forest Ecology and Management. 437: 27–40. https://doi.org/10.1016/j.foreco.2019.01.027.

Fettig, C.J.; Mortenson, L.A.; Bulaon, B.M.; Foulk, P.B. 2019. Tree mortality following drought in the central and southern Sierra Nevada, California, U.S. Forest Ecology and Management. 432: 164–178. https://doi.org/10.1016/j.foreco.2018.09.006.

Grundstein, A. 2009. Evaluation of climate change over the continental United States using a moisture index. Climatic Change. 93(1–2): 103–115. https://doi.org/10.1007/s10584-008-9480-3.

Guarín, A.; Taylor, A.H. 2005. Drought triggered tree mortality in mixed conifer forests in Yosemite National Park, California, USA. Forest Ecology and Management. 218: 229–244. https://doi.org/10.1016/j.foreco.2005.07.014.

Hanson, P.J.; Weltzin, J.F. 2000. Drought disturbance from climate change: response of United States forests. Science of the Total Environment. 262: 205–220. https://doi.org/10.1016/S0048-9697(00)00523-4.

Hubbart, J.A.; Guyette, R.; Muzika, R.-M. 2016. More than drought: precipitation variance, excessive wetness, pathogens and the future of the western edge of the Eastern Deciduous Forest. Science of the Total Environment. 566–567: 463–467. https://doi.org/10.1016/j.scitotenv.2016.05.108.

Jenkins, M.A.; Pallardy, S.G. 1995. The influence of drought on red oak group species growth and mortality in the Missouri Ozarks. Canadian Journal of Forest Research. 25(7): 1119–1127. https://doi.org/10.1139/x95-124.

Kareiva, P.M.; Kingsolver, J.G.; Huey, B.B., eds. 1993. Biotic interactions and global change. Sunderland, MA: Sinauer Associates, Inc. 559 p.

Keetch, J.J.; Byram, G.M. 1968. A drought index for forest fire control. Res. Pap. SE-38. Asheville, NC: U.S. Department of Agriculture Forest Service, Southeastern Forest Experiment Station. 35 p.

Koch, F.H.; Coulston, J.W. 2015. 1-year (2013), 3-year (2011–2013), and 5-year (2009–2013) drought maps for the conterminous United States. In: Potter, K.M.; Conkling, B.L., eds. Forest Health Monitoring: national status, trends, and analysis 2014. Gen. Tech. Rep. SRS-209. Asheville, NC: U.S. Department of Agriculture Forest Service, Southern Research Station: 57–71.

Koch, F.H.; Coulston, J.W. 2016. 1-year (2014), 3-year (2012–2014), and 5-year (2010–2014) maps of drought and moisture surplus for the conterminous United States. In: Potter, K.M.; Conkling, B.L., eds. Forest Health Monitoring: national status, trends, and analysis 2015. Gen. Tech. Rep. SRS-213. Asheville, NC: U.S. Department of Agriculture Forest Service, Southern Research Station: 61–78.

Koch, F.H.; Coulston, J.W. 2017. Moisture deficit and surplus in the conterminous United States for three time windows: 2015, 2013–2015, and 2011–2015. In: Potter, K.M.; Conkling, B.L., eds. Forest Health Monitoring: national status, trends, and analysis 2016. Gen. Tech. Rep. SRS-222. Asheville, NC: U.S. Department of Agriculture Forest Service, Southern Research Station: 63–80.

Koch, F.H.; Coulston, J.W. 2018. Moisture deficit and surplus in the conterminous United States for three time windows: 2016, 2014–2016, and 2012–2016. In: Potter, K.M.; Conkling, B.L., eds. Forest Health Monitoring: national status, trends, and analysis 2017. Gen. Tech. Rep. SRS-233. Asheville, NC: U.S. Department of Agriculture Forest Service, Southern Research Station: 65–84.

Koch, F.H.; Coulston, J.W. 2019. Drought and moisture surplus patterns in the conterminous United States: 2017, 2015–2017, and 2013–2017. In: Potter, K.M.; Conkling, B.L., eds. Forest Health Monitoring: national status, trends, and analysis 2018. Gen. Tech. Rep. SRS-239. Asheville, NC: U.S. Department of Agriculture Forest Service, Southern Research Station: 77–96.

Koch, F.H.; Coulston, J.W. 2020. Drought and moisture surplus patterns in the conterminous United States: 2018, 2016–2018, and 2014–2018. In: Potter, K.M.; Conkling, B.L., eds. Forest Health Monitoring: national status, trends, and analysis 2019. Gen. Tech. Rep. SRS-250. Asheville, NC: U.S. Department of Agriculture Forest Service, Southern Research Station: 83–102.

Koch, F.H.; Smith, W.D.; Coulston, J.W. 2013a. Recent drought conditions in the conterminous United States. In: Potter, K.M.; Conkling, B.L., eds. Forest Health Monitoring: national status, trends, and analysis 2011. Gen. Tech. Rep. SRS-185. Asheville, NC: U.S. Department of Agriculture Forest Service, Southern Research Station: 41–58.

Koch, F.H.; Smith, W.D.; Coulston, J.W. 2013b. An improved method for standardized mapping of drought conditions. In: Potter, K.M.; Conkling, B.L., eds. Forest Health Monitoring: national status, trends, and analysis 2010. Gen. Tech. Rep. SRS-176. Asheville, NC: U.S. Department of Agriculture Forest Service, Southern Research Station: 67–83.

Koch, F.H.; Smith, W.D.; Coulston, J.W. 2014. Drought patterns in the conterminous United States and Hawaii. In: Potter, K.M.; Conkling, B.L., eds. Forest Health Monitoring: national status, trends, and analysis 2012. Gen. Tech. Rep. SRS-198. Asheville, NC: U.S. Department of Agriculture Forest Service, Southern Research Station: 49–72.

Koch, F.H.; Smith, W.D.; Coulston, J.W. 2015. Drought patterns in the conterminous United States, 2012. In: Potter, K.M.; Conkling, B.L., eds. Forest Health Monitoring: national status, trends, and analysis 2013. Gen. Tech. Rep. SRS-207. Asheville, NC: U.S. Department of Agriculture Forest Service, Southern Research Station: 55–69.

Kolb, T.E.; Fettig, C.J.; Ayres, M.P. [and others]. 2016. Observed and anticipated impacts of drought on forest insects and diseases in the United States. Forest Ecology and Management. 380: 321–334. https://doi.org/10.1016/j.foreco.2016.04.051.

Laurance, S.G.W.; Laurance, W.F.; Nascimento, H.E.M. [and others]. 2009. Long-term variation in Amazon forest dynamics. Journal of Vegetation Science. 20(2): 323–333. https://doi.org/10.1111/j.1654-1103.2009.01044.x.

Littell, J.S.; Peterson, D.L.; Riley, K.L. [and others]. 2016. A review of the relationships between drought and forest fire in the United States. Global Change Biology. 22(7): 2353–2369. https://doi.org/10.1111/gcb.13275.

Marlier, M.E.; Xiao, M.; Engel, R. [and others]. 2017. The 2015 drought in Washington State: a harbinger of things to come? Environmental Research Letters. 12(11): 114008. https://doi.org/10.1088/1748-9326/aa8fde.

Martínez-Vilalta, J.; Lloret, F.; Breshears, D.D. 2012. Drought-induced forest decline: causes, scope and implications. Biology Letters. 8(5): 689–691. https://doi.org/10.1098/rsbl.2011.1059.

Mattson, W.J.; Haack, R.A. 1987. The role of drought in outbreaks of plant-eating insects. BioScience. 37(2): 110–118. https://doi.org/10.2307/1310365.

McDowell, N.; Pockman, W.T.; Allen, C.D. [and others]. 2008. Mechanisms of plant survival and mortality during drought: why do some plants survive while others succumb to drought? New Phytologist. 178: 719–739. https://doi.org/10.1111/j.1469-8137.2008.02436.x.

McEwan, R.W.; Dyer, J.M.; Pederson, N. 2011. Multiple interacting ecosystem drivers: toward an encompassing hypothesis of oak forest dynamics across eastern North America. Ecography. 34: 244–256. https://doi.org/10.1111/j.1600-0587.2010.06390.x.

McKee, T.B.; Doesken, N.J.; Kliest, J. 1993. The relationship of drought frequency and duration to time scales. In: Eighth conference on applied climatology, Anaheim, CA. Boston, MA: American Meteorological Society: 179–184.

Millar, C.I.; Westfall, R.D.; Delany, D.L. 2007. Response of high-elevation limber pine (*Pinus flexilis*) to multiyear droughts and 20th-century warming, Sierra Nevada, California, USA. Canadian Journal of Forest Research. 37: 2508–2520. https://doi.org/10.1139/X07-097.

Mitchell, P.J.; O'Grady, A.P.; Hayes, K.R.; Pinkard, E.A. 2014. Exposure of trees to drought-induced die-off is defined by a common climatic threshold across different vegetation types. Ecology and Evolution. 4(7): 1088–1101. https://doi.org/10.1002/ece3.1008.

Monteith, J.L. 1965. Evaporation and environment. Symposia of the Society for Experimental Biology. 19: 205–234.

Moore, G.W.; Edgar, C.B.; Vogel, J.G. [and others]. 2016. Tree mortality from an exceptional drought spanning mesic to semiarid ecoregions. Ecological Applications. 26(2): 602–611. https://doi.org/10.1890/15-0330.

Mueller, R.C.; Scudder, C.M.; Porter, M.E. [and others]. 2005. Differential tree mortality in response to severe drought: evidence for long-term vegetation shifts. Journal of Ecology. 93: 1085–1093. https://doi.org/10.1111/j.1365-2745.2005.01042.x.

National Oceanic and Atmospheric Adminstration (NOAA) National Centers for Environmental Information (NCEI). 2020a. National temperature and precipitation maps. https://www.ncdc.noaa.gov/temp-and-precip/us-maps/. [Date accessed: August 17, 2020].

National Oceanic and Atmospheric Adminstration (NOAA) National Centers for Environmental Information (NCEI). 2020b. State of the climate: drought for annual 2019. https://www.ncdc.noaa.gov/sotc/drought/201913. [Date accessed: August 19, 2020].

Norman, S.P.; Koch, F.H.; Hargrove, W.W. 2016. Review of broad-scale drought monitoring of forests: toward an integrated data mining approach. Forest Ecology and Management. 380: 346–358. https://doi.org/10.1016/j.foreco.2016.06.027.

Palmer, W.C. 1965. Metereological drought. Washington, DC: U.S. Department of Commerce, Weather Bureau. 58 p.

Peltier, D.M.P.; Ogle, K. 2019. Legacies of more frequent drought in ponderosa pine across the Western United States. Global Change Biology. 25(11): 3803–3816. https://doi.org/10.1111/gcb.14720.

Peng, C.; Ma, Z.; Lei, X. [and others]. 2011. A drought-induced pervasive increase in tree mortality across Canada's boreal forests. Nature Climate Change. 1(9): 467–471. https://doi.org/10.1038/nclimate1293.

Peters, M.P.; Iverson, L.R.; Matthews, S.N. 2015. Long-term droughtiness and drought tolerance of Eastern US forests over five decades. Forest Ecology and Management. 345: 56–64. https://doi.org/10.1016/j.foreco.2015.02.022.

Potter, C.S.; Klooster, S.A. 1999. Dynamic global vegetation modelling for prediction of plant functional types and biogenic trace gas fluxes. Global Ecology and Biogeography. 8(6): 473–488. https://doi.org/10.1046/j.1365-2699.1999.00152.x.

PRISM Climate Group. 2020. 2.5-arcmin (4 km) gridded monthly climate data. https://prism.oregonstate.edu. [Date accessed: July 13, 2020].

Raffa, K.F.; Aukema, B.H.; Bentz, B.J. [and others]. 2008. Cross-scale drivers of natural disturbances prone to anthropogenic amplification: the dynamics of bark beetle eruptions. BioScience. 58(6): 501–517. https://doi.org/10.1641/B580607.

Rahmstorf, S.; Foster, G.; Cahill, N. 2017. Global temperature evolution: recent trends and some pitfalls. Environmental Research Letters. 12(5): 54001. https://doi.org/10.1088/1748-9326/aa6825.

Rozas, V.; García-González, I. 2012. Too wet for oaks? Inter-tree competition and recent persistent wetness predispose oaks to rainfall-induced dieback in Atlantic rainy forest. Global and Planetary Change. 94–95: 62–71. https://doi.org/10.1016/j.gloplacha.2012.07.004.

Rozas, V.; Sampedro, L. 2013. Soil chemical properties and dieback of *Quercus robur* in Atlantic wet forests after a weather extreme. Plant and Soil. 373(1–2): 673–685. https://doi.org/10.1007/s11104-013-1835-5.

Schoennagel, T.; Veblen, T.T.; Romme, W.H. 2004. The interaction of fire, fuels, and climate across Rocky Mountain forests. BioScience. 54(7): 661–676. https://doi.org/10.1641/0006-3568(2004)054[0661:TIOFFA]2.0.CO;2.

Slette, I.J.; Post, A.K.; Awad, M. [and others]. 2019. How ecologists define drought, and why we should do better. Global Change Biology. 25(10): 3193–3200. https://doi.org/10.1111/gcb.14747.

Slette, I.J.; Smith, M.D.; Knapp, A.K. [and others]. 2020. Standardized metrics are key for assessing drought severity. Global Change Biology. 26(2): e1–e3. https://doi.org/10.1111/gcb.14899.

Steinemann, A. 2003. Drought indicators and triggers: a stochastic approach to evaluation. Journal of the American Water Resources Association. 39(5): 1217–1233. https://doi.org/10.1111/j.1752-1688.2003.tb03704.x.

Svoboda, M.; LeComte, D.; Hayes, M. [and others]. 2002. The drought monitor. Bulletin of the American Meteorological Society. 83(8): 1181–1190. https://doi.org/10.1175/1520-0477(2002)083<1181:TDM>2.3.CO;2 https://doi.org/10.1175/1520-0477-83.8.1181.

Swanston, C.; Brandt, L.A.; Janowiak, M.K. [and others]. 2018. Vulnerability of forests of the Midwest and Northeast United States to climate change. Climatic Change. 146(1): 103–116. https://doi.org/10.1007/s10584-017-2065-2.

Tei, S.; Sugimoto, A.; Yonenobu, H. [and others]. 2019. Effects of extreme drought and wet events for tree mortality: insights from tree-ring width and carbon isotope ratio in a Siberian larch forest. Ecohydrology. 12(8): e2143. https://doi.org/10.1002/eco.2143.

Thornthwaite, C.W. 1948. An approach towards a rational classification of climate. Geographical Review. 38(1): 55–94. https://doi.org/10.2307/210739.

Thornthwaite, C.W.; Mather, J.R. 1955. The water balance. Publications in Climatology. 8(1): 1–104.

Trouet, V.; Taylor, A.H.; Wahl, E.R. [and others]. 2010. Fire-climate interactions in the American West since 1400 CE. Geophysical Research Letters. 37(4): L04702. https://doi.org/10.1029/2009GL041695.

Vose, R.S.; Applequist, S.; Squires, M. [and others]. 2014. Improved historical temperature and precipitation time series for U.S. climate divisions. Journal of Applied Meteorology and Climatology. 53(5): 1232–1251. https://doi.org/10.1175/JAMC-D-13-0248.1.

Williams, A.P.; Allen, C.D.; Macalady, A.K. [and others]. 2013. Temperature as a potent driver of regional forest drought stress and tree mortality. Nature Climate Change. 3(3): 292–297. https://doi.org/10.1038/nclimate1693.

Williams, A.P.; Cook, E.R.; Smerdon, J.E. [and others]. 2020. Large contribution from anthropogenic warming to an emerging North American megadrought. Science. 368(6488): 314–318. https://doi.org/10.1126/science.aaz9600.

Willmott, C.J.; Feddema, J.J. 1992. A more rational climatic moisture index. Professional Geographer. 44(1): 84–88. https://doi.org/10.1111/j.0033-0124.1992.00084.x.

Zang, C.S.; Buras, A.; Esquivel-Muelbert, A. [and others]. 2020. Standardized drought indices in ecological research: why one size does not fit all. Global Change Biology. 26(2): 322–324. https://doi.org/10.1111/gcb.14809.

CHAPTER 5.
Tree Mortality

Mark J. Ambrose

INTRODUCTION

Tree mortality is a natural process in all forest ecosystems. High mortality can be an indicator of forest health problems. On a regional scale, high mortality levels may indicate widespread insect or disease impacts or stress from large-scale regional weather events, such as severe droughts. High mortality may also occur if a large proportion of the forest in a particular region is made up of older, senescent stands. The approach presented here seeks to detect mortality patterns that might reflect changes to ecosystem processes at large scales. In many cases, the proximate cause of mortality may be discernable. Understanding proximate causes of mortality ***may*** provide insight into whether the mortality is within the range of natural variation or reflects more fundamental changes to ecological processes.

DATA

Forest Inventory and Analysis (FIA) Phase 2 (P2) data were the basis of the mortality analysis. The FIA P2 data are collected across forested land throughout the United States, with approximately one plot per 6,000 acres of forest, using a rotating panel sample design (Bechtold and Patterson 2005). Field plots are divided into spatially balanced panels, with one panel being measured each year. A single cycle of measurements consists of measuring all panels. This "annualized" method of inventory was adopted, State by State, beginning in 1999. The cycle length (i.e., number of years required to measure all plot panels) ranges from 5 to 10 years.

An analysis of mortality requires data collected at a minimum of two points in time. Therefore, mortality analysis was possible for areas where data from repeated plot measurements using consistent sampling protocols were available (i.e., where one cycle of measurements had been completed and at least one panel of the next cycle had been measured, and where there had been no changes to the protocols affecting measurements of trees or saplings). In this report, as in recent years, the repeated P2 data were available for all of the Central and Eastern States. The most recent cycle of remeasurements for each State was used in this analysis.

In addition, mortality data have become available from parts of the Western United States. In the West, plots are remeasured on a 10-year cycle. Thus, estimates of growth and mortality from the Western States are based on less than a complete cycle of remeasurement. Working from an incomplete cycle of remeasurement, the effective sampling intensity for growth and mortality estimates is significantly lower than FIA's standard of one plot per 6,000 acres (table 5.1). Therefore, the sampling error percentage on growth and mortality estimates tends to be large. Results are not presented for ecoregion sections where fewer than 25 plots had been remeasured or

Table 5.1—Western States from which repeated Forest Inventory and Analysis Phase 2 measurements were available, the time period spanned by the data, and the effective sample intensity (based on the proportion of plots that had been remeasured) in the available datasets

State	Time period	Effective sample intensity
Arizona	2001–2018	one plot: 7,500 acres
California	2001–2017	one plot: 8,571 acres
Colorado	2002–2018	one plot: 8,571 acres
Idaho	2004–2018	one plot: 12,000 acres
Montana	2003–2018	one plot: 10,000 acres
Nevada	2004–2018	one plot: 12,000 acres
New Mexico	2005–2018	one plot: 15,000 acres
Oregon	2001–2017	one plot: 7,500 acres
Utah	2000–2018	one plot: 6,667 acres
Washington	2002–2017	one plot: 10,000 acres
Wyoming[a]	2000–2018	one plot: 7,500 acres

[a] Mortality estimates for Wyoming are based on a comparison of annualized inventory data with data from the final periodic inventory.

where the percentage of error was unacceptably high. Nevertheless, results presented for the West should be viewed as preliminary. Because of this, results from the West are discussed separately from those from the Eastern and Central United States. The division of Eastern/Central versus Western States, as well as the forest cover within those States, is shown in figure 5.1.

METHODS

The Forest Inventory and Analysis program calculates the annual growth, mortality, and removal volume on each plot over the interval between repeated measurements.[1] These values are stored in the FIA Database (version 8.0) (Burrill and others 2018). EVALIDator (ver. 1.8.0.01), an online tool for querying the FIA Database and generating area-based reports on forest characteristics (USDA Forest Service, FIA program 2019), was used to obtain annual gross growth[2] rates and mortality rates over the most recent measurement cycle for each of 113 ecoregion sections (Cleland and others 2007, McNab and others 2007) covering the Eastern and Central United States and 23 ecoregion sections in the Western[3] United States. For most States, the most recent cycle of available data ran through 2018[4] (e.g., data collected from 2012 through 2018).

[1] For a detailed explanation of how FIA calculates annualized growth, mortality, and removals, see Pugh and others (2018).

[2] Gross growth represents the increase in tree volume without adjusting for the volume of trees that died (i.e., mortality volume) in the ecoregion.

[3] At the time that this analysis was being completed, the method for estimating growth in the Interior West was different from that used in the rest of the United States. Because this would lead to results that would not be comparable to those in the rest of the United States, Interior West data were excluded and MRATIOs were only calculated for the West Coast States.

[4] Overall, the most recent data available for any State ranged from 2016 to 2019.

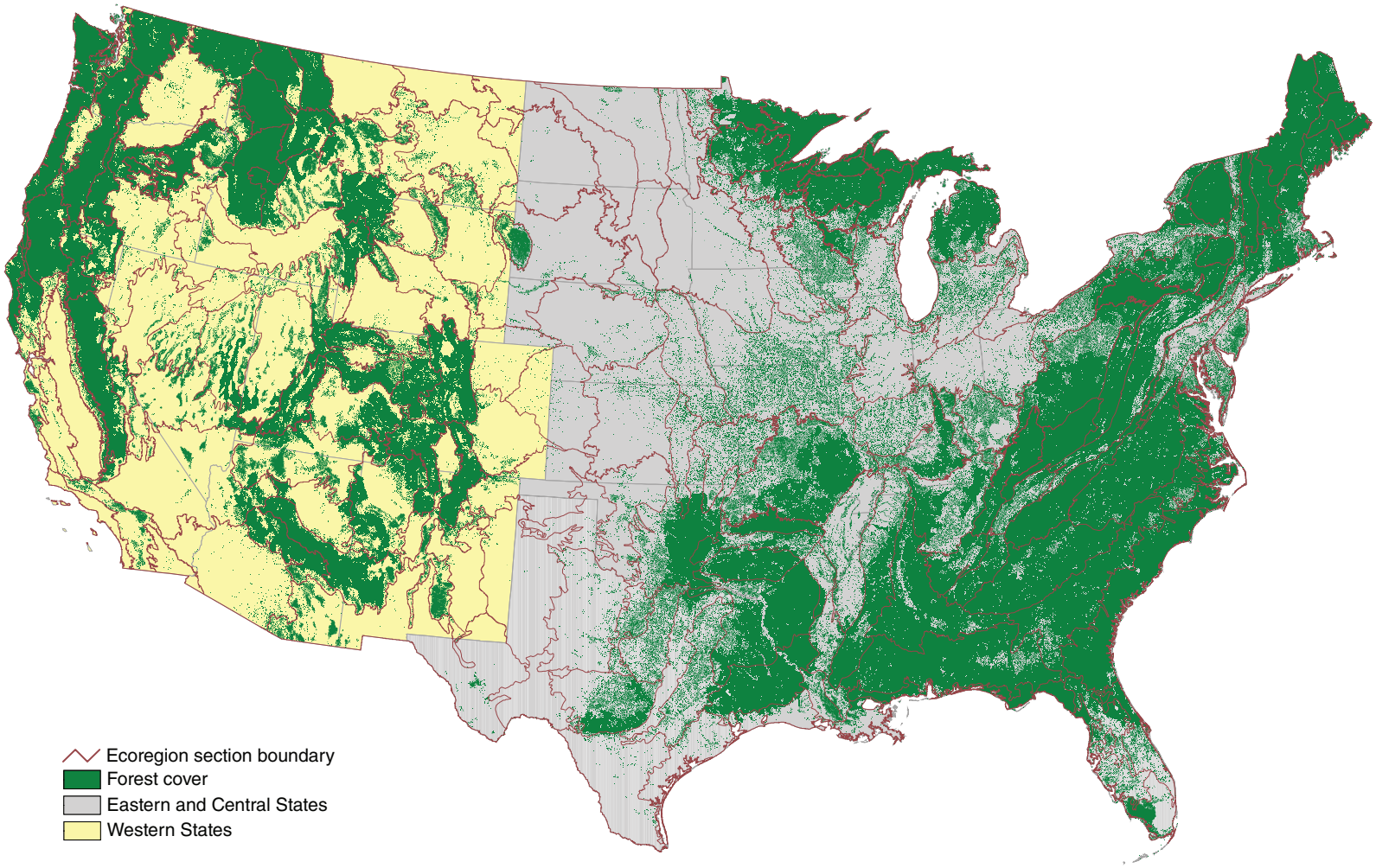

Figure 5.1—Forest cover in the States where mortality was analyzed by ecoregion section (Cleland and others 2007). Mortality in Eastern and Central States was analyzed using a complete remeasurement cycle; in most Western States, mortality was analyzed using a partial cycle of remeasurements, and results there should be considered preliminary. Forest cover was derived from Moderate Resolution Imaging Spectroradiometer (MODIS) satellite imagery (USDA Forest Service 2008).

To compare mortality across forest types and climate zones, the ratio of annual mortality to gross growth (MRATIO) was used as a standardized mortality indicator (Coulston and others 2005). The MRATIO has proven to be a useful indicator of forest health, but it can be a problematic indicator, especially when growth rates are very low. The MRATIO can also be difficult to interpret when there is high uncertainty to growth estimates. Both of these are the case with the data currently available from the West. Therefore, mortality as a percentage of total live volume also was calculated:

$$\text{Mortality percent} = m / v_l * 100$$

where

m = annual mortality (cubic feet per year)

v_l = total live tree volume (cubic feet)

When both this mortality percentage and the MRATIO are high, it suggests a possibly serious forest health concern.

To identify causal agents for the observed mortality, EVALIDator was also used to summarize by the reported "cause of death" associated with the observed mortality. Causes of death are reported as general categories (e.g., insects, fire, weather). For each ecoregion with a high MRATIO, EVALIDator was used to generate a table of annual mortality volume by FIA species group (Burrill and others 2018) and cause of death. From these tables, it is possible to make reasonable assumptions about the particular insects or diseases that may be affecting particular regions. Care must be used in interpreting these causes because tree mortality actually may be caused by a combination of factors (e.g., drought and insects). Further information about the causes of mortality is provided by the aerial survey of insects and disease (see ch. 2 in this report). It is difficult to directly match aerial survey data to mortality observed on FIA plots due to both the difference in timing when mortality is recorded and difficulty matching plot locations with aerial survey mortality polygons. However, aerial survey information has been incorporated into the discussion by referencing State Forest Health Highlights, which reflect in large part the results of aerial surveys.

In addition, mortality rates were derived for each forest type group (Burrill and others 2018, USDA Forest Service 2008) for each ecoregion section. At times, identifying the forest type experiencing high mortality can be more useful than identifying the species group, especially when the cause of death is abiotic.

RESULTS AND DISCUSSION

The MRATIO values are shown in figure 5.2. The MRATIO can be large if an over-mature forest is senescing and losing a cohort of older trees. If forests are not naturally senescing, a high MRATIO (>0.6) may indicate high mortality due to some acute cause (insects or pathogens) or due to generally deteriorating forest health conditions. The ecoregion sections

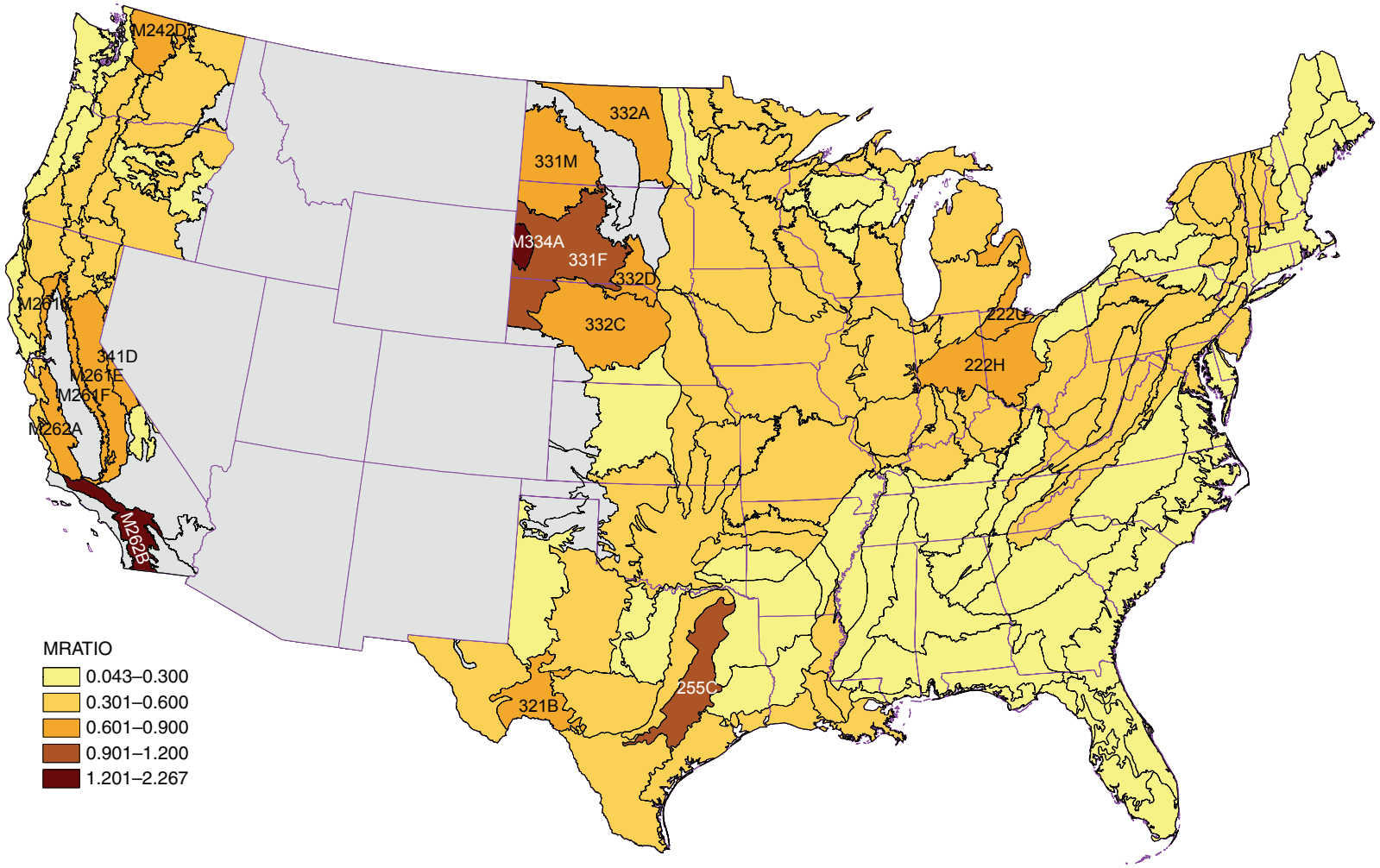

Figure 5.2—Tree mortality expressed as the ratio of annual mortality volume to gross annual volume growth (MRATIO) by ecoregion section (Cleland and others 2007). Data unavailable or insufficient for gray areas. (Data source: U.S. Department of Agriculture Forest Service, Forest Inventory and Analysis program)

with the highest MRATIOs are labeled on the map. In the discussion that follows, the focus is placed on the ecoregions having MRATIOs >0.6.

Eastern and Central States

The highest MRATIOs occurred in ecoregion sections 331F–Western Great Plains (MRATIO = 0.97) in South Dakota and Nebraska and M334A–Black Hills (MRATIO = 1.33). Other areas of high mortality relative to growth on the Great Plains were ecoregion sections 332C–Nebraska Sand Hills (MRATIO = 0.71) and 332D–North-Central Great Plains (MRATIO = 0.70) in South Dakota and Nebraska, 331M–Missouri Plateau (MRATIO = 0.73) in North and South Dakota, and 332A–Northeastern Glaciated Plains (MRATIO = 0.86) in North Dakota. In these Great Plains ecoregion sections where mortality is high relative to growth, the predominant vegetation is grassland. Although the ecoregion sections are quite large, there was relatively little forest land to measure (e.g., 64 forested plots in section 332A and 87 plots in region 331M). In the Plains, tree growth is generally slow because of naturally dry conditions. Where the number of sample plots is small and tree growth is naturally slow, care must be taken in interpreting mortality relative to growth.

In ecoregion section M334A–Black Hills (MRATIO = 1.33), the vast majority (93 percent) of mortality occurred in the ponderosa and Jeffrey pine species group. For the entire ecoregion section, 76 percent of mortality was caused by insects, while 14 percent was caused by fire (table 5.2); for ponderosa (*Pinus ponderosa*) and Jeffrey pine (*P. jeffreyi*), insects and fire were responsible for 74 and 16 percent of mortality, respectively. Mortality in this ecoregion is most likely related to mountain pine beetle (*Dendroctonus ponderosae*). There had been an ongoing pine beetle outbreak in the Black Hills region (Ball and others 2015, 2016; South Dakota Department of Agriculture 2011, 2012, 2013, 2014), though pine beetle activity has declined dramatically in the region since 2015 (Ball and others 2017, Wyoming State Forestry Division 2017). The pine beetle outbreak has ended, but reported mortality remains high because results reported, based on the most recent cycles of FIA data, reflect mortality over the period that includes the peak of the outbreak in 2015.

In ecoregion section 331F–Western Great Plains (MRATIO = 0.97), fire caused 64 percent of mortality; another 19 percent of mortality was weather-related (table 5.2). In this ecoregion section, most of the mortality (about 86 percent) occurred in the ponderosa and Jeffrey pine species group. In this species group, 64 percent of mortality was due to fire and 22 percent was due to adverse weather. Only 7 percent of pine mortality was related to insects.

The majority of the mortality in ecoregion 332A–Northeastern Glaciated Plains (MRATIO = 0.86) of North Dakota was split between the cottonwood and aspen (49 percent), white oak (24 percent), and other eastern soft hardwoods (18 percent) species groups. About 37 percent of

Table 5.2—Ecoregion sections in Eastern and Central States having the highest mortality relative to growth (MRATIO), annual mortality and growth rates, and associated causes of mortality

Ecoregion section	Average annual mortality	Average annual gross growth	MRATIO	Major causes of mortality
	------- *cubic feet per year* -------			
M334A–Black Hills	49,178,883	37,114,310	1.33	Insects (76%), fire (14%)
331F–Western Great Plains	12,075,815	12,396,781	0.97	Fire (64%), weather-related (19%)
255C–Oak Woods and Prairies	133,746,975	140,657,294	0.95	Weather-related (67%), disease (18%)
332A–Northeastern Glaciated Plains	8,025,426	9,296,699	0.86	Weather-related (37%), animals (13%)
321B–Stockton Plateau	8,149,276	9,953,146	0.82	Weather-related (69%), fire (30%)
331M–Missouri Plateau	6,393,366	8,777,223	0.73	Weather-related (71%)
332C–Nebraska Sand Hills	10,008,123	14,059,636	0.71	Insects (36%)
332D–North-Central Great Plains	7,993,301	11,460,800	0.70	Fire (39%), insects (19%), disease (18%)
222U–Lake Whittlesey Glaciolacustrine Plain	44,588,109	67,460,158	0.66	Insects (67%)
222H–Central Till Plains-Beech-Maple	111,024,790	176,893,434	0.63	Insects (51%)

the mortality overall (table 5.2) and 38 percent of cottonwood/aspen (*Populus* spp.) mortality was related to adverse weather. North Dakota experienced numerous storm events over the past several years, including 435 hail events and 66 tornadoes during the 2015 and 2016 growing seasons. Damage due to hail storms can make trees susceptible to a number of fungal diseases (North Dakota Forest Service 2015, 2016). Cottonwood canker fungi have been identified as a problem throughout North Dakota (North Dakota Forest Service 2014, 2015); these fungi may be contributing to the observed cottonwood mortality. About 13 percent of mortality was attributed to animals; almost all of this occurred in the cottonwood/aspen species group.

In ecoregion 331M–Missouri Plateau (MRATIO = 0.73), about 72 percent of the mortality (by volume) occurred in the cottonwood and aspen species group. About 71 percent of total mortality (table 5.2) and 90 percent of cottonwood/aspen mortality was identified as weather-related. Adverse weather conditions, including both drought and excessively wet conditions, occurred during the remeasurement cycle (Ball and others 2017; Johnson 2017; North Dakota Forest Service 2012, 2013; South Dakota Department of Agriculture 2012). Multiple tree-damaging storm events, including both hail storms and tornadoes, also occurred over that period (Johnson 2017, North Dakota Forest Service

2016). As mentioned above, cottonwood canker fungi have been identified as a problem throughout North Dakota (North Dakota Forest Service 2014, 2015) and may be contributing to the observed cottonwood mortality.

In ecoregion 332C–Nebraska Sand Hills (MRATIO = 0.71), about 45 percent of the mortality occurred in the cottonwood and aspen species group. About 36 percent of total mortality (table 5.2) and 30 percent of cottonwood/aspen mortality was due to insects. However, the cause of the majority of overall mortality (51 percent) as well as cottonwood/aspen mortality (68 percent) was classified as "unknown/other."

In 332D–North-Central Great Plains (MRATIO = 0.70), 39 percent of mortality was due to fire, while insects were responsible for 19 percent of mortality, and 18 percent of mortality was attributed to diseases (table 5.2). Mortality was high in multiple species groups, including the white oak, ponderosa and Jeffrey pine, other eastern softwoods, and other eastern soft hardwoods species groups. The majority of oak (*Quercus* spp.) and pine mortality was due to fire (74 percent and 65 percent, respectively). Disease was the major cause of mortality in the other eastern soft hardwoods species group (63 percent of mortality). A number of agents may have contributed to the mortality, including oak decline, which has been reported in northern and eastern Nebraska (Nebraska Forest Service 2017, 2018), bur oak blight (*Tubakia iowensis*), and Dutch elm disease (*Ophiostoma novo-ulmi*) (Ball and others 2017, 2018).

Mortality relative to growth was also rather high (MRATIO = 0.66) in ecoregion section 222U–Lake Whittlesey Glaciolacustrine Plain. There, the majority of the mortality (67 percent) was ash (*Fraxinus* spp.). About 67 percent of mortality in that ecoregion section was caused by insects (table 5.2), and insects were responsible for 98 percent of ash mortality. Most of this mortality was due to emerald ash borer (*Agrilus planipennis*), which has produced extremely high ash mortality throughout Ohio and Michigan (Michigan Department of Natural Resources 2014, 2015, 2016, 2017; Ohio Department of Natural Resources, Division of Forestry 2014, 2015). In fact, emerald ash borer has caused the death of the "vast majority" of native ash in northwestern Ohio (Ohio Department of Natural Resources, Division of Forestry 2016, 2017).

Similarly, in the adjacent ecoregion section 222H–Central Till Plains-Beech-Maple (MRATIO = 0.63) in Ohio and Indiana, much of the mortality (53 percent) was ash, and 96 percent of ash mortality was due to insects (table 5.2), most likely emerald ash borer. Indeed, emerald ash borer has been confirmed throughout the ecoregion as well as throughout Indiana (Marshall, 2017, 2018; Ohio Department of Natural Resources, Division of Forestry 2016, 2017). For species other than ash, the mortality-causing agent was most frequently not identified.

Ecoregion section 255C–Oak Woods and Prairies in Texas also had relatively high mortality (MRATIO = 0.95). About 49 percent

of the mortality occurred in the red and white oak species groups, and another 18 percent occurred in the loblolly and shortleaf pine species group. The majority (67 percent) of mortality in this ecoregion section was identified as weather-related (table 5.2). Weather was responsible for 72 percent of oak mortality and 43 percent of pine mortality. A record-setting drought in 2011 affected Oklahoma and Texas (Oklahoma Forestry Services 2014, 2015, 2016). It was reported as weakening both pines and hardwoods in Texas, making them susceptible to a variety of pests and pathogens (Smith 2013, 2014). Disease was the reported cause of another 18 percent of mortality (table 5.2). Disease was reported as responsible for 24 percent of oak mortality; fire was responsible for 41 percent of pine mortality. Oak wilt has been a major problem in oak woodlands in central Texas (Smith 2014; Texas A&M Forest Service 2015, 2016, 2019) and probably contributed to the red and white oak mortality. Pine engraver beetle (*Ips* spp.) has been a problem in Texas' pine forests and may have contributed to mortality in the loblolly and shortleaf pine species group (Smith 2014; Texas A & M Forest Service 2015, 2016, 2017).

In ecoregion 321B–Stockton Plateau (MRATIO = 0.82), 69 percent of mortality was related to adverse weather, and another 30 percent was due to fire (table 5.2). About 89 percent of mortality occurred in the western woodland softwoods species group. Most of this mortality probably was related to the previously discussed drought that affected Texas beginning in 2011.

Western States

As mentioned above, in all Western States, less than the full panel of plots have been remeasured. Thus, the mortality results presented here should be considered preliminary. Also, one must be aware that, because of the longer 10-year measurement cycle in the West, results shown represent mortality that may have occurred any time during the period spanned by the data (see table 5.1), which may have been as long as 18 years.

For a large portion of the West, no MRATIO has been presented. At the time this chapter was being written, the Interior West FIA region used a different method for estimating growth than the rest of the country. Thus, MRATIOs calculated for Interior West States were not comparable to values from the rest of the country, and no MRATIOs were presented for ecoregions in those States. MRATIOs were also not calculated for some ecoregions in West Coast States. This was because either (1) fewer than 25 plots had been remeasured in an ecoregion, or (2) the percent sampling error for the growth estimate was too high (>100 percent). Aside from the Interior West region, ecoregions omitted from the analysis were mostly nonforest (mostly desert or grassland, heavily urbanized, or mostly converted to agriculture).

West Coast ecoregion sections having the highest MRATIOs are shown in table 5.3 with the major causes of death identified. Seeing that fire and weather as well as insects and disease

Table 5.3—Ecoregion sections in West Coast States having the highest mortality relative to growth (MRATIO), annual mortality and growth rates, and associated causes of mortality

Ecoregion section	Average annual mortality	Average annual gross growth	MRATIO	Major causes of mortality
	------- *cubic feet per year* -------			
M262B–Southern California Mountain and Valley	30,749,476	13,564,463	2.27	Fire (67%), insects (10%), weather-related (10%)
341D–Mono	6,800,601	9,241,166	0.74	Insects (44%), fire (35%), disease (15%)
M242D–Northern Cascades	341,346,926	469,304,231	0.73	Insects (32%), fire (25%), weather-related (16%), disease (16%)
M261E–Sierra Nevada	435,027,997	641,958,197	0.68	Fire (32%), disease (30%), weather-related (12%), insects (13%)
M261C–Northern California Interior Coast Ranges	5,272,704	7,881,888	0.67	Fire (46%), disease (26%), weather-related (12%)
M261F–Sierra Nevada Foothills	20,425,732	32,442,906	0.63	Disease (20%), weather-related (16%), fire (12%)
M262A–Central California Coast Ranges	6,021,453	9,629,495	0.63	Disease (33%), fire (22%), weather-related (15%)

were responsible for significant mortality in these West Coast ecoregion sections, mortality was summarized by both forest type group and species group. One would expect that patterns of mortality caused by biotic factors (insects, disease) would be most apparent when looking at species groups affected, while patterns of mortality caused by abiotic factors (weather, fire) would be most apparent when looking at forest types affected.

Of the ecoregion sections of the West Coast States where the MRATIO could be calculated, ecoregion section M262B–Southern California Mountain and Valley (MRATIO = 2.27) stands out. This is the highest MRATIO found anywhere in the United States. Fire was responsible for 67 percent of this mortality (table 5.3). Insects were responsible for 10 percent of mortality, and adverse weather was responsible for another 10 percent. About 57 percent of the mortality in this ecoregion section occurred in the Western Oak forest type group, and most of that mortality (79 percent) was due to fire. Fire was also responsible for most of the mortality (76 percent) in the Pinyon/juniper forest type group, where 7 percent of the ecoregion's mortality occurred. Insects were responsible for almost all the mortality in the Ponderosa Pine forest type group and about 43 percent of the mortality in the California Mixed Conifer forest type group; they were responsible for about 21 percent of the mortality in the ponderosa and Jeffrey pine species group and about 17 percent of the other western softwoods species group.

In ecoregion section 341D–Mono (MRATIO = 0.74), about 64 percent of mortality occurred in the western woodland softwoods species

group, and about 21 percent was lodgepole pine (*P. contorta*). All of the lodgepole pine mortality was attributed to insects, while for western woodland softwoods, about 49 percent of mortality was due to fire, about 28 percent was due to insects, and 19 percent was due to disease.

In M261E–Sierra Nevada (MRATIO = 0.68), mortality occurred in a large number of species groups, with the highest mortality suffered by true firs (43 percent), ponderosa and Jeffrey pine (17 percent), and sugar pine (11 percent). A variety of agents (insects, disease, fire, and weather) contributed to the observed mortality. Disease was the single most important cause of mortality in the true firs and sugar pine.

In M261C–Northern California Interior Coast Ranges (MRATIO = 0.67), almost all of the mortality occurred in the Western Oak forest type group (which does not include tanoak-dominated forest types). About 41 percent of the mortality was oaks, and about 54 percent was the other western softwoods species group. About 52 percent of the oak mortality and about 40 percent of the softwood mortality was due to fire. Another 40 percent of softwood mortality was attributed to disease.

Similarly, in M261F–Sierra Nevada Foothills (MRATIO = 0.63), almost all of the mortality occurred in the Western Oak forest type group. About 65 percent of the mortality was oaks, about 17 percent was other western softwoods, and 8 percent was ponderosa/Jeffrey pine. However, in this ecoregion section, a variety of agents (disease, fire, and weather) all contributed to the observed mortality (table 5.3).

Likewise, in ecoregion section M262A–Central California Coast Ranges (MRATIO = 0.63), almost all of the mortality occurred in the Western Oak forest type group. About 81 percent of the mortality was oaks. In this ecoregion section, disease was responsible for 33 percent of mortality, fire caused 22 percent of mortality, and 15 percent of mortality was attributed to adverse weather (table 5.3).

At a broad scale, we see that in much of California tree mortality is often related to a combination of prolonged drought (2011–2015 statewide; 2011–2017 in parts of the State), bark beetles, and fire (California Forest Pest Council 2015, 2016, 2017). These factors have interacted, leading to high mortality, especially in southern California. Overstocked stands in many parts of the State have contributed to the drought stress and susceptibility of forests to insects and wildfires (California Forest Pest Council 2015, 2016, 2017). It should also be noted that the same drought which led to high mortality (directly or indirectly) would also have reduced growth over the measurement period; reduced growth also contributes to a high MRATIO (see Methods section).

Aside from California, the highest MRATIO (0.73) occurred in ecoregion section M242D–Northern Cascades. There, mortality occurred in a large number of species groups, including

Engelmann and other spruces (22 percent), true firs (24 percent), lodgepole pine (15 percent), and Douglas-fir (17 percent). While insects and fire were the most significant mortality-causing agents, other factors, including disease and adverse weather, also contributed significantly to the observed mortality (table 5.3).

Figure 5.3 shows the ratio of annual mortality to standing live tree volume for the United States. In most of the country, the ecoregions having high mortality relative to standing volume are the same regions that had high MRATIOs (fig. 5.2).

Focusing on the Interior West, we see two clusters of ecoregion sections where mortality is high relative to standing live volume: a cluster of mountain ecoregion sections in western Montana, central Idaho, and northwestern Wyoming (M331A–Yellowstone Highlands, M331J–Wind River Mountains, M332A–Idaho Batholith, M332B–Northern Rockies and Bitterroot Valley, M332D–Belt Mountains, M332E–Beaverhead Mountains, and M332F–Challis Volcanics) and a cluster including the Front Range of Colorado and southern Wyoming (M331I–Northern Parks and Ranges) and the south-central highlands of Colorado and northern New Mexico (M331G–South-Central Highlands) together with the Uinta Mountains of Utah (M331E–Uinta Mountains). In all of these ecoregion sections, annual mortality exceeded 2.5 percent of live volume (table 5.4).

In Colorado and Wyoming, 61 percent of the mortality in ecoregion section M331I–Northern Parks and Ranges was lodgepole pine, and another 20 percent was the Engelmann and other spruces species group; almost all of this mortality was attributed to insects. The ecoregion includes areas that have experienced major outbreaks of mountain pine beetle as well as spruce beetle (*D. rufipennis*) (Colorado State Forest Service 2016; Wyoming State Forestry Division 2016, 2017). These same pests have been affecting ecoregion M331E–Uinta Mountains (USDA Forest Service, Uinta-Wasatch-Cache National Forest [N.d.], Utah Department of Natural Resources, Forestry, Fire, & State Lands 2016), where 62 percent of mortality was lodgepole pine, and 18 percent was the Engelmann and other spruces species group. Here, also, most of the mortality was caused by insects. In ecoregion section M331G–South-Central Highlands, about two-thirds of mortality overall was caused by insects. In this ecoregion section, about 64 percent of mortality was the Engelmann and other spruces species group; 88 percent of spruce mortality was due to insects. In this area, spruce beetle has caused significant mortality (Colorado State Forest Service 2016, 2017; Zegler 2015, 2016; Zegler and Formby 2017).

In the areas of high mortality in Montana, Idaho, and northwestern Wyoming (ecoregion sections M331A, M331J, M332A, M332B, M332D, M332E, and M332F), insects and fire

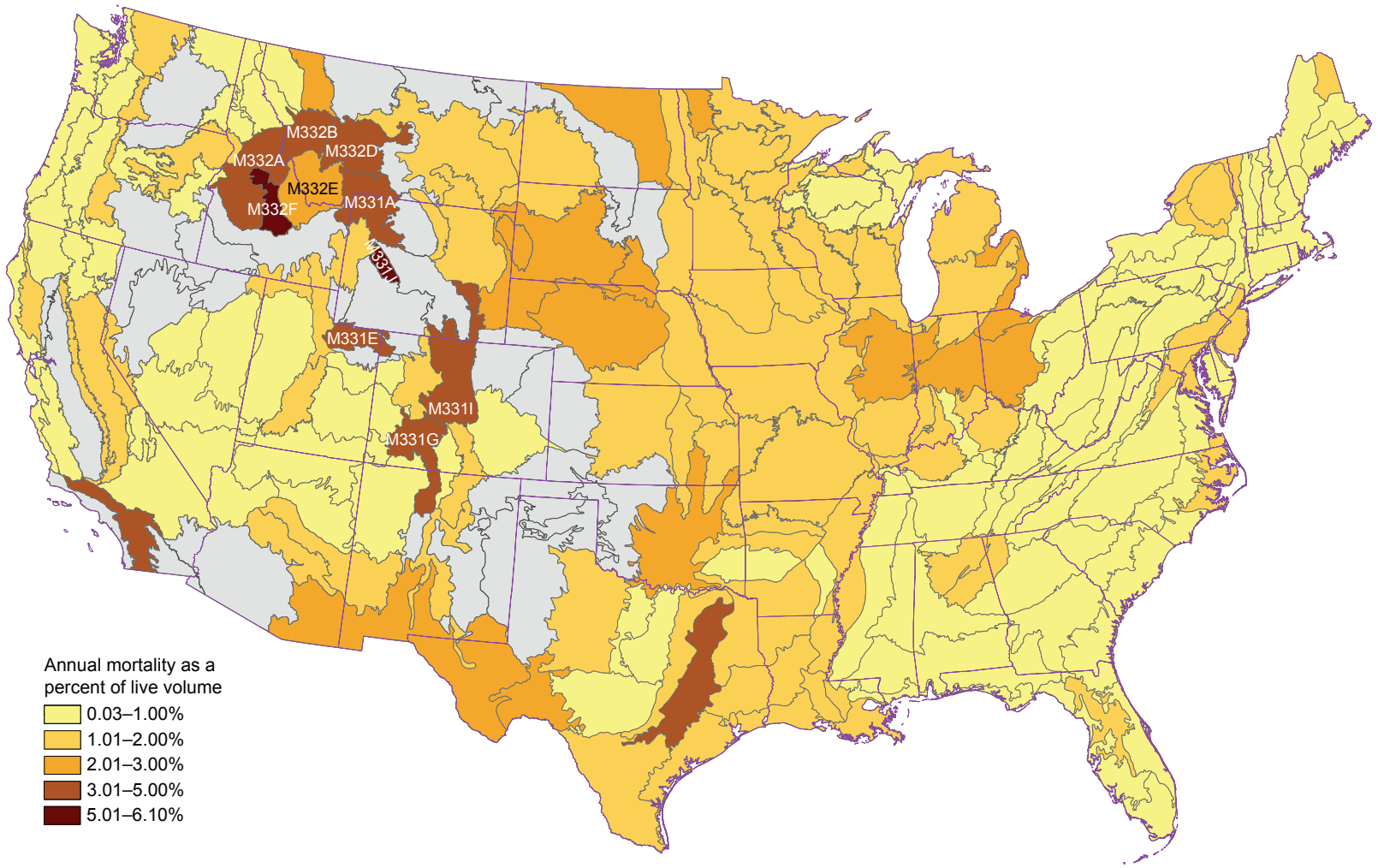

Figure 5.3—Annual tree mortality expressed as a percentage of live tree volume by ecoregion section (Cleland and others 2007). Data unavailable or insufficient for gray areas. (Data source: U.S. Department of Agriculture Forest Service, Forest Inventory and Analysis program)

Table 5.4—Ecoregion sections in Interior West States having the highest mortality relative to standing tree volume and associated causes of mortality

Ecoregion section	Average annual mortality	Standing tree volume	Mortality relative to standing volume	Major causes of mortality
	cubic feet per year	*cubic feet*		
M332F–Challis Volcanics	130,337,369	2,137,789,144	6.10%	Fire (51%), insects (40%)
M331J–Wind River Mountains	51,284,166	950,316,430	5.40%	Insects (69%), fire (20%)
M332D–Belt Mountains	203,919,686	4,906,754,034	4.16%	Insects (87%)
M331I–Northern Parks and Ranges	514,041,199	12,391,505,232	4.15%	Insects (84%)
M331A–Yellowstone Highlands	327,715,284	8,192,840,314	4.00%	Insects (57%), fire (27%)
M331E–Uinta Mountains	103,858,588	2,766,471,956	3.75%	Insects (72%), disease (17%)
M331G–South-Central Highlands	326,038,823	9,383,451,487	3.47%	Insects (67%), fire (13%), disease (11%)
M332B–Northern Rockies and Bitterroot Valley	191,975,434	5,921,485,532	3.24%	Insects (50%), fire (36%)
M332A–Idaho Batholith	532,620,433	17,627,954,803	3.02%	Fire (55%), insects (25%), disease (11%)
M332E–Beaverhead Mountains	149,432,898	5,317,108,378	2.81%	Insects (76%), fire (15%)

were the most significant causes of mortality (table 5.4). This region includes areas suffering outbreaks of mountain pine beetle (Montana Department of Natural Resources and Conservation 2014, 2016) as well as major fires (Idaho Department of Lands 2014). However, several other insect and disease issues have been identified in this region and may have contributed to the mortality. In most of these ecoregion sections (M331A, M331J, M332A, M332B, M332D, M332E), lodgepole pine was the species suffering the highest mortality, most of which was due to insects. However, many other species groups, including Douglas-fir, true firs, and Engelmann and other spruces also suffered non-trivial mortality.

SUMMARY

This analysis shows that in most of the Eastern and Central United States, mortality is low relative to tree growth. The areas of highest mortality occur in the mostly riparian forests of Great Plains ecoregions. A common characteristic of most of the ecoregions having high mortality is that they are on the margins of land suitable for forest growth, being very dry. Thus, they tend to be extremely vulnerable to changes in weather patterns that might produce prolonged and/or extreme drought. Drought, combined with a variety of other biotic and/or abiotic stressors, is likely responsible for much of the mortality observed.

However, one insect pest issue does stand out in the East. In ecoregions 222H–Central Till Plains-Beech-Maple and 222U–Lake Whittlesey Glaciolacustrine Plain, ash mortality due to emerald ash borer was extremely high.

The preliminary analysis of the Western United States shows that, in many parts of the Interior West, mortality is very high as a percentage of live volume and that several West Coast ecoregion sections have high MRATIOs. All of these areas correspond to regions where insect outbreaks (see ch. 2) as well as fire (ch. 3) and/or severe drought (ch. 4) have occurred. These three mortality-causing agents are related in that drought stresses trees, making them more susceptible to insect attack, while both drought and insect-killed trees create conditions favorable for wildfires.

It is also important to realize that the analyses presented in this chapter alone cannot tell the complete story regarding tree mortality. Mortality that is concentrated in highly fragmented forest or nonforest areas adjacent to human development may not be detected because the available FIA data do not cover most urban areas or other places not defined as forest by FIA. Also, these analyses are unlikely to detect a pest or pathogen attacking a particular tree species in a mixed-species forest where other species are growing vigorously. This is especially true of species (e.g., ash) that make up a relatively small proportion of many eastern forests. For example, it is known that emerald ash borer has been causing very high ash mortality in many Eastern and Central States in recent years (Ohio Department of Natural Resources, Division of Forestry 2016; USDA APHIS 2018), yet this mortality stands out only in ecoregions 222H–Central Till Plains-Beech-Maple and 222U–Lake Whittlesey Glaciolacustrine Plain. Elsewhere in the East, though ash mortality is known to be extremely high, the mortality is masked because ash is a relatively minor component of the forest.

To gain a more complete understanding of mortality, one should consider the results of this analysis together with other indicators of forest health. Forest Inventory and Analysis tree damage data (Burrill and others 2018), as well as Evaluation Monitoring projects that focus on particular mortality-causing agents (ch. 8–13) can provide insight into smaller scale or species-specific mortality issues. Large-scale analyses of forest-damaging events, including insect and disease activity (ch. 2) and fire (ch. 3) are also important for understanding mortality patterns. This can be especially important in the West, where mortality data are limited.

LITERATURE CITED

Ball, J.; Pyser, N.; Warnke, M. 2016. Forest health highlights in South Dakota 2016. Pierre: South Dakota Department of Agriculture, Division of Resource Conservation and Forestry. 6 p. https://www.fs.fed.us/foresthealth/protecting-forest/forest-health-monitoring/monitoring-forest-highlights.shtml. [Date accessed: May 9, 2018].

Ball, J.; Seidl, A.; Warnke, M. 2017. State of South Dakota forest health highlights. Pierre: South Dakota Department of Agriculture, Division of Resource Conservation and Forestry. 8 p. https://sdda.sd.gov/conservation-forestry/forest-health/SDHighlights_2017-2.pdf. [Date accessed: July 23, 2019].

Ball, J.; Seidl, A.; Warnke, M. 2018. State of South Dakota forest health highlights. Pierre: South Dakota Department of Agriculture, Division of Resource Conservation and Forestry. 12 p. https://sdda.sd.gov/conservation-forestry/forest-health/SDHighlights_2018.pdf. [Date accessed: July 1, 2019].

Ball, J.; Warnke, M.; Garbisch, B. 2015. Forest health highlights in South Dakota 2015. Pierre: South Dakota Department of Agriculture, Division of Resource Conservation and Forestry. 9 p. https://www.fs.fed.us/foresthealth/protecting-forest/forest-health-monitoring/monitoring-forest-highlights.shtml. [Date accessed: May 9, 2018].

Bechtold, W.A.; Patterson, P.L., eds. 2005. The enhanced Forest Inventory and Analysis program—national sampling design and estimation procedures. Gen. Tech. Rep. SRS-80. Asheville, NC: U.S. Department of Agriculture Forest Service, Southern Research Station. 85 p.

Burrill, E.A.; Wilson, A.M.; Turner, J.A. [and others]. 2018. The Forest Inventory and Analysis Database: database description and user guide for Phase 2 (version 8.0). Washington, DC: U.S. Department of Agriculture Forest Service. 946 p. http://fia.fs.fed.us/library/database-documentation/. [Date accessed: July 16, 2019].

California Forest Pest Council. 2015. 2015 California forest health highlights. 21 p. https://www.fs.fed.us/foresthealth/protecting-forest/forest-health-monitoring/monitoring-forest-highlights.shtml. [Date accessed: July 9, 2018].

California Forest Pest Council. 2016. 2016 California forest health highlights. 31 p. https://www.fs.fed.us/foresthealth/protecting-forest/forest-health-monitoring/monitoring-forest-highlights.shtml. [Date accessed: May 9, 2018].

California Forest Pest Council. 2017. 2017 California forest health highlights. 38 p. https://www.fs.usda.gov/Internet/FSE_DOCUMENTS/fseprd578578.pdf. [Date accessed: May 9, 2018].

Cleland, D.T.; Freeouf, J.A.; Keys, J.E. [and others]. 2007. Ecological subregions: sections and subsections for the conterminous United States. Gen. Tech. Rep. WO-76D. Washington, DC: U.S. Department of Agriculture Forest Service. Map; Sloan, A.M., cartographer; presentation scale 1:3,500,000; colored. Also on CD-ROM as a GIS coverage in ArcINFO format.

Colorado State Forest Service. 2016. 2015 report on the health of Colorado's forests: 15 years of change. Fort Collins, CO: Colorado State Forest Service. 32 p. https://csfs.colostate.edu/media/sites/22/2016/02/ForestHealthReport-2015.pdf. [Date accessed: July 30, 2019].

Colorado State Forest Service. 2017. 2016 report on the health of Colorado's forests: fire and water. Fort Collins, CO: Colorado State Forest Service. 36 p. https://csfs.colostate.edu/media/sites/22/2017/02/CSU_304464_ForestReport-2016-www.pdf. [Date accessed: July 30, 2019].

Coulston, J.W.; Ambrose, M.J.; Stolte. K.S. [and others]. 2005. Criterion 3 – health and vitality. In: Conkling, B.L.; Coulston, J.W.; Ambrose, M.J., eds. Forest Health Monitoring 2001 national technical report. Gen. Tech. Rep. SRS-81. Asheville, NC: U.S. Department of Agriculture Forest Service, Southern Research Station. 204 p.

Idaho Department of Lands. 2014. 2014 forest health highlights. 7 p. https://www.fs.fed.us/foresthealth/docs/fhh/ID_FHH_2014.pdf. [Date accessed: July 30, 2019].

Johnson, L. 2017. North Dakota forest health highlights 2017. 12 p. https://www.ag.ndsu.edu/ndfs/documents/north-dakota-forest-health-highlights-2017.pdf. [Date accessed: July 23, 2019].

Marshall, P.T. 2017. 2017 Indiana forest health highlights. Vallonia, IN: Indiana Department of Natural Resources. 17 p. https://www.in.gov/dnr/forestry/files/fo-Forest_Health_Highlights_2017.pdf. [Date accessed: June 20, 2019].

Marshall, P.T. 2018. 2018 Indiana forest health highlights. Vallonia, IN: Indiana Department of Natural Resources. 17 p. https://www.in.gov/dnr/forestry/files/fo-Forest_Health_Highlights_2018.pdf. [Date accessed: June 20, 2019].

McNab, W.H.; Cleland, D.T.; Freeouf, J.A. [and others], comps. 2007. Description of ecological subregions: sections of the conterminous United States. [CD-ROM]. Gen. Tech. Report WO-76B. Washington, DC: U.S. Department of Agriculture Forest Service. 80 p. https://doi.org/10.2737/WO-GTR-76B.

Michigan Department of Natural Resources. 2014. 2014 forest health highlights. 51 p. https://www.fs.fed.us/foresthealth/protecting-forest/forest-health-monitoring/monitoring-forest-highlights.shtml. [Date accessed: April 27, 2018].

Michigan Department of Natural Resources. 2015. 2015 forest health highlights. 50 p. https://www.fs.fed.us/foresthealth/protecting-forest/forest-health-monitoring/monitoring-forest-highlights.shtml. [Date accessed: April 8, 2018].

Michigan Department of Natural Resources. 2016. 2016 forest health highlights. 51 p. https://www.fs.fed.us/foresthealth/protecting-forest/forest-health-monitoring/monitoring-forest-highlights.shtml. [Date accessed: April 8, 2018].

Michigan Department of Natural Resources. 2017. 2017 forest health highlights. 31 p. https://www.michigan.gov/documents/dnr/frsthlthhghlghts_513144_7.pdf. [Date accessed: May 8, 2018].

Montana Department of Natural Resources and Conservation, Forest Pest Management Program. 2014. Montana forest health highlights 2014. 4 p. https://www.fs.fed.us/foresthealth/docs/fhh/MT_FHH_2014.pdf. [Date accessed: July 30, 2019].

Montana Department of Natural Resources and Conservation, Forest Pest Management Program. 2016. Montana forest health highlights 2016. 4 p. http://dnrc.mt.gov/divisions/forestry/docs/assistance/pests/conditions-highlights/fhh_2016.pdf. [Date accessed: July 30, 2019].

Nebraska Forest Service. 2017. Nebraska forest health highlights 2017. 6 p. https://www.fs.fed.us/foresthealth/docs/fhh/NE_FHH_2017.pdf. [Date accessed: August 25, 2018].

Nebraska Forest Service. 2018. Nebraska forest health highlights 2018. 3 p. https://nfs.unl.edu/publications/downloads/NE2018Forest%20Health%20Highlights-3.pdf. [Date accessed: July 12, 2019].

North Dakota Forest Service. 2012. North Dakota forest health highlights 2012. 12 p. https://www.fs.fed.us/foresthealth/protecting-forest/forest-health-monitoring/monitoring-forest-highlights.shtml. [Date accessed: May 15, 2018].

North Dakota Forest Service. 2013. North Dakota forest health highlights 2013. 12 p. https://www.fs.fed.us/foresthealth/protecting-forest/forest-health-monitoring/monitoring-forest-highlights.shtml. [Date accessed: April 26, 2018].

North Dakota Forest Service. 2014. North Dakota forest health highlights 2014. 24 p. https://www.fs.fed.us/foresthealth/protecting-forest/forest-health-monitoring/monitoring-forest-highlights.shtml. [Date accessed: April 12, 2018].

North Dakota Forest Service. 2015. North Dakota forest health highlights 2015. 24 p. https://www.fs.fed.us/foresthealth/protecting-forest/forest-health-monitoring/monitoring-forest-highlights.shtml. [Date accessed: April 12, 2018].

North Dakota Forest Service. 2016. North Dakota forest health highlights 2016. 4 p. https://www.ag.ndsu.edu/ndfs/documents/north-dakota-forest-health-highlights-2016.pdf. [Date accessed: August 25, 2018].

Ohio Department of Natural Resources, Division of Forestry. 2014. 2014 Ohio forest health highlights. 7 p. Columbus, OH: Ohio Department of Natural Resources, Division of Forestry. https://www.fs.fed.us/foresthealth/protecting-forest/forest-health-monitoring/monitoring-forest-highlights.shtml. [Date accessed: April 27, 2018].

Ohio Department of Natural Resources, Division of Forestry. 2015. 2015 Ohio forest health highlights. 8 p. Columbus, OH: Ohio Department of Natural Resources, Division of Forestry. https://www.fs.fed.us/foresthealth/protecting-forest/forest-health-monitoring/monitoring-forest-highlights.shtml. [Date accessed: April 17, 2018].

Ohio Department of Natural Resources, Division of Forestry. 2016. 2016 Ohio forest health highlights. 8 p. Columbus, OH: Ohio Department of Natural Resources, Division of Forestry. https://www.fs.fed.us/foresthealth/protecting-forest/forest-health-monitoring/monitoring-forest-highlights.shtml. [Date accessed: April 17, 2018].

Ohio Department of Natural Resources, Division of Forestry. 2017. 2017 Ohio forest health highlights. 7 p. Columbus, OH: Ohio Department of Natural Resources, Division of Forestry. https://www.fs.fed.us/foresthealth/docs/fhh/OH_FHH_2017.pdf. [Date accessed: July 7, 2019].

Oklahoma Forestry Services. 2014. Oklahoma forest health highlights 2014. 5 p. https://www.fs.fed.us/foresthealth/protecting-forest/forest-health-monitoring/monitoring-forest-highlights.shtml. [Date accessed: April 2, 2018].

Oklahoma Forestry Services. 2015. Oklahoma forest health highlights 2015. 6 p. https://www.fs.fed.us/foresthealth/protecting-forest/forest-health-monitoring/monitoring-forest-highlights.shtml. [Date accessed: April 3, 2018].

Oklahoma Forestry Services. 2016. Oklahoma forest health highlights 2016. 6 p. https://www.fs.fed.us/foresthealth/protecting-forest/forest-health-monitoring/monitoring-forest-highlights.shtml. [Date accessed: April 2, 2018].

Pugh, S.A.; Turner, J.A.; Burrill, E.A.; David, W. 2018. The Forest Inventory and Analysis Database: population estimation user guide (edition: November 2018). U.S. Department of Agriculture Forest Service. 166 p. http://www.fia.fs.fed.us/library/database-documentation/. [Date accessed: July 25, 2020].

Smith, L.A. 2013. Forest health insects and diseases conditions Texas 2013. Longview, TX: Texas A & M Forest Service. 5 p. https://www.fs.fed.us/foresthealth/protecting-forest/forest-health-monitoring/monitoring-forest-highlights.shtml. [Date accessed: April 27, 2018].

Smith, L.A. 2014. Forest health highlights in Texas 2014. Longview, TX: Texas A & M Forest Service. 1 p. https://www.fs.fed.us/foresthealth/protecting-forest/forest-health-monitoring/monitoring-forest-highlights.shtml. [Date accessed: April 27, 2018].

South Dakota Department of Agriculture. 2011. South Dakota forest health highlights 2011. Pierre: South Dakota Department of Agriculture, Division of Resource Conservation and Forestry. 4 p. https://www.fs.fed.us/foresthealth/protecting-forest/forest-health-monitoring/monitoring-forest-highlights.shtml. [Date accessed: May 1 2018].

South Dakota Department of Agriculture. 2012. South Dakota 2012 forest health highlights. Pierre: South Dakota Department of Agriculture, Division of Resource Conservation and Forestry. 5 p. https://www.fs.fed.us/foresthealth/protecting-forest/forest-health-monitoring/monitoring-forest-highlights.shtml. [Date accessed: March 15, 2018].

South Dakota Department of Agriculture. 2013. South Dakota 2013 forest health highlights. Pierre: South Dakota Department of Agriculture, Division of Resource Conservation and Forestry. 5 p. https://www.fs.fed.us/foresthealth/protecting-forest/forest-health-monitoring/monitoring-forest-highlights.shtml. [Date accessed: March 15, 2018].

South Dakota Department of Agriculture. 2014. South Dakota 2014 forest health highlights. Pierre: South Dakota Department of Agriculture, Division of Resource Conservation and Forestry. 7 p. https://www.fs.fed.us/foresthealth/protecting-forest/forest-health-monitoring/monitoring-forest-highlights.shtml. [Date accessed: March 15, 2018].

Texas A & M Forest Service. 2015. Forest health highlights in Texas 2015. Longview, TX: Texas A & M Forest Service. 1 p. https://www.fs.fed.us/foresthealth/protecting-forest/forest-health-monitoring/monitoring-forest-highlights.shtml. [Date accessed: April 20, 2018].

Texas A & M Forest Service. 2016. Forest health highlights in Texas 2016. Longview, TX: Texas A & M Forest Service. 1 p. https://www.fs.fed.us/foresthealth/protecting-forest/forest-health-monitoring/monitoring-forest-highlights.shtml. [Date accessed: April 20, 2018].

Texas A & M Forest Service. 2017. Forest health highlights 2017. Longview, TX: Texas A & M Forest Service. 2 p. https://www.fs.fed.us/foresthealth/protecting-forest/forest-health-monitoring/monitoring-forest-highlights.shtml. [Date accessed: May 21, 2018].

Texas A & M Forest Service. 2019. Forest health highlights 2019. Longview, TX: Texas A & M Forest Service. 2 p. https://www.fhm.fs.fed.us/foresthealth/docs/fhh/TX_FHH_2019.pdf. [Date accessed: May 21, 2020].

U.S. Department of Agriculture (USDA) Animal and Plant Health Inspection Service (APHIS). 2018. Emerald ash borer. https://www.aphis.usda.gov/aphis/resources/pests-diseases/hungry-pests/the-threat/emerald-ash-borer/emerald-ash-borer-beetle. [Date accessed: August 31, 2018].

U.S. Department of Agriculture (USDA) Forest Service. 2008. National forest type dataset. [Online]. http://data.fs.usda.gov/geodata//rastergateway/forest_type/index.php. [Date accessed: September 13, 2016].

U.S. Department of Agriculture (USDA) Forest Service, Forest Inventory and Analysis (FIA) program. 2019. Forest Inventory EVALIDator web-application version 1.8.0.01 St. Paul, MN: U.S. Department of Agriculture Forest Service, Northern Research Station. http://apps.fs.fed.us/Evalidator/evalidator.jsp. [Date accessed: July 13, 2020].

U.S. Department of Agriculture (USDA) Forest Service, Uinta-Wasatch-Cache National Forest. [N.d.]. Beetle activity on the Uinta-Wasatch-Cache National Forest. http://www.fs.usda.gov/detail/uwcnf/home/?cid=STELPRDB5145143. [Date accessed: July 25, 2017].

Utah Department of Natural Resources, Forestry, Fire, & State Lands. 2016. Utah forest health highlights 2016. 3 p. https://www.fs.fed.us/foresthealth/protecting-forest/forest-health-monitoring/monitoring-forest-highlights.shtml. [Date accessed: April 24, 2018].

Wyoming State Forestry Division. 2016. 2016 Wyoming forest health highlights. 16 p. https://www.fs.fed.us/foresthealth/docs/fhh/WY_FHH_2016.pdf. [Date accessed: August 25, 2018].

Wyoming State Forestry Division. 2017. 2017 Wyoming forest health highlights. 17 p. https://www.fs.fed.us/foresthealth/docs/fhh/WY_FHH_2017.pdf. [Date accessed: August 25, 2018].

Zegler, T. 2015. New Mexico forest health conditions, 2015. 17 p. http://www.emnrd.state.nm.us/SFD/FWHPlan/documents/2015_NMconditionsreport_low_shortIIpdf.pdf. [Date accessed: July 30, 2019].

Zegler, T. 2016. New Mexico forest health conditions, 2016. 18 p. http://www.emnrd.state.nm.us/SFD/FWHPlan/documents/2016_NMconditionsreport_short.pdf. [Date accessed: July 30, 2019].

Zegler, T.; Formby, J.P. 2017. New Mexico forest health conditions 2017. 35 p. http://www.emnrd.state.nm.us/SFD/FWHPlan/documents/NMForestHealthConditionsReportComplete.pdf. [Date accessed: July 30, 2019].

SECTION 2.

Analyses of Long-Term Forest Health Trends and Presentations of New Techniques

CHAPTER 6.

Changes in Coarse Woody Material Attributes, U.S. Forests, 2002–2011 to 2012–2019

Christopher W. Woodall
Matthew B. Russell
Shawn Fraver
Brian F. Walters
Grant M. Domke

INTRODUCTION

Coarse woody materials (CWM) are often defined as dead wood of a certain minimum size in forest ecosystems (Harmon and others 1986). For the purposes of the U.S. national inventory, CWM has a minimum diameter of 3.0 inches at the point of intersection with a sampling transect (i.e., transect diameter) in addition to having a lean angle <45 degrees from vertical to delineate it from standing dead trees (Woodall and others 2019). For decades now, CWM has been recognized as an important component of forest ecosystems (Harmon and others 1986) serving as a substrate for tree regeneration (Bolton and D'Amato 2011), habitat for wildlife (Nordén and others 2004), and store of carbon (Bradford and others 2008), among a host of other functions (e.g., Stokland and others 2012). In recognition of these critical functions, the Forest Inventory and Analysis (FIA) program of the U.S. Department of Agriculture Forest Service has been conducting a nationwide inventory of CWM since ca. 2000 as a component of its strategic-scale forest inventory (Woodall and Monleon 2008, Woodall and others 2019). Concomitant with this resource inventory, there has been documentation and concern regarding tree mortality and associated forest health issues at various scales around the world (e.g., McDowell and Allen 2015). Along present trajectories of global change (e.g., tree mortality from climate change and/or insects/disease), it can be hypothesized that increasing rates of tree mortality will have impacts to related forest resources such as CWM. Because one of the largest hurdles to monitoring CWM change is its inherent nature at small scales (e.g., spatially and temporally heterogeneous tree mortality combined with various decay pathways), quantifying how CWM attributes are changing across large spatial domains is an important first step towards future conservation efforts.

As a means to objectively evaluate CWM change across U.S. forests within the context of expected global change impacts, fundamental parameters (e.g., changes in size distribution) of CWM resources (e.g., biomass) were examined across spatial scales of inference ranging from inventory survey units to the conterminous United States using FIA's multidecadal inventory (2002–2011 to 2012–2019). Specific objectives of this study were to: (1) evaluate changes in CWM biomass, in terms of stocks and spatial trends; (2) evaluate changes in CWM transect diameter and decay class distributions; (3) evaluate changes in CWM species composition; and (4) within the context of identified CWM changes, suggest novel indicators of CWM change and associated monitoring refinements.

METHODS

Data

Downed dead wood are sampled by the FIA program using line-intersect sampling (LIS) on a subset of inventory plots that are classified as forested. Forest land is defined as having at least 10-percent canopy cover of live tree species or the potential to support such cover if recently cut/disturbed along with a spatial size requirement of 1 acre and at least 120 feet

in width (USDA Forest Service 2016). The FIA design is based on a spatially balanced sample of approximately one plot per 6,000 acres (Reams and others 2005). Each inventory plot consists of four points arranged in a cluster with one point at the center and three points oriented from the central subplot at 0, 120, and 240 degrees. Each of these four points is referred to as a subplot. The distance from the central point to the center of the surrounding points is 120 feet. These four points form the center of fixed-area plots (24-foot fixed radius) used to tally live and standing dead trees in addition to serving as the origin of transects used to measure CWM pieces.

For most regions of the United States, CWM is sampled using LIS on a subset of forest inventory plots whose sample intensity has changed over time (ranging from every inventory plot to $1/16^{th}$ of inventory plots) (Woodall and others 2019). Line-intersect sampling itself consists of arraying one-dimensional sampling transects across forest domains of interest with any piece of CWM intersecting a transect being considered part of the sample (Woodall and Monleon 2008, USDA Forest Service 2016). Population estimators are constructed based on the length of transect, CWM piece transect diameter, and the attributes of interest derived from measurements of each sampled piece (e.g., CWM piece volume). Population estimates are calculated from combined plots using the standard, FIA post-stratification estimators (Scott and others 2005). A major delineation in the execution of the national inventory of CWM was a major national change in the plot sampling protocols between the 2002–2011 and 2012–present inventories. As these changes can be considered independent inventories valid for evaluation of changes in the U.S. CWM population over 2 decades, they form the basis of this assessment. In terms of the quality analysis and quality control of the CWM inventory program, despite the often decayed and fractured state of much of the CWM population, the measurement repeatability of various CWM attributes such as diameter and species identification (Campbell and others 2019) is on par with various live tree attributes such as tree grade. The model error associated with estimating carbon stocks of highly decayed CWM pieces and sampling error associated with the 2002–2011 inventories are examples of sources of uncertainty that may outweigh the error from a number of CWM field measurement errors. (For details regarding the evolution of the CWM inventory along with all relevant field protocols, inference procedures, and database documentation, see Woodall and others [2019].) Finally, it is strongly noted that the downed dead wood inventory conducted by the FIA program contains more dead wood components than CWM, including residue piles, fine woody debris, duff, and litter. We chose to focus solely on CWM in this study as a precursor to examining all aforementioned components as the CWM inventory measures numerous attributes (e.g., size, decay, and species) of interest by themselves and in concert with the standing tree inventory. We hypothesize that a firmer foundation for understanding changes

in fine woody debris or residue piles should be built upon robust understanding of changes in the CWM population.

Analyses

The FIA CWM inventory, sampled from 2002–2011 to 2012–2019, is the basis for the analysis presented in this assessment. Valid CWM samples for each State were pulled from the FIA Database (Burrill and others 2017) for each decade to enable change estimation for all States where possible, except for Nevada, New Mexico, Wyoming, Hawaii, and Alaska, where annual inventories were implemented at later dates. Although there are contemporary CWM inventories for those excluded States (and territories such as Puerto Rico and the U.S. Virgin Islands), we decided to focus on CWM change estimation in the conterminous United States where there were valid CWM inventories for change estimation across nearly 2 decades. Unlike resource-change analysis for live trees, where individuals are tracked over time for estimation of live tree resource changes, the tracking of individual CWM pieces does not form the basis of FIA CWM monitoring, although it can be brought to bear when modeling CWM dynamics (Russell and others 2014). Instead, a "stock-change" approach is used where valid estimates of CWM populations are compared across time. Therefore, in this study, CWM changes are evaluated at relatively large scales such as the survey unit or State level. The procedures for developing CWM population estimates across these varying domains are described in Woodall and Monleon (2008).

RESULTS AND DISCUSSION

As FIA's CWM inventory has varied in its plot protocols and sample intensity across space and time since its inception in ~2000 (Woodall and others 2019), there are various approaches to data analysis and associated interpretations of CWM resource attributes. If remeasured individual CWM inventory plots are used as a mode of inference, the result is a greatly reduced number of plots across time (fig. 6.1A). In addition, extreme care must be given when comparing such results at the individual plot level due to changes in plot sampling protocols and sample intensity across time (e.g., fig. 6.1A, western Texas and the West Coast). In contrast to only using remeasured plots, entire collections (i.e., panels) of CWM inventory plots can be considered independent samples of the CWM population at discrete points in time. All contemporary (~2012–2019) CWM inventory plots number in the tens of thousands (fig. 6.1B), forming the basis of rigorous examination of CWM at strategic scales. Using all available within-State CWM inventory plots at two points in time for States that had such inventories, the amount of CWM biomass is seen as mostly increasing across FIA survey units with an average increase of a few tons per acre (fig. 6.2). For the area considered in this study (i.e., remeasured State CWM inventories), an estimate of 2.3 billion tons of CWM from 2002–2011 has increased by 17 percent to 2.7 billion tons in 2012–2019. In a general sense, the balance of CWM biomass across large scales is driven by changes in tree mortality, harvest, decay/combustion, and salvage utilization. It

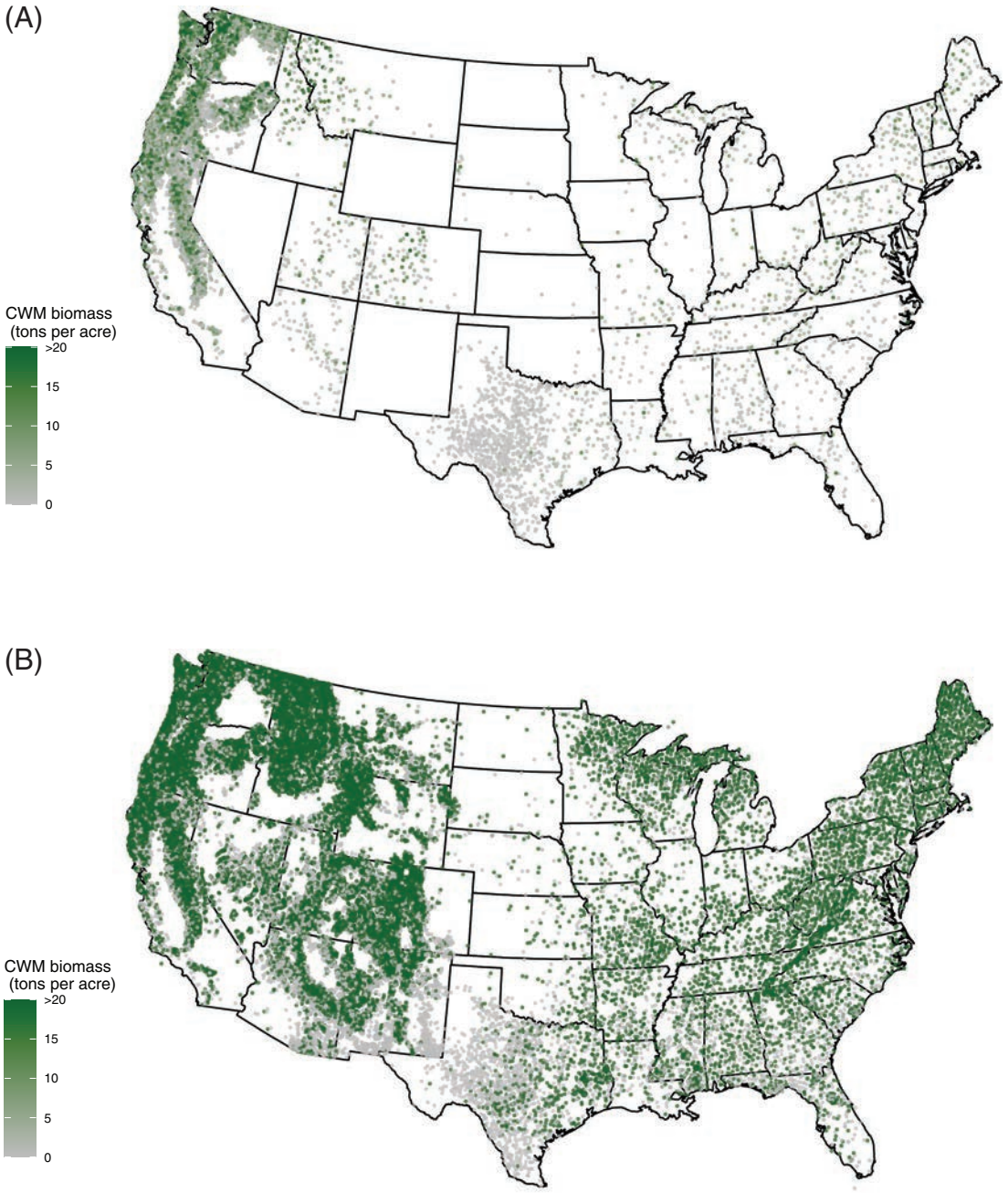

Figure 6.1—(A) Total coarse woody material (CWM) biomass (2012–2019) for only remeasured, forested down woody material (DWM) plots (2002–2011 to 2012–2019). (B) Total CWM biomass for all plots with at least one forested condition measured between 2012 and 2019.

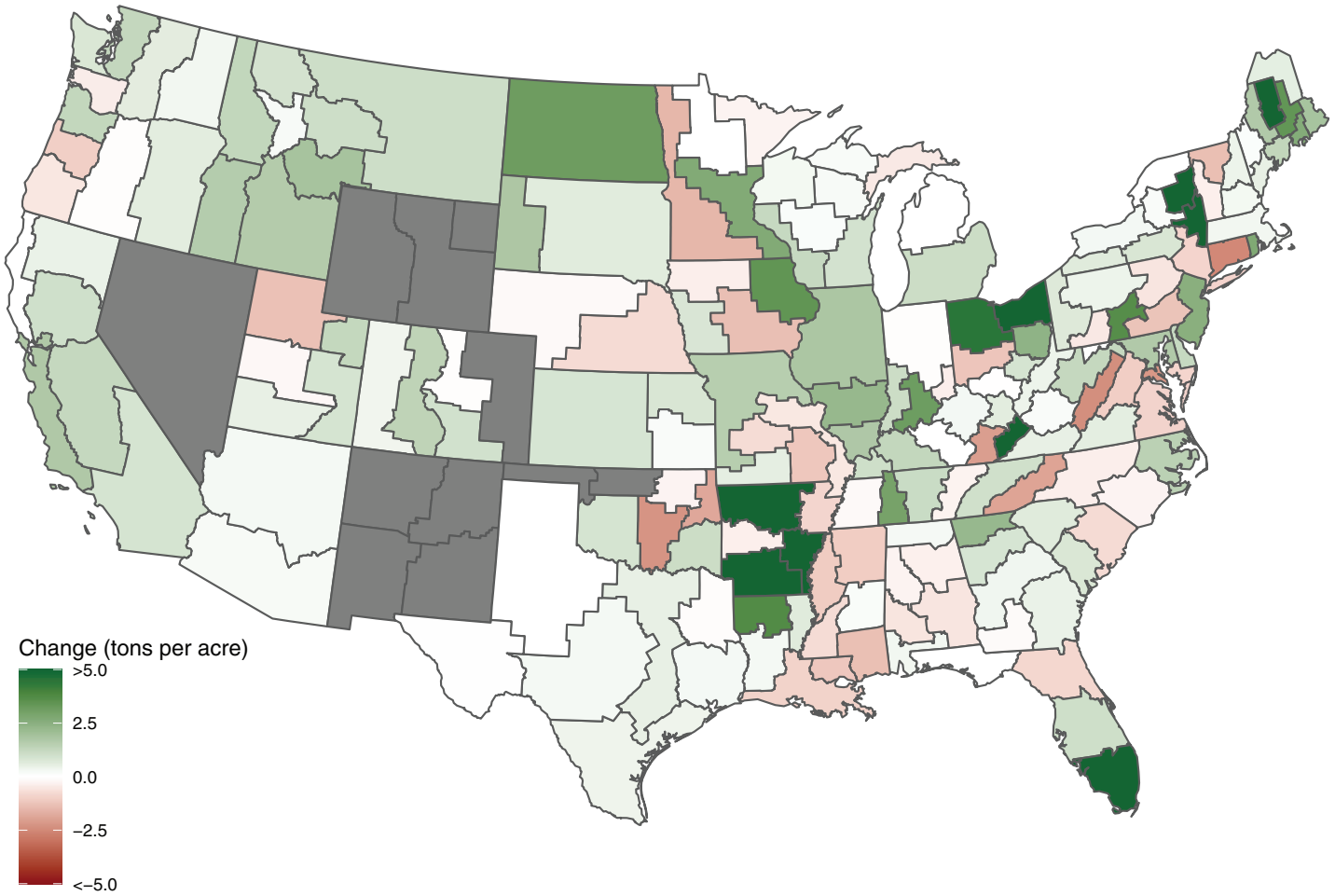

Figure 6.2—Change in coarse woody material (CWM) biomass (tons per acre) in U.S. forests by survey unit, 2002–2011 to 2012–2019. Gray States/survey units indicate no remeasured plots.

can be hypothesized that increases in CWM observed for most areas of the country resulted from mortality/harvest inputs exceeding decay/combustion and/or salvage utilization. Despite this overall increase in CWM biomass, some areas of the United States saw some minor reductions, including the Midwest, Louisiana and Mississippi, and along the Appalachian Mountains. These reductions may be attributed to declining mortality/harvest in combination with continuing decay processes. However, if decay is assumed to be relatively stable over decadal time scales, these CWM reductions suggest lower mortality rates and/or harvest utilization in these regions, which might be attributed to recovery from acid rain deposition along the Appalachian Mountains (Kosiba and others 2018) and vigorous post-hurricane recovery in the Gulf of Mexico.

To further unravel the dynamics of CWM change, the general attributes of decay, size, and species can be examined. The distribution of decay status for CWM is normally distributed and centered on moderately decayed pieces (decay class 3; fig. 6.3). Since the 2000s, the CWM population has slightly shifted towards a more advanced decay status with a notable increase in the total biomass of moderately decayed pieces. Changes in CWM stage of decay has varied across States, with the greatest increase in freshly fallen CWM pieces (decay class 1) occurring in Midwestern States (fig. 6.4). In a similar manner, there was disparity in slightly decayed CWM pieces (decay class 2) across States with some States showing large

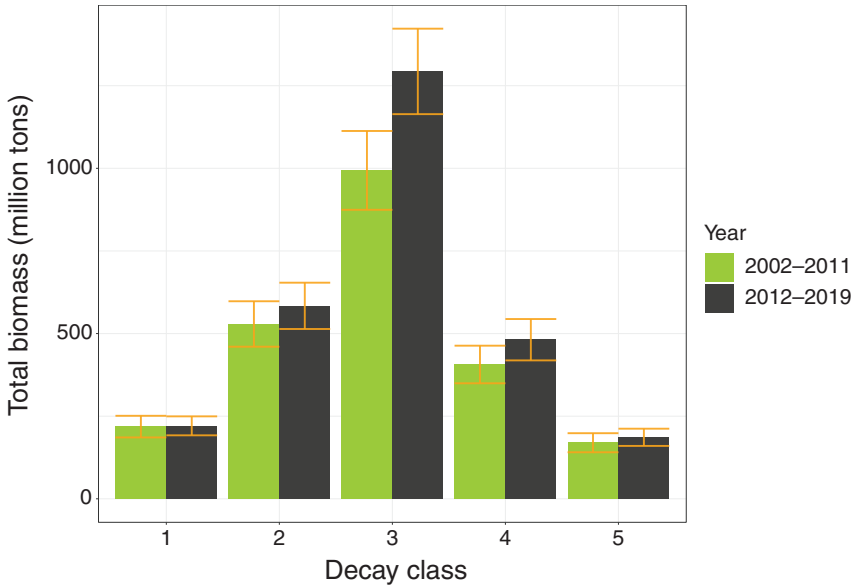

Figure 6.3—U.S. coarse woody material (CWM) decay class distribution, 2002–2011 to 2012–2019.

increases (e.g., Maine, Arkansas, Montana, North Dakota, and South Dakota) and others showing decreases (e.g.,Washington, Oregon, Idaho, Vermont, and Michigan). For the more advanced stages of decay (decay classes 3–5; Woodall and Monleon 2008), there was a more consistent increase across all States, especially for decay classes 3 and 4. The percentage of change of moderately to advanced decayed CWM biomass compared to freshly fallen or slightly decayed biomass across States indicates that most States are experiencing overall increases in the amount of advanced decayed

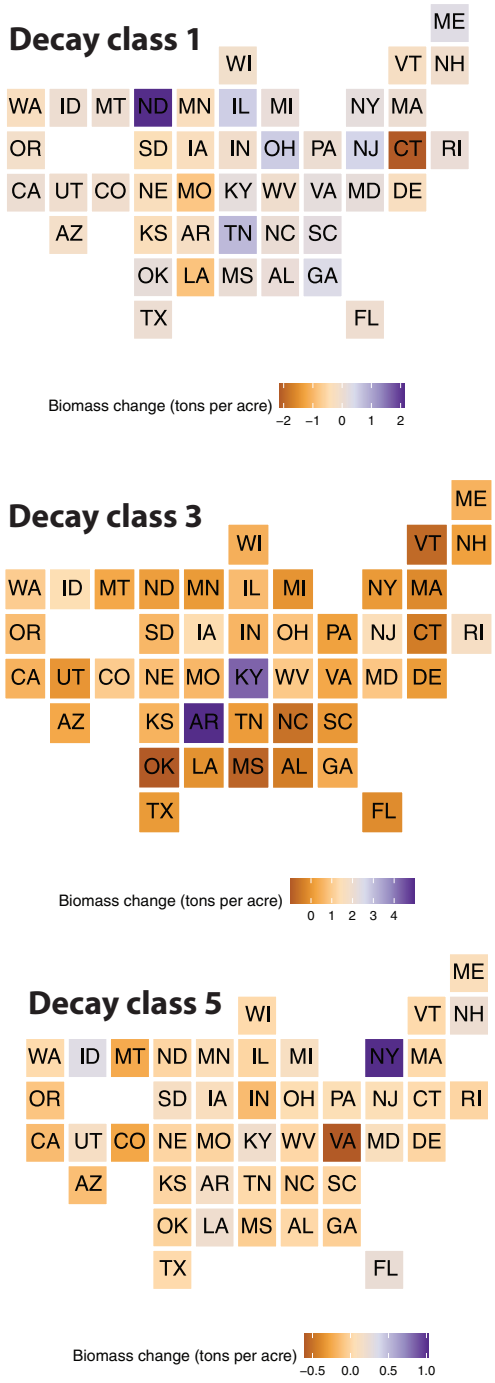

Figure 6.4—Change in coarse woody material (CWM) decay classes, 2002–2011 to 2012–2019.

CWM biomass (fig. 6.5). The States that have had an increase in the amount of fresh CWM compared to advanced decayed CWM were North Dakota, Mississippi, Maine, Tennessee, North Carolina, and Oklahoma.

The biomass of CWM is largely represented by smaller sized CWM pieces if transect diameter is considered an indicator of CWM size (fig. 6.6). Over the course of nearly 2 decades, the plurality of CWM biomass has been in pieces with a transect diameter between 4.1 and 16.0 inches. In terms of change, the largest-sized CWM pieces (transect diameter >24.0 inches) approximately doubled in biomass from ~300 million tons to ~600 million tons. Most States had increases in the amount of CWM biomass residing in smaller sized pieces (3.0 to 8.0 inches), while higher latitude States appeared to experience greater increase in moderately sized CWM (8.1 to 16.0 inches) over 2 decades (fig. 6.7). Increases in the largest sized CWM (>16.0 inches) appeared to be equally distributed among States. When viewing the change of large-sized versus smaller sized CWM pieces over time, it is evident that

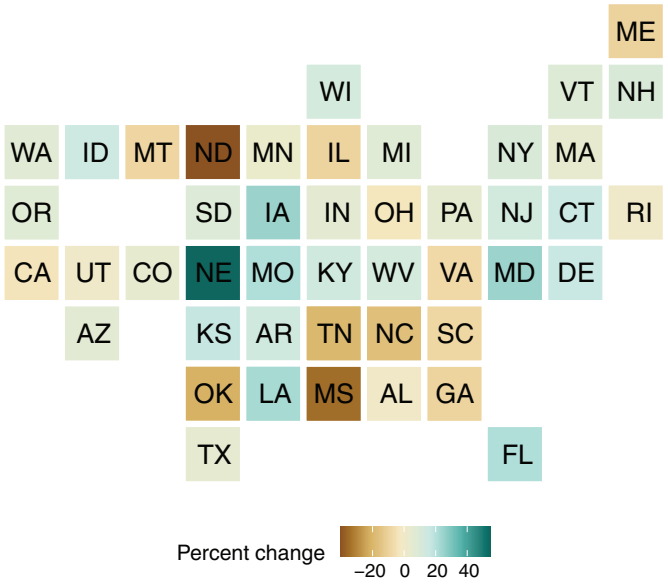

Figure 6.5—Change in percentage of moderately to advanced decayed coarse woody material (CWM) biomass, 2002–2011 to 2012–2019. (Note: a positive value indicates that the State's population of CWM biomass is becoming more advanced in decay over nearly 20 years.)

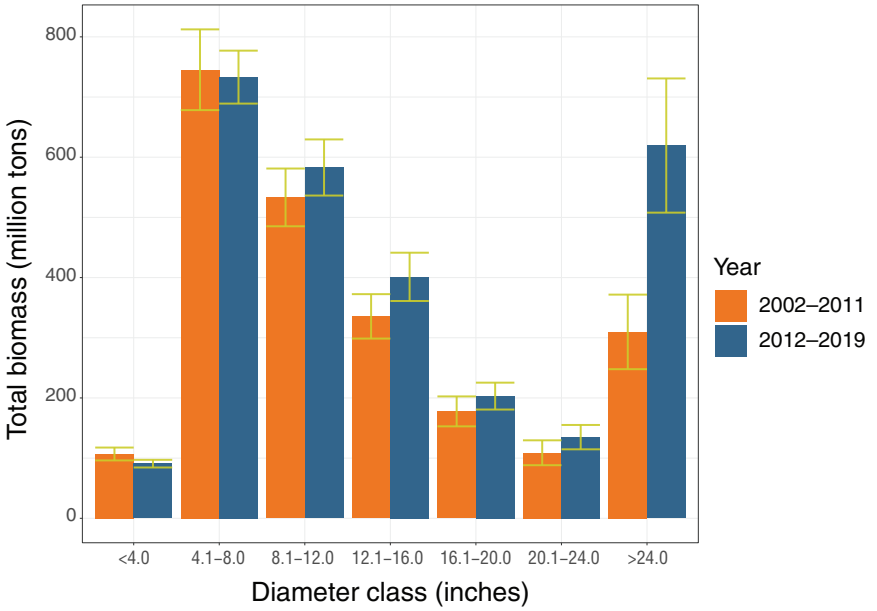

Figure 6.6—U.S. coarse woody material (CWM) transect diameter class distribution, 2002–2011 to 2012–2019.

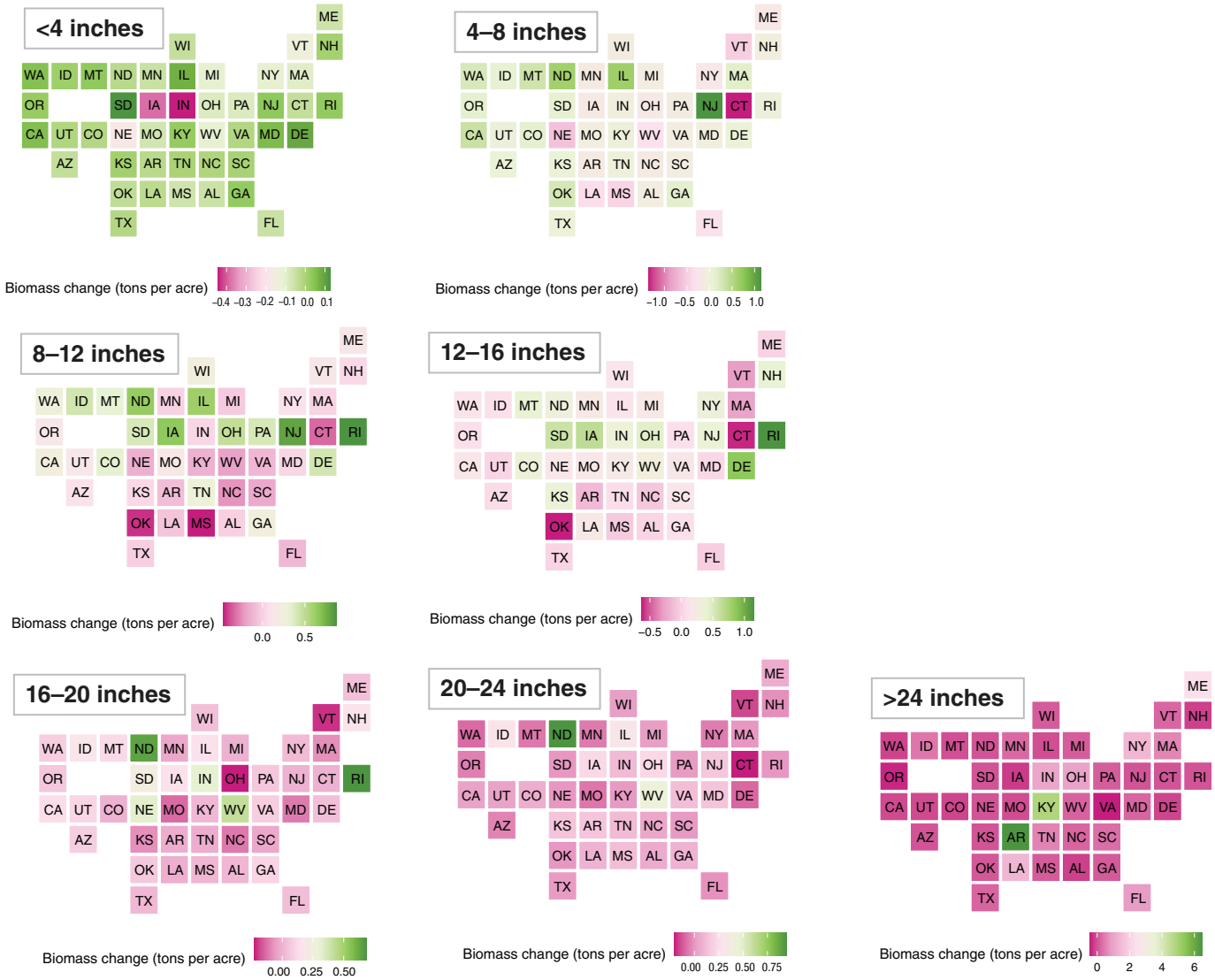

Figure 6.7—Changes in coarse woody material (CWM) transect diameter class distribution, 2002–2011 to 2012–2019.

most States are at least experiencing a minor increase in the relative prevalence of larger sized CWM pieces (fig. 6.8). In particular, the States of Maine, Florida, Arkansas, Kentucky, Louisiana, Texas, Mississippi, West Virginia, Indiana, North Dakota, Nebraska, and New York had higher levels of large-sized CWM increases relative to smaller sized pieces over 2 decades.

Very few studies have evaluated changes in CWM species composition, although such analyses might help evaluate the influence of large-scale forest mortality events (e.g., Woodall and Nagel 2006) on subsequent CWM accumulation and depletion (Russell and others 2015, Woodall and others 2015; i.e., decay and/or combustion). As no CWM species types and/or documented CWM species assemblages exist for monitoring purposes (i.e., forest types for dead trees as opposed to just live trees), the top three CWM species in terms of biomass prevalence can be examined (fig. 6.9). For a plurality of States, the top three CWM species are of such advanced decay they are recorded as an unknown species or unknown hardwood. However, in many cases, the prevalence of any particular CWM species can be attributed to past forest health issues, disturbance events, or long-term stand development/successional pathways. Certainly for the West Coast, the prevalence of Douglas-fir (*Pseudotsuga menziesii*) CWM can be attributed to Douglas-fir being a dominant tree species that has been a focus of dead wood studies for decades (e.g., Spies and others 1988). In Rocky Mountain States, ponderosa pine (*Pinus ponderosa*) is often a top

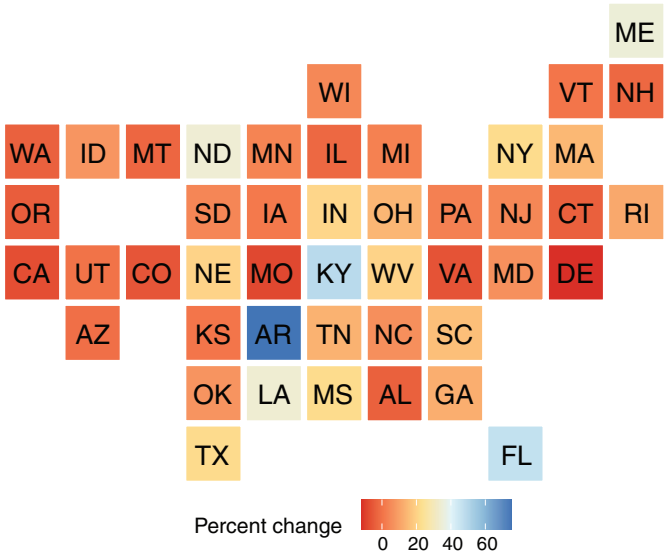

Figure 6.8—Change in percentage of large-sized coarse woody material (CWM) biomass (transect diameter >16.0 inches), 2002–2011 to 2012–2019. (Note: a negative value indicates that the State's population of CWM biomass is becoming increasingly represented by large-sized CWM pieces.)

CWM species owing to both its prevalence and widespread mortality events stemming from droughts, wildfire, and insects/disease (Bottero and others 2017). In the East, the prevalence of beech (*Fagus* spp.), eastern white pine (*P. strobus*), and red maple (*Acer rubrum*) may be an indicator of past diseases (e.g., beech bark disease; Morin and others 2007), trajectories of old-field succession, and/or natural progression of stand development. Akin to relative changes in decay and transect-diameter distributions of CWM biomass (e.g., figs. 6.5 and 6.8), the change in the relative percentage of the top five

CWM species relative to all other species over time can be examined by State (fig. 6.10). For a few States, CWM biomass is becoming more dominated by fewer species such as found in Arkansas, Massachusetts, Tennessee, Indiana, Florida, Texas, and Idaho; in contrast, Vermont, Connecticut, Kansas, and Oklahoma exhibited less dominance of the top five CWM species. The dominance of one species accounting for a plurality of CWM biomass across a State may be an indicator of past mortality events that primarily affected one major tree species in the context of perhaps a less diverse live tree diversity (e.g., ponderosa pine and mountain pine beetle [*Dendroctonus ponderosae*] mortality in Idaho) compared to the mortality of a less dominant tree species in a highly diverse system (e.g., flowering dogwood [*Cornus florida*] mortality in the Great Smoky Mountains).

The results of this national CWM change evaluation can be used to indicate trends in forest health dynamics with implications for CWM resource trajectories. Additionally, such an analysis may help identify CWM resource metrics of utility for conserving forest resources inclusive of dead wood (e.g., forest carbon stocks or habitat). Overall, CWM biomass has increased across forests of the United States, which is not surprising given concomitant increases in live tree volume and biomass during the same time period (Oswalt and others 2019). However, CWM biomass is increasingly represented by larger sized pieces of more advanced decay with a species composition that is less dominated by a few species (i.e., perhaps greater species diversity and/or species evenness). It can only be speculated as to what this CWM resource trend indicates as much more research into uncertainty analyses and relationships between CWM and standing live/dead trees needs to occur. However, the following hypotheses can be suggested. First, the increasing amounts of CWM biomass of larger sized pieces are probably indicative of the maturing forest resource across the United States. Second, as CWM pieces are increasingly of advanced decay, it suggests that there are fewer episodic disturbances (e.g., blowdown events) relative to mortality from stand development (i.e., tree suppression, senescence) and/or insects/disease (e.g., spruce budworm [*Choristoneura freeman*] or beech bark disease). Third, the somewhat steady or slightly reduced dominance of CWM species composition by a few species by State suggests that widespread species-specific mortality events are not imparting substantial additions to the CWM population beyond that of natural mortality dynamics (e.g., stand development). However, the relatively sparse sample intensity of the CWM inventory (especially during the 2002–2011 period) prevents further conclusions regarding mortality events that operate at the stand level (e.g., root rots). Overall, examinations of CWM resource dynamics provide an insight into past trajectories of forest development across large scales with implications for carbon and nutrient cycles, as well as an amenity of ecosystem services.

Beyond strategic-scale resource assessments, additional research is needed to enable further refinement of the initial analyses provided in

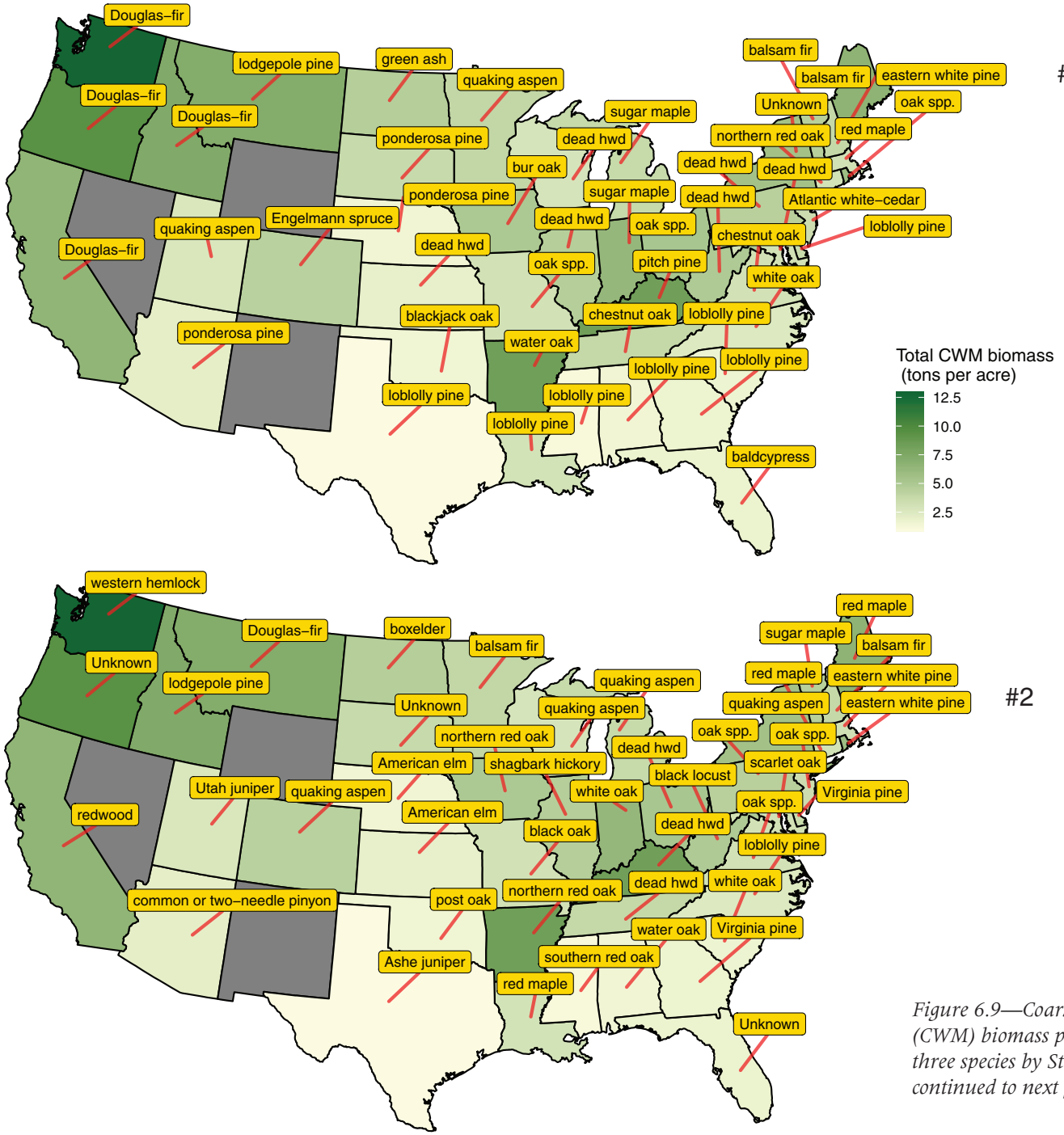

Figure 6.9—Coarse woody material (CWM) biomass per forested acre and top three species by State, 2012–2019.
continued to next page

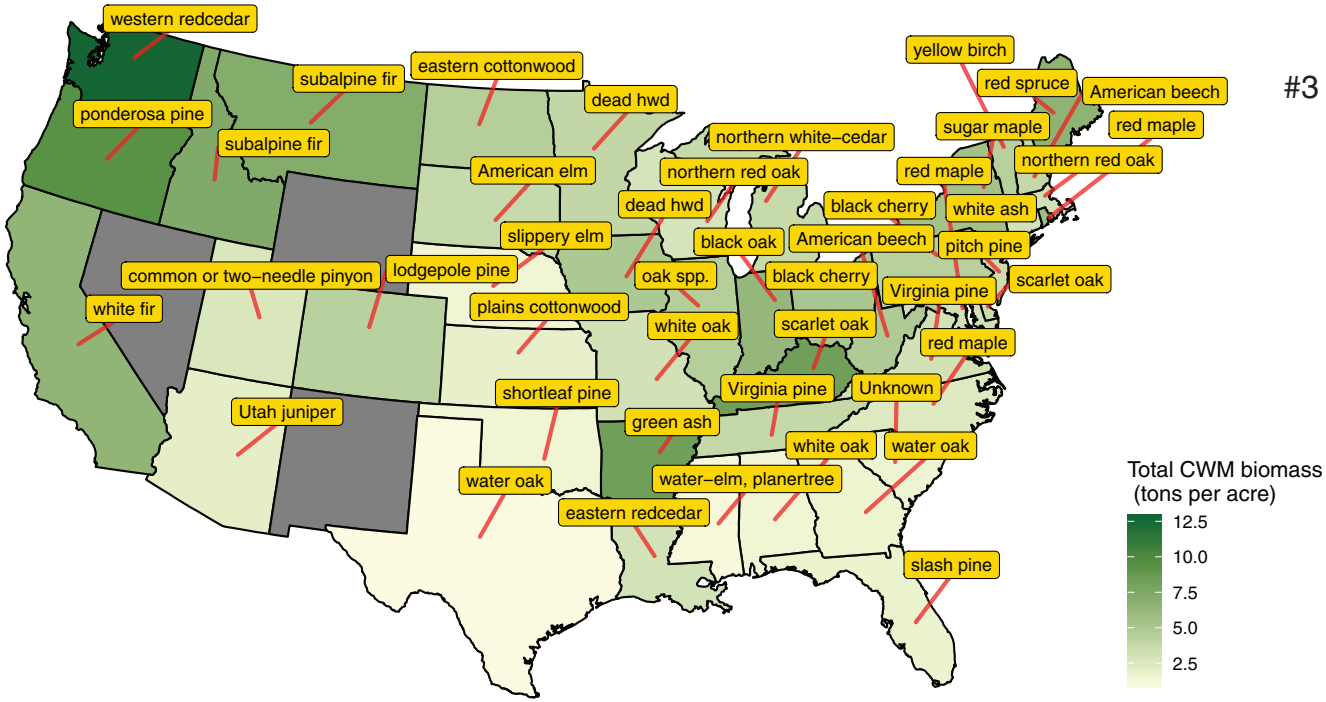

Figure 6.9 (continued)—Coarse woody material (CWM) biomass per forested acre and top three species by State, 2012–2019.

this study. Explicit linkages to standing live/dead trees provides a more comprehensive assessment of tree life cycles, stand development processes, and successional changes. Such a linkage is beyond the objectives of this study but would greatly aid efforts to manage carbon stocks and adapt forest management for future global change (e.g., climate change events or insects/disease). Furthermore, although individual CWM pieces are not explicitly tracked in FIA's strategic inventory, refinement of change estimation procedures beyond coarse large-scale stock change estimation paradigms would assist with unraveling CWM dynamics. It can be suggested that numerous resource monitoring paradigms for live trees do not necessarily apply to CWM given that CWM populations decline (volume and biomass loss) over time with a dependence on tree mortality for accretion, quite the opposite of live trees. Another topic of critical importance is the assessment of total uncertainty in CWM resource assessments. The FIA program enables the determination of sampling error associated with CWM data through online tools and documented procedures (Woodall and others 2019). However, there are numerous other sources of error that should be acknowledged in CWM resource analyses such as model

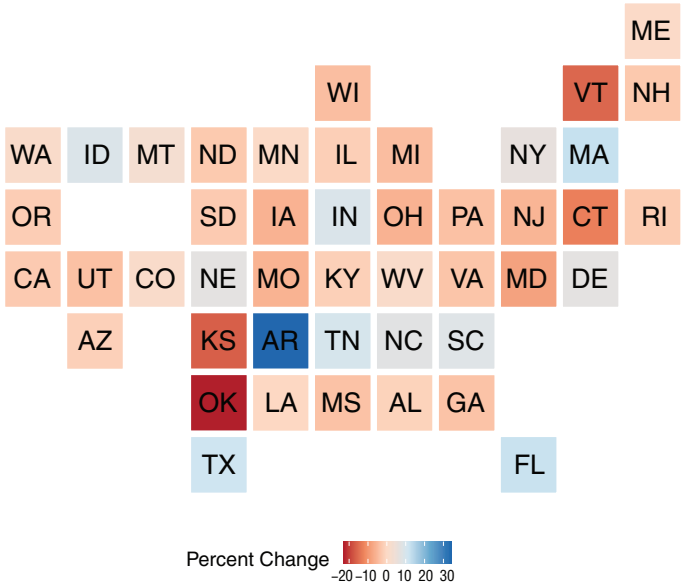

Figure 6.10—Change in percentage of biomass of top five coarse woody material (CWM) species accounting for total CWM by State, 2002–2011 to 2012–2019. (Note: a positive value indicates that the State's population of CWM biomass is becoming more dominated by fewer species over nearly 20 years.)

error (e.g., log volume) and uncertainties in decay reduction factors (Campbell and others 2019). Finally, more robust approaches to quantifying CWM diversity (e.g., species, size, decay state) are needed that are reflective of the unique aspects of this resource. Can functional traits indicative of tree decay pathways be incorporated to assist with interpretation of future resource trajectories? Relative to the lengthy history of forest management and associated sciences, the science of CWM resource monitoring and management has many opportunities for substantial advancement.

In conclusion, nearly 20 years of effort invested in a consistent, national inventory of CWM has established a baseline of data regarding the attributes of the CWM population at the outset of the 21st century as U.S. forests face increasing stressors (e.g., episodic precipitation, invasive species, and/or development). Although comparisons between the 2002–2011 and 2012–present CWM inventories should be at the population scale (e.g., survey units or States) due to revisions to plot measurement protocols, there remains an abundance of analytical possibilities that will only be expanded upon once the 2012–present inventory is fully remeasured. Not only will remeasured plots enable more sophisticated CWM dynamics modeling and longitudinal analysis (e.g., Russell and others 2014), the initial results of this study suggest that refining paradigms of CWM resource analysis in the context of live and standing dead tree attributes would greatly advance our understanding of forest structure, carbon pools, and nutrient cycles, among a host of vital forest ecosystem processes that all tier to dead wood.

LITERATURE CITED

Bolton, N.W.; D'Amato, A.W. 2011. Regeneration responses to gap size and coarse woody debris within natural disturbance-based silvicultural systems in northeastern Minnesota, USA. Forest Ecology and Management. 262: 1215–1222. https://doi.org/10.1016/j.foreco.2011.06.019.

Bottero, A.; D'Amato, A.W.; Palik, B.J. [and others]. 2017. Density-dependent vulnerability of forest ecosystems to drought. Journal of Applied Ecology. 54: 1605–1614. https://doi.org/10.1111/1365-2664.12847.

Bradford, J.B.; Birdsey, R.A.; Joyce, L.A.; Ryan, M.G. 2008. Tree age, disturbance history, and carbon stocks and fluxes in subalpine Rocky Mountain forests. Global Change Biology. 14: 2882–2897. https://doi.org/10.1111/j.1365-2486.2008.01686.x.

Burrill, E.A.; Wilson, A.M.; Turner, J.A. [and others]. 2017. The Forest Inventory and Analysis Database: database description and user guide version 7.2 for Phase 2. Washington, DC: U.S. Department of Agriculture Forest Service. 946 p. http://www.fia.fs.fed.us/library/database-documentation/. [Date accessed: July 2018].

Campbell, J.; Green, M.B.; Yanai, R.D. [and others]. 2019. Estimating uncertainty in the volume and carbon storage of downed coarse woody debris. Ecological Applications. 29: e01844. https://doi.org/10.1002/eap.1844.

Harmon, M.E.; Franklin, J.F.; Swanson, F.J. [and others]. 1986. Ecology of coarse woody debris in temperate ecosystems. Advances in Ecological Research. 15: 133–302. https://doi.org/10.1016/S0065-2504(08)60121-X.

Kosiba, A.M.; Schaberg, P.G.; Rayback, S.A.; Hawley, G.J. 2018. The surprising recovery of red spruce growth shows links to decreased acid deposition and elevated temperature. Science of the Total Environment. 637–638: 1480–1491. https://doi.org/10.1016/j.scitotenv.2018.05.010.

McDowell, N.G.; Allen, C.D. 2015. Darcy's law predicts widespread forest mortality under climate warming. Nature Climate Change. 5: 669–672. https://doi.org/10.1038/nclimate2641.

Morin, R.S.; Liebhold, A.M.; Tobin, P.C. [and others]. 2007. Spread of beech bark disease in the Eastern United States and its relationship to regional forest composition. Canadian Journal of Forest Research. 37: 726–736.

Norden, B.; Ryberg, M.; Gotmark, F.; Olausson, B. 2004. Relative importance of coarse and fine woody debris for the diversity of wood-inhabiting fungi in temperate broadleaf forests. Biological Conservation. 117: 1–10. https://doi.org/10.1016/S0006-3207(03)00235-0.

Oswalt, S.N.; Smith, W.B.; Miles, P.D.; Pugh, S.A. 2019. Forest resources of the United States, 2017: a technical document supporting the Forest Service 2020 RPA Assessment. Gen. Tech. Rep. WO-97. Washington, DC: U.S. Department of Agriculture Forest Service, Washington Office. 223 p. https://doi.org/10.2737/WO-GTR-97.

Reams, G.A.; Smith, W.D.; Hansen, M.H. [and others]. 2005. The Forest Inventory and Analysis sampling frame. In: Bechtold, W.A.; Patterson, P.L., eds. The enhanced Forest Inventory and Analysis program – national sampling design and estimation procedures. Gen. Tech. Rep. SRS-80. Asheville, NC: U.S. Department of Agriculture Forest Service, Southern Research Station: 11–26.

Russell, M.B.; Fraver, S.; Aakala, T. [and others]. 2015. Quantifying carbon stores and decomposition in dead wood: a review. Forest Ecology and Management. 350: 107–128. https://doi.org/10.1016/j.foreco.2015.04.033.

Russell, M.B.; Woodall, C.W.; Fraver, S. [and others]. 2014. Residence time and rate of decay for downed woody debris biomass/carbon in Eastern US forests. Ecosystems. 17: 765–777. https://doi.org/10.1007/s10021-014-9757-5.

Scott, C.T.; Bechtold, W.A.; Reams, G.A. 2005. Sample-based estimators used by the Forest Inventory and Analysis national information management system. In: Bechtold, W.A.; Patterson, P.L., eds. The enhanced Forest Inventory and Analysis program – national sampling design and estimation procedures. Gen. Tech. Rep. SRS-80. Asheville, NC: U.S. Department of Agriculture Forest Service, Southern Research Station: 43–67.

Spies, T.A.; Franklin, J.F.; Thomas, T.B. 1998. Coarse woody debris in Douglas-fir forests of western Oregon and Washington. Ecology. 69: 1689–1702. https://doi.org/10.2307/1941147.

Stokland, J.N.; Siitonen, J.; Jonsson, B.G. 2012. Biodiversity in dead wood. Cambridge, UK: Cambridge University Press. 509 p. https://doi.org/10.1017/CBO9781139025843.

U.S. Department of Agriculture (USDA) Forest Service. 2016. Forest Inventory and Analysis national core field guide, volume I: field data collection procedures for Phase 2 plots, version 7.1. Washington, DC: U.S. Department of Agriculture Forest Service, Forest Inventory and Analysis. https://www.fia.fs.fed.us/library/field-guides-methods-proc/index.php. [Date accessed: June 2018].

Woodall, C.W.; Monleon, V.J. 2008. Sampling protocol, estimation, and analysis procedures for the down woody materials indicator of the FIA program. Gen. Tech. Rep. NRS-22. Newtown Square, PA: U.S. Department of Agriculture Forest Service, Northern Research Station. 68 p. https://doi.org/10.2737/NRS-GTR-22.

Woodall, C.W.; Monleon, V.J.; Fraver, S. [and others]. 2019. The downed and dead wood inventory of forests in the United States. Scientific Data. 6: 180303. https://doi.org/10.1038/sdata.2018.303.

Woodall, C.W.; Nagel, L.M. 2006. Coarse woody type: a new method for analyzing coarse woody debris and forest change. Forest Ecology and Management. 227: 115–121. https://doi.org/10.1016/j.foreco.2006.02.032.

Woodall, C.W.; Russell, M.; Walters, B.F. [and others]. 2015. Net carbon flux of dead wood in forests of the Eastern US. Oecologia. 177: 861–874.

CHAPTER 7.

Advancing Broad-scale Forest Health Evaluation and Monitoring with rFIA

Hunter Stanke
Andrew O. Finley
Grant M. Domke

INTRODUCTION

The U.S. Department of Agriculture Forest Inventory and Analysis (FIA) program collects data describing the condition and change of forest ecosystems across all lands in the United States (Smith 2002, USDA Forest Service 2019b). The extraordinary size of the spatial domain and breadth of forest variables sampled by the FIA program make it a unique and powerful resource for determining the extent and severity of undesirable changes in forest health across large spatial domains in the United States. Due to a lack of flexible, user-friendly tools for estimation of forest variables (Tinkham and others 2018), the richness and utility of the FIA data are not always realized for forest health assessment. We developed rFIA (Stanke and others 2020, https://rfia.netlify.app/), an open-source R package (R Core Team 2020), to reduce these data accessibility hurdles and unlock the potential of FIA for broad-scale forest health evaluation and monitoring.

rFIA achieves two primary objectives: (1) improve the accessibility of FIA data for the estimation of status and change in forest ecosystems and (2) offer enhanced flexibility in estimation strategies and defining populations of interest. Using a simple yet powerful design, rFIA implements the design-based estimation procedures described in Bechtold and Patterson (2005) for more than 60 forest variables and allows users to return intermediate (i.e., plot, condition, and/or tree-level) estimates of all variables for use in modeling studies. With rFIA, users can easily summarize forest variables for populations defined by any combination of spatial units (i.e., spatial polygons), temporal domains (e.g., most recent measurements), and/or biophysical attributes (e.g., species, site classifications). Furthermore, rFIA implements five design-based estimators that enhance the value of FIA for temporal change detection and offer flexibility in a tradeoff between precision and temporal specificity.

Here we present three case studies chosen to demonstrate some aspects of rFIA's potential to advance forest health evaluation and monitoring in the United States. First, we highlight rFIA's spatiotemporal estimation capacity by estimating current down woody material (DWM) biomass within HUC6 watershed boundaries across the conterminous United States (CONUS) by combining the most recent FIA inventories available in each State. We next illustrate how rFIA enhances the value of FIA for temporal change detection by examining trends in lodgepole pine (*Pinus contorta*) mortality in Colorado using multiple design-based estimators. Finally, we use rFIA to estimate plot-level live tree density and develop a Bayesian hierarchical model to estimate changes in live tree abundance (i.e., net response of recruitment, growth, and mortality) within ecoregion subsections (Cleland and others 2007) across the CONUS (excluding Wyoming due to a lack of remeasurements), thereby demonstrating how rFIA can aid model-based analyses.

METHODS

Data

Since 1999, FIA has operated an extensive, nationally consistent forest inventory designed to monitor changes in forests across all lands in the United States (Smith 2002). The program measures forest variables on a network of permanent ground plots that are systematically distributed at a rate of approximately one plot/2428 ha (one plot per 6,000 acres) across the United States (Smith 2002). Ground plots are remeasured approximately every 5 to 7 years in the Eastern United States and 10 years in the Western United States, with remeasurements currently available in most States. Data collected on ground plots are stored in a large public database (i.e., the FIA Database) (USDA Forest Service 2019a). rFIA includes utility functions to retrieve, process, and visualize data stored in the FIA Database (Stanke and others 2020). Herein, we demonstrate potential applications of rFIA to forest health evaluation and monitoring, drawing solely from data collected by the FIA program. The code to reproduce these analyses (including sample sizes and results) are available at our official website (https://rfia.netlify.app/project/fhm2020/).

National-scale DWM Biomass Stocks

The FIA program measures variables related to DWM volume, biomass, and carbon on a subset of ground plots in most FIA regions (i.e., intensive or forest health plots). The *dwm* function in rFIA uses FIA data to produce plot-level or population estimates of DWM variables by ecosystem components, including: coarse woody debris (i.e., 1,000-hour fuels), fine woody debris (i.e., 1-, 10-, and 100-hour fuels), slash piles, litter, and duff. We used the *getFIA* function in rFIA to download an appropriate subset of the FIA Database from the FIA DataMart and selected the most recent subset of inventories within each State using the *clipFIA* function. We then used the most recent subset of the FIA Database to estimate the current biomass density of 100-hour fuels (1.00–2.99-inch diameter) on forest land (including public and private lands) within HUC6 watershed boundaries across the CONUS. All estimates were produced using the temporally indifferent (TI) estimator (i.e., the same methods implemented by FIA's flagship online estimation tool, EVALIDator [Miles 2019]).

Trends in Colorado Lodgepole Pine Mortality

The FIA program uses an annual panel system to estimate current inventories and change, where inventory cycles consist of multiple panels, and individual panels comprise mutually exclusive subsets of ground plots measured in the same year within a region. Precision of point and change estimates can often be improved by combining annual panels within an inventory cycle (i.e., by augmenting current data with data collected previously). While FIA does not prescribe a core procedure for combining panels (Bechtold and Patterson 2005), the TI estimator, which effectively pools data from annual panels into a single periodic inventory, is likely the most widely known and used.

rFIA implements the TI estimator by default for consistency with EVALIDator (Miles 2019). Alternatively, users may choose to return estimates from individual annual panels (ANNUAL estimator) or use one of three moving-average-based estimators, including the simple moving average (SMA), linear moving average (LMA), and exponential moving average (EMA). The SMA estimator applies equal weight to all annual panels within an inventory cycle; hence, its estimates tend to align closely with those of the TI estimator. In contrast, the LMA and EMA estimators apply weights that decay linearly or exponentially as a function of time since measurement, respectively. The EMA estimator requires specification of a decay parameter, λ (ranging between 0 and 1, default 0.5), that controls the rate at which panel weights decline with time (higher values of λ indicate more even distribution of weights across panels).

The FIA program calculates growth, mortality, and removals between repeated measurements of inventory plots. To provide early estimates of mortality (i.e., prior to availability of remeasurements on annual inventory plots), FIA draws on inventory data collected prior to the implementation of the annual design (i.e., periodic inventory plots; where many annual plots were established on top of previous periodic plots). The *growMort* function in rFIA seamlessly integrates both procedures (periodic-annual and annual-annual) to provide unbiased estimates of tree mortality processes over time.

We used the *growMort* function to estimate trends in the mortality rate (trees per acre per year) of lodgepole pine in Colorado over the period 2002–2018. We estimate mortality rates and associated uncertainty using each design-based estimator currently offered in rFIA (i.e., TI, SMA, LMA, EMA, and ANNUAL estimators) and visually compare trends across estimators. To highlight the flexibility and utility of the EMA estimator for use in temporal change detection, we estimate mortality rates and associated uncertainty with multiple values of λ (i.e., effectively varying the temporal kernel from which mortality rates are estimated) and visually compare short-range and long-range trends.

National-scale Shifts in Live Tree Abundance

Traditionally, FIA has relied on sample plot data and design-based estimators to produce point and change estimates of forest variables (Tinkham and others 2018). These estimators are familiar and generally unbiased (McRoberts 2010), though low sample sizes often limit their ability to yield sufficiently precise estimates for small populations (e.g., small spatial domains, rare species/events). Model-based estimators offer a versatile alternative to design-based estimation, relying on predictions from models and ancillary variables to produce estimates of forest variables and often yielding more precise estimates for small populations. To aid model-based analyses using FIA data, rFIA allows users to return estimates of all forest variables within subpopulation response units (e.g., plot,

subplot, condition, tree-level). These estimates can then be used (along with ancillary variables) to develop models of ecological patterns and processes, estimate population parameters, and predict to unobserved domains (e.g., forecast future change).

Here, we use the *tpa* function in rFIA to estimate plot-level number of live trees per acre (TPA) and live tree basal area per acre (BAA) for all plot visits under the annual inventory design across the CONUS. Using estimates from plots visited more than once (i.e., remeasured annual plots), we construct a Bayesian hierarchical model to estimate the average rate of change in live TPA and BAA at individual plots, within ecoregion subsections (Cleland and others 2007), and across the CONUS over the period 1999–2019:

$$y_{i,j,k} \sim normal(\beta_{j,k} t_{i,j,k} + \alpha_{j,k}, \varsigma^2_{j,k}) \quad (1)$$

$$\alpha_{j,k} \sim normal(\alpha_k, \sigma^2_{\alpha,k}) \quad (2)$$

$$\beta_{j,k} \sim normal(\beta_k, \sigma^2_{\beta,k}) \quad (3)$$

$$\alpha_k \sim normal(\alpha, \sigma^2_{\alpha}) \quad (4)$$

$$\beta_k \sim normal(\beta, \sigma^2_{\beta}) \quad (5)$$

where

y = the log of live TPA or BAA at visit i, on plot j, in ecoregion subsection k

t = year of visit

α = a random intercept describing y at $t = 0$

β = a random slope describing the average annual rate of change in y

$\varsigma^2_{j,k}$ = the residual variance of the linear model relating log TPA/BAA to time at the plot level [equation (1)]

We allow $\alpha_{j,k}$ and $\beta_{j,k}$ to vary across plots, with their values drawn from subsection-level distributions [equations (2–3)] characterized by a corresponding mean (α_k and β_k) and variance ($\sigma^2_{\alpha,k}$, $\sigma^2_{\beta,k}$) for each coefficient. Parameters of subsection-level distributions are in turn drawn from a CONUS-level distribution defined by means (α and β) and variances (σ^2_{α}, σ^2_{β}) of each coefficient. As our response (live TPA or live BAA) is log scaled, we can transform estimates of β_k and β to annual rates:

$$r_k = 100(e^{\beta_k} - 1) \quad (6)$$

$$r = 100(e^{\beta} - 1) \quad (7)$$

where

r = percentage of annual change in live TPA or BAA (Crawley 1993)

The hierarchical form of our model allows us to draw inference regarding temporal trends in live tree abundance across multiple ecological scales (i.e., stand, landscape, and subcontinental). For brevity, we highlight results at the landscape and subcontinental scale here. Specifically, we estimate the percentage of annual change in live TPA and live BAA of tree populations [equations (6 and 7)] within ecoregion subsections and across the CONUS. We estimate the probability of direction, or probability that the estimated rate for each population excludes 0, to highlight the "significance" of the estimated trends.

RESULTS AND DISCUSSION

National-scale DWM Biomass Stocks

We mapped estimates and associated uncertainty of current 100-hour fuel biomass density (tons per acre) by HUC6 units across the CONUS to demonstrate the spatiotemporal estimation capacity of rFIA (fig. 7.1). In the Eastern United States, 100-hour fuel density generally appears to be higher in regions dominated by oak-hickory forest types relative to regions dominated by southern pines, northern hardwoods, and spruce/fir forest. In the Western United States, 100-hour fuel density appears to be elevated in regions dominated by Douglas-fir forest types (e.g., Pacific Northwest) relative to other regions. Uncertainty (measured as sampling error percentage, or coefficient of variation percentage) tended to be highest in the Plains and desert Southwest, presumably due to low sample sizes. Estimates presented herein are similar to those from previous efforts to characterize DWM biomass in U.S. forests (Chojnacky and others 2004, Woodall and others 2013).

Down woody material is an important component of forest ecosystems across the United States. Specifically, DWM biomass may help describe fuel loading, wildlife habitat, structural diversity, and biogeochemical processes in forests (Woodall and Monleon 2008). The national-scale DWM inventory provided by FIA is unprecedented in scope and spatial extent, and of extraordinary value in many forest health monitoring efforts. We anticipate the *dwm* function in rFIA will be of particular interest to wildlife biologists, ecologists, mycologists, foresters, and fuels specialists seeking to estimate the status, change, and future states of DWM stocks. For brevity, we only present results of 100-hour fuel density (biomass per acre). However, it is important to note that our analysis (i.e., a single call to *dwm*) simultaneously produced estimates of DWM biomass, carbon, and volume (totals and density) for the following ecosystem components/fuel classes: litter, duff, 1-hour (0.00–0.24-inch diameter), 10-hour (0.25–0.99-inch diameter), 100-hour (1.00–2.99-inch diameter), and 1,000-hour fuels (≥3 inch diameter).

While the analysis presented here is relatively simple, it represents a substantial advance in spatial estimation capacity relative to other FIA estimation tools (USDA Forest Service 2019a). That is, we used unique areal units (i.e., HUC6 watershed boundaries) to define populations of interest, rather than relying on fields recorded in

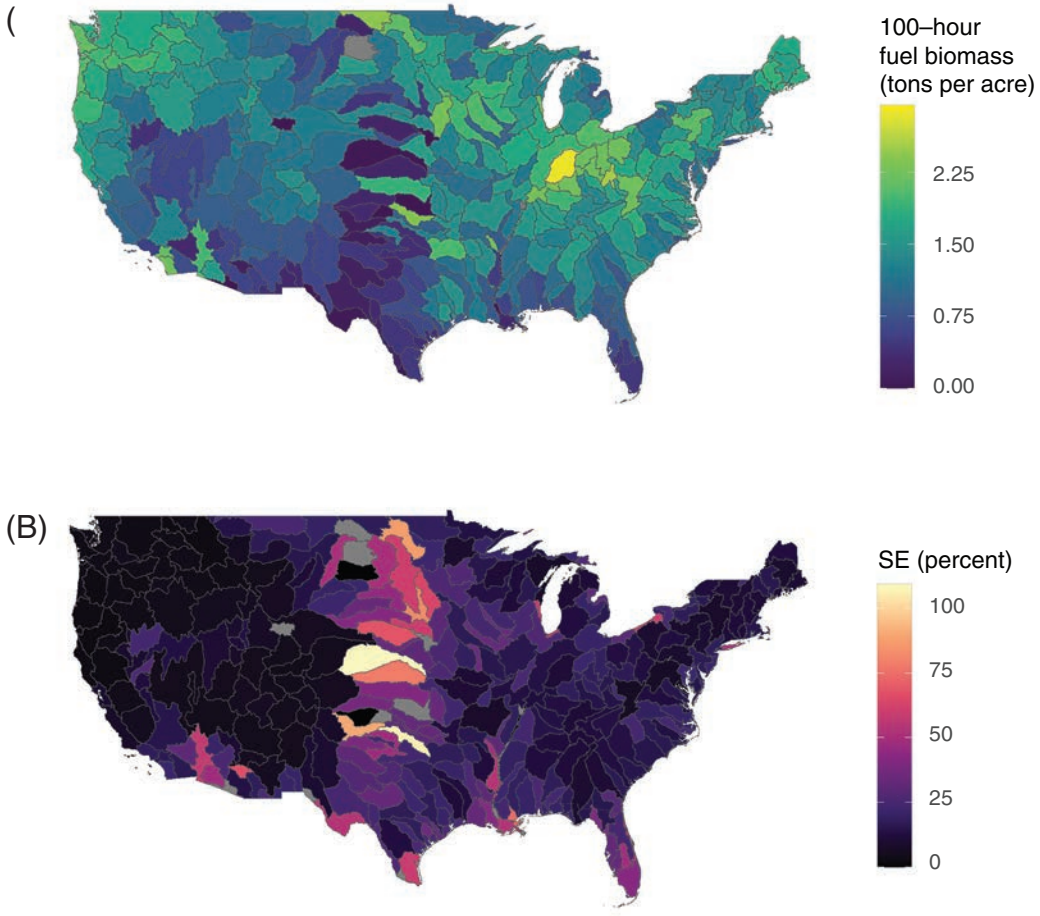

Figure 7.1—(A) Estimated current 100-hour fuel biomass (tons per acre) and (B) associated uncertainty (percent sampling error [SE]) within HUC6 watershed boundaries across the conterminous United States. All estimates produced using the dwm *function in the rFIA package, using the temporally indifferent estimator.*

the FIA Database. With rFIA, users can specify any spatial polygon object to use as a grouping variable (i.e., region contained within each areal unit is treated as a unique population). For example, spatial polygons describing historic fire regimes could be used to group estimates of current DWM fuel stocks (or other variables of interest, e.g., size-class distributions, mortality, invasive species abundance). While we use the *dwm* function to highlight rFIA's spatial estimation capacity, all rFIA estimator functions have been designed with the same functionality.

Trends in Colorado Lodgepole Pine Mortality

We used multiple design-based estimators to examine temporal trends in Colorado lodgepole pine mortality (TPA per year) and highlight how rFIA enhances the value of FIA for temporal change detection. A general pattern of increasing mortality through time was evident across all estimators, likely linked to recent outbreaks of mountain pine beetle (*Dendroctonus ponderosae*) in the region (Page and Jenkins 2007). Specifically, we observe an approximately fourfold increase in lodgepole pine mortality across all estimators in 2015 relative to 2005 levels. Point-estimates of mortality (estimated mortality in any given year) and associated uncertainty (i.e., sampling error percentage) varied considerably among estimators, with the ANNUAL estimator exhibiting the highest degree of interannual variability and uncertainty and the SMA and TI estimators exhibiting the smoothest temporal trends and lowest uncertainty (fig. 7.2). In general, a decrease in uncertainty was evident across estimators over

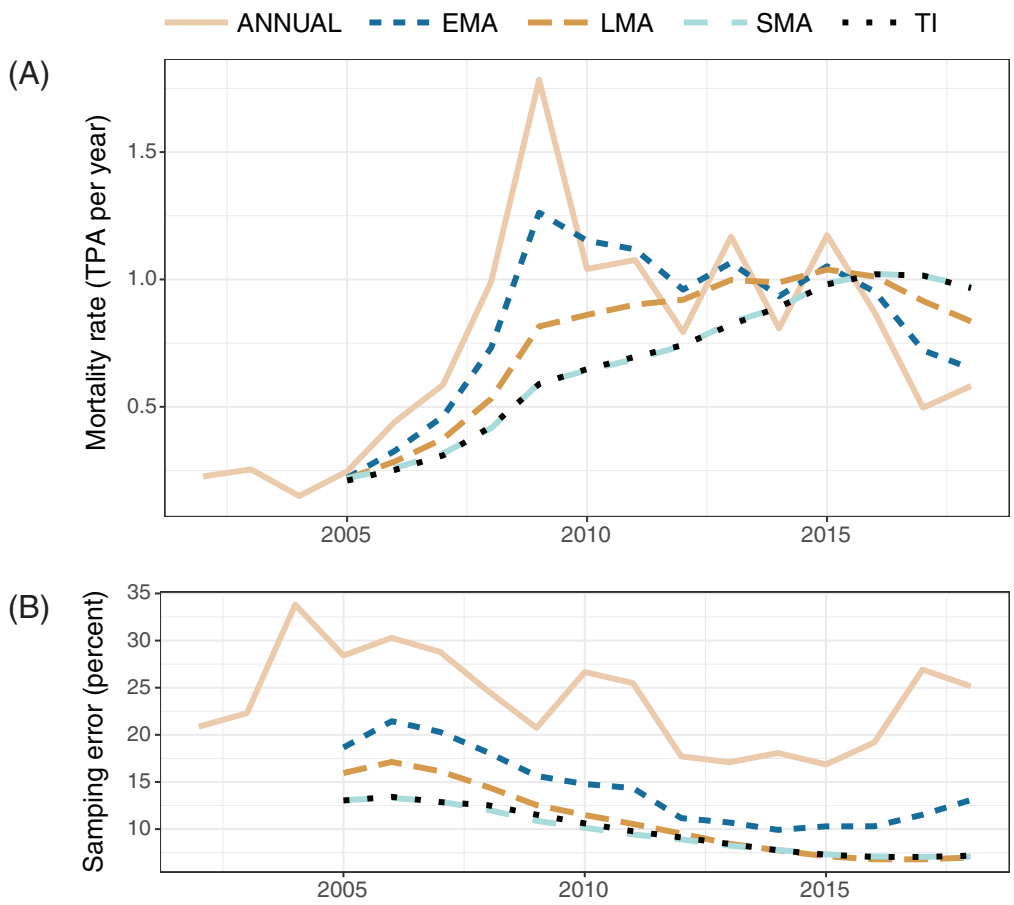

*Figure 7.2—(A) Estimated trends in lodgepole pine (*Pinus contorta*) mortality rates (trees per acre [TPA] per year) and (B) associated uncertainty (percent sampling error) in the State of Colorado over the period 2002–2018. Estimates were produced using five design-based estimators: annual (ANNUAL), exponential moving average (EMA), linear moving average (LMA), simple moving average (SMA), and temporally indifferent (TI). All estimates were produced using the* growMort *function in the rFIA package.*

time, likely due to increasing sample size (i.e., availability of plot remeasurements). While the estimators presented herein vary considerably in their temporal specificity, it is important to note that plot remeasurements occur on 10-year intervals in the Western United States. Hence, all estimates of mortality should be interpreted as an average over a decade (ANNUAL) or more (SMA, LMA, EMA, TI).

Point-estimates of mortality and associated uncertainty varied with the value of λ (i.e., decay parameter controlling distribution of weights across an inventory cycle) specified in the EMA estimator, illustrating the estimator's pronounced flexibility and an inherent tradeoff between precision and temporal specificity (fig. 7.3). As λ approaches 0, higher weight is given to more recent panels in the inventory cycle, and the behavior of the EMA approaches that of the ANNUAL estimator (high temporal specificity; increased uncertainty). In contrast, as λ approaches 1, panel weights are distributed more evenly across inventory cycle, and the behavior of the EMA approaches that of the SMA (low temporal specificity; decreased uncertainty). Sample variance is generally minimized when panel weights are evenly distributed across the inventory cycle, though improved precision comes at the cost of introducing temporal lag-bias (Bechtold and Patterson 2005). Hence, equal weighting schemes (e.g., SMA, TI, or EMA with a high λ) could be undesirable in settings where the variable of interest is suspected to change rapidly over time (as seen here).

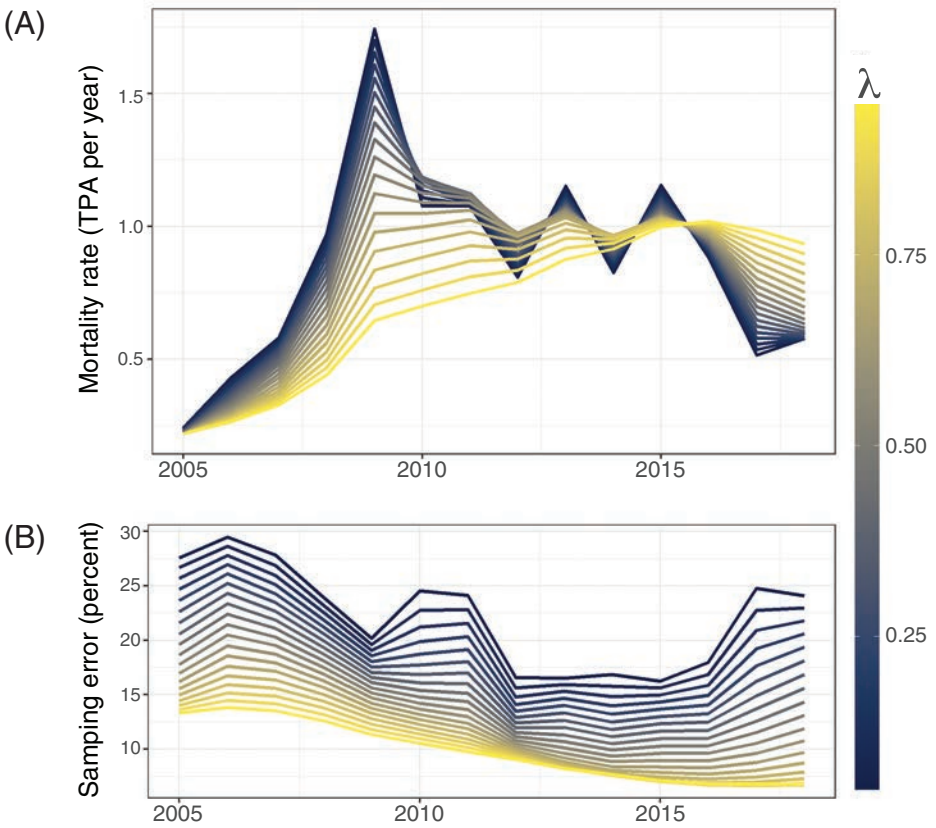

*Figure 7.3—(A) Variation in short-range and long-range temporal trends of lodgepole pine (*Pinus contorta*) mortality rates (trees per acre [TPA] per year) and (B) associated uncertainty (percent sampling error) in the State of Colorado over the period 2002–2018. Estimates produced by varying the value of λ specified in the exponential moving average (EMA) estimator, where high values of λ characterize long-range temporal trends and low values characterize short-range temporal trends. All estimates produced using the* growMort *function in the rFIA package.*

In practice, the choice of estimator should be guided by user objectives. That is, no single estimator presented herein is "best" for all estimation objectives or across a wide variety of spatial, temporal, and population conditions. As a general guide, estimators that distribute weights approximately evenly across panels (i.e., SMA, TI, or EMA with a high λ) should be employed when users seek to minimize uncertainty around estimates and no considerable change is suspected in the underlying population. In contrast, if users are primarily interested in characterizing temporal change in the population of interest, estimators that give higher weight to more recent observations (i.e., ANNUAL, LMA, EMA with low λ) are likely to be more suitable.

In rFIA, users can easily produce "moving-average ribbons" as seen in fig. 7.3 where estimates are produced for multiple, sequential values of λ using the EMA estimator (i.e., effectively characterizing change across multiple temporal scales). Such plots are particularly useful for detecting periods of rapid change in a population. That is, rapid change is likely when large gaps appear between point-estimates produced with different values of λ, with increases in the state variable indicated when short-range (i.e., low λ) estimates exceed long-range estimates (i.e., high λ) (fig. 7.3, 2008–2012) and decreases indicated when long-range estimates exceed short-range estimates (fig. 7.3, 2017–2018).

National-scale Shifts in Live Tree Abundance

To demonstrate how rFIA can aid model-based analyses using FIA data, we use rFIA to estimate plot-level live tree TPA and BAA and develop a Bayesian hierarchical model to estimate temporal changes in each variable across multiple ecological scales. Across the entire CONUS (i.e., subcontinental scale, excluding Wyoming due to a lack of remeasurements), we found a decline in live TPA at a rate of 0.41 percent per year (probability of direction = 99.9 percent, i.e., very high confidence rate is different from 0). In contrast, we found live BAA to be expanding at a rate of 0.99 percent per year across the CONUS (probability of direction = 99.9 percent). Considerable variability was evident across ecoregion subsections (i.e., landscape scale; fig. 7.4); however, broad-scale patterns of decline in live TPA and expansion in live BAA emerge across much of the CONUS. Notable exceptions appear in northern Minnesota, where both variables are expanding, and in the southern Rocky Mountains, where both variables frequently indicate decline or zero net change in live tree abundance.

Shifts in live tree abundance emerge from the net demographic response of tree populations to endogenous (e.g., competition) and exogenous drivers (e.g., climate, disturbance). Hence, the patterns we observe in figure 7.4 represent the net result of spatially varying tree mortality, recruitment, and growth (BAA only) processes in U.S. forests over the period 1999–2019. General patterns of decline in live TPA and

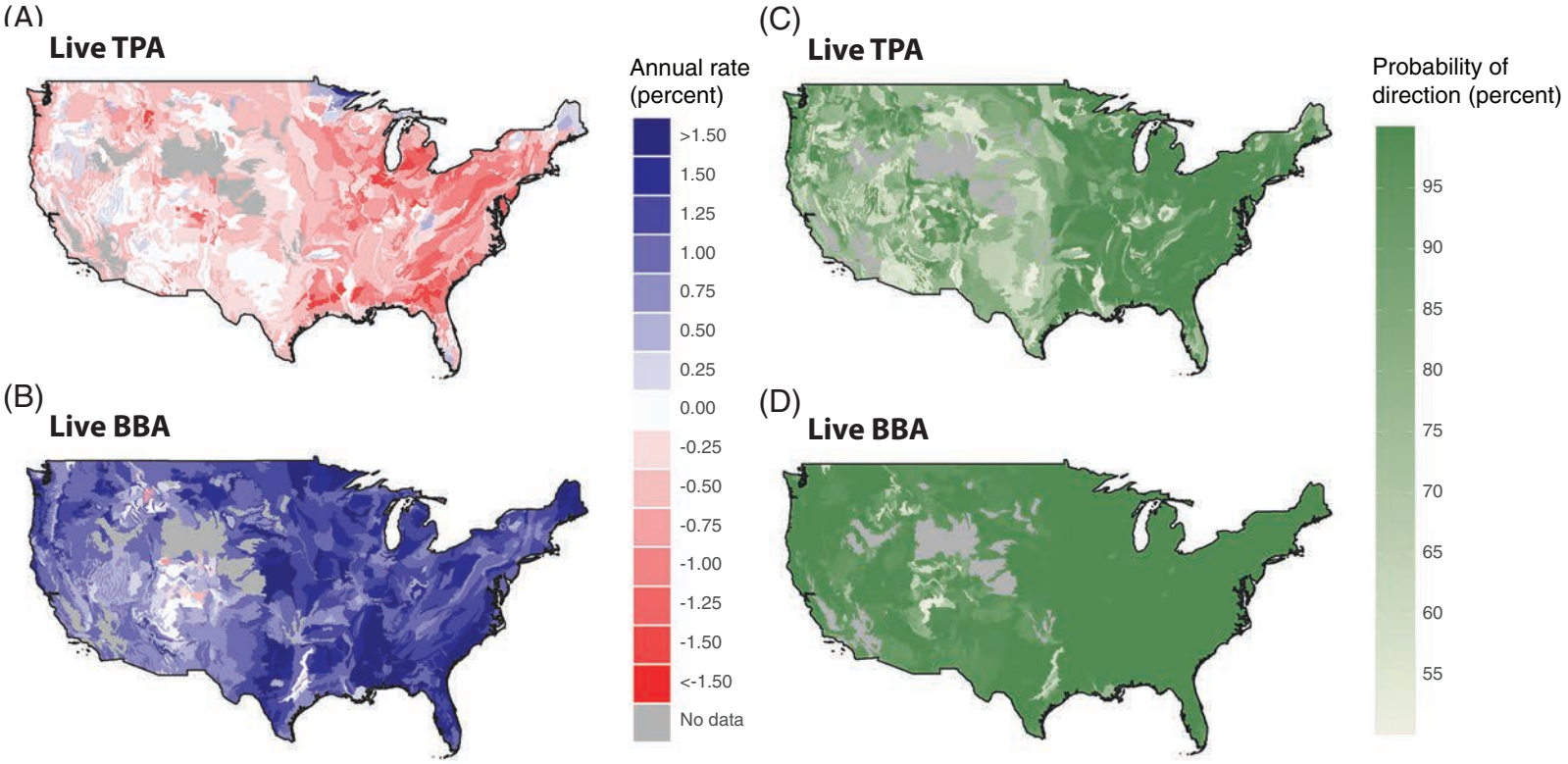

Figure 7.4—Estimated annual rate of change (percent per year) in (A) live number of trees per acre (TPA) and (B) live basal area per acre (BAA), and (C, D) associated indices of significance (probability of direction) within ecoregion subsections (Cleland and others 2007) across the conterminous United States from 1999–2019. All estimates produced using a Bayesian hierarchical model fit to plot-level indices of live TPA and BAA on remeasured Forest Inventory and Analysis (FIA) plots. Plot-level indices of live tree abundance produced using the tpa *function in the rFIA package.*

expansion in live BAA likely emerge in part from transient dynamics associated with stand structural development and succession (Franklin and others 2002) (synchronous maturation of secondary forest across broad spatial domains); hence, it is difficult to determine if/when shifts result primarily from exogenous stressors. Previous efforts have restricted their population of interest to old forest to account for such dynamics (Van Mantgem and others 2009); however, these analyses are unlikely to properly characterize demographic responses at the landscape level, where tree populations are dispersed amongst a mosaic of stand structural classes and successional stages.

rFIA's capacity to return estimates of forest variables within subpopulation response units (e.g., plot-level estimates, as used here) is unique relative to other public FIA estimation tools (i.e., others are designed primarily for design-based population estimation). This capacity eliminates the need for users to navigate the complex structure and data coding of the FIA Database to retrieve data for use in modeling or other applications (e.g., plot-level mapping). We anticipate this capacity will be particularly valuable in applications related to forest health evaluation and monitoring by allowing users to: (1) draw on auxiliary variables to augment sparse FIA data (e.g., Phase 2+ and Phase 3 plot networks) and improve estimation of forest health variables; and (2) draw on multiple remeasurements of FIA plots (when available) to improve estimation of demographic indices and change attributes (as shown here).

Future Extensions of rFIA

In short, we designed rFIA to reduce the hurdles of accessing and manipulating FIA data. Specifically, we aim to improve the accessibility of FIA data for the estimation of status and change in forest ecosystems, and to offer enhanced flexibility in estimation strategies and defining populations of interest. At present, rFIA is capable of estimating more forest variables (>60) from FIA data than any other publicly available tool. This suite of forest variables includes multiple important forest health indicators, including: tree mortality, tree growth, DWM, and tree diversity (i.e., species diversity, structural diversity). Current development aims to broaden the scope of rFIA to provide advanced estimation capacity for indicators of ozone damage, tree crown condition, soil quality, lichen diversity, and understory plant diversity.

Furthermore, we intend to expand the capacity of rFIA to include a suite of spatially enabled model-assisted estimators aimed at improving estimation within small domains (e.g., spatial/temporal extents, rare events). Model-assisted estimators will allow users to easily incorporate auxiliary data in the estimation of forest variables, offering substantial improvements in spatial prediction and change detection for sparsely sampled forest health variables.

Interested users can track updates to rFIA at our official website (https://rfia.netlify.app/). We encourage users to report any issues and/or desired extensions on our active issues page (https://github.com/hunter-stanke/rFIA/issues).

LITERATURE CITED

Bechtold, W.A.; Patterson, P.L. 2005. The enhanced forest inventory and analysis program—national sampling design and estimation procedures. Gen. Tech. Rep. SRS-80. Asheville, NC: U.S. Department of Agriculture Forest Service, Southern Research Station. 85 p. https://www.srs.fs.usda.gov/pubs/gtr/gtr_srs080/gtr_srs080.pdf. [Date accessed: June 15, 2020].

Chojnacky, D.C.; Mickler, R.A.; Heath, L.S.; Woodall, C.W. 2004. Estimates of down woody materials in Eastern US forests. Environmental Management. 33(1): S44–S55. https://doi.org/10.1007/s00267-003-9116-3.

Cleland, D.T.; Freeouf, J.A.; Keys, J.E. [and others]. 2007. Ecological subregions: sections and subsections for the conterminous United States. Gen. Tech. Rep. WO-76D. Washington, DC: U.S. Department of Agriculture Forest Service. Map; Sloan, A.M., cartographer; presentation scale 1:3,500,000; colored. Also on CD-ROM as a GIS coverage in ArcINFO format or at http://data.fs.usda.gov/geodata/edw/datasets.php. [Date accessed: June 15, 2020].

Crawley, M.J. 1993. GLIM for ecologists. Hoboken: Wiley-Blackwell. 396 p.

Franklin, J.F.; Spies, T.A.; Van Pelt, R. [and others]. 2002. Disturbances and structural development of natural forest ecosystems with silvicultural implications, using Douglas-fir forests as an example. Forest Ecology and Management. 155: 399–423. https://doi.org/10.1016/S0378-1127(01)00575-8.

McRoberts, R.E. 2010. Probability-and model-based approaches to inference for proportion forest using satellite imagery as ancillary data. Remote Sensing of Environment. 114: 1017–1025. https://doi.org/10.1016/j.rse.2009.12.013.

Miles, P. 2019. Forest inventory EVALIDator web-application version 1.8.0.01. St. Paul, MN: U.S. Department of Agriculture Forest Service, Northern Research Station. https://apps.fs.usda.gov/Evalidator/evalidator.jsp. [Date accessed: June 15, 2020].

Page, W.G.; Jenkins, M.J. 2007. Mountain pine beetle-induced changes to selected lodgepole pine fuel complexes within the intermountain region. Forest Science. 53: 507–518.

R Core Team. 2020. R: a language and environment for statistical computing. Vienna, Austria: R Foundation for Statistical Computing. https://www.R-project.org/. [Date accessed: June 15, 2020].

Smith, W.B. 2002. Forest Inventory and Analysis: a national inventory and monitoring program. Environmental Pollution. 116: S233–S242. https://doi.org/10.1016/S0269-7491(01)00255-X.

Stanke, H.; Finley, A.O.; Weed, A.S. [and others]. 2020. rFIA: an R package for estimation of forest attributes with the US Forest Inventory and Analysis Database. Environmental Modelling & Software. 127: 104664. https://doi.org/10.1016/j.envsoft.2020.104664.

Tinkham, W.T.; Mahoney, P.R.; Hudak, A.T. [and others]. 2018. Applications of the United States Forest Inventory and Analysis dataset: a review and future directions. Canadian Journal of Forest Research. 48: 1251–1268. https://doi.org/10.1139/cjfr-2018-0196.

U.S. Department of Agriculture (USDA) Forest Service. 2019a. FIA tools and data. https://www.fia.fs.fed.us/tools-data/. [Date accessed: June 15, 2020].

U.S. Department of Agriculture (USDA) Forest Service. 2019b. Forest Inventory and Analysis national program. https://www.fia.fs.fed.us/. [Date accessed: June 15, 2020].

Van Mantgem, P.J.; Stephenson, N.L.; Byrne, J.C. [and others]. 2009. Widespread increase of tree mortality rates in the Western United States. Science. 323: 521–524. https://doi.org/10.1126/science.1165000.

Woodall, C.W.; Monleon, V.J. 2008. Sampling protocol, estimation, and analysis procedures for the down woody materials indicator of the FIA program. Gen. Tech. Rep. NRS-22. Newtown Square, PA: U.S. Department of Agriculture Forest Service, Northern Research Station. 68 p. https://doi.org/10.2737/NRS-GTR-22.

Woodall, C.W.; Walters, B.F.; Oswalt, S.N. [and others]. 2013. Biomass and carbon attributes of downed woody materials in forests of the United States. Forest Ecology and Management. 305: 48–59. https://doi.org/10.1016/j.foreco.2013.05.030.

Each year, the Forest Health Monitoring (FHM) Program funds a variety of Evaluation Monitoring (EM) projects, which are "designed to determine the extent, severity, and causes of undesirable changes in forest health identified through Detection Monitoring (DM) and other means" (FHM 2015). In addition, EM projects can produce information about forest health improvements. Evaluation Monitoring projects are submitted, reviewed, and selected through an established process. More detailed information about how EM projects are selected, the most recent call letter, lists of EM projects awarded by year, and EM project poster presentations can all be found on the FHM website: https://www.fs.fed.us/foresthealth/protecting-forest/forest-health-monitoring/index.shtml.

Beginning in 2008, each FHM annual national report contains summaries of recently completed EM projects. Each summary provides an overview of the project and results, citations for products and other relevant information, and a contact for questions or further information. The summaries provide an introduction to the kinds of monitoring projects supported by FHM and include enough information for readers to pursue specific interests. Six project summaries are included in this report.

LITERATURE CITED

Forest Health Monitoring (FHM). 2015. Evaluation monitoring. https://www.fs.fed.us/foresthealth/fhm/em/index.shtml. [Date accessed: August 5, 2019].

SECTION 3.

Evaluation Monitoring Project Summaries

CHAPTER 8.

Determining What Species Regenerate in Forest Stands Impacted by Heterobasidion Root Disease in Wisconsin and Michigan

Michael Hillstrom
Michael Demchik
Monique Sakalidis
Kyoko Scanlon
Trevor Adams
Katherine Minnix

INTRODUCTION

Heterobasidion root disease (*Heterobasidion irregulare*; HRD) causes substantial pine (*Pinus* spp.) mortality in North America and other regions of the Northern Hemisphere. It first appeared in Wisconsin in 1993 and has since been documented in 28 counties. It was first documented in Michigan in 1963, and recent survey work found it was present in 19 counties. New infestations mainly occur when spores carried by wind land on freshly cut pine and spruce (*Picea* spp.) stumps. Expanding mortality gaps develop as the fungus spreads along interconnected roots. Treating cut conifer stumps with a fungicide effectively prevents HRD infestation.

The continued spread and impact of HRD in the Lake States has increased awareness and concern about the disease. Recent research has filled some knowledge gaps, but many questions are yet to be answered. One knowledge gap in the Lake States is determining what species naturally regenerate in pine plantations infested with HRD. The objective of this research was to evaluate the composition of natural regeneration in red pine (*P. resinosa*) stands impacted by HRD in Wisconsin and Michigan.

METHODS

Thirty-one sites in Wisconsin and Michigan with known HRD infestations were assessed. *H. irregulare* was confirmed via laboratory cultures for all sites. Forty-nine expanding mortality gaps were studied across the 31 sites (three or fewer per site). Expanding mortality gaps were typically not concentric and varied in size from 0.02 to 8.5 acres with a mean of 0.96 acres. All understory regeneration was evaluated in three 10-m^2 round plots for each expanding mortality gap. The species and height class (0.6-m intervals) were recorded for every plant in the plots. "Desirable" regeneration included aspen (*Populus tremuloides*), balsam fir (*Abies balsamea*), black cherry (*Prunus serotina*), jack pine (*P. banksiana*), oak (*Quercus* spp.), red maple (*Acer rubrum*), red pine, white pine (*P. strobus*), and white spruce (*P. glauca*). "Undesirable" regeneration included boxelder (*A. negundo*) and three invasive plant groups: barberry (*Berberis thunbergii*), buckthorn (*Frangula alnus* and *Rhamnus cathartica*), and honeysuckle (*Lonicera* spp.).

Overstory tree species were recorded in variable radius plots (10 BAF [basal area factor] prism; square feet) 10 m and 100 m in each cardinal direction from the edge of expanding mortality gaps. See Demchik and others (2020) for full methods including statistical analyses.

RESULTS

The majority of expanding mortality gaps had sufficient desirable regeneration to fill them over time (Demchik and others 2020). Regeneration was a mix of hardwood and conifer species (Demchik and others 2019) (figs. 8.1 and 8.2). Woody invasive plants were discovered on 39 percent of sites (Demchik and others 2020). Red maple or oak in the overstory 10 m from a gap were correlated with more regeneration of that species in the understory (Demchik and others

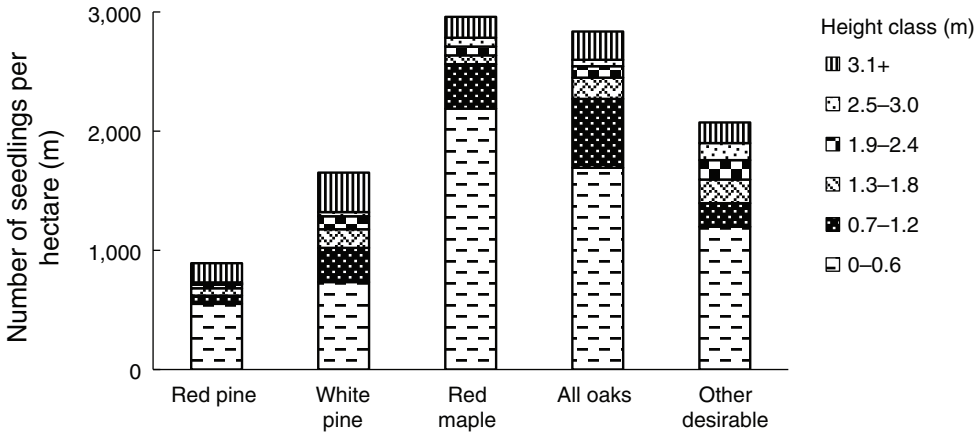

Figure 8.1—Regeneration in Heterobasidion irregulare*-caused expanding mortality pockets or gaps (number of seedlings per hectare by height class) in Wisconsin and Michigan.*

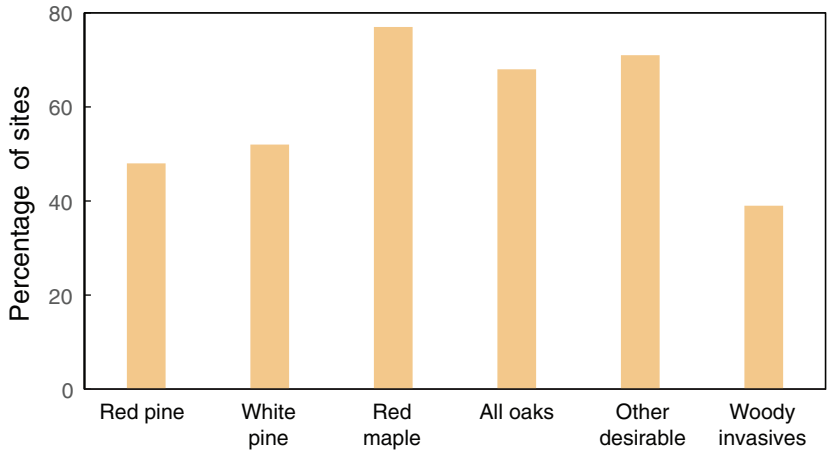

Figure 8.2—Percentage of sites in Wisconsin and Michigan that included each species or species group.

2020). Basal area, soil type, and gap size also impacted regeneration of some species (Demchik and others 2020).

DISCUSSION AND CONCLUSIONS

Although most gaps had satisfactory levels of desirable regeneration, a considerable amount was of HRD- susceptible conifer species. We predict that impacts to pine regeneration may increase as seedlings become saplings and their root systems have a greater chance of contacting HRD-infected trees, stumps, or spores in the soil. Pine regeneration is currently considered desirable because the impacts of HRD on pine regeneration over time in the Lake States still needs to be studied. Nonetheless, because HRD can remain active on infested sites for decades, we expect that these pine stands will increasingly become dominated by hardwood species that are not impacted by HRD. Forestry professionals should be consulted to determine what species of regeneration are most appropriate for an infested site. Management recommendations will vary depending on how many HRD infection centers exist in a pine stand. The quantity of invasive plants will also impact management recommendations. In highly infested stands, regenerating to pine species is not advised; therefore, additional management that converts the stand away from pine may be necessary. These changes in species composition are likely to impact the ecology and economic value of HRD-infested stands. For HRD management recommendations, see Wisconsin's guidelines for stump treatment to reduce the risk of introduction and spread of Heterobasidion root disease (Wisconsin DNR 2020).

For more information, contact: Michael Hillstrom, michael.hillstrom@wisconsin.gov.

ACKNOWLEDGMENTS

We thank all the landowners who allowed us access to their land for this study and the group of individuals who helped collect data for this project. We thank the U.S. Department of Agriculture Forest Service, Forest Health Monitoring (FHM) coordinators Karen Ripley, Chris Asaro, and Stephen Burr for reviewing this project summary. This project (NC-EM-17-03) was funded by the Forest Service FHM Evaluation Monitoring program through grant 17-DG-11420004-297.

LITERATURE CITED

Demchik, M.C.; Sakalidis, M.L.; Hillstrom, M. [and others]. 2020. Evaluating regeneration in Heterobasidion root disease infested stands in the Lake States. Forest Science. 66(2): 141–144. https://doi.org/10.1093/forsci/fxz074.

Wisconsin Department of Natural Resources (DNR). 2020. Guidelines for stump treatment to reduce the risk of introduction and spread of Heterobasidion root disease in Wisconsin. PUB-FR-768 2020. https://dnr.wi.gov/news/input/documents/guidance/final/20200406/FA-20-0012-C.pdf. [Date accessed: March 11, 2020.]

CHAPTER 9.

Legacy Effects of Emerald Ash Borer on Vegetation in Riparian Forests and Communities of Woodboring Cerambycid Beetles

Patrick Engelken
Deborah G. McCullough

INTRODUCTION

The emerald ash borer (EAB) (*Agrilus planipennis* Fairmaire) (Coleoptera: Buprestidae) invasion has resulted in the death of millions of ash (*Fraxinus* spp.) trees since its 2002 detection in southeastern Michigan and nearby Ontario. Previous studies assessed ash mortality and effects of EAB in urban and forested areas, but to date impacts of EAB in riparian forests have not been evaluated. These forests border rivers and streams, are often hydric, and experience periods of inundations. Riparian forest ecosystems are functionally linked to adjacent waterways. For example, riparian forests regulate transfers of energy into streams via inputs of leaf litter, provide stream structure through inputs of fallen branches and logs, and provide shade to ameliorate aquatic temperatures. Black ash (*Fraxinus nigra*) and green ash (*F. pennsylvanica*) are often abundant in riparian forests across Michigan and represent a substantial component of the riparian overstory. Impacts of EAB invasion, including mortality of overstory ash, could substantially influence terrestrial and aquatic conditions with potentially cascading secondary effects. We conducted three separate studies, described below, to assess ash mortality and effects of EAB in riparian forests.

Project 1. Legacy Effects of Emerald Ash Borer on Riparian Forest Vegetation and Structure

Methods

We identified three watersheds in southern Michigan that represented the general east-to-west temporal progression of the EAB invasion. Selected watersheds included the Clinton, Grand, and Kalamazoo River watersheds (fig. 1 in Engelken and McCullough 2020a). In each watershed, we identified a major canopy gap resulting from EAB-caused ash mortality along four first-order streams (12 sites total). In each site, we surveyed vegetation and other variables in the canopy gap and the surrounding, intact forest using a combination of fixed-radius plots and linear transects. Variables recorded included the amount of light (photosynthetically active radiation) available to vegetation in summer and winter; species and diameter at breast height (d.b.h.) of all standing live and dead trees (d.b.h. ≥10.2 cm); species and number of saplings (diameter 2.5–10 cm and height ≥0.5 m) and seedlings (diameter <2.5 cm and height ≤0.5 m); species and percentage of cover of shrubs and herbaceous plants; and species, diameter, length, and decay class of coarse woody debris (≥7.6-cm diameter). Variables were standardized per hectare for analysis. Comparisons between canopy gaps and

surrounding forests and among watersheds were performed using two-factor split plot analysis of variance (ANOVA). Nonmetric multidimensional scaling ordinations, permutational analysis of variance (PERMANOVA), and indicator species analysis (ISA) were performed to compare pre-EAB overstory with the current saplings and to compare composition of vegetation in canopy gaps and forests.

Results

Prior to EAB invasion, canopy gaps were dominated largely by green ash and black ash, but >85 percent of the ash basal area was killed by EAB across all watersheds. Currently, species richness and live basal area are lower in canopy gaps than in the surrounding forests (table 1 in Engleken and others 2020). Live overstory trees were scarce in canopy gaps and consisted primarily of American elm (*Ulmus americana*), maples (*Acer* spp.), and swamp white oak (*Quercus bicolor*). Ash trees were rare in forests surrounding canopy gaps. These forests comprised oaks (*Quercus* spp.), maples, and a mix of other hardwoods such as black cherry (*Prunus serotina*) and American beech (*Fagus grandifolia*). A lower percentage of dead ash trees remained standing in southeastern sites and, not surprisingly, volume of ash coarse woody debris was higher in these sites than the areas invaded more recently. Ash saplings were abundant in canopy gaps, reflecting the species composition of overstory trees prior to EAB invasion. Saplings in forested areas adjacent to gaps were dominated by red maple (*A. rubrum*), while northern red oak (*Q. rubra*), black cherry, sugar maple (*A. saccharum*), and red maple were common in overstories. Understory vegetation in canopy gaps was dominated by dense mats of sedges (*Carex* spp.). Tree seedlings were rare and often absent in canopy gaps, presumably as a result of these sedge mats.

Discussion

In the riparian forests we surveyed, the EAB invasion has resulted in the functional loss of mature green and black ash trees. Despite the almost complete lack of a mature ash cohort, consistently high sapling densities combined with reduced EAB densities could facilitate ash persistence in post-invasion areas. If EAB densities increase, however, recruitment of ash saplings into the overstory will be limited. Continued monitoring will be important to assess the future status and dynamics of ash and other species in post-EAB riparian forests.

Project 2. Species Diversity and Assemblages of Cerambycidae in the Aftermath of the Emerald Ash Borer (Coleoptera: Buptrestidae) Invasion in Riparian Forests of Southern Michigan

Methods

We conducted this project in the same field sites that were surveyed in Project 1. In each site, we deployed two Fluon®-coated cross-vane

panel traps. One trap was deployed at ground level at the edge of an EAB-caused canopy gap. The other trap was suspended in the canopy of a living hardwood tree, directly above the ground trap. Each trap was baited with a lure containing racemic 3-hydroxyhexan-2-one, an aggregation pheromone known to be broadly attractive to an array of species in several tribes of the subfamily Cerambycinae, along with a pouch of ultra-high-release ethanol. Traps were deployed from May into October of 2017 and 2018. Traps were checked at 2- to 3-week intervals to retrieve captured insects, which were stored in 70-percent ethanol until identification. Two-factor ANOVA was performed on capture and species richness data to make comparisons among the three watersheds and between canopy and ground traps. Nonmetric multidimensional scaling ordinations, permutational analysis of variance (PERMANOVA), and indicator species analysis (ISA) were performed on cerambycid capture data. Vegetation and coarse woody debris recorded in sites were overlaid on the final ordination to assess site-related features that were potentially correlated with changes in communities.

Results

We captured a total of 3,645 beetles representing 65 species and five subfamilies of cerambycids. Communities of cerambycids captured in southeast sites, with the longest history of EAB invasion, differed from those collected in south-central and southwest Michigan, which were similar. Results of ISA suggested these differences were largely due to three cerambycid species that were abundant in the southeast sites. Correlation of site-related variables and beetle captures indicated cerambycid species assemblages were associated most strongly with abundance and decay stage of coarse woody debris. During both years, >90 percent of cerambycid species were captured by mid-summer, but seasonal activity differed among and within tribes. Numbers of beetles captured by canopy and ground traps were similar, but species richness was higher in canopy traps than ground traps. Additionally, communities of cerambycids captured in canopy traps differed from those in ground traps.

Discussion

Results of this study suggest that influx of ash coarse woody debris following the EAB invasion can have temporally lagged, secondary effects on communities of native cerambycids. This has resulted in changes in distribution and potentially population-level changes of several species as ash trees break down and accumulate on the forest floor. Our results also indicate that for surveys to assess nonnative cerambycid presence or native cerambycid communities, deploying traps early in the growing season and including both canopy and ground traps will yield a wide array of species.

Project 3. Riparian Forest Conditions Along Three Northern Michigan Rivers Following Emerald Ash Borer Invasion

Methods

We selected three rivers in northwest Michigan, the Betsie, Platte, and Little Manistee Rivers (fig. 1 in Engelken and McCullough 2020b), for this project. All are important spawning rivers for Great Lakes salmon and trout, provide recreational opportunities, and have substantial stretches running through public land. We used time-lapsed aerial images to identify the onset and progression of canopy gaps likely resulting from EAB-caused ash mortality along the length of the rivers. Perimeters of each gap were outlined and then analyzed using ArcMap® to quantify frequency and size of canopy gaps along each river and to estimate the proportion of the riparian buffer along each river that has been lost as a result of the EAB invasion. We then surveyed a 3–5-km stretch of each river where multiple canopy gaps occurred. We used kayaks to access three canopy gaps and three areas of intact forest between gaps along each river and then established fixed-radius plots and linear transects within the sites. Variables recorded included species and d.b.h. of standing live and dead trees (d.b.h. ≥10.2 cm); species and number of recruits (d.b.h. 2.4–10.2 cm and height >2 m), saplings (diameter <2.4 cm and height 0.5–2 m), and seedlings (diameter <2.4 cm and height ≤0.5 m); species and percentage of cover of herbaceous plants; and species, diameter, length, and decay of coarse woody debris (≥7.6-cm diameter). Variables were standardized per hectare and two-factor ANOVA was used to compare canopy gaps and intact forests.

Results

Invasion by EAB has killed >95 percent of overstory ash trees along all three rivers. Density of canopy gaps resulting from EAB-caused ash mortality ranged from 3.6 to 7.1 canopy gaps/km. Ash distribution largely followed the rivers prior to EAB invasion. Canopy gaps caused by dead ash trees now comprise 13 to 21 percent of the area in the riparian forests within 100 m of the banks of all three rivers (table 3.1 in Engelken and McCullough 2020b). These gaps were originally dominated by a mixture of green and black ash, which comprised 46 to 71 percent of the total basal area prior to EAB invasion. Ash trees were rare in intact forests, comprising <10 percent of basal area. Overstory composition of forests surrounding canopy gaps varied among rivers but were generally dominated by maples mixed with bigtooth aspen (*Populus grandidentata*), swamp white oak, eastern white pine (*Pinus strobus*), or eastern hemlock (*Tsuga canadensis*). Advance regeneration was abundant in gaps, and green ash accounted for >40 percent of recruits and >60 percent of saplings along all rivers. Black ash regeneration, however, was rare or nonexistent. Similar to observations in southern Michigan, sedge mats dominated canopy gap understories and few tree seedlings occurred in gaps.

Discussion

Our results indicate that EAB-caused mortality has created substantial and frequent canopy gaps in riparian forests bordering the three rivers in northwestern Michigan, potentially threatening stability of riparian buffers and altering aquatic conditions. As in southern Michigan, green ash saplings and recruits are abundant in canopy gaps, but whether they will persist and eventually move into the overstory remains unknown. The absence of new seedlings in canopy gaps indicates that if saplings and recruits do not reach maturity, these canopy gaps may persist over time. The lack of black ash regeneration is particularly troubling. Continued monitoring to quantify long-term dynamics of tree species and effects of ash mortality on aquatic conditions of these and other affected rivers will be important.

For more information, contact: Patrick Engelken engelke2@msu.edu; Deborah G. McCullough, mccullo6@msu.edu.

LITERATURE CITED

Engelken, P.J.; Benbow, M.E.; McCullough, D.G. 2020. Legacy effects of emerald ash borer on riparian forest vegetation and structure. Forest Ecology and Management. 457: 117684. https://doi.org/10.1016/j.foreco.2019.117684.

Engelken, P.J.; McCullough, D.G. 2020a. Species diversity and assemblages of Cerambycidae in the aftermath of the emerald ash borer (Coleoptera: Buptrestidae) invasion in riparian forests of southern Michigan. Environmental Entomology. 49(2): 391–404. https://doi.org/10.1093/ee/nvaa013.

Engelken, P.J.; McCullough, D.G. 2020b. Riparian forest conditions along three northern Michigan rivers following emerald ash borer invasion. Canadian Journal of Forest Research. 50(8): 800–810. https://doi.org/10.1139/cjfr-2019-0387.

CHAPTER 10.

Vulnerability of Rocky Mountain Bristlecone Pine to Mountain Pine Beetle

Barbara Bentz
David Soderberg
Justin Runyon
Sharon Hood
Jim Vandygriff
Matt Hansen
Sky Stephens

INTRODUCTION

Conifers growing at alpine and subalpine habitats are disproportionately affected by climatic changes. Increasing temperatures are reducing suitable growing habitat and impacting regeneration patterns as snowpack timing is altered. In addition to these direct effects, tree survival at high elevations is indirectly being affected by recent shifts in thermal regimes favoring biotic disturbance agents including bark beetles. Development of strategies for conservation and protection of high-elevation conifer species therefore requires an understanding of their vulnerability to bark beetle-caused mortality. Many high-elevation pine species, for example, have become susceptible to mortality due to the mountain pine beetle (MPB) (*Dendroctonus ponderosae*, Coleoptera: Curculionidae, Scolytinae) as favorable thermal conditions for population success have increased in recent decades (Bentz and others 2014). The mountain pine beetle is a native bark beetle found across western North America and is among the most important tree mortality agents in pine forests. The majority of pine species that grow in the Western United States are known hosts, although some species appear to be less vulnerable to attack. Warming in recent years has increased MPB activity, including at high elevations where extensive mortality has occurred in whitebark pine (*Pinus albicaulis*), lodgepole pine (*P. contorta*), and limber pine (*P. flexilis*) (Cleaver and others 2015, Macfarlane and others 2013). The relative vulnerability of other high-elevation pine species to MPB, however, remains unclear. Also unclear is the role that evolved resinous defenses play in vulnerability of a particular pine species to MPB-caused mortality.

Pines have resinous secondary metabolite (SM) defenses, both constitutive and induced, that have evolved for protection against bark beetle attack, but they are metabolically expensive and divert resources from other processes including growth (Franceschi and others 2005). In general, constitutive defenses are considered reliable because they are always available. Induced defenses, in contrast, occur in response to an insect attack; therefore, costs are hypothesized to be only incurred as needed. Slow-growing and longer lived conifer species with high costs for tissue replacement are hypothesized to invest more in constitutive defenses because of their reliability, and investment in both constitutive and induced responses is considered redundant (Cipollini and others 2014). In a recent study, MPB attacks on the high-elevation Great Basin (GB) bristlecone pine (*P. longaeva*) were rare despite extensive mortality of adjacent limber pine. Similarly, in mixed stands of foxtail pine (*P. balfouriana*) and limber pine, attacks on foxtail pine were low despite high MPB-caused mortality of limber pine. In both species with rare or low preference by MPB, constitutive SM defense concentrations were up to eight times that of concentrations in co-occurring limber pine (Bentz and others 2017). These results suggest a level of protection from high constitutive SM concentrations, although induced responses have not been investigated in these species.

Great Basin bristlecone and foxtail pine are long-lived species, and together with Rocky Mountain (RM) bristlecone pine (*P. aristata*), they make up the bristlecone or foxtail pine group (Lanner 2007). Although MPB attacks have been reported in RM bristlecone (Klutsch and others 2011), the vulnerability and defense capacity of this species, relative to its long-lived cousins, remains unclear. Our objectives were to (1) quantify MPB-caused mortality within the past 10 years in stands where RM bristlecone and limber pines co-occur, (2) evaluate in the field if MPB is capable of successful brood production in RM bristlecone pine, and (3) quantify the timing and concentration of constitutive and induced SM defenses, and morphological defenses, in RM bristlecone and limber pine growing in the same stands across the range of RM bristlecone pine.

METHODS

Location of mixed RM bristlecone and limber pine stands were determined using several sources including the U.S. Department of Agriculture Forest Service, Forest Inventory and Analysis (FIA) Database (USDA Forest Service 2017a), Forest Service District and U.S. Department of the Interior National Park Service vegetation maps, and personal communication. Tree mortality surveys were conducted in 13 stands throughout the Colorado portion of the RM bristlecone pine range where MPB activity had been noted in Insect and Disease Surveys (USDA Forest Service 2017b) or FIA plots within the past 10 years (fig. 10.1). Sampling for constitutive and induced resin characteristics of the species was conducted at three sites in Colorado and two additional sites at the southern edge of the RM bristlecone pine distribution in Arizona and New Mexico (fig. 10.1). To quantify relative MPB preference for RM bristlecone pine and other co-occurring pines growing in the same stands, we used contiguous 405-m^2 fixed-radius circular plots extending linearly along a randomly chosen azimuth for as far as MPB-infested pine continued within the location. Live trees of all species were measured for diameter at breast height (d.b.h.; 7.5-cm minimum). Pines were examined for status (live, MPB-killed, or other mortality) and for signs of dwarf mistletoe (*Arceuthobium* spp.) and white pine blister rust caused by the nonnative pathogen *Cronartium ribicola*. Mountain pine beetle-killed trees were confirmed by the presence of egg galleries typical for MPB. For pines attacked by MPB, year of attack can be estimated for up to 3 years post-attack using characters of foliage color and needle retention. Basal area (BA) of live and dead trees, by species, was calculated (see Bentz and others 2021).

Defense measurements were taken on 12 RM bristlecone and 12 limber pines at each of 5 sites (see Soderberg and others, in preparation). At one site, co-occurring lodgepole pines were also sampled. Constitutive SM defenses were measured by taking a 1.8- x 6-mm phloem plug at d.b.h. from six equidistant locations around the circumference of the bole of each sampled tree. The removed tissue was placed in a vial, sealed, immediately placed on dry ice for transport, and stored at -40 °C until processing.

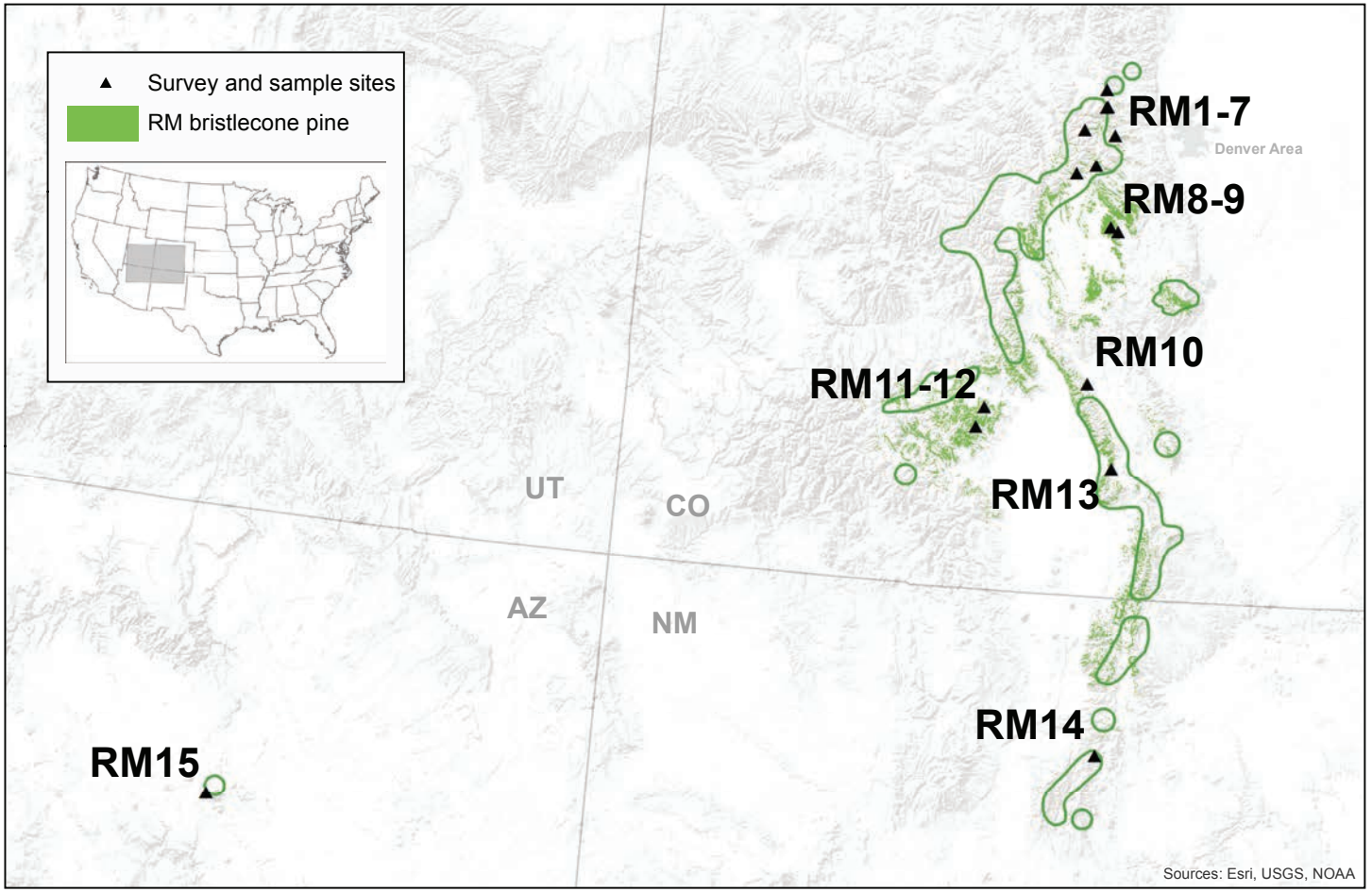

Figure 10.1—Location of Rocky Mountain (RM) bristlecone pine mortality survey (RM 1–13) and defense sample (RM 5, 9, 13, 14, 15) sites. Mortality surveys were conducted in 2017 and defense sampling in 2018 and 2019. Rocky Mountain bristlecone pine distribution based on Little (1971) and Ellenwood and others (2015).

To measure an induced response, the 12 constitutive sample trees were randomly chosen to receive either a mechanical wound (n = 6) or a wound plus fungal inoculant to simulate an MPB attack (n = 6). For the latter, we used a fungal inoculation of *Grosmannia clavigera*, a fungal symbiont of MPB that was placed into the 1.8- x 6-mm wound created by the constitutive sample. Inoculating trees with this MPB fungal associate has been shown to produce an induced response that differs from mechanical wounding alone (e.g., Keefover-Ring and others 2016). The timing, concentration, and composition of induced responses on each simulated attack and mechanical wounding tree were measured 1, 4, and 30 days after inoculation using a Trephor microtome sampling tool. Induced samples were transported and stored as indicated above for constitutive samples. Extracted phloem from constitutive, simulated attack and mechanical wounding sampling was analyzed using a coupled gas chromatography-mass spectrometry (GC-MS), and quantifications were made relative to an internal standard. Monoterpenoids, sesquiterpenoids, benzenoids, and a non-isoprenoid hydrocarbon were quantified and identified by comparison of chromatographic retention times and mass spectra with those of commercially available standards (Soderberg and others, in preparation). Only total SMs (sum of all compounds) are included in this report. A phloem sample and two cores per tree recording the preceding 10 years of growth were collected to analyze phloem and xylem resin ducts, and basal area increment (10-year BAI).

RESULTS AND DISCUSSION

Stands in the mortality surveys contained a mix of pine species, including RM bristlecone, limber, lodgepole, and ponderosa (*P. ponderosa*) pines, with RM bristlecone pine comprising a range of 4–92 percent of all pines at each site (table 10.1). No signs of white pine blister rust or dwarf mistletoe were observed on RM bristlecone pine within our plots. Based on galleries beneath the bark of dead trees, MPB was confirmed as the causal agent of death in all pine species surveyed. Emergence holes leading to pupal chambers on attacked trees also confirmed that MPB reproduced

Table 10.1—Stand conditions and metrics of mountain pine beetle (MPB)-killed pines at mortality survey sites (non-pines were a minor component)

Site	Species	Total pine	MPB-killed trees	Basal area (live, pre-outbreak)	Basal area (MPB-killed)	d.b.h. (live, pre-outbreak)	d.b.h. (MPB-killed)
		percent	*number*	*m^2/ha*	*m^2/ ha*	*cm*	*cm*
RM1	*P. aristata*	4.0	0	1.25	0.0	18.9	—
	P. flexilis	96.0	31	28.68	7.54	18.8	21.7
RM2	*P. aristata*	92.4	58	52.68	12.65	31.9	33.8
	P. flexilis	7.6	0	1.48	0.0	18.9	—
RM3	*P. aristata*	48.3	21	12.45	4.62	22.5	32.3
	P. flexilis	51.7	62	34.45	24.79	35.9	45.3
RM4	*P. aristata*	19.4	14	6.56	4.13	26.7	28.6
	P. contorta	80.6	17	15.09	3.54	18.3	24.2
RM5	*P. aristata*	35.7	1	6.01	0.37	22.5	28.7
	P. contorta	9.8	0	3.45	0.0	34.0	—
	P. flexilis	54.5	22	20.23	9.05	34.8	39.3

continued to next page

Table 10.1 (*continued*)—Stand conditions and metrics of mountain pine beetle (MPB)-killed pines at mortality survey sites (non-pines were a minor component)

Site	Species	Total pine	MPB-killed trees	Basal area (live, pre-outbreak)	Basal area (MPB-killed)	d.b.h. (live, pre-outbreak)	d.b.h. (MPB-killed)
		percent	*number*	*m^2/ha*	*m^2/ ha*	*cm*	*cm*
RM6	*P. aristata*	42.7	0	11.23	0.0	27.0	—
	P. contorta	57.3	5	14.51	1.90	25.7	32.4
RM7	*P. aristata*	81.9	37	21.43	11.67	20.9	27.9
	P. contorta	18.1	11	11.38	5.86	33.0	35.4
RM8	*P. aristata*	72.4	2	19.05	0.94	21.1	25.0
	P. flexilis	27.6	0	9.84	0.0	23.9	—
RM9	*P. aristata*	70.7	12	10.35	2.65	23.2	25.5
	P. flexilis	24.0	1	4.99	1.07	25.8	57.2
	P. ponderosa	5.3	0	1.35	0.0	31.8	—
RM10	*P. aristata*	10.5	0	1.58	0.0	20.4	—
	P. contorta	32.3	5	5.37	1.04	21.8	30.1
	P. flexilis	50.4	26	11.82	5.96	25.7	30.7
	P. ponderosa	6.8	2	2.19	1.41	28.8	56.0
RM11	*P. aristata*	88.9	10	10.16	2.34	19.6	34.4
	P. contorta	2.2	0	0.81	0.0	30.1	—
	P. ponderosa	8.9	3	2.55	1.16	31.7	46.5
RM12	*P. aristata*	90.9	2	10.50	1.62	24.0	33.5
	P. contorta	6.1	0	0.32	0.0	17.9	—
	P. ponderosa	3.0	0	0.38	0.0	27.9	—
RM13	*P. aristata*	59.9	24	12.97	3.60	22.8	32.5
	P. flexilis	36.9	10	17.74	2.10	31.6	39.1
	P. ponderosa	3.2	3	1.79	0.94	35.1	47.2
	P. flexilis	54.5	22	20.23	9.05	34.8	39.3

d.b.h. = diameter at breast height

— = no trees killed

successfully in RM bristlecone pine. We found that the proportion of each MPB-killed pine species at a site was correlated with host species availability. The proportion of a pine species killed by MPB over the 10-year period was best predicted by the proportion of BA of that species in the stand pre-outbreak ($F_{1,19} = 55.41$, $p < 0.0001$) (table 10.1, fig. 10.2). These results are similar to attack patterns found in mixed stands of hosts with known vulnerability to MPB including whitebark and lodgepole pine stands in Wyoming (Bentz and others 2015) and mixed lodgepole and ponderosa pine stands in Colorado (West and others 2014). Our results, however, are in contrast to surveys where the closely related GB bristlecone and foxtail pines grew in mixed stands with limber pine. Mountain pine beetle attacks were extensive on limber pine, low on foxtail pine, and rare on GB bristlecone pine regardless of the proportions of each species in the area (Bentz and others 2017). Rocky Mountain bristlecone pine appears to be more vulnerable to MPB attack than its close bristlecone relatives (Bentz and others 2021).

Across all sites, RM bristlecone pine was slower growing over the most recent 10 years than both limber and lodgepole pine. Rocky Mountain bristlecone also had greater concentrations of constitutive (day 0) SMs than both limber and lodgepole pines (fig. 10.3A). Similarly, the closely related and slower growing GB bristlecone and foxtail pines were also found to have greater constitutive SMs than co-occurring limber pine (Bentz and others 2017). Although simulated attack

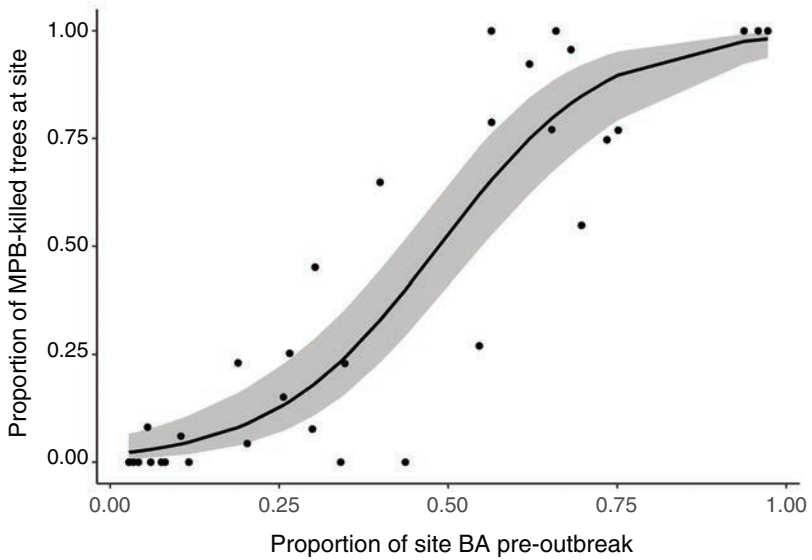

Figure 10.2—The proportion of a mountain pine beetle (MPB)-killed pine species at a site over a 10-year period (2006 to 2016) was best predicted by the proportion of basal area (BA) (m^2/ha) of that species in the stand pre-outbreak. Shown is the linear mixed model (SAS version 9.4, GLIMMIX) regression prediction (solid line) and the 95-percent confidence intervals (shaded area) for all species combined (Bentz and others 2021).

trees of RM bristlecone, limber, and lodgepole pine showed an induced increase in total SM compounds by day 4, the response was not different than mechanical wounding trees on that sample date. By day 30, however, the total response in simulated attack trees was >10x greater than day 0 (fig. 10.3D), and also greater than the day 30 mechanical wounding tree responses for all species and sites (Soderberg and others, in preparation). These results suggest that response to a simulated attack did not occur rapidly (i.e., within 4 days). Although a large number of MPB attacks can occur within a few days (Bentz and others 1996), attacks can also be sustained over a month or longer (Bentz and others 2014). Our results suggest trees invest in induced defenses over a sustained period rather than a short period immediately following attack. In addition to having a greater level of constitutive SMs, RM bristlecone pine also had a greater overall induced response at day 30 than the response in limber pine. At the one site where RM bristlecone pine and lodgepole pine were sampled, however, lodgepole pine had a greater induced response on day 30. Our results suggest that investment in constitutive and induced defenses are not mutually exclusive, and in RM bristlecone pine, greater constitutive defenses were correlated with greater induced defenses (Soderberg and others, in preparation). Pines killed by MPB have been shown to invest less in resin duct-related defenses compared to trees that survived MPB attack (Hood and others 2015). In addition to xylem resin ducts, our ongoing analyses also include phloem resin ducts of the three species. Resin duct sampling included constitutive (day 0), 30 days, and 1 year post-induction.

Although RM bristlecone had much greater constitutive and induced defenses than limber pine, trees of both species were attacked, and attacks were most common on the species with the greatest frequency in the stand pre-outbreak. In addition to overall concentrations, composition of SM defenses may also influence

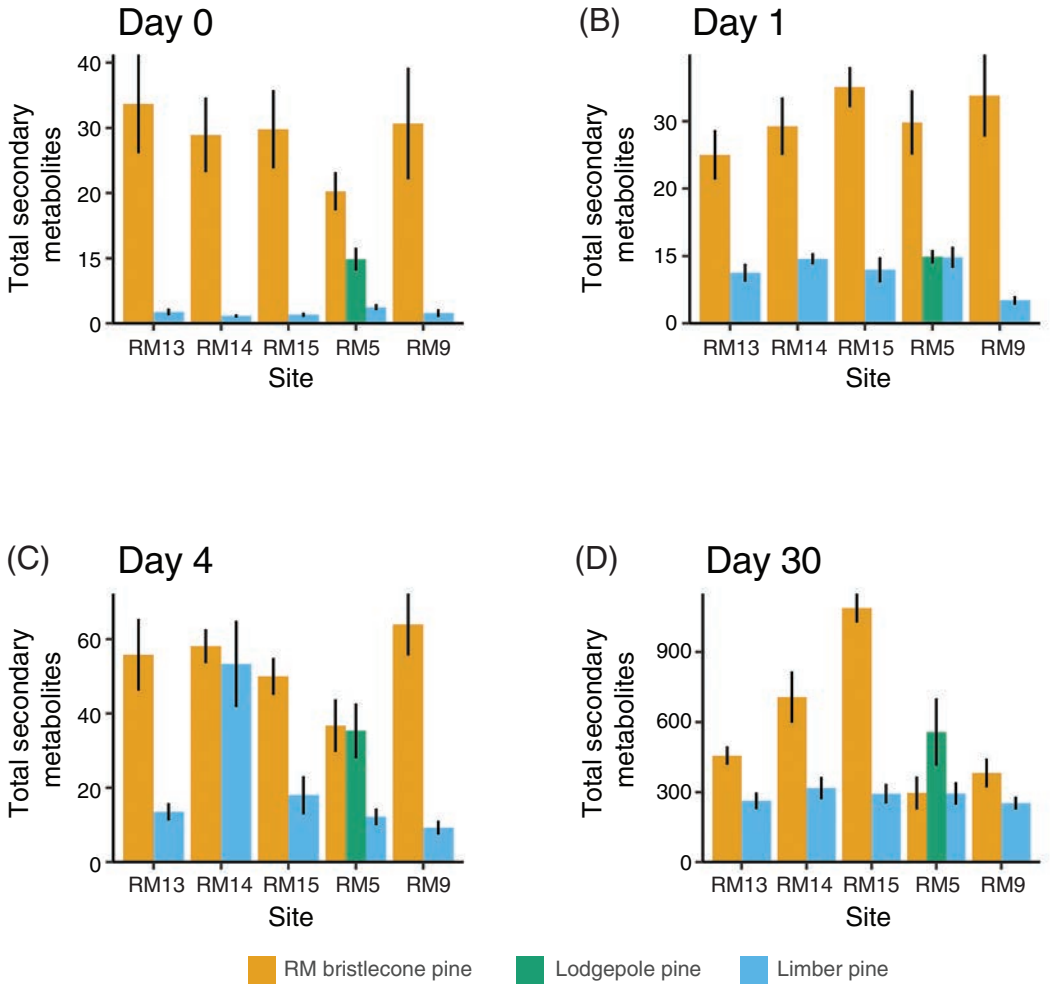

Figure 10.3—Total secondary metabolites (mg compound/g dry weight) in three pine species at five sites across the range of Rocky Mountain (RM) bristlecone pine (see fig. 10.1). Samples were collected at (A) day 0 (constitutive) and post-inoculation with a mountain pine beetle fungal associate (i.e., simulated attack) on (B) day 1, (C) day 4, and (D) day 30 (Soderberg and others, in preparation). Note the different y-axis scales among the days and that lodgepole pine was sampled at a single site.

MPB tree attack. Great Basin bristlecone and foxtail pine, which had rare to low attacks, contained >85-percent α-Pinene (- and + enantiomers combined) (Bentz and others 2017), and high levels of this terpenoid are known to be repellent to MPB as it can oxidize to verbenone (Lindgren and Miller 2002). In this study, RM bristlecone and limber pines had high proportions of δ-3-Carene, which can have both negative and positive roles in the attack process and survival of MPB and its associates (Boone and others 2013, Miller and Borden 2000).

Our results provide baseline data for building a foundation to better understand MPB responses to high-elevation pines and evolved tree defenses. More information is needed relating defense metrics of individual trees to successful versus unsuccessful attacks, in addition to knowledge of individual and ratios of compounds that influence MPB attack and reproductive success.

For more information, contact: Barbara Bentz, barbara.bentz@usda.gov.

LITERATURE CITED

Bentz, B.J.; Boone, C.; Raffa, K.F. 2015. Tree response and mountain pine beetle attack preference, reproduction and emergence timing in mixed whitebark and lodgepole pine stands. Agricultural and Forest Entomology. 17: 421–432. https://doi.org/10.1111/afe.12124.

Bentz, B.J.; Hansen, E.M.; Vandygriff, J.C. [and others]. 2021. Rocky Mountain bristlecone pine (*Pinus aristata*) is a confirmed host to mountain pine beetle (*Dendroctonus ponderosae*). Western North American Naturalist. 81(1): 19–26. https://doi.org/10.3398/064.081.0102.

Bentz, B.J.; Hood, S.A.; Hansen, E.M. [and others]. 2017. Defense traits in the long-lived Great Basin bristlecone pine and resistance to the native herbivore mountain pine beetle. New Phytologist. 213: 611–624. https://doi.org/10.1111/nph.14191.

Bentz, B.J.; Powell, J.A.; Logan, J.A. 1996. Localized spatial and temporal attack dynamics of the mountain pine beetle. Res. Pap. INT-494. Ogden, UT: U.S. Department of Agriculture Forest Service, Intermountain Research Station. 8 p. https://doi.org/10.5962/bhl.title.68955.

Bentz, B.J.; Vandygriff, J.C; Jensen, C. [and others]. 2014. Mountain pine beetle voltinism and life history characteristics across latitudinal and elevational gradients in the Western United States. Forest Science. 60: 434–449. https://doi.org/10.5849/forsci.13-056.

Boone, C.K.; Keefover-Ring, K.; Mapes, A.C. [and others]. 2013. Bacteria associated with a tree-killing insect reduce concentrations of plant defense compounds. Journal of Chemical Ecology. 39: 1003–1006. https://doi.org/10.1007/s10886-013-0313-0.

Cipollini, D.; Walters, D.; Voelkel, C. 2014. Costs of resistance in plants: from theory to evidence. Annual Plant Reviews. 47: 263–307.

Cleaver, C.M.; Jacobi, W.R.; Burns, K.S.; Means, R.E. 2015. Limber pine in the central and southern Rocky Mountains: stand conditions and interactions with blister rust, mistletoe, and bark beetles. Forest Ecology and Management. 358: 139–153. https://doi.org/10.1016/j.foreco.2015.09.010.

Ellenwood, J.R.; Krist F.J.; Romero S.A. 2015. National individual tree species atlas. FHTET-15-01. Fort Collins, CO: U.S. Department of Agriculture Forest Service, Forest Health Protection Enterprise Team. 320 p.

Franceschi, V.R.; Krokene, P.; Christiansen, E.; Krekling, T. 2005. Anatomical and chemical defenses of conifer bark against bark beetles and other pests. New Phytologist. 167: 353–376. https://doi.org/10.1111/j.1469-8137.2005.01436.x.

Hood, S.; Sala, A.; Heyerdahl, E.K.; Boutin, M. 2015. Low-severity fire increases tree defense against bark beetle attacks. Ecology. 96: 1846–1855. https://doi.org/10.1890/14-0487.1.

Keefover-Ring, K.; Trowbridge, A.; Mason, C.J.; Raffa, K.F. 2016. Rapid induction of multiple terpenoid groups by ponderosa pine in response to bark beetle-associated fungi. Journal of Chemical Ecology. 42: 1–12. https://doi.org/10.1007/s10886-015-0659-6.

Klutsch, J.G.; Goodrich, B.A.; Schoettle, A.W. 2011. Limber pine forests on the leading edge of white pine blister rust distribution in northern Colorado. In: Keane, R.E.; Tomback, D.F.; Murray, M.P.; Smith, C.M., eds. Proc. RMRS-P-63. The future of high-elevation, five-needle white pines in western North America: Proceedings of the high five symposium. Fort Collins, CO: U.S. Department of Agriculture Forest Service, Rocky Mountain Research Station: 222–225.

Lanner, R.M. 2007. The bristlecone book: a natural history of the world's oldest trees. Missoula, MT: Mountain Press Publishing Company. 117 p.

Lindgren, B.S.; Miller, D.R. 2002. Effect of verbenone on five species of bark beetles (Coleoptera: Scolytidae) in lodgepole pine forests. Environmental Entomology. 31: 759–765. https://doi.org/10.1603/0046-225X-31.5.759.

Little, E. 1971. Atlas of United States trees. Vol. 1. Conifers and important hardwoods. Misc. Publ. 1146. Washington, DC: U.S. Department of Agriculture Forest Service. 9 p. plus maps.

Macfarlane, W.W.; Logan, J.A.; Kern, W.R. 2013. An innovative aerial assessment of Greater Yellowstone Ecosystem mountain pine beetle-caused whitebark pine mortality. Ecological Applications. 23: 421–437. https://doi.org/10.1890/11-1982.1.

Miller, D.R.; Borden, J.H. 2000. Dose-dependent and species-specific responses of pine bark beetles (Coleoptera: Scolytidae) to monoterpenes in association with pheromones. The Canadian Entomologist. 132: 183–195.

Soderberg, D.; Bentz, B.J.; Runyon, J. [and others]. Defense metrics of Rocky Mountain bristlecone pine and co-occurring pines. In preparation.

U.S. Department of Agriculture (USDA) Forest Service. 2017a. Forest Inventory and Analysis Database. https://www.fia.fs.fed.us/tools-data/. [Date accessed: June 2017].

U.S. Department of Agriculture (USDA) Forest Service. 2017b. 1997–2016 National Insect and Disease Detection Surveys. https://www.fs.fed.us/foresthealth/applied-sciences/mapping-reporting/detection-surveys.shtml. [Date accessed: June 2017].

West, D.R.; Briggs, J.S.; Jacobi, W.R.; Negrón, J.F. 2014. Mountain pine beetle-caused mortality over eight years in two pine hosts in mixed-conifer stands of the southern Rocky Mountains. Forest Ecology and Management. 334: 321–330. https://doi.org/10.1016/j.foreco.2014.09.012.

Chapter 11.

Tree Mortality and Fuel Changes due to Extreme Drought and Concurrent Bark Beetle Outbreaks in California

Sharon M. Hood
Charlotte C. Reed
Daniel R. Cluck
Beverly Bulaon
Stacy Hishinuma
Andrea Hefty
Sheri Smith

INTRODUCTION

Tree mortality associated with drought and concurrent bark beetle outbreaks in the Western United States is expected to increase under warmer and drier climate regimes (Kolb and others 2016). The combined impacts of drought and insect outbreaks on tree mortality have important implications for predicting forest dynamics under climate change, yet forecasting tree mortality is one of the most uncertain processes in dynamic vegetation models. To improve predictions of how climate change will alter forest dynamics, models must be informed by a better understanding of how tree-level factors influence probability of mortality when multiple disturbance agents co-occur. Some tree-level early warning signals for drought-related mortality have been identified, but few patterns have emerged across tree species, and most studies do not consider drought interactions with insects (Cailleret and others 2019, Camarero and others 2015). Similarly, despite recent advances in the understanding of physiological mechanisms underlying drought-related tree mortality (Adams and others 2017, Sevanto and others 2014), much remains unclear. This is especially true when insects are involved (Anderegg and others 2015), as they can affect tree carbon and water balance, both important links to drought-related tree mortality (McDowell and others 2008). A handful of studies have examined why some trees die and others survive in the face of drought combined with insect outbreaks (Csank and others 2016, McDowell and others 2010), but it is still unclear whether generalizable tree-level mortality risk factors or early warning signals exist in the face of these interacting disturbances.

Tree die-off events can cause rapid, drastic changes to forest structure and fuel loads, with cascading effects on potential fire behavior and severity (Hicke and others 2012). Dead trees in the red stage, when needles remain in the crowns, alter canopy fuel availability and may have higher ignition potential and burn more intensely. However, the red stage is transient, and needles fall to the ground within a few years of tree death. Surface fuel loading may then increase as foliage, branches, and trees decompose and fall to the ground. Previous research on changes to fuels in beetle-impacted forests suggests responses may vary by forest type, with studies in the Northern Rockies showing little change to surface fuel loads (Donato and others 2013, Stalling and others 2017) and others from the Southeastern and Southwestern United States reporting increased surface fuel loading and more rapid snag fall (Hoffman and others 2012, Xie and others 2020). Likewise, research into how high levels of tree mortality influence fire behavior and fire severity is also mixed and dependent on fire weather, outbreak conditions, and time since attack (Hood 2019, Sieg and others 2017).

The 2012–2016 drought and associated bark beetle outbreaks in California resulted in extensive tree mortality and provided a unique opportunity to examine questions of why some trees die while others survive these co-occurring

disturbances and to increase understanding of how subsequent bark beetle-caused tree mortality alters fuel profiles and forest flammability over time. Our study objectives were to: (1) identify factors relating to conifer tree mortality and monitor changes in vegetation after mortality and (2) determine temporal changes in fuel loading and hazard due to bark beetle- and drought-associated tree mortality.

METHODS

Sampling areas were established in 2016 in two separate geographical areas affected by the 2012–2016 California drought and concurrent beetle outbreaks. We installed plots in areas of low and high recent tree mortality on the Los Padres National Forest (LPNF; 27 plots) in singleleaf pinyon (*Pinus monophylla* Torr. & Frém) woodlands and on the Sierra National Forest (SNF; 49 plots) in areas dominated by ponderosa pine (*P. ponderosa* Lawson & C. Lawson), white fir (*Abies concolor* [Gord. & Glend.] Lindl. ex Hildebr.), and incense cedar (*Calocedrus decurrens* [Torr.] Florin). Plots in the SNF sampling area utilized an existing plot network within areas of specific forest type and mortality level, excluding areas of recent forest management (Pile and others 2019). We selected a subset of 50 plots in the network in 2016 based on mortality level determined from 2015 Insect and Disease Survey (IDS) data and species composition. We selected approximately half of the plots based on low mortality (<5 percent), and the other half based on relatively high mortality (>40 percent). Plots in the LPNF sampling area were selected based on singleleaf pinyon presence and mortality levels similarly determined from IDS data. Individual plot selection was random within areas of high and low mortality with singleleaf pinyon dominance. In California, singleleaf pinyon is a primary host to pinyon ips (*Ips confusus* LeConte); ponderosa pine is the primary host to western pine beetle (*Dendroctonus brevicomis* LeConte); and white fir is the primary host to fir engraver (*Scolytus ventralis* LeConte) (Fettig 2016). Cedar bark beetles (*Phloeosinus* spp.) are secondary mortality agents on incense cedar (Fettig 2016).

We installed 0.04-ha macroplots in 2016 and monitored changes in vegetation and fuels annually through 2019. At each macroplot, we recorded tree species, diameter at breast height (1.37 m aboveground, d.b.h.; groundline diameter [GLD] for singleleaf pinyon), tree height, crown base height, and status of all trees ≥12.7-cm d.b.h. Mortality agent was assessed for dead trees (i.e., no green needles remaining) based on presence and pattern of insect-specific galleries. We estimated the percentage of faded, dead needles remaining in the crown each year for all dead trees. We tallied saplings (≥1.37 m and <10-cm d.b.h.) by species, diameter class, and status and seedlings (<1.37 m) by species, height class, and status on a nested 0.01-ha microplot inside the macroplot. We collected two 4.5-mm cores near groundline on two living and two dead trees for each available species at each plot to assess tree growth patterns and responses to drought. We estimated fine fuel (1–100 hour), shrub, and herbaceous loading using the Photoload method (Keane and Dickinson 2007)

at eight 1-m^2 quadrats within the macroplot. We measured litter and duff depth at one point in each quadrat. Coarse fuel loading (1,000 hour) and decay classes were estimated by measuring the small and large end diameter and length of each log ≥7.6 cm on the macroplot.

All data were entered into FFI (FEAT/FIREMON Integrated) (Lutes and others 2009) for surface fuel and stand density calculations. We assessed all tree species for needle retention and snag fall but only singleleaf pinyon, ponderosa pine, white fir, and incense cedar for the tree ring-based analyses of tree mortality due to limited sample sizes (<14 cores per species) in the other tree species. For growth analyses and chronology building, cores were sanded and crossdated, and rings were measured to develop species-specific chronologies using standard dendrochronological techniques (Stokes and Smiley 1996). We selected a subset of six live and six dead trees per species for stable carbon isotope analysis based on tree dominance or codominance within the canopy. A subset of 10 live and 10 dead trees each for singleleaf pinyon and ponderosa pine was additionally randomly selected from the group of successfully dated trees to assess resin ducts (see Reed and Hood [2021] for full tree ring methods).

RESULTS

Tree Mortality and Risk Factors

Over the course of sampling (2016–2019), tree mortality remained fairly steady within LPNF plots (from 27 percent in 2016 to 30 percent in 2019) but increased within SNF plots (from 43 percent to 54 percent), particularly for ponderosa pine (from 78 percent to 92 percent). At the end of the study, mean plot-level tree mortality for individual species ranged from 30 percent for singleleaf pinyon to 91 percent for ponderosa pine but varied considerably by low versus high mortality level. Mortality attributed to host-specific beetles was high for singleleaf pinyon (97 percent; pinyon ips), ponderosa pine (93 percent; western pine beetle), and white fir (91 percent; fir engraver), and all cored trees had evidence of successful attack by primary bark beetles. Mortality agents for incense cedar were unknown or attributed to suppression and drought.

Differences in radial growth between surviving and dying trees were apparent only for ponderosa pine and incense cedar. Ponderosa pine that survived tended to have lower basal area increment (BAI) than trees that died until around the late 1980s–early 1990s, a time period corresponding to a multiyear regional drought and bark beetle outbreaks, at which point growth differences between dying and surviving trees decreased. In contrast, BAI of incense cedar that survived tended to be higher than for trees that died throughout the study period, and particularly in recent decades. Across species, differences in carbon isotope discrimination ($\Delta^{13}C$) between live and dead trees were inconsistent. Ponderosa pine that survived had higher $\Delta^{13}C$ throughout most of the study period than trees that died. The other three species showed weak or inconsistent differences in $\Delta^{13}C$ between live and dead trees. Resin duct

analysis of pines showed that in the 5 years leading up to the 2012–2016 drought, some differences emerged. Surviving ponderosa pines had higher relative duct area and weakly greater duct density. Singleleaf pinyon that survived had a greater duct production (i.e., number of ducts) and weakly higher total duct area. Full results of tree mortality and risk factors are reported in Reed and Hood (2021).

Needle Retention

During the first year of sampling in 2016, there were 26 white fir, 21 sugar pine, 12 singleleaf pinyon, and 102 ponderosa pine that had recently died with high needle retention for which we could track needle loss annually. Needle loss was rapid and followed a similar pattern for all species (fig. 11.1). In the second year, 28 to 43 percent of needles remained, and by year 4, all trees had virtually no needles left.

Snag Longevity

Of the 1,402 trees (including nine species) recorded on the plots, we estimated 536 (38 percent) died from the 2012–2016 drought and successful beetle attacks. By the last year of sampling in 2019, 41 percent of the recently dead trees had broken, and 20 percent of these had broken below 1.37 m. Snag fall varied by species, with pines (all species) falling most quickly (table 11.1).

Fuel Loads

Fine woody surface fuel loads (1–100-hour fuel components) were generally low for both the LPNF and SNF sites (table 11.2). On the LPNF, areas of high tree mortality increased in fine woody fuel more than the low tree mortality plots. On the SNF, there was not as clear of a pattern, with some fuel components increasing and others decreasing. The largest change occurred in the 1,000-hour fuels in the areas of high mortality. In just 4 years, 1,000-hour fuels in the high-mortality areas quadrupled from 0.38 kg m^{-2} to 1.50 kg m^{-2} on the LPNF and more than doubled on the SNF from 3.05 kg m^{-2} to 7.55 kg m^{-2}. Fuel loads of 1,000-hour logs

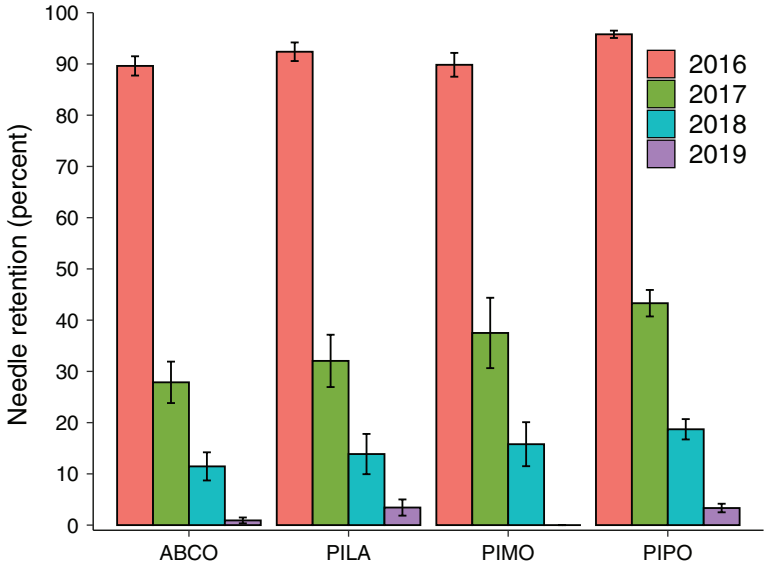

Figure 11.1—Needle retention (percent) of recently killed trees over time by species. ABCO = Abies concolor *(white fir); PILA* = Pinus lambertiana *(sugar pine); PIMO* = Pinus monophyla *(singleleaf pinyon pine); PIPO* = Pinus ponderosa *(ponderosa pine).*

Table 11.1—Number and percentage of new snags created during the drought and bark beetle outbreaks by species that were broken by end of the sampling in 2019

Snag condition		White fir n = 91	Red fir n = 26	Incense cedar n = 55	Lodgepole pine n = 13	Jeffrey pine n = 2	Sugar pine n = 48	Singleleaf pinyon n = 120	Ponderosa pine n = 177	Black oak n = 4	Total 536
Broken: any height	n	15	5	20	5	0	16	45	114	0	220
	%	16	19	36	38	0	33	38	64	0	41
Broken: below 1.37 m	n	2	0	12	4	0	9	31	47	0	105
	%	2	0	22	31	0	19	26	27	0	20

Table 11.2—Mortality and fuel loads on the Los Padres and Sierra National Forests by low- (<5 percent) and high- (>40 percent) mortality plots

	Low-mortality plots						High-mortality plots					
	2016		2019		Difference		2016		2019		Difference	
	Mean	SE	Mean	SE	Mean	SE	Mean	SE	Mean	SE	Mean	SE
Los Padres National Forest												
Mortality (%)	8	3	13	5	5	4	61	5	62	4	1	1
1-hour (kg m^{-2})	0.13	0.02	0.14	0.02	0.00	0.02	0.09	0.02	0.13	0.02	0.04	0.01
10-hour (kg m^{-2})	0.18	0.05	0.15	0.03	-0.03	0.04	0.12	0.04	0.17	0.04	0.05	0.02
100-hour (kg m^{-2})	0.06	0.03	0.08	0.03	0.02	0.01	0.02	0.00	0.10	0.02	0.08	0.02
1,000-hour (kg m^{-2})	0.06	0.01	0.10	0.03	0.04	0.03	0.38	0.27	1.50	0.44	1.12	0.28
Sierra National Forest												
Mortality (%)	21	3	29	3	7	2	66	4	76	3	10	2
1-hour (kg m^{-2})	0.09	0.02	0.10	0.02	0.01	0.01	0.06	0.01	0.09	0.01	0.02	0.01
10-hour (kg m^{-2})	0.26	0.06	0.15	0.02	-0.11	0.05	0.16	0.03	0.17	0.02	0.01	0.03
100-hour (kg m^{-2})	0.34	0.09	0.13	0.03	-0.21	0.09	0.34	0.10	0.20	0.04	-0.14	0.10
1,000-hour (kg m^{-2})	2.65	0.62	3.43	0.64	0.78	0.24	3.05	0.62	7.55	0.95	4.51	0.89

SE = standard error

increased positively with tree mortality level (fig. 11.2). More detailed surface and canopy fuels and fire hazard analyses are ongoing.

DISCUSSION AND CONCLUSIONS

The predicted increase in the intensity and/or length of droughts, combined with changes in bark beetle dynamics associated with climate change (Kolb and others 2016), requires a better understanding of how severe disturbance events influence mortality at the tree level if we are to effectively predict future forest mortality. Risk factors associated with tree-level mortality differ among tree species, and generalizable patterns become less clear when bark beetle outbreaks occur in concert with a particularly long, hot drought, likely a reflection of unique strategies for dealing with these disturbances. For ponderosa pine, both long-term differences in tree physiology and shorter term beetle-related selection and variability in defenses influence susceptibility to drought and beetle attacks. For singleleaf pinyon and white fir, however, long-term variability between trees that survived and those that died is less clear, and beetle dynamics may play a more prominent role in mortality patterns. Incense cedar, in contrast, for which we see limited evidence of beetle-related mortality, appears to be primarily influenced by long-term differences in growth rate and stand dominance, which likely impact resource availability and susceptibility to drought. It is also possible that cedar bark beetles may have contributed to incense cedar death (Stephenson and others 2019). Models that aim to predict tree-level mortality under future climate scenarios will need to account for extreme drought events and may need to consider multiple species-specific risk factors to more accurately predict tree death.

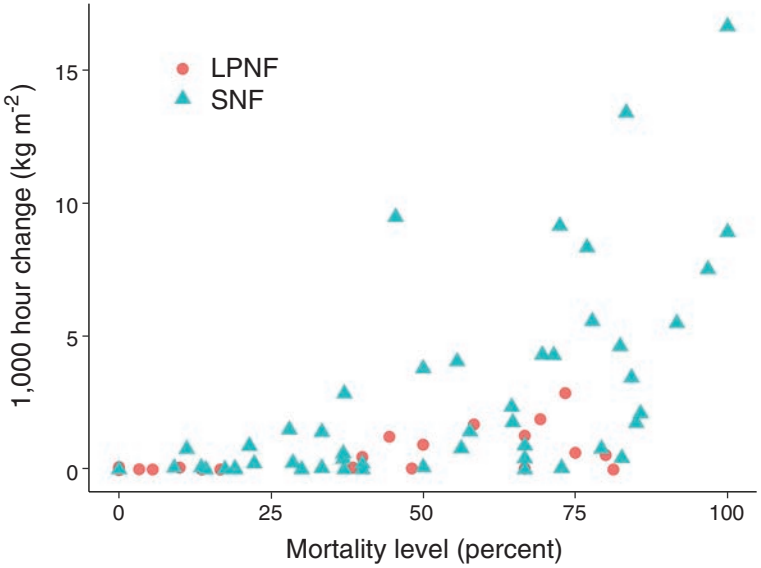

Figure 11.2—Change in 1,000-hr fuel loads from 2016 to 2019 by overstory (≥12.7-cm d.b.h.) tree mortality level on the Los Padres National Forest (LPNF) and Sierra National Forest (SNF).

Failure of newly dead trees was high, especially for pine species and incense cedar, considering we only monitored trees for 4 years from 2016 to 2019. Our results are conservative, as our sampling does not include trees that died in the 2012–2016 drought but that fell before 2016. Landram and others (2002) conducted a large study of snag demography in California over 9 years. While our monitoring period

was much shorter and sample sizes lower than theirs, our dead ponderosa pine annual fall rates are consistent with that study at an annual 6.5 percent versus 6.9 percent. However, our fall rates are higher for lodgepole pine (7.8 versus 3.8) and incense cedar (4.3 versus 2.5) and lower for white fir (0.5 versus 3.7) than what Landram and others (2002) reported. The high snag fall raises concerns for people working, including fire fighters, and recreating in areas of high tree mortality.

The timing and degree of change to fuel profiles from bark beetle outbreaks varies greatly by forest type, with implications for subsequent wildfire behavior and severity (Hicke and others 2012, Jenkins and others 2012). Falling snags increased 1,000-hour fuel loading in the areas of high mortality, whereas we found fewer changes in fine woody surface fuels despite heavy needle loss. Given that trees dropped their needles within about 3 years of death and the high snag fall rates, we anticipate that any increase to potential crown fire behavior would be short-lived as canopy fuel loads will continue to decrease over time, but additional analysis is needed. High levels of tree mortality influence other aspects of subsequent wildland fire besides potential fire behavior, such as spotting potential, fire severity, fire suppression tactics, and firefighter safety (Fettig and others 2021, Hood 2019). The vast area impacted by the drought and outbreaks will likely influence wildfire hazard, with increased connectivity of fuels over thousands of acres. Stephens and others (2018) raised the possibility of mass fires occurring in these forests over the next several decades that are much higher in intensity and have unpredictable fire behavior compared to individual wildfires. Ecological changes related to altered forest structure and composition from the drought and bark beetle outbreaks are also anticipated (Fettig and others 2019, Stephenson and others 2019, Young and others 2020).

ACKNOWLEDGMENTS

This work was supported by the U.S. Department of Agriculture Forest Service, Forest Health Protection EM-18-WC-03, Region 5, and Rocky Mountain Research Station. The thoughtful reviews of Marc Meyer and Christopher Fettig improved previous versions of the manuscript.

For more information, contact: Sharon Hood, sharon.hood@usda.gov.

LITERATURE CITED

Adams, H.D.; Zeppel, M.J.; Anderegg, W.R. [and others]. 2017. A multi-species synthesis of physiological mechanisms in drought-induced tree mortality. Nature Ecology and Evolution. 1: 1285–1291. https://doi.org/10.1038/s41559-017-0248-x.

Anderegg, W.R.L.; Hicke, J.A.; Fisher, R.A. [and others]. 2015. Tree mortality from drought, insects, and their interactions in a changing climate. New Phytologist. 208(3): 674–683. https://doi.org/10.1111/nph.13477.

Cailleret, M.; Dakos, V.; Jansen, S. [and others]. 2019. Early-warning signals of individual tree mortality based on annual radial growth. Frontiers in Plant Science. 9: 1964. https://doi.org/10.3389/fpls.2018.01964.

Camarero, J.J.; Gazol, A.; Sangüesa-Barreda, G. [and others]. 2015. To die or not to die: early warnings of tree dieback in response to a severe drought. Journal of Ecology. 103(1): 44–57. https://doi.org/10.1111/1365-2745.12295.

Csank, A.Z.; Miller, A.E.; Sherriff, R.L. [and others]. 2016. Tree-ring isotopes reveal drought sensitivity in trees killed by spruce beetle outbreaks in south-central Alaska. Ecological Applications. 26(7): 2001–2020. https://doi.org/10.1002/eap.1365.

Donato, D.C.; Harvey, B.J.; Romme, W.H. [and others]. 2013. Bark beetle effects on fuel profiles across a range of stand structures in Douglas-fir forests of Greater Yellowstone. Ecological Applications. 23(1): 3–20. https://doi.org/10.1890/12-0772.1.

Fettig, C.J. 2016. Native bark beetles and wood borers in Mediterranean forests of California. In: Lieutier, F.; Paine, T.D., eds. Insects and diseases of Mediterranean forest systems. Cham, Switzerland: Springer International Publishing: 499–528. https://doi.org/10.1007/978-3-319-24744-1_18.

Fettig, C.J.; Hood, S.M.; Runyon, J.B.; Stalling, C.M. 2021. Bark beetle and fire interactions in western coniferous forests: research findings. Fire Management Today. 79(1): 14–23.

Fettig, C.J.; Mortenson, L.A.; Bulaon, B.M.; Foulk, P.B. 2019. Tree mortality following drought in the central and southern Sierra Nevada, California, US. Forest Ecology and Management. 432: 164–178. https://doi.org/10.1016/j.foreco.2018.09.006.

Hicke, J.A.; Johnson, M.C.; Hayes, J.L.; Preisler, H.K. 2012. Effects of bark beetle-caused tree mortality on wildfire. Forest Ecology and Management. 271(0): 81–90. https://doi.org/10.1016/j.foreco.2012.02.005.

Hoffman, C.M.; Sieg, C.H.; McMillin, J.D.; Fulé, P.Z. 2012. Fuel loadings 5 years after a bark beetle outbreak in South-western USA ponderosa pine forests. International Journal of Wildland Fire. 21(3): 306–312. https://doi.org/10.1071/WF11019.

Hood, S.M. 2019. Fire and bark beetle interactions. In: Manzello, S.L., ed. Encyclopedia of wildfires and wildland-urban interface (WUI) fires. Cham, Switzerland: Springer International Publishing: 1–6. https://doi.org/10.1007/978-3-319-51727-8_251-1.

Jenkins, M.J.; Page, W.G.; Hebertson, E.G.; Alexander, M.E. 2012. Fuels and fire behavior dynamics in bark beetle-attacked forests in western North America and implications for fire management. Forest Ecology and Management. 275: 23–34. https://doi.org/10.1016/j.foreco.2012.02.036.

Keane, R.; Dickinson, L. 2007. The Photoload sampling technique: estimating surface fuel loadings using downward looking photographs. Gen. Tech. Rep. RMRS-190. Fort Collins, CO: U.S. Department of Agriculture Forest Service, Rocky Mountain Research Station. 44 p. https://doi.org/10.2737/RMRS-GTR-190.

Kolb, T.E.; Fettig, C.J.; Ayres, M.P. [and others]. 2016. Observed and anticipated impacts of drought on forest insects and diseases in the United States. Forest Ecology and Management. 380: 321–334. https://doi.org/10.1016/j.foreco.2016.04.051.

Landram, F.M.; Laudenslayer, W.F., Jr.; Atzet, T. 2002. Demography of snags in eastside pine forests of California. In: Laudenslayer, W.F., Jr.; Shea, P.J.; Valentine, B.E. [and others], tech. coords. Proceedings of the symposium on the ecology and management of dead wood in western forests. Gen Tech. Rep. PSW-181. Albany, CA: U.S. Department of Agriculture Forest Service, Pacific Southwest Research Station: 605–620. https://doi.org/10.2737/PSW-GTR-181.

Lutes, D.C.; Benson, N.C.; Keifer, M. [and others]. 2009. FFI: a software tool for ecological monitoring. International Journal of Wildland Fire. 18(3): 310–314. https://doi.org/10.1071/WF08083.

McDowell, N.; Pockman, W.T.; Allen, C.D. [and others]. 2008. Mechanisms of plant survival and mortality during drought: Why do some plants survive while others succumb to drought? New Phytologist. 178(4): 719–739. https://doi.org/10.1111/j.1469-8137.2008.02436.x.

McDowell, N.G.; Allen, C.D.; Marshall, L. 2010. Growth, carbon-isotope discrimination, and drought-associated mortality across a *Pinus ponderosa* elevational transect. Global Change Biology. 16(1): 399–415. https://doi.org/10.1111/j.1365-2486.2009.01994.x.

Pile, L.S.; Meyer, M.D.; Rojas, R. [and others]. 2019. Drought impacts and compounding mortality on forest trees in the southern Sierra Nevada. Forests. 10: 237. https://doi.org/10.3390/f10030237.

Reed, C.C.; Hood, S.M. 2021. Few generalizable patterns of tree-level mortality during extreme drought and concurrent bark beetle outbreaks. Science of the Total Environment. 750: 141306. https://doi.org/10.1016/j.scitotenv.2020.141306.

Sevanto, S.; McDowell, N.G.; Dickman, L.T. [and others]. 2014. How do trees die? A test of the hydraulic failure and carbon starvation hypotheses. Plant, Cell & Environment. 37(1): 153–161. https://doi.org/10.1111/pce.12141.

Sieg, C.H.; Linn, R.R.; Pimont, F. [and others]. 2017. Fires following bark beetles: factors controlling severity and disturbance interactions in ponderosa pine. Fire Ecology. 13(3): 1. https://doi.org/10.4996/fireecology.130300123.

Stalling, C.; Keane, R.E.; Retzlaff, M. 2017. Surface fuel changes after severe disturbances in northern Rocky Mountain ecosystems. Forest Ecology and Management. 400: 38–47. https://doi.org/10.1016/j.foreco.2017.05.020.

Stephens, S.L.; Collins, B.M.; Fettig, C.J. [and others]. 2018. Drought, tree mortality, and wildfire in forests adapted to frequent fire. BioScience. 68(2): 77–88. https://doi.org/10.1093/biosci/bix146.

Stephenson, N.L.; Das, A.J.; Ampersee, N.J. [and others]. 2019. Which trees die during drought? The key role of insect host-tree selection. Journal of Ecology. 107: 2383–2401. https://doi.org/10.1111/1365-2745.13176.

Stokes, M.A.; Smiley, T.L. 1996. An introduction to tree-ring dating. Tucson, AZ: University of Arizona Press. 73 p.

Xie, H.; Fawcett, J.E.; Wang, G.G. 2020. Fuel dynamics and its implication to fire behavior in loblolly pine-dominated stands after southern pine beetle outbreak. Forest Ecology and Management. 466: 118130. https://doi.org/10.1016/j.foreco.2020.118130.

Young, D.J.; Meyer, M.; Estes, B. [and others]. 2020. Forest recovery following extreme drought in California, USA: natural patterns and effects of pre-drought management. Ecological Applications. 30(1): e02002. https://doi.org/10.1002/eap.2002.

CHAPTER 12.

Accuracy Assessment of Insect and Disease Survey and eDaRT for Monitoring Forest Health

Michèle R. Slaton
Kayanna Warren
Alexander Koltunov
Sheri Smith

INTRODUCTION

The historic drought and bark beetle outbreak in California that peaked 2014–2016 resulted in high levels of tree mortality at a landscape scale. Millions of trees were reportedly affected, primarily ponderosa pine (*Pinus ponderosa*), but also Jeffrey pine (*P. jeffreyi*), sugar pine (*P. lambertiana*), white fir (*Abies concolor*), and red fir (*A. magnifica*) (USDA Forest Service 2020b). U.S. Department of Agriculture Forest Service, State and Private Forestry, Forest Health Protection (FHP) delivers forest health information, including Aerial Detection Survey (ADS) data in support of the national Insect and Disease Survey (IDS). Aerial Detection Survey polygons are sketch-mapped from aircraft and attributed with disturbance agent and host and with estimated trees per acre (TPA) with mortality. Focus is typically on the upper forest stratum, defined for our study in the Sierra Nevada as conifers >11 inches diameter at breast height (d.b.h.).

As tree mortality progressed in 2014, high-quality, near real-time data were needed to facilitate timely management response. Toward this end, FHP undertook an evaluation of potential improvements to ADS, including integration of alternate technologies. Recently, satellite-based remote sensing methods and processing systems have emerged to detect stand- and landscape-level changes, including the Ecosystem Disturbance and Recovery Tracker (eDaRT; Koltunov and others 2020). eDaRT products provide information on vegetation disturbance events derived from Landsat satellite imagery at the 98-foot (30-m) scale. The onset of these events is attributed to a 2-week time period, and each event has a relative intensity that corresponds to canopy cover loss. The eDaRT system is both flexible and efficient for operational implementation needs, has demonstrated high accuracy (Koltunov and others 2020), and is in use for several applications in California.

Although both eDaRT and ADS may be used to represent forest mortality information, each one reports different metrics at different spatial and temporal scales. The overall goal of our Evaluation Monitoring project (EM-18-WC) funded by the Forest Service, Forest Health Monitoring program was to provide a rigorous assessment of ADS and eDaRT products and outline recommendations for complementary use by land managers. To meet this goal, our specific objectives were to (1) develop and execute a ground-based sampling strategy to compare ADS and eDaRT to reference validation data, and (2) make recommendations for appropriate use of data in varied applications.

METHODS

Our study area (104,795 acres) was located on the Sierra National Forest (SNF) in ponderosa pine and mixed conifer forests at elevations between 2,800 and 7,600 feet (fig. 12.1). Our sample consisted of 57 total ADS polygons (Damage Type 2 for mortality) and eDaRT (version 2.9) outputs for the entire study area

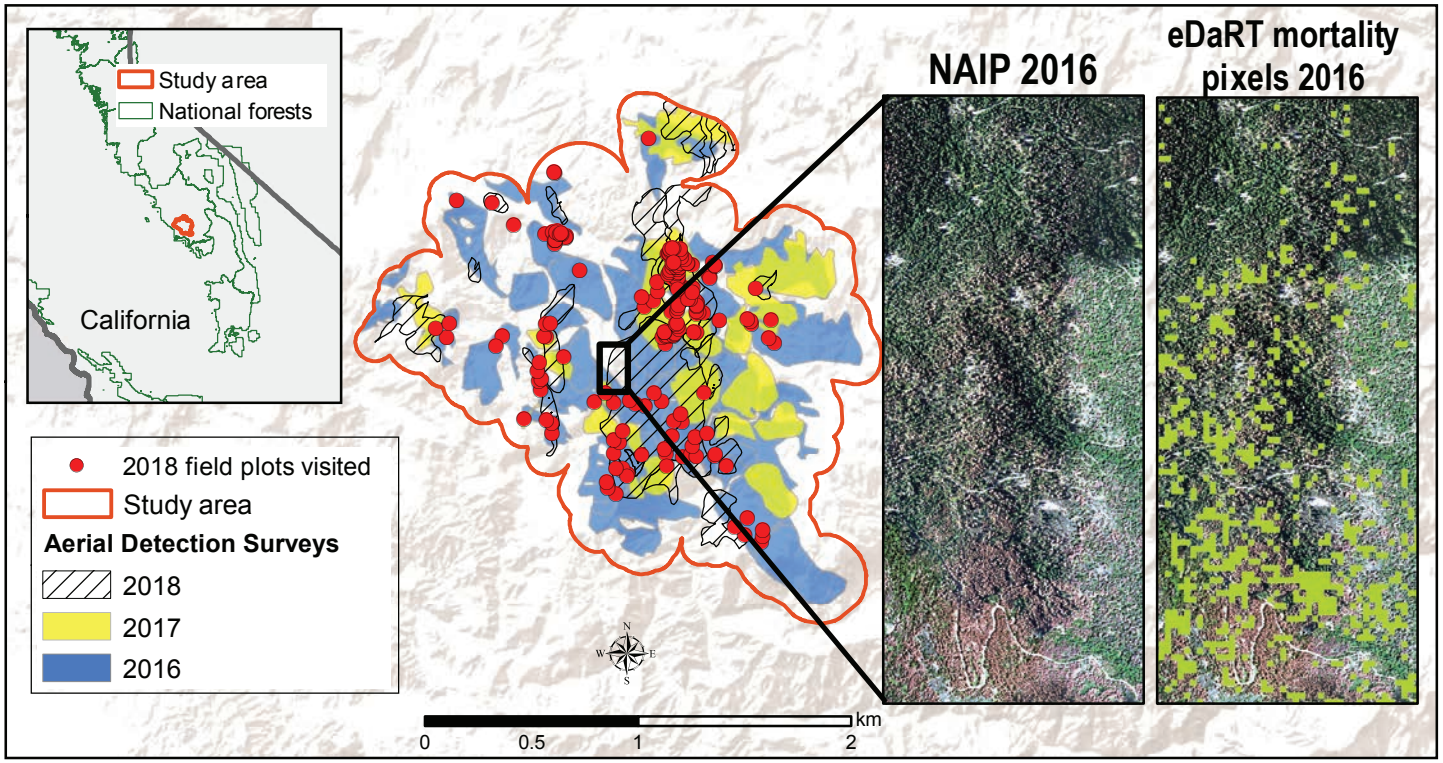

Figure 12.1—Map of study area on the Sierra National Forest, CA, including field plots and Aerial Detection Survey (ADS) polygons (years 2016 and 2018 only used in analysis).

for 2016 and 2018, years for which several ADS mortality polygons were mapped in the study area. Our analysis focused on ADS locality and relative severity data, which could be compared to eDaRT. All field sampling occurred in 2018, and our design targeted a primary sampling area based on *a priori* information about tree mortality occurrence (fig. 12.1). Within this area, we sampled 161 Landsat pixels (98 x 98 feet) within ADS polygons, and 21 pixels outside polygons, all randomly selected within forest types, excluding known fires or vegetation management projects, and prioritized by accessibility. Field technicians recorded tree needle color and decay class, as based on fine twig, bole, and bark characteristics to estimate year of death as presumptively recorded by aerial survey. Decay classes followed Forest Service procedures (USDA Forest Service 2020a), and needle color characteristics were based upon

Miller and Keen (1960) and further refined for the Sierra Nevada montane belt based on input from Forest Service pathologists and entomologists (key available upon request).

At the time of this project, the primary metric for magnitude of change for eDaRT events was a relative proxy for canopy cover loss, based on the temporally integrated standardized residuals of modeling vegetation indices (e.g., normalized difference vegetation index [NDVI]) before and after tree mortality events, a metric termed "confidence" (Koltunov and others 2020). We used field and imagery inspections to identify a threshold for spectral change, above which pixels were determined to be significantly affected by tree mortality, a class hereafter referred to as mortality pixels (eDaRT confidence >50). This relatively simple calibration would not necessarily apply elsewhere in the State, but at the time of this project, the threshold provided a simple and consistent method to deliver an estimate, while more robust estimators of event severity are under development in eDaRT. It is important to note that eDaRT products do not directly describe the number of trees, live or dead, but the degree to which each pixel is affected. Therefore, tree density products were created using F3, an interpolation algorithm developed at the Forest Service Pacific Southwest Region Remote Sensing Lab that uses Forest Inventory and Analysis (FIA) data and Landsat imagery to map forest stand metrics (Huang and others 2018). By overlaying F3 density of trees (prior to mortality) with eDaRT mortality products, we derived estimates of dead tree numbers from this combined eDaRT-F3 product. Resulting values are single estimates per pixel, with error rates for F3 and eDaRT as reported by Koltunov and others (2020) and Huang and others (2018), respectively.

Total dead tree numbers as derived from plots, ADS, and eDaRT were computed at the scale of individual ADS polygons and across the entire study area. For the plots, we multiplied mean density of dead trees by respective area acreage to determine the plot-based total for dead trees. For ADS data, we multiplied the dead TPA for each polygon by its acreage to derive total dead tree numbers. eDaRT mortality pixels were combined with F3 tree density data to compute a combined eDaRT-F3 result for the total quantity of dead trees. Error matrices comparing ADS to plot-based TPA estimates were created by computing means of dead tree densities for field plots within each polygon and binning values into TPA categories in increments of 10. User's, producer's, and overall accuracy were calculated for ADS following Pontius and Millones (2011). Logistical difficulty in precisely colocating ground plots with Landsat pixels led us to rely upon the polygon-scale comparisons of eDaRT to plot-based and ADS data, and also upon the high-resolution imagery-based assessment as reported by Koltunov and others (2020) for pixel-based error rates.

RESULTS

For 31 out of 36 ADS polygons mapped in 2016 (one of 37 polygons was discarded due to an apparently mislabeled TPA value of zero), the plot-derived densities of dead trees in the polygons (tallied in 2018; red phase; decay classes 2, 3, and 4; i.e., estimated 2–4 years since mortality) were lower than ADS data (fig. 12.2). For year 2018 ADS polygons, plot-based TPA estimates (tallied in 2018, red or yellow phase, decay classes 1 and 2) were also lower than ADS assignments in 17 out of 19 polygons. User's and producer's accuracies, representing omission and commission errors for each TPA class, ranged from 0–50 percent, and overall accuracies for 2016 and 2018 report years were 3 and 10 percent, respectively (fig. 12.2). Because of the difficulty in assigning year of tree death in the field, we allowed for a 1–2-year systematic misassignment by field technicians (i.e., up to three decay classes to represent the 2016 ADS report year, and two decay classes for 2018) but still found that ADS routinely over-estimated TPA. When compiling all TPA bins and examining accuracy only in terms of presence/absence of mortality in polygons, we found overall 40-percent accuracy for 2018 and 75-percent accuracy for 2016.

Across the study area, we found 48,414 acres in year 2016 ADS mortality polygons, in contrast to 7,048 acres as estimated by eDaRT. At the extent of the entire SNF, ADS mapped 181,725 acres with mortality in 2016 compared to 51,298 acres mapped by eDaRT, demonstrating a consistent pattern of greater area estimates from ADS compared to eDaRT. Aerial Detection

(A) **2018**

ADS TPA class \ Plot TPA class	0	1–10	11–20	>20	Grand Total	User's accuracy (%)
0	0	1[a]	0	0	1	0
1–10	6	2	0	0	8	25
11–20	2	3	0	0	5	0
>20	3	3	0	0	6	0
Grand total	11	9	0	0	20	
Producer's accuracy (%)	0	22	0	0		Overall accuracy = 10%

[a] Indicates one apparently mislabeled ADS polygon with TPA value of zero.

(B) **2016**

ADS TPA class \ Plot TPA class	0	1–10	11–20	>20	Grand Total	User's accuracy (%)
0	1	1[a]	0	0	2	50
1–10	1	0	0	0	1	0
11–20	4	2	0	0	6	0
>20	20	8	0	0	28	0
Grand total	26	11	0	0	37	
Producer's accuracy (%)	4	0	0	0		Overall accuracy = 3%

[a] Indicates one apparently mislabeled ADS polygon with TPA value of zero.

Figure 12.2—Error matrices representing disagreement between Aerial Detection Survey (ADS) and plot-based dead trees per acre (TPA) in polygons. Cell values are numbers of ADS polygons. Plot-based trees were >11 inches d.b.h. and included decay classes 1 and 2 for year 2018 (A) and decay classes 2, 3, and 4 for year 2016 (B). Raw values only are displayed; an area-based matrix with corrections following Pontius and Millones (2011) produced almost identical values.

Survey estimated a total of 1,954,086 dead trees in 2016 across our study area. This is in contrast to the plot-based estimate of 154,453 total dead trees (measured in 2018 as red phase decay class 2, >11 inches d.b.h.). A temporal allowance of +/- 2 years for potential misassignment of time of death by field technicians would be required to bring ADS estimates within the plot-based range of values for both flight years 2016 and 2018 (data not shown). Given the criteria we used to assess timing of death, and the fact that the criteria were largely developed for disease agents and hosts within our study area, it is unlikely that misassignment in timing of death explains the large departures between datasets. The combined eDaRT-F3 data indicated that the study area contained 488,945 dead trees in 2016. In both years 2016 and 2018, eDaRT-F3 estimates fell within the range of plot-based data given +/- 1-year error allowed for field assignment in time of death (fig. 12.3).

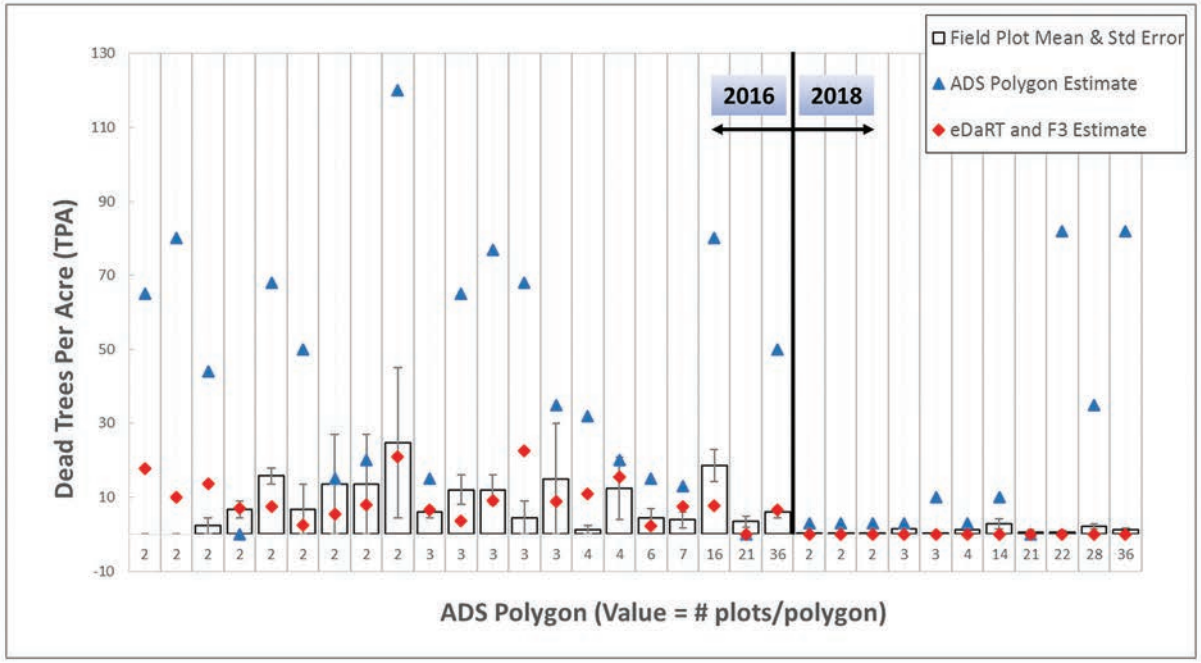

Figure 12.3—Dead trees per acre (TPA) estimates from ADS polygons, eDaRT-F3, and plot-measured means with standard error (SE) bars, with plot sample size per polygon for 2 years.

DISCUSSION

We generally found fewer dead trees within plots than corresponding ADS polygons indicated, both for 2016 and 2018 report years. Even given a temporal margin of error for field personnel assigning time of tree death of up to 2 years, we found that overall, plot-based estimates matched polygon estimates in TPA bins in only 3–10 percent of cases. Notably, a previous assessment of ADS across multiple States in the United States during less severe mortality events found a general pattern of underestimation of dead TPA as compared to ground- and imagery-based measurements (Coleman and others 2018). In our study area, extremely severe mortality occurred over numerous years, and in numerous species with inconsistent crown fade patterns. As a result, sketch-mapping required representation of complex patterning. Aerial Detection Survey practitioners report that in large events such as this, observations of dead tree patches are "lassoed" into larger and potentially more diffuse polygons to facilitate consistent tracking during flight; practitioners typically refer to polygons as areas "with" (i.e., that contain) mortality rather than "of" (i.e., totally affected by) mortality to make this distinction. Our findings were consistent with that trend, in which polygons with high TPA labels contained areas without dead trees. At the scale of the study area and of the SNF administrative unit, acreages of eDaRT mortality were generally lower than those reported by ADS. This may be partially due to the "lasso" effect of mapping extensive mortality that essentially lumps together several areas of acres *with* mortality, rather than splitting more tightly defined acres *of* mortality. Accordingly, FHP specifies in ADS metadata that products should be utilized at spatial scales of 1:100,000 or smaller and that overlays with other spatial products should be approached cautiously (USDA Forest Service 2020b).

Some discrepancy may also be explained by missed detections of low-magnitude mortality in eDaRT. However, levels as low as 5-percent cover loss have up to a 56-percent chance of detection, making missed detections relatively uncommon, especially in denser forests (Koltunov and others 2020). Another source of disagreement is likely rooted in each dataset's method to identify timing of tree death. eDaRT timing is identified by the date of the first Landsat image (every 8–16 days) in which an anomaly is detected, and which may include invisible changes, such as canopy drying. Aerial Detection Survey mappers use visual cues based on canopy color to determine the year of mortality onset. However, because the severity of drought advanced the rate of canopy change, and because mortality expanded and intensified over numerous years, identifying precise timing of mortality onset from aircraft during this extreme event was challenging. There is also error associated with back-dating mortality on the ground given different fade patterns by species and in different microclimates; however, our 2–3-year temporal allowance for error in plot-based assignments reduces the likelihood that this factor explains the discrepancy. Lastly, eDaRT identifies disturbance dates based on the first image in which an anomaly is expressed.

However, if clouds or other factors compromise image quality, detection onset may be delayed, in some cases even until the following year.

The difference in total numbers of dead trees between ADS and the eDaRT-F3 across the study area in part reflects the differences in the areal extent (acreage) of mortality between the datasets. However, our findings show that the disagreement also stemmed from the ADS TPA estimate itself, which was greater than both the plot-based and eDaRT-F3-based values. Importantly, at the time of our analysis, ADS polygons were not labeled with an estimate of the proportion of the polygon (percentage of area) affected by mortality; this method was implemented in 2019. Additional validation will be required for this new metric, but it may be expected to increase the accuracy of derived metrics for numbers of dead trees from ADS because it potentially corrects for overestimation caused by the "lasso" effect.

Although deriving total numbers of dead trees from either ADS or eDaRT is possible, both methods should be approached with caution. Because tree numbers are not easily counted from aircraft, nor are they strongly correlated to spectral indicators in imagery, alternative mortality metrics, such as basal area, volume, biomass, or percentage of area affected may provide more reliable indicators for the magnitude of change. The former two metrics are currently available using eDaRT and F3, and the latter is a standard attribute for ADS products since 2019.

CONCLUSIONS

Practically speaking, forest health information must be accurate enough to guide allocation of funds and resources at a subregional scale and to plan and implement project prescriptions at the stand scale. Table 12.1 provides a simple decision-making matrix to assist users in data selection for determining tree mortality levels for land management applications and analyses. This matrix reinforces the importance of recent direction in the IDS program to enhance integration between aerial detection, ground-based assessments, and a range of remote sensing techniques, such as eDaRT and F3. Recommendations for future development and assessment of ADS and eDaRT methods are summarized into a few main points:

- The new ADS label for the percentage of a polygon affected is expected to improve the accuracy and utility of ADS dead tree products, although it will require both validation and quality control to reduce bias between observers. Similarly, the confidence-based threshold used to estimate severity of eDaRT events will be improved upon through the upcoming release of a Mortality Magnitude Index to directly estimate canopy cover loss, and F3 products will be improved by the recent implementation of intensification of remeasurement from a 10-year to a 5-year cycle.
- Demand for reference validation datasets remains high. "Virtual plots" in which analysts measure canopy cover change within Landsat pixels using high-resolution

Table 12.1—A decision-making matrix to assist users in data selection for determining tree mortality levels for land management applications and analyses

Information needed	Suitability of data currently available	Recommended developments
Agent and host tree species affecting area	ADS attributes for host type affected and agent are generally highly accurate (refer to Coleman and others [2018] and citations therein for assessment).	An eDaRT mortality-type classifier is currently under development, and ADS and ground plots may assist in training.
Acreage of tree mortality events	ADS is available but subject to error as reported in this chapter. ADS reports acres with mortality rather than acres of mortality. eDaRT is appropriate from stand scale to State scale but relies on proxy for magnitude of events.	Validation of ADS percentage of area affected metric eDaRT Mortality Magnitude Index to quantify canopy cover loss is planned to replace proxy method (data release targeted for 2021).
Number of trees affected at district or broader scale	ADS is available but subject to error as reported in this chapter. eDaRT-F3 was found to be highly accurate in our study area.	Validation of ADS percentage of area affected metric Investigation of dependency of accuracy on polygon size and proximity to polygon perimeter Additional eDaRT-F3 validation is recommended elsewhere prior to use.
Basal area or volume affected by mortality event	ADS may be used with standard tree allometry to derive these metrics, but no validation is available, and is subject to potential overestimation as found for number of trees. Combine eDaRT with F3; validation is not available, but basal area and volume are generally more readily modeled than number of trees.	Metrics are best suited to imagery and LiDAR-based approaches and are not likely to be developed in ADS. Combined eDaRT and F3 products require additional validation for these metrics.
Settings and situations most appropriate for current use	ADS highlights broad-scale and annual trends, and detects small-scale and highly dispersed or light-severity events where agent and host identification are important. eDaRT-F3 is suitable for stand-level to regional analysis and currently best detects tree mortality in denser stands. eDaRT is also suitable for applications where high temporal resolution for disturbance onset is required.	The current study mainly compared ADS and eDaRT in the context of a severe and discrete mortality event. Continued exploration of product integration to exploit the strengths of each will be highly valuable.

ADS = Aerial Detection Survey; eDaRT = Ecosystem Disturbance and Recovery Tracker; F3 = an interpolation algorithm that uses Forest Inventory and Analysis data and Landsat imagery to map forest stand metrics.

imagery such as National Agriculture Imagery Program (NAIP) or from Google Earth provide an efficient means to create reference data for eDaRT (Koltunov and others 2020). Statewide LiDAR acquisitions, especially in conjunction with high-resolution imagery to assess crown fade and moisture, will provide for continued broad-scale assessment of both ADS and eDaRT. Implementation of these remote sensing-based methods will allow for improved targeting and efficiency of smaller scale ground-based validation efforts.

- Leveraging the unique strengths of diverse monitoring methods is becoming increasingly important as broad-scale tree mortality events unfold. Directing ADS flights toward core areas for targeted host and agent assessment will not only minimize risk for flight personnel but will complement remote sensing techniques by helping to train broad-scale models and to direct on-the-ground assessments.

For more information (including full EM-18-WC report), contact: Michèle Slaton, michele.slaton@usda.gov.

ACKNOWLEDGMENTS

We are grateful to Carol Clark for assistance with this analysis and to Adrian Das, Derek Young, Ryan Hanavan, and Jeff Moore for their comments that improved upon earlier versions of this manuscript.

LITERATURE CITED

Coleman, T.W.; Graves, A.D.; Heath, Z. [and others]. 2018. Accuracy of aerial detection surveys for mapping insect and disease disturbances in the United States. Forest Ecology and Management. 430: 321–336. https://doi.org/10.1016/j.foreco.2018.08.020.

Huang, S.L.; Ramirez, C.; McElhaney, M.; Evans, K. 2018. F-3: simulating spatiotemporal forest change from field inventory, remote sensing, growth modeling, and management actions. Forest Ecology and Management. 415: 26–37. https://doi.org/10.1016/j.foreco.2018.02.026.

Koltunov, A.; Ramirez, C.M.; Ustin, S.L. [and others]. 2020. eDaRT: The Ecosystem Disturbance and Recovery Tracker system for monitoring landscape disturbances and their cumulative effects. Remote Sensing of Environment. 238: 111482. https://doi.org/10.1016/j.rse.2019.111482.

Miller, J.M.; Keen, F.P. 1960. Biology and control of the western pine beetle. Misc. Publ. 800. Washington, DC: U.S. Department of Agriculture Forest Service. 318 p.

Pontius, R.G.; Millones, M. 2011. Death to Kappa: birth of quantity disagreement and allocation disagreement for accuracy assessment. International Journal of Remote Sensing. 32: 4407–4429. https://doi.org/10.1080/01431161.2011.552923.

U.S. Department of Agriculture (USDA) Forest Service. 2020a. Forest Inventory and Analysis national core field guide volume 1: field data collection procedures for Phase 2 plots, version 9.0. Washington, DC: U.S. Department of Agriculture Forest Service. 449 p.

U.S. Department of Agriculture (USDA) Forest Service, Pacific Southwest Region, Forest Health Protection. 2020b. Aerial Detection Monitoring. https://www.fs.usda.gov/detail/r5/forest-grasslandhealth/?cid=fsbdev3_046696. [Date accessed: June 30, 2020].

CHAPTER 13.

Emerald Ash Borer Infestation in Arkansas: Extent, Severity, and Progression

Mohammad M. Bataineh
Benjamin L. Walters
Stephen R. Clarke
Benjamin Babst
Robert Ficklin

INTRODUCTION

The invasive emerald ash borer (*Agrilus planipennis*; EAB) is currently present in five Canadian provinces and 35 States, including Arkansas, and has caused mortality of millions of ash (*Fraxinus* spp.) trees across the continent (Herms and McCullough 2014). The regulatory response following the initial 2002 EAB discovery took the form of large-scale detection surveys and establishment of quarantines to slow or prevent human-aided spread (BenDor and others 2006). Imposed quarantines restricted the movement of ash nursery stock and products, including firewood, from known infested areas. In Arkansas, a quarantine was implemented in September 2014 covering 25 counties, including six with confirmed EAB infestation sites. This quarantine was expanded in October 2016 to include eight additional counties, following confirmations in Randolph County and additional counties within the original quarantine area, and was further expanded to a statewide quarantine in March 2018. Detection surveys were usually not followed by delimiting surveys to establish infestation extent, estimate EAB population density, and provide baseline data for monitoring.

Quarantine and management strategies rely on understanding the current extent and severity of the infestation. Satellite colony establishment complicates making management decisions (Muirhead and others 2006) and, based on distances from known infested locations, may highlight quarantine effectiveness and relative contribution of human transport. More realistic parameterization of local and regional EAB spread models requires empirical data on realized spread (Siegert and others 2015). Moreover, information on the current infestation extent and severity would provide the basis for risk assessments and prioritization of treatment areas. The objectives of this study are to (1) document the extent, severity, and progression of EAB infestation in Arkansas; and (2) reconstruct EAB-induced ash tree mortality patterns as a surrogate for realized spread and infestation progression.

METHODS

The study area encompassed 17 southern Arkansas counties in which EAB was confirmed as of December 2017. The area is within the South Central Plains and Ouachita Mountains ecoregions (Woods and others 2004). Ash trees are sparse, representing 1 percent of gross live tree total bole volume within each of the two ecoregions, and are mainly distributed along major streams and rivers. The most pronounced ash distribution within the study area is found along the Little Missouri River and the Ouachita River in Clark and Ouachita Counties, respectively (fig. 13.1A).

Adult catches from EAB detection efforts since 2014 were compiled into a geodatabase. Data sources included original trapping, which was used to confirm EAB presence in a county as part of EAB national surveys, and any additional detection traps that were deployed within a county after confirmation. Detection traps (purple panel traps with [Z]-3-hexenol lures

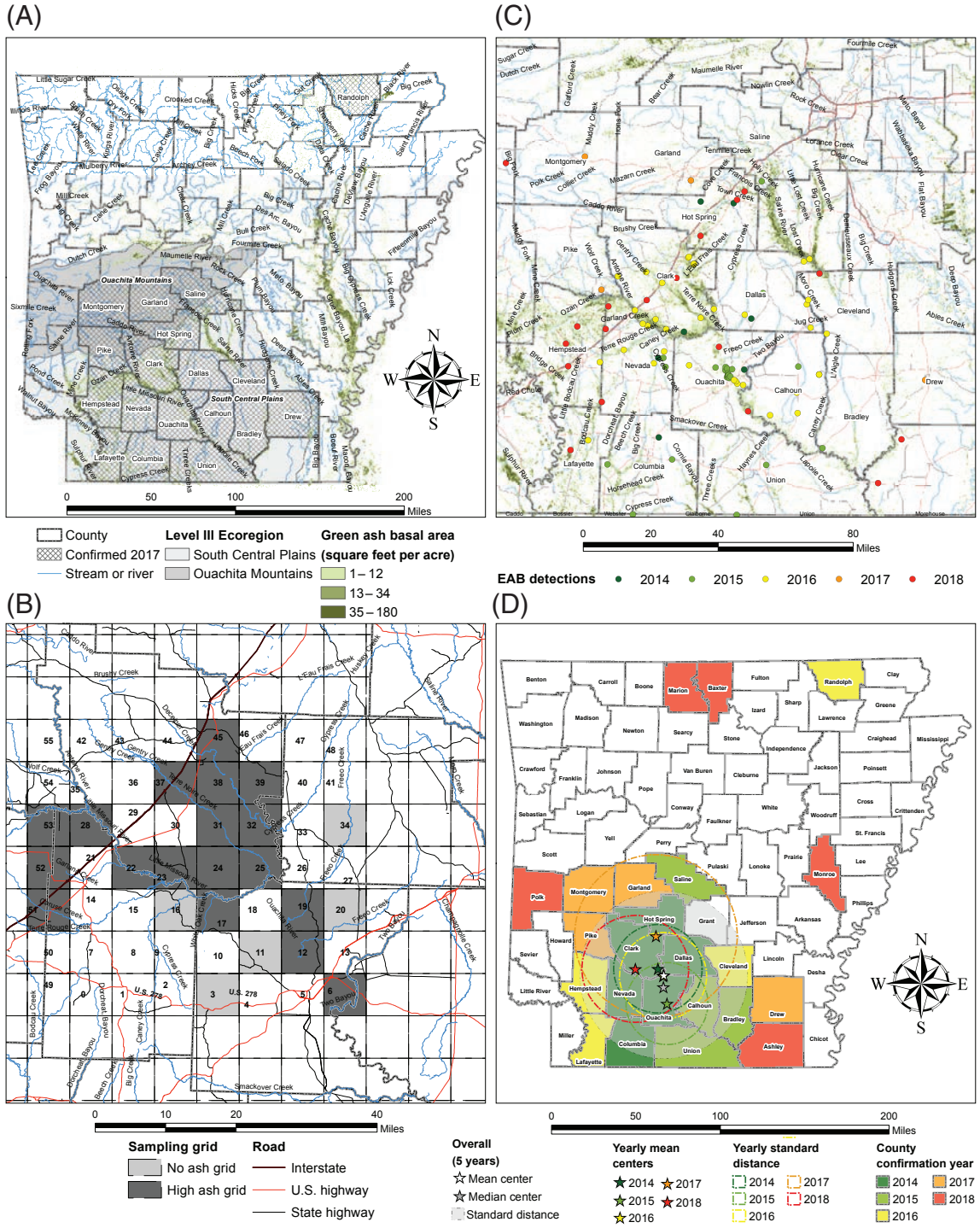

Figure 13.1—(A) Green ash basal area distribution along major streams and rivers within the two Arkansas ecoregions that encompass the 17 counties of the study area; (B) the 6- x 6-mile grid used for trapping of emerald ash borer (EAB) and reconstruction of EAB-induced ash tree mortality patterns; (C) EAB detections (positive adult catches), over a 5-year period from 2014 through 2018; (D) EAB county-level yearly confirmation with yearly and 5-year spatial summary statistics (mean, median, and standard distance circle of one standard deviation) of positive detections. Ecoregion level III boundaries (Woods and others 2004) are included for reference. Green ash distribution data derived from Individual Species Parameter Maps by the U.S. Department of Agriculture Forest Service, Forest Health Protection (FHP), Forest Health Assessment and Applied Sciences Team (FHAAST). (Data sources: FHP, FHAAST, and Arkansas GIS Office)

placed in the lower crowns of ash trees) were deployed within confirmed counties using a 6- x 6-mile grid encompassing the 17-county study area (fig. 13.1B), following the U.S. Department of Agriculture Animal and Plant Health Inspection Service (APHIS) EAB national survey guidelines (USDA APHIS 2015). Species identity of captured EAB adults in detection traps was confirmed under the microscope as outlined in Parsons (2008). Using the compiled geodatabase for EAB adult catches, infestations were mapped for the 17 counties over a 5-year period from 2014 to 2018 (fig. 13.1C).

To reconstruct EAB-induced ash mortality patterns, as a surrogate for realized spread and progression, the year of death at an annual resolution was determined for standing dead ash trees (i.e., snags). Radial increment cores were collected from declining, dead, and live trees across an area encompassing the majority of four counties with an initial confirmation in 2014, approximately 2,000 square miles (fig. 13.1B). The four counties (Clark, Dallas, Ouachita, and Nevada) represented an area with the earliest infestation date in Arkansas and highest abundance of ash. Systematic ash tree surveys were conducted in March and April of 2019 to locate and georeference EAB-symptomatic trees: trees with D-shaped exit holes, epicormic branching, woodpecker feeding, bark splits, and general canopy decline. Field visits utilized the 6- x 6-mile grid previously used for detection traps and included a total of 56 grid cells (fig. 13.1B). Due to higher abundance of ash trees along rivers and waterways, 18 grid cells covering the Little Missouri River, Ouachita River, Two Bayou, Freeo Creek, Terre Noire Creek, Deceiper Creek, Terre Rouge Creek, and Antoine River were sampled with higher intensity with an average of five ash trees sampled per grid cell (fig. 13.1B). No ash trees were found within five grid cells. Three ash trees per grid cell, on average, were randomly selected for sampling from the remaining 33 grid cells. Ash selection focused on dead and dying trees but included a minor component of asymptomatic live and symptomatic declining trees to ensure feasibility of crossdating ash snag cores. A total of 179 ash trees were sampled, 77 percent of which were snags.

Within each grid cell, snags were defined as standing dead ash trees with no visible buds or leaves but exhibiting symptoms of EAB infestation. Ash trees were classified into five decline classes ranging from 1 to 5, with a rank of 1 being healthy and 5 being standing dead (Knight and others 2012, Smith 2006). Trees with decline classes 1 through 4 were used as reference in crossdating and determination of year of death. To capture EAB-induced mortality and not that of other causal factors, such as density-dependent mortality, trees were selected if they were currently or previously in the canopy as judged from size and characteristics of trees, and gaps when tops were broken. Consequently, trees along edges of forest stands and trees with dominant and codominant crown positions were favored in sample selection. Sampled locations represented urban, rural residential, and forested or wooded areas. Georeferenced asymptomatic and declining ash trees' and snags' diameter at

breast height (d.b.h.), total height, crown position class (dominant, codominant, intermediate, or suppressed), and decline status were recorded. Snag decay status was also recorded using a three-level categorical variable as: 1 = recently dead tree with fine branches present and intact bark and top; 2 = declining snag with most fine branches missing but large limbs present or broken, broken top, and loose or sloughing bark; 3 = decayed snag with no coarse branches and sloughed off bark.

Two radial increments were collected at breast height at right angles for each sampled tree. Tree cores were air dried, glued, sanded, and processed following standard methodology (Stokes and Smiley 1968). Tree cores were scanned using an Epson® Expression 11000XL scanner and Epson® scanner software. The width of each tree ring was measured to the nearest 0.000039 inches (0.001 mm) using WinDendro™ software. Cores were visually, graphically, and statistically crossdated by matching patterns in tree ring widths among samples from the same tree and then trees within a grid cell. COFECHA software was used to verify measurement quality and perform statistical crossdating (Grissino-Mayer 2001, Holmes 1983). Master chronologies developed using COFECHA from asymptomatic and declining ash trees with calendar year assigned to each annual growth ring were compared to tree ring widths from dead trees. Year of death was assigned to the outermost ring based on marker years and pattern matching with the master chronology, and quality of dating was checked using the undated series option in COFECHA (Bataineh and Daniels 2014, Daniels and others 1997, Siegert and others 2014).

Year of death estimates for each tree location were mapped and used in spatial overlays with adult trap catches. Ash distribution maps from the Individual Tree Species Parameter (ITSP) maps (Ellenwood and others 2015) were also used in the overlay analysis to examine effect of host abundance and distribution on EAB realized spread. The ITSP green ash (*Fraxinus pennsylvanica*) raster basal area estimates were clipped to the study area and then reclassified into three basal area-based abundance classes. Other available spatial datasets including roads, public land boundaries, and number of camp and lodge structures (used for hunting, fishing, hiking, and other recreational purposes) were also used in overlays. Spatial statistics and point density estimates were calculated for year of tree death and trap catch layers using ArcGIS 10.7 tools.

RESULTS AND DISCUSSION

For the 5-year period, 2014 through 2018, 229 traps were deployed across the study area. Overall detection rate was 47 percent for the entire time period, with 107 positive catch traps and 122 traps with no catches. The EAB detections radiated outward from the original seven locations encompassed by the six counties confirmed in 2014 (figs. 13.1C and 13.1D). In some cases, EAB was detected 80 to 90 miles away from known infestations as was the case for detections in Monroe County, outside the study area. Similar to other areas nationwide,

outlier populations continued to appear within the designated quarantine zone in Arkansas, and outreach campaigns did not seem effective in limiting infested material transport as was previously hypothesized (Siegert and others 2015). The median location for the point pattern created by adult trap catches for the 5-year period was centered at latitude 33.70833°N and longitude -92.893242°W, located along the Ouachita River between Old River Island to the north and Tulip Creek to the south (fig. 13.1D). The mean location (33.81212°N, -92.890096°W) was centered 7 miles due north of median near the corners of Dallas, Clark, and Ouachita Counties (fig. 13.1D). The mean and median locations represented the spatial centers of the detection pattern over the 5-year period with less influence of perimeter traps on the median than mean center. A standard distance of 50 miles, one standard deviation, radiating from the mean center contained 81 percent of positive trap catch locations over the 5-year period. For each trapping year, mean centers and standard distances reflected the outward spread and dispersion of EAB detections with 1.8- and 1.2-fold increases in standard distance for 2017 and 2018, respectively (fig. 13.1D). Increases in standard distance were more drastic when detection records outside the study area were included, with 1.5-, 2-, and 3-fold increases in standard distance for 2016, 2017, and 2018, respectively.

A total of 179 ash trees were georeferenced and measured. Ash snags made up 77 percent of the sample (138 trees) with an additional 11 percent (19 trees) in severe decline. Mean ± SD (standard deviation) of d.b.h. and total height for all sampled trees were 9.4 ± 4.3 inches and 48.6 ± 19.1 feet, respectively. Ash trees, live and dead, were mainly of the dominant or codominant crown positions (82 percent), and the remaining were of intermediate or suppressed position (18 percent). Most ash snags were also dominant or codominant (82 percent). Based on branch, top, and bark conditions, most ash snags were recently dead (65 percent) or in a moderate decline stage (21 percent).

Trap detection of EAB appeared to lag behind EAB-induced ash tree mortality by at least 1 year (fig. 13.2). Earliest EAB-induced mortality occurred in 2013 with the majority (68 percent) dying within 2 years of the first State detection, indicating that ash trees may be dying within a shorter time frame compared to the 6-year period reported at the northern range (Knight and others 2012). Stand density was reported to influence ash mortality rates with more rapid mortality in stands, as those reported in this study, with low density (Knight and others 2012). Only a few trees along the Terre Noire and Terre Rouge Creeks in Clark and Nevada Counties, respectively, had died in 2013. Ash tree mortality had progressed along the Little Missouri River in 2014, spanning 20 to 30 miles in a counter flow direction, when the first State detections were reported. About half (55 percent) of 2014 ash snags were in Clark County, with 18, 14, 5, and 5 percent of 2014 snags in Nevada, Ouachita, Hempstead, and Dallas Counties, respectively. Nearest positive trap detections, in

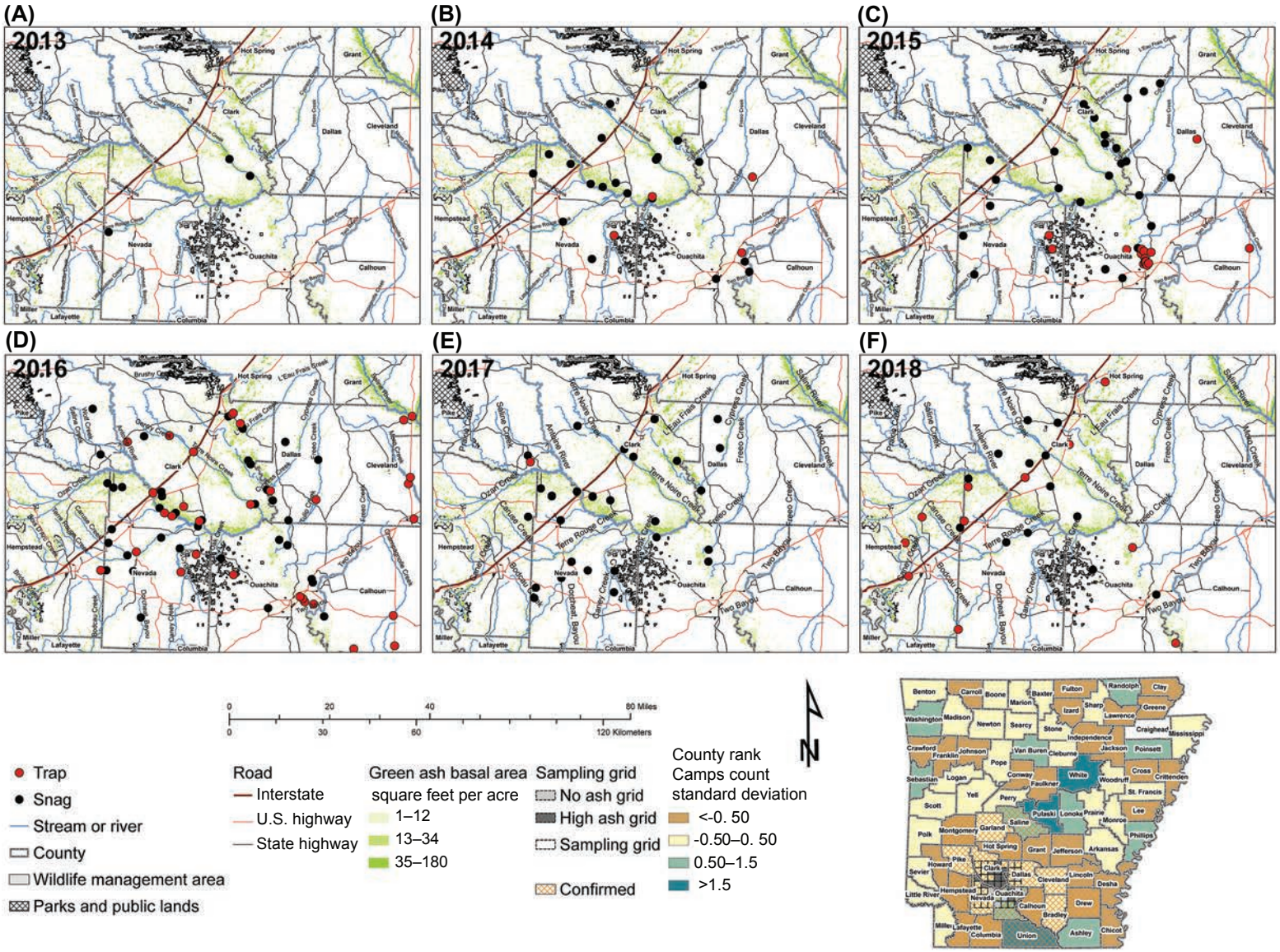

Figure 13.2—Annual progression in (A) 2013, (B) 2014, (C) 2015, (D) 2016, (E) 2017, and (F) 2018 of emerald ash borer-induced mortality in relation to annual positive trap detections, host abundance and distribution, and other cultural features such as roads, camps, and public lands within an area encompassing the majority of four Arkansas counties. Green ash distribution data derived from Individual Species Parameter Maps by the U.S. Department of Agriculture Forest Service, Forest Health Protection (FHP), Forest Health Assessment and Applied Sciences Team (FHAAST). (Data sources: FHP, FHAAST, and Arkansas GIS Office)

2014, were between 0.3 and 11 miles from an ash snag killed that year, but a distance of 6.5 to 15.6 miles separated these detections from an ash snag killed in 2013. Public lands in Clark and Nevada Counties included DeGray Lake Recreational Area and Poison Springs State Forest and Wildlife Management Area, respectively. Interstate 30 (I-30) traverses Clark County from northeast to southwest and passes through the upper northwest corner of Nevada County. Using density of camps and lodges as a surrogate for human movement of firewood, Clark and Nevada Counties had a relatively low number of camps and lodges, 19 and 13 respectively, compared to Ouachita County, which contained 104 camps and lodges (fig. 13.2). Ash snags in Pike and Hempstead Counties were dated at earliest to 2016 and 2014, respectively, whereas earliest positive trap catches were reported in 2017 and 2016, respectively (fig. 13.2).

The concentration of ash hosts along major streams and rivers within the study area appeared to facilitate both short-distance colonization and long-distance dispersal by EAB (fig. 13.2). Aggregates of ash trees with relatively sequential death dates from 2013 through 2017 or 2018 were evident along the Little Missouri River, Terre Noire Creek, Terre Rouge Creek, and Deceiper Creek (fig. 13.2). Simultaneously, latest ash snag death dates radiated perpendicularly away from drainage channels as host abundance declined. Thus, abundance of hosts along drainage channels appeared to facilitate short-distance colonization, whereas scarcity of hosts away from drainage channels seemed to facilitate long-distance dispersal and therefore support the establishment of outlier populations. The effect of host proximity in this spatiotemporal pattern is consistent with reports of substantially increased colonization likelihood with abundant ash within 650 feet of infestation centers (Siegert and others 2010). The onset of EAB infestation appeared to be concentrated in Clark and Nevada Counties, which is not surprising given the high ash abundance, proximity to public land and recreational areas, and the fact that a major road artery, I-30, traverses both counties.

Point density estimates of adult counts per unit area showed high EAB density along I-30 and along the Little Missouri and Ouachita Rivers (fig. 13.3A). Highest density of one adult caught per square mile was recorded at the northwestern border of Cleveland County along the Saline River. This highlighted the high risk of potential mortality along this drainage. The relatively high ash abundance along the Saline River coupled with lack of field observations of ash mortality indicate that EAB spread may continue northward and southward along the Saline River, threatening valuable ash trees within these bottomland hardwood forests. Therefore, areas along the Saline River should be of high priority in scheduling salvage and sanitation harvests. Other high-density locations included: an area near Camden between the Ouachita River and Two Bayou; and an area 13 miles north of Hope, near Ozan (fig. 13.3A). Ash snag point density estimates per unit area showed clustering of dead trees along the Little Missouri River, Deceiper Creek, Terre Noire Creek, Ouachita River, and

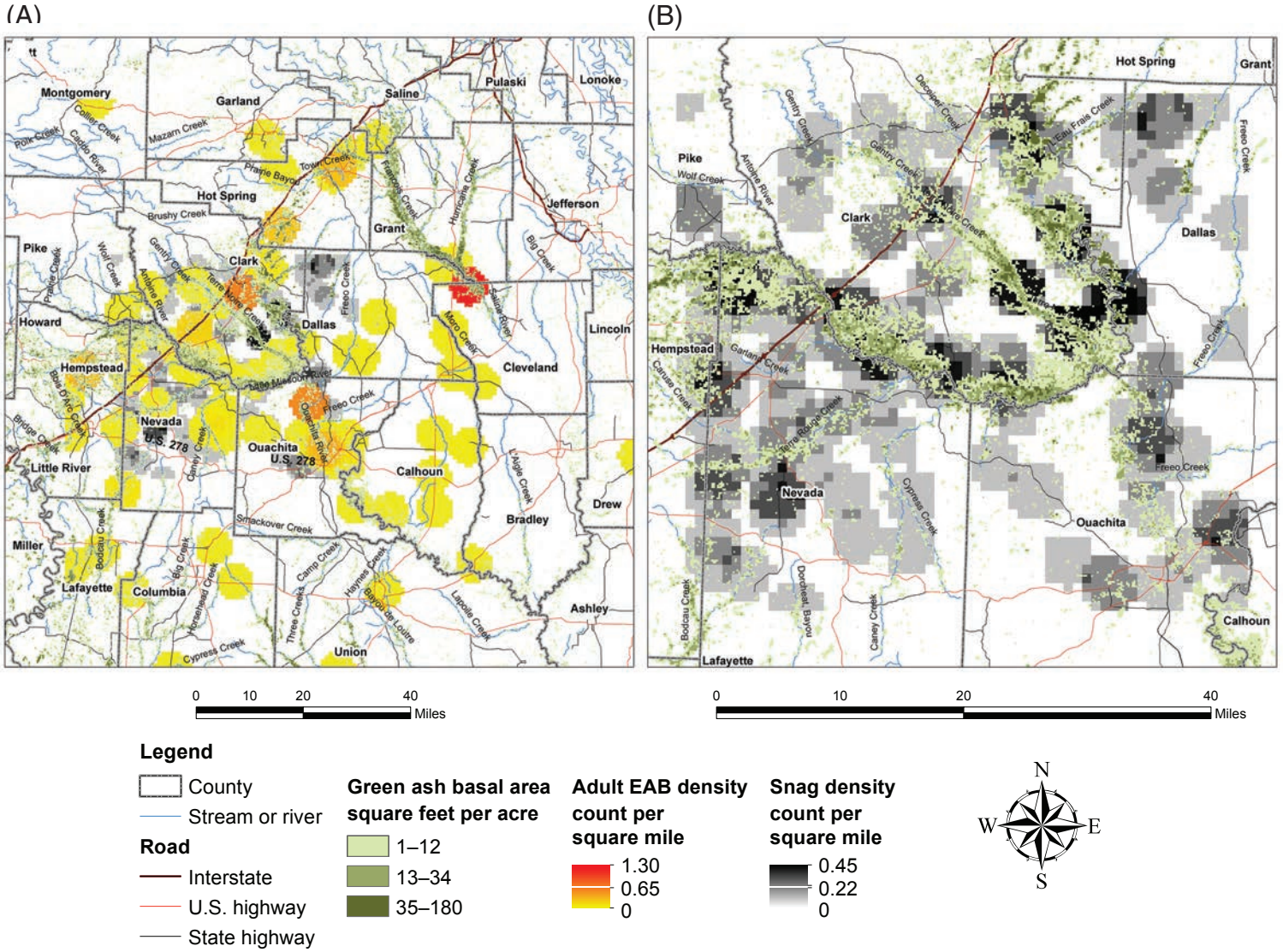

Figure 13.3—(A) Density of emerald ash borer (EAB) detections and (B) EAB-killed ash snags, counts per square mile, over a 5-year period from 2014 through 2018. Green ash distribution data derived from Individual Species Parameter Maps by the Forest Service, Forest Health Protection, Forest Health Assessment and Applied Sciences Team. (Data sources: Forest Health Protection, FHAAST, and Arkansas GIS Office)

along the I-30 corridor (fig. 13.3B). Highest density of one snag per 2 square miles was recorded at the confluence of Terre Noire and Deceiper Creeks. Ash snag and EAB population densities provided somewhat similar accounts of the severity of the current infestation (fig. 13.3). This concordance highlights the feasibility of using EAB population density as an indirect measure of potential ash mortality at larger landscape scales. It appears, however, that in areas of low host abundance, trap detection is less effective in highlighting infestation severity, which may be circumvented by placing traps along waterways where hosts are abundant.

CONCLUSIONS

To inform EAB regulatory and management response, the extent, severity, and progression of the Arkansas infestation were documented and mapped. Reconstruction of ash tree mortality coupled with spatially explicit trap detection records provided the basis for examination of realized spread and progression of the EAB infestation. Human transport of infested material appeared to continue to play a role in expanding the spread, but the spatial arrangement of the ash host in linear fashions along waterways also appeared to play a role in spread expansion by facilitating both short-distance colonization and long-distance dispersal. Outward progression was characteristic of satellite population establishment as opposed to expansion of original infestations. Human transport of infested material, which is the focus of quarantine implementation, did not seem to be hindered, and EAB satellite populations were detected 20 to 30 miles away from known infested areas. Trap detections lagged behind the onset of ash tree mortality by at least 1 year, highlighting the difficulty of early detection of invasive borers like EAB. Trap detections also appeared to be less effective in highlighting infestation severity in areas of low host abundance, which may be improved by placing traps along waterways where the host is more abundant. A multitude of factors including host abundance, road networks, and proximity to public land and recreational areas seem to have contributed to the highest infestation severity occurring in Clark County. The onset of EAB infestations appeared to be concentrated in Clark and Nevada Counties. As EAB spread continues, bottomland hardwood forests along the Saline River have high risk of potential EAB-induced ash tree mortality.

ACKNOWLEDGMENTS

We thank the Arkansas Department of Agriculture, Forestry Division and Ag. Pest Survey Program, and the U.S. Department of Agriculture Animal and Plant Health Inspection Service, Plant Protection and Quarantine, for their support in conducting research activities. Funding for this project was provided by the U.S. Department of Agriculture Forest Service, Forest Health Monitoring, Evaluation Monitoring program (project no. SO-DG-11083150-014 [M.M.B.]), with partial funding provided by the McIntire-Stennis Cooperative Forestry Research Program (project number 1005987-ARK02472).

For more information, contact: Mohammad Bataineh, Bataineh@uamont.edu.

LITERATURE CITED

Bataineh, M.M.; Daniels, L.D. 2014. An objective classification of largewood in streams. Forest Ecology and Management. 313: 1–9. https://doi.org/10.1016/j.foreco.2013.10.037.

BenDor, T.K.; Metcalf, S.S.; Fontenot, L.E. [and others]. 2006. Modeling the spread of the emerald ash borer. Ecological Modelling. 197(1–2): 221–236. https://doi.org/10.1016/j.ecolmodel.2006.03.003.

Daniels, L.D.; Dobry, J.; Klinka, K.; Feller, M.C. 1997. Determining year of death of logs and snags of *Thuja plicata* in southwestern coastal British Columbia. Canadian Journal of Forest Research. 27(7): 1132–1141. https://doi.org/10.1139/x97-055.

Ellenwood, J.; Krist, F.J.; Romero, S.A. 2015. Individual tree species parameter maps. https://www.fs.fed.us/foresthealth/applied-sciences/mapping-reporting/indiv-tree-parameter-maps.shtml#:~:text=Individual Tree Species Parameter Maps,density of a given species/. [Date accessed: January 1, 2018].

Grissino-Mayer, H.D. 2001. Evaluating crossdating accuracy: a manual and tutorial for the computer program COFECHA. Tree-Ring Research. 57(2): 205–221.

Herms, D.A.; McCullough, D.G. 2014. Emerald ash borer invasion of North America: history, biology, ecology, impacts, and management. Annual Review of Entomology. 59: 13–30. https://doi.org/10.1146/annurev-ento-011613-162051.

Holmes, R.L. 1983. Computer-assisted quality control in tree-ring dating and measurement. Tree-Ring Bulletin. 43(1): 69–78.

Knight, K.S.; Brown, J.P.; Long, R.P. 2012. Factors affecting the survival of ash (*Fraxinus* spp.) trees infested by emerald ash borer (*Agrilus planipennis*). Biological Invasions. 15(2): 371–383. https://doi.org/10.1007/s10530-012-0292-z.

Muirhead, J.R.; Leung, B.; Overdijk, C. [and others]. 2006. Modelling local and long-distance dispersal of invasive emerald ash borer *Agrilus planipennis* (Coleoptera) in North America. Diversity and Distributions. 12(1): 71–79. https://doi.org/10.1111/j.1366-9516.2006.00218.x.

Parsons, G.L. 2008. Emerald ash borer: a guide to identification and comparison to similar species. East Lansing, MI: Michigan State University. 56 p.

Siegert, N.W.; McCullough, D.G.; Liebhold, A.M.; Telewski, F.W. 2014. Dendrochronological reconstruction of the epicentre and early spread of emerald ash borer in North America. Diversity and Distributions. 20(7): 847–858. https://doi.org/10.1111/ddi.12212.

Siegert, N.W.; McCullough, D.G.; Williams, D.W. [and others]. 2010. Dispersal of *Agrilus planipennis* (Coleoptera: Buprestidae) from discrete epicenters in two outlier sites. Enivronmental Entomology. 39(2): 253–265. https://doi.org/10.1603/EN09029.

Siegert, N.W.; Mercader, R.J.; McCullough, D.G. 2015. Spread and dispersal of emerald ash borer (Coleoptera: Buprestidae): estimating the spatial dynamics of a difficult-to-detect invasive forest pest. The Canadian Entomologist. 147: 338–348. https://doi.org/10.4039/tce.2015.11.

Smith, A. 2006. Effects of community structure on forest susceptibility and response to the emerald ash borer invasion of the Huron River Watershed in southeast Michigan. Columbus, OH: The Ohio State University. 122 p. M.S. thesis.

Stokes, M.A.; Smiley, T.L. 1968. An introduction to tree-ring dating. Chicago, IL: University of Chicago Press. 73 p.

U.S. Department of Agriculture (USDA) Animal and Plant Health Inspection Service (APHIS). 2015. Emerald ash borer program manual, *Agrilus planipennis* (Fairmaire), ver. 1.6. Riverdale, MD. 111 p.

Woods, A.J.; Foti, T.L.; Chapman, S.S. [and others]. 2004. Ecoregions of Arkansas. Reston, VA: U.S. Department of the Interior, U.S. Geological Survey. Color poster with map, descriptive text, summary tables, and photographs; presentation scale: 1:1,000,000.

ACKNOWLEDGMENTS

This research presented in this report was supported in part through the project "Forest Health Monitoring, Analysis, and Assessment" of Cost Share Agreement 19-CS-11330110-027 (May 23, 2019 through September 22, 2020) and the project "Forest Health Monitoring, Assessment, and Analysis" of Cost Share Agreement 20-CS-11330180-020 (June 20, 2020 through August 31, 2021) between North Carolina State University (this institution is an equal opportunity provider) and the U.S. Department of Agriculture Forest Service, Southern Research Station, Asheville, NC. This research was supported by funds provided by the U.S. Department of Agriculture Forest Service, Southern Research Station, Asheville, NC.

The editors and authors of this report thank the following for their reviews and constructive comments: Chris Asaro, Erik Berg, Stephen Burr, Jennifer Costanza, Adrian Das, Tom Eager, Jim Ellenwood, Christopher Fettig, Andrew Gray, Ryan Hanavan, Wood Johnson, Justin Keyzer, Marc Meyer, Jeff Moore, Randy Morin, Jose Negrón, Steve Norman, Karen Ripley, Matt Russell, Tom Smith, Robin Usborne, William Van Doren, Kayanna Warren, Denys Yemshanov, and Derek Young.

AUTHOR INFORMATION

Sections 1 and 2, Forest Health Monitoring Research

Mark J. Ambrose, Research Assistant, North Carolina State University, Department of Forestry and Environmental Resources, Raleigh, NC 27695.

Erin M. Berryman, Quantitative Ecologist, RedCastle Resources, Inc., Fort Collins, CO 80526.

John W. Coulston, Supervisory Research Forester, U.S. Department of Agriculture Forest Service, Southern Research Station, Blacksburg, VA 24060.

Shawn Fraver, Associate Professor, University of Maine, School of Forest Resources, Orono, ME 04473.

Grant M. Domke, Research Forester, U.S. Department of Agriculture Forest Service, Northern Research Station, Forest Inventory and Analysis, St. Paul, MN 55108.

Andrew O. Finley, Professor, Michigan State University, Department of Forestry, East Lansing, MI 48825.

Frank H. Koch, Research Ecologist, U.S. Department of Agriculture Forest Service, Southern Research Station, Eastern Forest Environmental Threat Assessment Center, Research Triangle Park, NC 27709.

Jeanine L. Paschke, Geographic Information Systems Analyst, RedCastle Resources, Inc., Fort Collins, CO 80526.

Kevin M. Potter, Research Professor, North Carolina State University, Department of Forestry and Environmental Resources, Raleigh, NC 27695.

Matthew B. Russell, Associate Professor/Extension Specialist, University of Minnesota, Department of Forest Resources, St. Paul, MN 55108.

Hunter Stanke, Research Assistant, University of Washington, School of Environmental and Forest Sciences, Seattle, WA 98195.

Brian F. Walters, Forester, U.S. Department of Agriculture Forest Service, Northern Research Station, Forest Inventory and Analysis, St. Paul, MN 55108.

Christopher W. Woodall, Research Forester, U.S. Department of Agriculture Forest Service, Northern Research Station, Forest Inventory and Analysis, Durham, NH 03824.

Author Information, cont.

Trevor Adams, Forestry Specialist, Minnesota Department of Natural Resources, Northome, MN 56661.

Benjamin Babst, Associate Professor, University of Arkansas at Monticello, Monticello, AR 71656.

Mohammad M. Bataineh, Associate Professor, University of Arkansas at Monticello, Monticello, AR 71656.

Barbara Bentz, Research Entomologist, U.S. Department of Agriculture Forest Service, Rocky Mountain Research Station, Logan UT 84321.

Beverly Bulaon, Entomologist, U.S. Department of Agriculture Forest Service, Forest Health Protection, Sonora, CA 95370.

Stephen R. Clarke, Forest Entomologist, U.S. Department of Agriculture Forest Service, Forest Health Protection, Lufkin, TX 75901.

Daniel R. Cluck, Entomologist, U.S. Department of Agriculture Forest Service, Forest Health Protection, Susanville, CA 96130.

Michael Demchik, Professor, University of Wisconsin-Stevens Point, Stevens Point, WI 54481.

Patrick Engelken, Research Technician, Michigan State University, East Lansing, MI 48824.

Robert Ficklin, Professor, University of Arkansas at Monticello, Monticello, AR 71656.

Matt Hansen, Entomologist, U.S. Department of Agriculture Forest Service, Rocky Mountain Research Station, Logan, UT 84321.

Andrea Hefty, Entomologist, U.S. Department of Agriculture Forest Service, Forest Health Protection, San Bernardino, CA 92408.

Michael Hillstrom, Forest Health Specialist, Wisconsin Department of Natural Resources, Fitchburg, WI 53711.

Stacy Hishinuma, Entomologist, U.S. Department of Agriculture Forest Service, Forest Health Protection, San Bernardino, CA 92408.

Sharon M. Hood, Research Ecologist, U.S. Department of Agriculture Forest Service, Rocky Mountain Research Station, Missoula, MT 59808.

Alexander Koltunov, Remote Sensing Scientist, U.S. Department of Agriculture Forest Service, Pacific Southwest Region Remote Sensing Lab, McClellan, CA 95652 and University of California Davis, Center for Spatial Technologies and Remote Sensing (CSTARS), Davis CA 95616.

Katherine Minnix, PhD Candidate, Michigan State University, East Lansing, MI 48824.

Deborah G. McCullough, Professor, Michigan State University, East Lansing, MI 48824.

Charlotte Reed, Ecologist, U.S. Department of Agriculture Forest Service, Rocky Mountain Research Station, Missoula, MT 59808.

Justin Runyon, Research Entomologist, U.S. Department of Agriculture Forest Service, Rocky Mountain Research Station, Bozeman, MT 59715.

Monique Sakalidis, Assistant Professor, Michigan State University, East Lansing, MI 48824.

Kyoko Scanlon, Forest Pathologist, Wisconsin Department of Natural Resources, Fitchburg, WI 53711.

Michèle R. Slaton, Ecologist, U.S. Department of Agriculture Forest Service, Pacific Southwest Region Remote Sensing Lab, McClellan, CA 95652.

Sheri Smith, Regional Entomologist, U.S. Department of Agriculture Forest Service, Pacific Southwest Region, Vallejo, CA 94592.

David Soderberg, PhD Candidate, Wildland Resources Department, Utah State University, Logan, UT 84322.

Sky Stephens, Entomologist, U.S. Department of Agriculture Forest Service, Forest Health Protection, Lakewood, CO 80401.

Jim Vandygriff, Entomologist, U.S. Department of Agriculture Forest Service, Rocky Mountain Research Station, Logan, UT 84321.

Benjamin L. Walters, Graduate Research Assistant, University of Arkansas at Monticello, Monticello, AR 71656.

Kayanna Warren, Ecologist, U.S. Department of Agriculture Forest Service, Pacific Southwest Region, State and Private Forestry, Vallejo, CA 94592.

Potter, Kevin M.; Conkling, Barbara L., eds. 2021. Forest health monitoring: national status, trends, and analysis 2020. Gen. Tech. Rep. SRS-261. Asheville, NC: U.S. Department of Agriculture, Forest Service, Southern Research Station. 211 p. https://doi.org/10.2737/SRS-GTR-261.

The annual national report of the Forest Health Monitoring (FHM) program of the Forest Service, U.S. Department of Agriculture, presents forest health status and trends from a national or multi-State regional perspective using a variety of sources, introduces new techniques for analyzing forest health data, and summarizes results of recently completed Evaluation Monitoring projects funded through the FHM national program. In this 20th edition in a series of annual reports, national survey data are used to identify recent geographic patterns of insect and disease activity. Satellite data are employed to detect geographic patterns of forest fire occurrence. Recent drought and moisture surplus conditions are compared across the conterminous United States. Data collected by the Forest Inventory and Analysis (FIA) program are employed to detect regional differences in tree mortality. Nearly 20 years of FIA coarse woody material (CWM) data are examined across spatial scales to assess change over time in CWM biomass, diameter and decay class, and species composition. Case studies demonstrate the potential of rFIA, an open-source R package developed to improve the accessibility of FIA data and offer enhanced flexibility in estimation strategies, to advance forest health evaluation and monitoring. Six recently completed Evaluation Monitoring projects are summarized, addressing forest health concerns at smaller scales.

Keywords—Change detection, coarse woody material, drought, fire, forest health, forest insects and disease, tree canopy, tree mortality.

Scan this code to submit your feedback, or go to www.srs.fs.usda.gov/pubeval.

A copy of this report is available for download at www.srs.fs.usda.gov/pubs/.

Please direct inquiries about the availability of hard copies to pubrequest@fs.fed.us. Number of copies is limited to two per person.

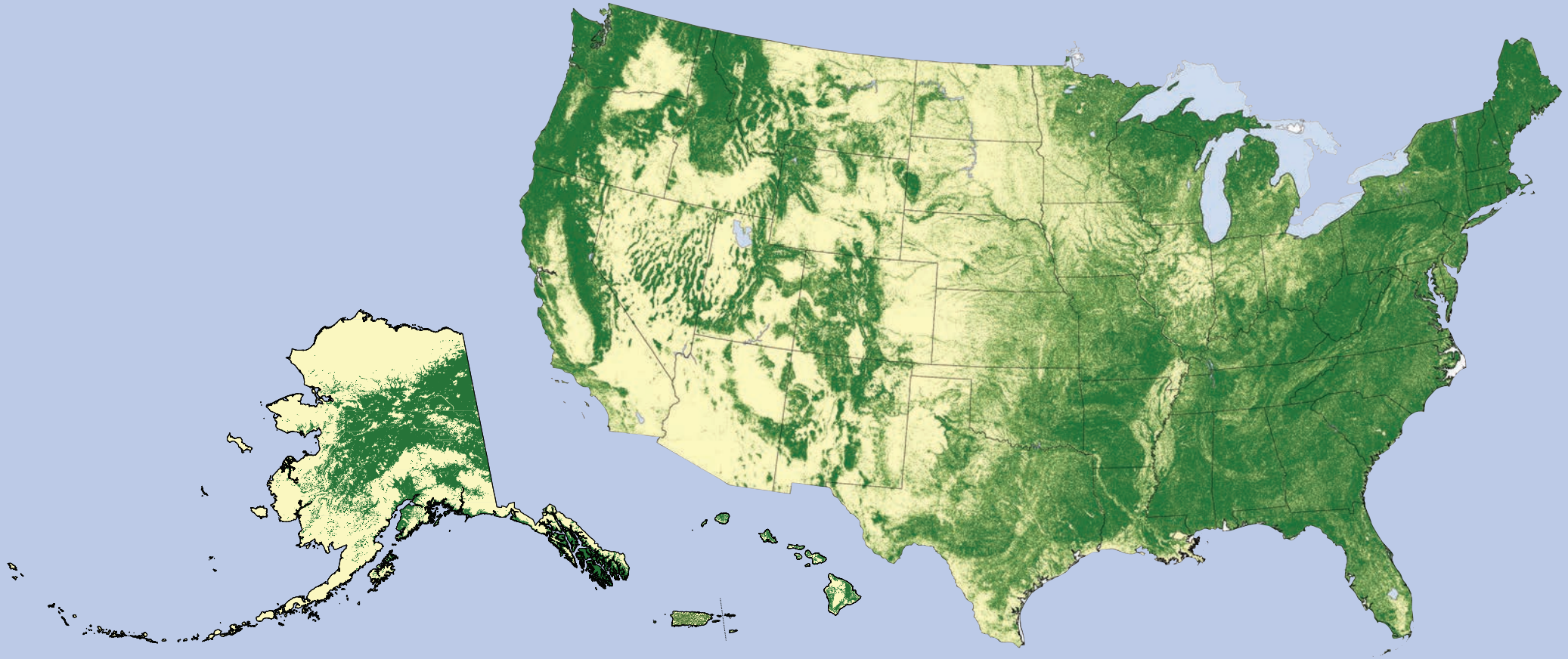

In accordance with Federal civil rights law and U.S. Department of Agriculture (USDA) civil rights regulations and policies, the USDA, its Agencies, offices, and employees, and institutions participating in or administering USDA programs are prohibited from discriminating based on race, color, national origin, religion, sex, gender identity (including gender expression), sexual orientation, disability, age, marital status, family/parental status, income derived from a public assistance program, political beliefs, or reprisal or retaliation for prior civil rights activity, in any program or activity conducted or funded by USDA (not all bases apply to all programs). Remedies and complaint filing deadlines vary by program or incident.

Persons with disabilities who require alternative means of communication for program information (e.g., Braille, large print, audiotape, American Sign Language, etc.) should contact the responsible Agency or USDA's TARGET Center at (202) 720-2600 (voice and TTY) or contact USDA through the Federal Relay Service at (800) 877-8339. Additionally, program information may be made available in languages other than English.

To file a program discrimination complaint, complete the USDA Program Discrimination Complaint Form, AD-3027, found online at http://www.ascr.usda.gov/complaint_filing_cust.html and at any USDA office or write a letter addressed to USDA and provide in the letter all of the information requested in the form. To request a copy of the complaint form, call (866) 632- 9992. Submit your completed form or letter to USDA by: (1) mail: U.S. Department of Agriculture, Office of the Assistant Secretary for Civil Rights, 1400 Independence Avenue, SW, Washington, D.C. 20250-9410; (2) fax: (202) 690-7442; or (3) email: program.intake@usda.gov" program.intake@usda.gov.

USDA is an equal opportunity provider, employer, and lender.

Forest Health Monitoring: National Status, Trends, and Analysis 2020

2021